NASA CR-134812
GIT A-1651

S-BAND OMNIDIRECTIONAL ANTENNA FOR THE SERT-C SATELLITE

By
H. L. Bassett, J. W. Cofer, Jr., R. R. Sheppard, and M. J. Sinclair

JULY 1975

ENGINEERING EXPERIMENT STATION
Georgia Institute of Technology

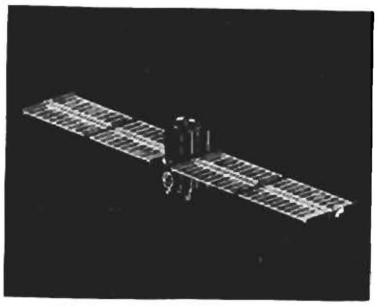

Prepared for
NATIONAL AERONAUTICS AND SPACE ADMINISTRATION

NASA LEWIS RESEARCH CENTER
Contract NAS3-18901

1. Report No.	2. Government Accession No.	3. Recipient's Catalog No.
CR-134812		

4. Title and Subtitle	5. Report Date
S-BAND OMNIDIRECTIONAL ANTENNA FOR THE SERT-C SATELLITE	May 1975
	6. Performing Organization Code
7. Author(s) H. L. Bassett, J. W. Cofer, Jr. R. R. Sheppard and M. J. Sinclair	8. Performing Organization Report No. A-1651
	10. Work Unit No.
9. Performing Organization Name and Address Engineering Experiment Station Georgia Institute of Technology Atlanta, Georgia 30332	11. Contract or Grant No. NAS3-18901
	13. Type of Report and Period Covered Contractor Final Report 6-74 - 4-75
12. Sponsoring Agency Name and Address NASA Lewis Research Center 21000 Brookpark Road Cleveland, Ohio 44135	14. Sponsoring Agency Code

15. Supplementary Notes

Project Manager, Martin J. Conroy, Systems Engineering Branch, NASA, LeRC, Cleveland, Ohio
Design, test and evaluation results reported; May 1975

16. Abstract

This report details the program to design an S-band omnidirectional antenna system for the SERT-C spacecraft. The program involved the tasks of antenna analyses by computer techniques, scale model radiation pattern measurements of a number of antenna systems, full-scale RF measurements, and the recommended design, including detailed drawings. A number of antenna elements were considered: the cavity-backed spiral, quadrifilar helix, and crossed-dipoles were chosen for in-depth studies. The final design consisted of a two-element array of cavity-backed spirals mounted on opposite sides of spacecraft and fed in-phase through a hybrid junction. This antenna system meets the coverage requirement of having a gain of at least -10 dBi over 50 percent of a 4π steradian sphere with the solar panels in operation. This coverage level is increased if the ground station has the capability to change polarization.

17. Key Words (Suggested by Author(s))	18. Distribution Statement
SERT-C Satellite, S-Band, Omnidirectional Antenna, Scale-Model, Radiation Patterns, Contour Plots Quadrifilar Helix Spiral Antenna	Unclassified

19. Security Classif. (of this report)	20. Security Classif. (of this page)	21. No. of Pages	22. Price*
Unclassified	Unclassified		

* For sale by the National Technical Information Service, Springfield, Virginia 22151

FOREWORD

This final report was prepared by the Systems and Techniques Department of the Engineering Experiment Station, Georgia Institute of Technology, under Contract NAS3-18901. This contract was initiated by the Space Flight Programs Directorate of NASA Lewis Research Center, Cleveland, Ohio. The contract was administered by Edward J. Domino and Martin J. Conroy of the Systems Engineering Branch, Spacecraft Communications Section.

The period of performance covered by this report extends from 24 June 1974 to 24 March 1975.

Report authors are Harold L. Bassett, James W. Cofer, Jr., Richard R. Sheppard, and Michael J. Sinclair, all of the Systems and Techniques Department. Other personnel participating in this work include G. R. Loefer and C. E. Summers. Mr. W. P. Allen, Lockheed-Georgia, is due acknowledgement for his contributions in the scale model testing.

The views and conclusions contained in this document are those of the authors and should not be interpreted as necessarily representing the official policies, either expressed or implied, of NASA LeRC or the U. S. Government.

TABLE OF CONTENTS

LIST OF FIGURES

LIST OF FIGURES (Continued)

LIST OF FIGURES (Continued)

LIST OF FIGURES (Continued)

LIST OF TABLES

S-BAND OMNIDIRECTIONAL ANTENNA FOR THE SERT-C SATELLITE

Harold L. Bassett, James W. Cofer, Jr., Richard R. Sheppard
and Michael J. Sinclair

Engineering Experiment Station
Georgia Institute of Technology

SUMMARY

This report details the program to design an S-band omnidirectional antenna system for the SERT-C spacecraft. The program involved the tasks of antenna analyses by computer techniques, scale model radiation pattern measurements of a number of antenna systems, full-scale RF measurements, and the recommended design, including detailed drawings. A number of antenna elements were considered; the cavity-backed spiral, quadrifilar helix, and crossed-dipoles were chosen for in-depth studies. The final design consisted of a two-element array of cavity-backed spirals mounted on opposite sides of the spacecraft and fed in-phase through a hybrid junction. This antenna system meets the coverage requirement of having a gain of at least -10 dBi over 50 pecent of a 4π steradian sphere with the solar panels in operation. This coverage level is significantly increased if the ground station has the capability to change polarization.

I. INTRODUCTION

A. Background

The analyses and test results for an S-band omnidirectional antenna system for the SERT-C spacecraft are presented in this report. The SERT-C spacecraft will provide a practical demonstration of the use of ion engines to propel a spacecraft from a low parking orbit to synchronous orbit. The spacecraft will also demonstrate precise station keeping, attitude control, and rendezvous capability at synchronous altitude.

The spacecraft will be launched from ETR by a McDonnell-Douglas Delta 2910 launch vehicle and placed in a parking orbit of 3150 km altitude. After orientation, the spacecraft will be separated from the launch vehicle, the solar arrays will be deployed, and a checkout of the spacecraft systems will be performed by means of telemetry and command. Two of the 30-cm ion engines will then be started, and the spacecraft will describe a spiral ascent trajectory until synchronous altitude is attained. The omnidirectional S-band antenna system will be utilized for telemetry and command during the ascent period. At synchronous altitude, the spacecraft will be rotated until the high gain antenna is pointed at the earth, and demonstrations of attitude control, station keeping, and rendezvous capability will be performed.

B. Summary of Tasks

The S-band telemetry and command antenna used during the ascent stage is the subject of this report. The work period was from 24 June 1974 through 24 February 1975. The program was divided into five tasks. The first task was entitled "Analysis and Preliminary Design," and was a sixty-day effort. This particular task centered on the analysis of a number of different type antenna systems and the selection of three candidate omnidirectional antennas for evaluation. Representatives from NASA LeRC and Georgia Tech were to choose the appropriate antenna system from the three candidates. The particular area of emphasis was in the determination of the shadowing

of the antenna by the rotating solar panels. Calculations were to be performed to show the estimated percent coverage of the antenna system with the solar panel shadowing included.

In addition to the computer analyses of the antenna system, the advisability of scale model testing was determined in Task I. The appropriate scaling factors, test facility, and test methods were also presented at the conclusion of the initial sixty-day effort. Detailed discussions of the antenna analyses and the scale model factors are presented in Section II of this report.

Upon approval of the preliminary design, the engineering model of the antenna was to be designed. This effort was designated Task II. The finalization of this particular task depended on the results of Task IV, "Scale Model Testing." The three antenna systems recommended at the conclusion of Task I were an array of quadrifilar helices, an array of cavity-backed spirals, and an array of crossed-dipoles. It was recommended at the conclusion of Task I that scale model testing on each of these systems be done prior to choosing the final system. A detailed discussion of the scale model testing and rationale for choosing an array of two cavity-backed spiral antennas is presented in Section II.C.

The Task III effort was designated as "Fabrication of the Antenna." As it turned out, the fabrication effort consisted in main of a scale model satellite and scale model antennas. Since the final choice of the antenna system was cavity-backed spirals, it was felt that it would be cost-effective to purchase the antennas. This particular task is discussed further in Section II.E. The recommended antenna configuration is presented in a separate chapter, Section III.

The testing of the engineering model was done under Task IV. As a minimum, the tests would include amplitude pattern tests, polarization test, maximum power gain test, input impedance test, and a power handling test. The amplitude pattern tests were made with the use of a scale model and are discussed in Section II.C. The remainder of the tests were performed on a full-scale model of the SERT-C satellite and these results are presented in Section II.D.

The fifth task was designated "Reporting" and this included monthly progress reports including financial and performance analysis reports. A presentation was made at the conclusion of the sixty-day analysis effort to appropriate personnel at NASA LeRC. Task V also included the writing of this final report and a final presentation of results at NASA LeRC.

The following is a summary of the research and development program on the SERT-C S-Band omnidirectional antenna system:

(1) Evaluation of candidate antennas.

(2) Reduction of candidate list to three antenna types using analytical techniques and a tradeoff study.

(3) Preliminary scale model testing and a recommendation of crossed-dipoles, quadrifilar helices, or cavity-backed spirals based on patterns alone.

(4) Scale model testing utilizing both the quadrifilar helix and cavity-backed spiral as antenna elements. The patterns of two element and four element arrays were measured. Both radiation contour plots and polar plots were recorded.

(5) Performance of VSWR tests. It was found that the quadrifilar helix was marginal when considering RF design specifications. Thus, the cavity-backed spiral was the final choice for the antenna element. Two of these mounted on opposite sides of the spacecraft met all specifications.

(6) Perform power handling test on the two-element spiral array.

C. Antenna Specifications

(1) Coverage and Gain

The antenna shall provide a minimum gain of 10 dB below isotropic in all areas of a 4π steradian sphere that are not shadowed by the spacecraft body or the solar arrays. Before the solar arrays are deployed the coverage of a sphere shall be at least 65 percent. After the solar arrays are deployed the coverage of a sphere shall be at least 50 percent.

(2) Polarization

The antenna shall provide right hand circular polarization along the positive roll axis during the orbit raising phase of the mission.

(3) Frequency Bands

The command carrier frequency will be 2.069673 GHz. The telemetry carrier frequency will be 2.2475 GHz.

(4) Power

The antenna system shall operate continuously with a power input of 20 watts at any carrier frequency in the telemetry band.

(5) Antenna Connector

A single coaxial RF connector shall be used to connect the antenna to the spacecraft S-band transponder. This connector shall be either the TNC or miniature types such as the OSM series.

(6) Impedance

a. In a band of 20 MHz, centered at the command frequency specified in above paragraph C.3, the antenna shall have an impedance of 50 ohms, at a VSWR of 1.5:1 or lower.

b. In a band of 20 MHz, centered at the telemetry frequency specified in above paragraph C.3, the antenna shall have an impedance of 50 ohms, at a VSWR of 1.5:1 or lower.

D. Thermal Specifications

(1) Louver Constraint

The north and south faces of the spacecraft contain louvers which act as temperature control devices. These louvered faces shall not be used as antenna mounting surfaces.

(2) Temperature Cycle

Due to rotation of the spacecraft body about the axis of the solar arrays, the exposure of the spacecraft faces to solar flux will cycle periodically. The minimum period of this cycle will be 2.5 hours. The maximum period will be 24 hours.

(3) Thermal Isolation

The antenna shall be designed so that it is thermally isolated from the spacecraft.

(4) Eclipse Survival

The antenna shall be capable of surviving a 72 minute eclipse (no solar illumination) once per day.

(5) Sunlight Survival

The antenna shall be capable of surviving exposure to full sunlight (one solar constant) from any angle, using a spacecraft blockage factor appropriate to the installation.

(6) Solar Array Constraint

The antenna shall not interfere with the solar illumination of the solar array.

E. Weight

The omnidirectional antenna weight goal shall be 3.63 kg (8 pounds) or less.

II. TECHNICAL APPROACH

This section of the report is an elaboration of the program followed by Georgia Tech in the determination of the S-band omnidirectional antenna design. It includes the candidate antennas, the theoretical modeling of certain antenna types located on the spacecraft, the rationale for the choice of the final antenna, the scale model testing, the full-scale model antenna measurements, and the mechanical design aspects.

A. Candidate Antennas

A number of antenna types were evaluated as possible candidates for the SERT-C spacecraft omnidirectional directional antenna elements. The element requirements were:

(1) circular polarization (RHC)
(2) handle 20 watts CW power
(3) broadband (2.0 GHz to 2.3 GHz)
(4) lightweight.

A listing of the candidate antennas that evolved is:

(1) slots in a ground plane
(2) crossed-dipoles
(3) quadrifilar helix (Volute) [1,2,3]
(4) wraparound [4]
(5) loops
(6) spirals
(7) log conical
(8) monopole arrays
(9) regular helix.

Some of these are similar type antennas and were categorized as follows and further studied:

(1) slots and wraparound
(2) crossed-dipoles, monopole arrays, and loops
(3) quadrifilar helix and regular helix
(4) spiral and log conical.

The wraparound antenna types were felt to be too complex for this application. Since the slots and crossed dipoles are complementary elements and because considerable success [5] has been found with dipoles, it was decided to consider the crossed-dipoles as one of the three candidates.

The quadrifilar helix had excellent potential and it was felt that it should be given due consideration as an antenna element. The cavity-backed spiral antenna had the desired element radiation pattern characteristics and it is a broadband device. Normally, these spirals are used in the receive mode only, but there are high power designs available. Since these three element designs when used in an array had the potential to meet all the performance requirements, were simple in design, lightweight, normally possess circular polarization characteristics, and were also simple to model, the crossed-dipoles, quadrifilar helix, and cavity-backed spiral were chosen for further evaluation.

The crossed-dipole array, the quadrifilar helix array, and the cavity-backed spiral array were presented as candidate antennas to NASA LeRC at the sixty-day review meeting. Also presented were the computer computations of estimated coverage for a number of antenna array configurations. These data are presented in Section II.C, "Theoretical Modeling".

B. S-Band Antenna Systems

It seems appropriate, in this discussion, to consider antenna systems in general. In principle, it is impossible to achieve isotropic coverage for a singly polarized antenna system. A null-free pattern will consist of different polarizations. To obtain an S-band antenna system with near isotropic coverage is very difficult for structures large compared to the wavelength. It is possible to obtain near null-free coverage if the ground station has polarization diversity. In the days of VHF TM systems, antennas were mounted on vehicles whose diameters might be on the order of a couple of wavelengths. Thus, one or two of these antennas gave excellent ground station coverage with the exception of nose-on or tail-on look angles. When the TM frequencies were changed to S-band, the wavelength decreased by a factor of ten. This meant that two antennas would, in general, produce

scalloped patterns in the azimuth plane of a vehicle with many deep nulls. These effects are caused by interference and shadowing. Normally, it took an array of S-band antennas to provide adequate coverage. We have seen a number of these array designs in the literature [5,6,7]. Another approach has been to extend an antenna away from the structure so that the structure becomes negligible [8].

Instead of the closely spaced multi-element array or the extended antennas, a theoretical analysis of the two-element and four-element arrays was performed. This approach was taken for three reasons:

(1) only two faces of the spacecraft were available for mounting antennas

(2) simplicity and

(3) weight.

Many of these configurations are presented in Section II.C. A near-omnidirectional pattern in the equatorial plane was desired, where nulls near the poles were acceptable. It was anticipated that either a two-element or four-element array would meet the coverage factor. This factor indicates the percent of the total space angle, 4π steradians, for which a certain gain will be exceeded. There is no doubt that these arrays will provide much more than adequate coverage if the ground station utilizes polarization diversity.

There is good reasoning for considering the two-element and four-element arrays based on the experiences of other spacecraft antenna systems. Two excerpts from the literature are included as Appendix I of this report.

These excerpts are typical of comments that were found in most of the literature. In general, the majority of the past and current spacecraft communications systems which require near-omnidirectional antenna coverage rely in main on either the space and/or polarization diversity of the ground stations. The aspect of space and/or polarization diversity has become more popular since systems engineers have become more familiar with the propagation characteristics of the earth's atmosphere. Typical characteristics that cause an apparent attenuation of signal are: atmospheric water vapor, clouds and fog, rainfall and hail, refraction,

reflection and scattering, decorrelation, polarization rotation, and Doppler frequency shift. These are all frequency dependent and, fortunately, S-Band systems are not affected as much as systems in other frequency bands. These effects, coupled with both the deep nulls in the spacecraft antenna pattern coverage and the changes of polarization of the spacecraft antenna with respect to aspect angle, require that ground stations possess, at least, polarization diversity.

C. Theoretical Modeling

In order to evaluate the performance of an antenna system such as that required for the present satellite application, the percentage of a 4π steradian sphere over which the gain level is greater than or equal to a specified level must be known. A typical plot of one such power distribution for an unknown antenna system is shown in Figure 1. In this plot, the percentage of the sphere over which the gain level is less than the power level shown (abscissa) is plotted as a function of the abscissa. This type of plot resembles in form the familiar probability distribution function. For example in Figure 1, one can tell that the peak of the power pattern has a gain of +5 dBi, since the gain is less than (or equal) to this value 100% of the time. Likewise, the gain is less than -1.7 dBi over 35% of the sphere, or in the context of this application is greater than or equal to -1.7 dBi over 65% (100%-35%) of an arbitrary far-field spherical surface. Thus, the total electric field (and therefore the power pattern) must be calculated (or measured) as a vector summation of the contributions from all radiating structures in the system for a large number of points (R, θ, Φ) on an arbitrary far-field sphere. The points are then treated as samples from a random process and a probability distribution found. It is important to note that the number of spherical points having a given gain level are not merely counted but the areas (i.e., $R^2 \sin\theta \, \Delta\theta \, \Delta\Phi$) having a given gain are summed.

Several techniques are available for calculation of the far-field pattern depending on the particular geometry involved and/or the level of rigor deemed necessary. Three such techniques commonly used are the geometrical theory of diffraction (GTD), moment methods, and scalar array calculations.

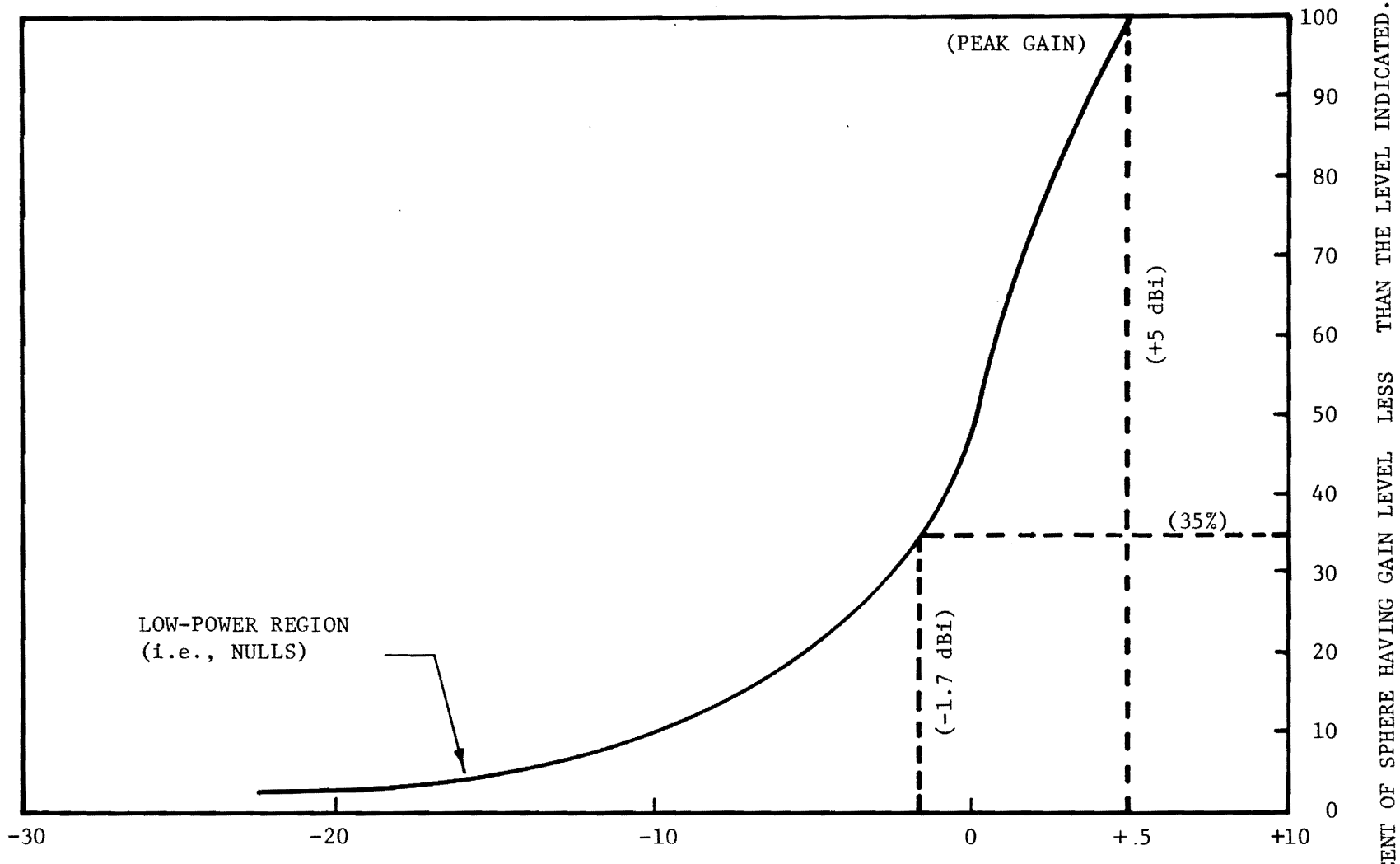

Figure 1. Typical percent coverage function for an arbitrary antenna system.

The method of GTD is useful when it is desired to calculate the field in a shadow region behind an obstacle. For this particular application, the electric field intensity in the far-field of the vehicle may be calculated theoretically (using GTD) from the equation

$$\bar{E}(\theta,\phi) = \sum_{n=1}^{N} \bar{A}_n(\theta,\phi) e^{-j\beta R_n} + \sum_{m=1}^{M} \bar{B}_m(\theta,\phi) e^{-j\beta \rho_m} \qquad (1)$$

where

$\bar{A}_n(\theta,\phi)$ = the radiation pattern (including polarization) of the n^{th} element,

N = total number of elements,

β = propagation constant,

$$R_n = \sqrt{(X_2 - X_{in})^2 + (Y_2 - Y_{in})^2 + (Z_2 - Z_{in})^2}$$

(X_{in}, Y_{in}, Z_{in}) = coordinates of element location on vehicle,

(X_2, Y_2, Z_2) = coordinates of far-field point

$= (R_o \sin\theta \cos\phi,\ R_o \sin\theta \sin\phi,\ R_o \cos\theta)$,

$\bar{B}_m(\theta,\phi)$ = the field scattered by the edges of the box-shaped vehicle in the direction θ,ϕ,

$$\rho_m = \sqrt{(X_2 - U_m)^2 + (Y_2 - V_m)^2 + (Z_2 - W_m)^2}$$

(U_m, V_m, W_m) = coordinates of the m^{th} edge point from which scattered fields originate,

M = total number of edge scattering points.

In antenna systems having highly directive elements or very few obstacles in the near vicinity, the second part of Equation (1) containing the scattered fields can be ignored. Scattered fields arise when a ray leaving the element strikes an edge of the vehicle instead of radiating directly away. This ray then scatters into a cone of rays whose cone half-angle depends on the angle between the edge and the incident ray. If the cone from a particular point (U_m, V_m, W_m) passes along the direction θ,ϕ, that point is considered to be a scattering point for the direction θ,ϕ. Therefore, the number of scattering points (M) could be much larger or much smaller (possibly zero)

than the number of elements (N). Multiple scattered fields (from one edge to another and then to the far-field) are considered second order effects and usually are not included in the analysis.

The moment method technique takes into account the effect of the vehicle by calculating the currents which are induced on its surface and the radiated electric field corresponding to those currents. A moment method evaluation of the wire radiating and scattering geometries has been formulated by Professors D. C. Kuo and B. J. Strait of Syracuse University [9]. A listing of this program was obtained and coded for the Univac U-1108 computer at Georgia Tech. Input and output data have been compared with those of Professor Strait and identical results were obtained.

The moment method computer program operates in the following fashion. First, the vehicle is considered to be made up of a large number of wire segments instead of continuous smooth surfaces. A wire geometry is specified in terms of the location and size of the wire elements. Next, the mutual impedances between the various portions of the wires are calculated in terms of an impedance matrix; then the impedance matrix is inverted to obtain the admittance matrix between the various portions of the wires. Specified input voltages are applied to those wires which are desired as radiators (i.e., the antenna elements), and then the currents induced in these wire elements as well as those incuded in the rest of the structure are calculated. Using these currents the far-field pattern obtained from the composite structure is calculated. Due to the nature of the computational technique, the antennas on the vehicle are modeled as wire radiators (e.g., an electrically small loop). These radiators are placed at predetermined points around the vehicle and the far-field pattern from the composite structure is calculated.

The third and simplest computational technique, termed the scalar method, results when the polarization of the far-field pattern is assumed to be the same as that of the element, and the scattered field (second term in Equation (1)) is neglected. This method is by far the simplest to model; however, the results do not carry as much credibility as those of the other two methods. A modified version of this approach was used on this contract

since (1) a knowledge of the lower portion of the gain distribution was not desired (i.e., lowest specification was for 35%), and (2) the extremely large size in wavelengths of the vehicle would have consumed an excessive amount of computer time. A concerted effort was made to verify the scalar calculations by applying the method of moments to some of the antenna configurations. It became immediately obvious that the solar panels could not be handled since they required admittance matrices with element numbers much greater than the storage capacity of the Georgia Tech Univac 1108 computer. Even with the neglecting of the panels and half of the vehicle, the required storage was on the order of four times that available. It was felt that to further approximate the vehicle would yield unrealistic results; consequently, this approach was abandoned. The method of GTD is also very time consuming since for each point in the far-field (e.g., increments of 1° each in θ and Φ yields 64,800 points), all edges of the vehicle must be searched iteratively to determine the origin, phase, and amplitude of energy which scatters to that point. Consequently, the method of moments and GTD were abandoned in favor of a scalar method which takes into account the loss of coverage due to shadowing by the solar panels.

This shadowing effect was handled by calculating the pattern using the first term of Equation (1) and replacing the field in the shadow region by zero. A common shadow region was derived for all elements by placing one element on top (i.e., location of the engines) and calculating the outline of the panels in the θ-Φ domain. A plot of these points is shown in Figure 2. The contour is very nearly approximated by the equation

$$\theta(\Phi) > 90° + 45° \left|\sin \Phi\right|^{0.8} \tag{2}$$

where the coordinate system used is shown in Figure 3. The element pattern $A_n(\theta,\Phi)$ in Equation (1) was assumed to vary according to the equation

$$A_n(\theta,\Phi) = \left\{[1 + \cos (\theta - \theta_n)]\ [1 + \cos (\theta - \Phi_n)]\right\}^p \tag{3}$$

where (θ_n,Φ_n) specify the angular pointing direction of the n^{th} element,

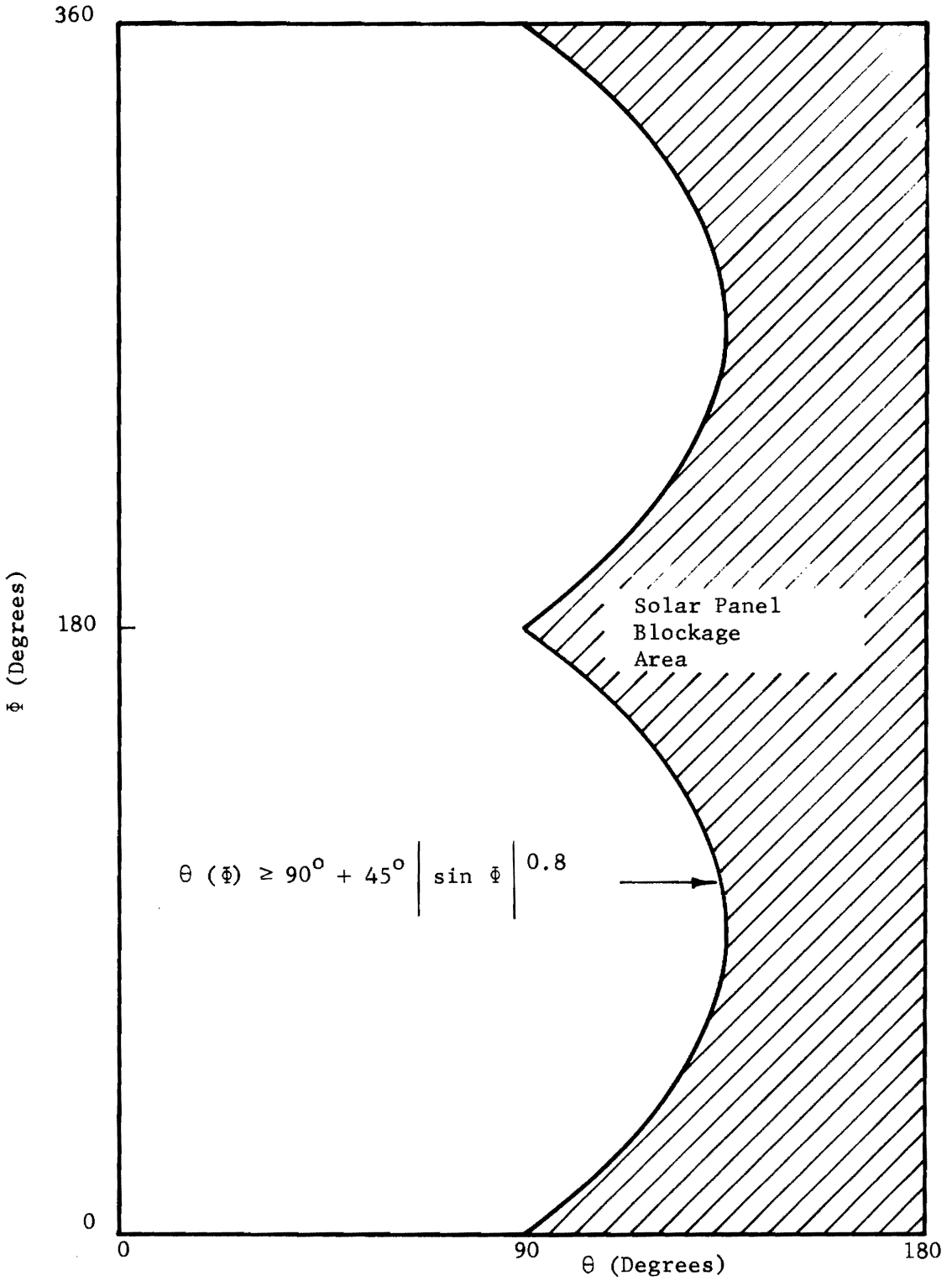

Figure 2. Rectangular plot of the θ - Φ domain showing region blocked by the solar panels.

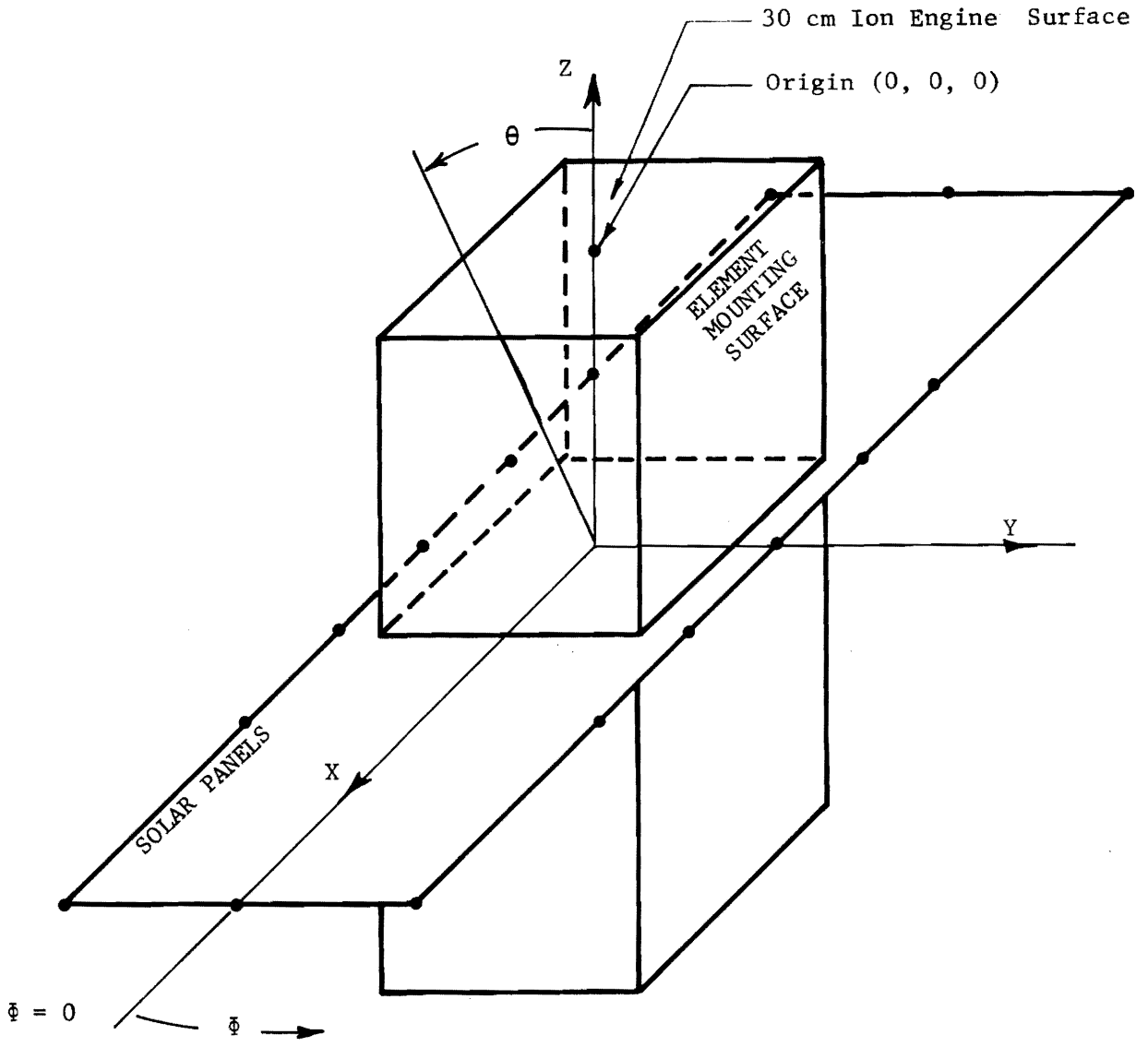

Figure 3 . Geometry of the SERT-C satellite used to calculate optical blockage (as a function of θ and Φ) by the solar panels for an element located at the origin.

and p is a measure of the directivity of the element pattern (e.g., highly directive for large p). One method for choosing p is by calculating the value required to cause the element pattern to decrease by a specified number of dB at $(\theta-\theta_m, \phi-\phi_n)$ either equal to (0°, 90°) or (90°, 0°) (horizon taper) as this connotes the type of element used. For example, the values of p used to calculate patterns under this contract are listed below along with their horizon tapers ($\pm$ 90° edge taper):

p = 0.00 (0 dB)
p = 0.83 (-5 dB)
p = 1.66 (-10 dB)
p = 3.32 (-20 dB)

Patterns were calculated for several combinations of element numbers and locations and with element patterns described by Equation (3) and the values of p above. These patterns are portrayed as three-dimensional functions (power) of the spherical angles θ and Φ. Such a plot for one particular case is shown in Figure 4. This particular case is that of two elements with 5-dB horizon tapers and located at the top center edges of the sides not containing the solar panels [coordinates = (0,27,0) and (0,-27,0)] and pointing along opposite directions. The two relatively flat plateau regions in the pattern correspond to the pointing directions of the individual elements where that element is dominant, while the rapidly fluctuating areas correspond to regions of cancellation and reinforcement by the two elements. The effect of making the elements more directive by assigning horizon tapers of 10 and 20 dB may be observed from Figures 5 and 6, respectively. A more directive element broadens the "quiet region" in front of each element and decreases the interaction region; however, the percent coverage may also decrease due to the low power areas between the peaks.

A large number of patterns were also calculated for four-element arrays. Pairs of elements were placed at the top corner edges [coordinates = (19.8, 27,0), (-19.8,27,0), (-19.8,-27,0), and (19.8,-27,0) inches] of the two previously described sides of the vehicle. The element pointing directions

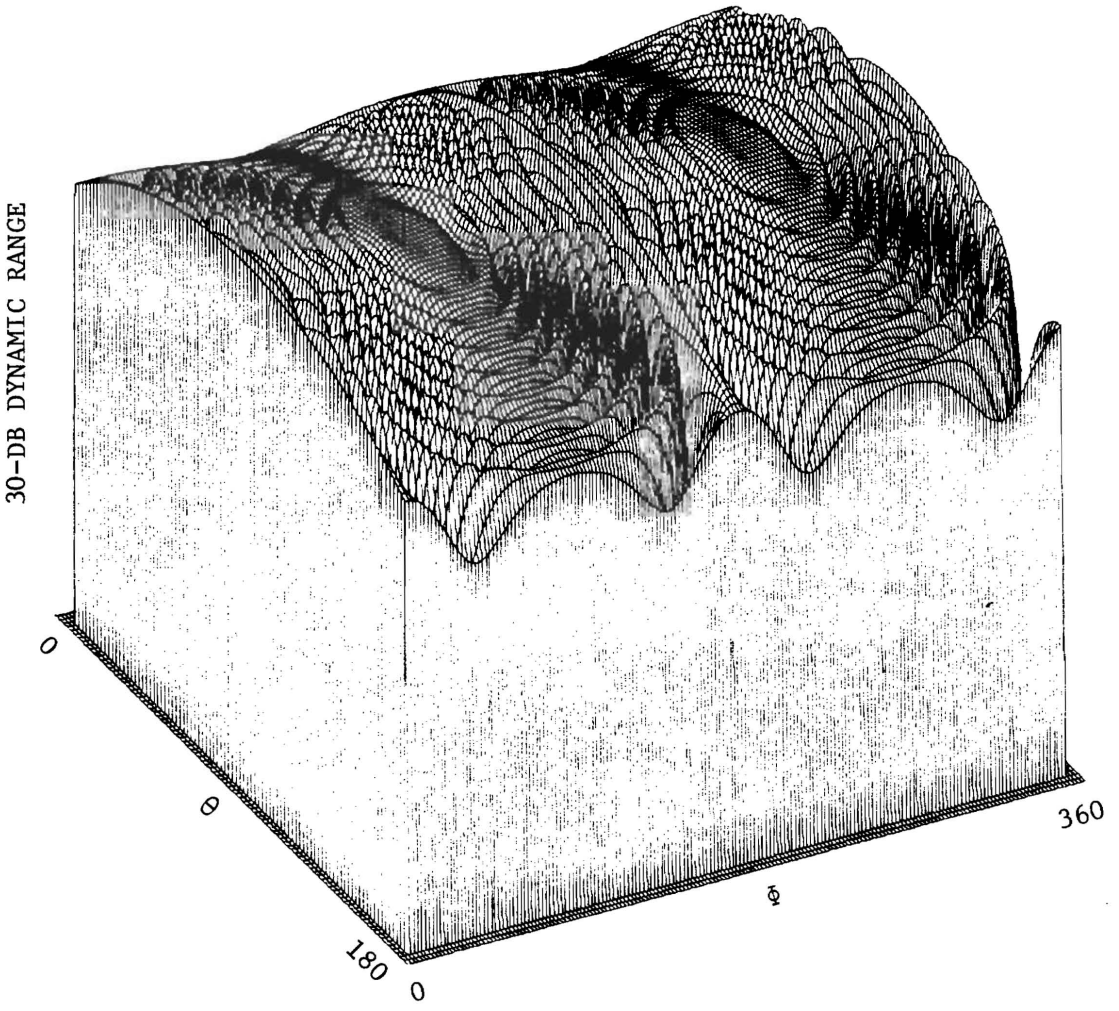

Figure 4. Calculated radiation pattern from a 2 element array located on the SERT-C satellite. The elements have a 5 dB taper 90^{o} away from boresight. The elements have θ-Φ pointing directions of (90,90) and (90,270). Solar panel blockage was not included.

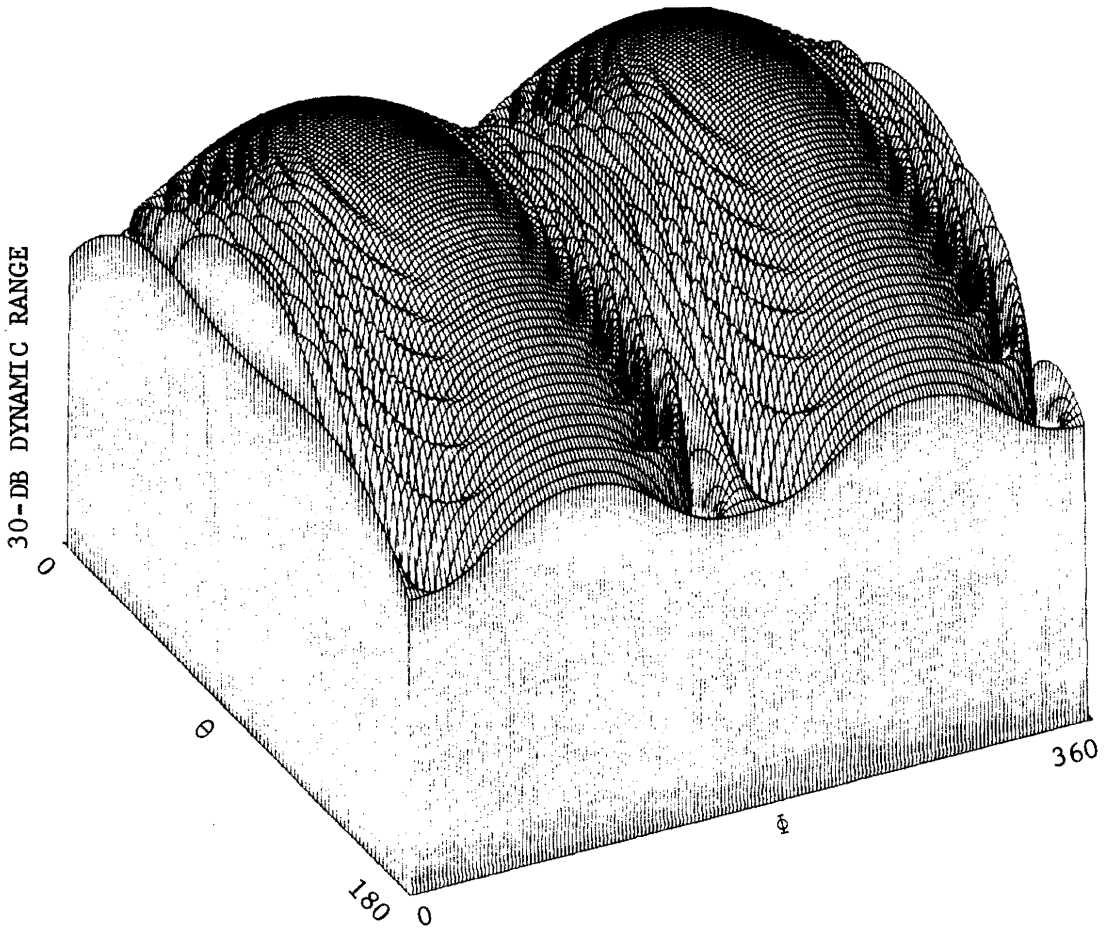

Figure 5. Calculated radiation pattern from a 2 element array located on the SERT-C satellite. The elements have a 10 dB taper 90° away from boresight. The elements have θ - Φ pointing directions of (90, 90) and (90, 270). Solar panel blockage was not included.

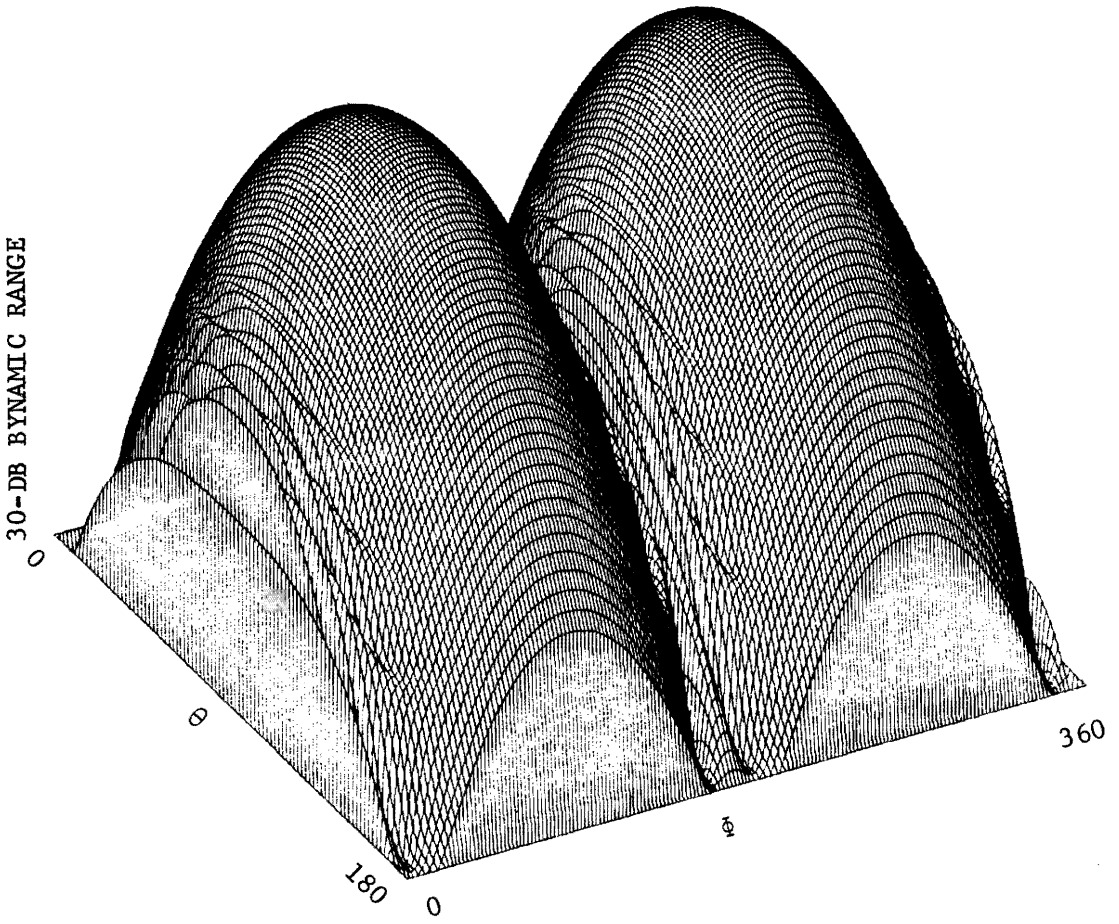

Figure 6. Calculated radiation pattern from a 2 element array located on the SERT-C satellite. The elements have a 20 dB taper 90^{o} away from boresight. The elements have θ - Φ pointing directions of (90, 90) and (90, 270). Solar panel blockage was not included.

were equally spaced in Φ (i.e., $\Phi = 45^{o}$, 135^{o}, 225^{o}, 315^{o}), and various combinations of θ-pointing directions such as (45^{o}, 45^{o}, 45^{o}, 45^{o}), (90^{o}, 90^{o}, 90^{o}, 90^{o}), (90^{o}, 45^{o}, 90^{o}, 45^{o}), (120^{o}, 45^{o}, 120^{o}, 45^{o}), etc., were investigated. The calculated results for such a four-element array having 10-dB horizon tapers is shown in Figure 7 (no solar panel blockage). The entire 4π spherical region is one of strong interaction with little or no plateau area present. The effect of increasing the horizon taper to 20 dB (shown in Figure 8) is to reduce the element interaction and to produce a corresponding low power region between the element pointing directions.

The effect of considering the solar panels (blockage) may be accounted for by neglecting any signal which would pass into the shadow region of Figure 6. This is a worst case assumption since some of the field will diffract into this region from the panel edges. The effect of this blockage on the calculated pattern of Figure 5 may be observed in Figure 9, where the field in the subject region has been constrained to be zero. The percent coverage functions for the blocked and unblocked configurations may be compared in Figure 10. These coverage functions are obtained by normalizing the peak value of the calculated field to 0 dB, grouping the spherical areas which have power levels within a given range (e.g., -20 dB $\pm$ 0.5 dB), adding a calculated directivity to each level of the coverage function and subtracting any known losses. The ideal directivity is the ratio of the maximum radiation intensity (P_m) to the average radiation intensity (P_a).

$$D = \frac{P_m(\theta,\Phi)}{P_a} \quad . \tag{4}$$

The average intensity is simply the total power radiated (P_t) divided by the area of the particular spherical surface being investigated.

$$P_a = \frac{P_t}{4\pi R^2} \quad . \tag{5}$$

P_t is then the total power contained in the calculated pattern $P(\Phi,\theta)$ and is given by

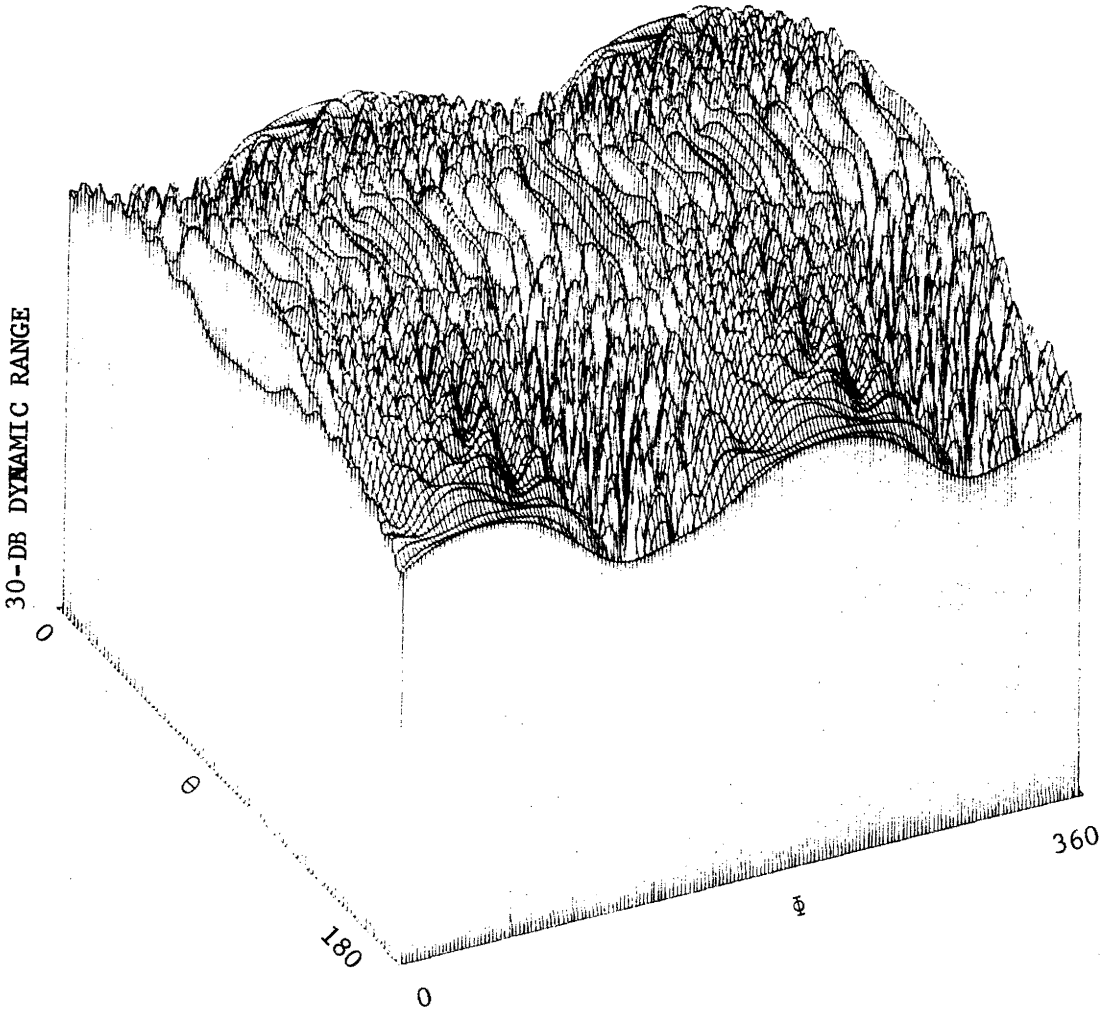

Figure 7. Calculated radiation pattern from a 4 element array located on the SERT-C satellite. The elements have a 10 dB taper 90° away from boresight. The elements have θ - Φ pointing directions of (120, 45), (45, 135), (120, 225), and (45, 315). Solar panel blockage was not included.

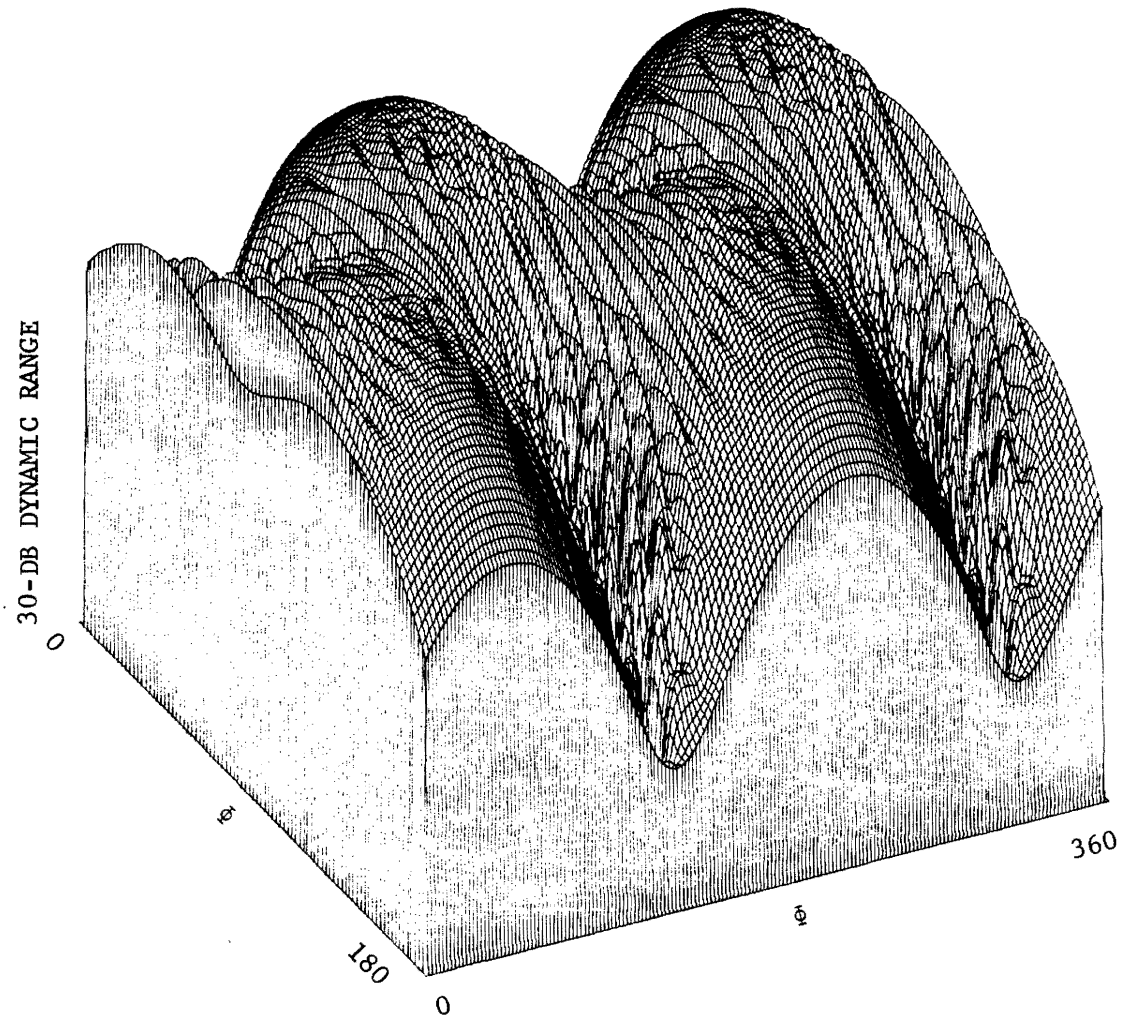

Figure 8. Calculated radiation pattern from a 4 element array located on the SERT-C satellite. The elements have a 20 dB taper 90^{o} away from boresight. The elements have θ - Φ pointing directions of (120, 45), (45, 135), (120, 225), and (45, 315). Solar panel blockage was not included.

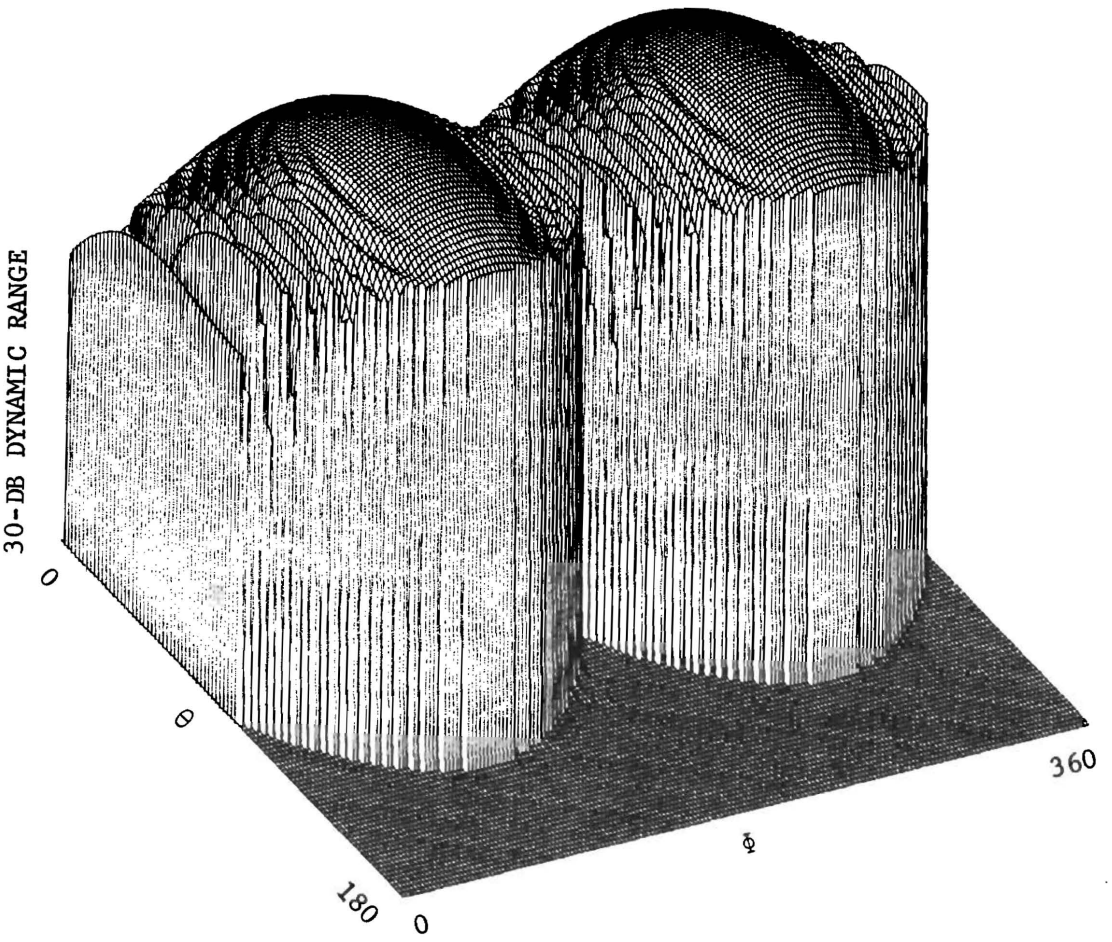

Figure 9. Calculated radiation pattern from a 2 element array located on the SERT-C satellite. The elements have a 10 dB taper 90^{o} away from boresight. The elements have θ - Φ pointing directions of (90, 90) and (90, 270). Solar panel blockage was included.

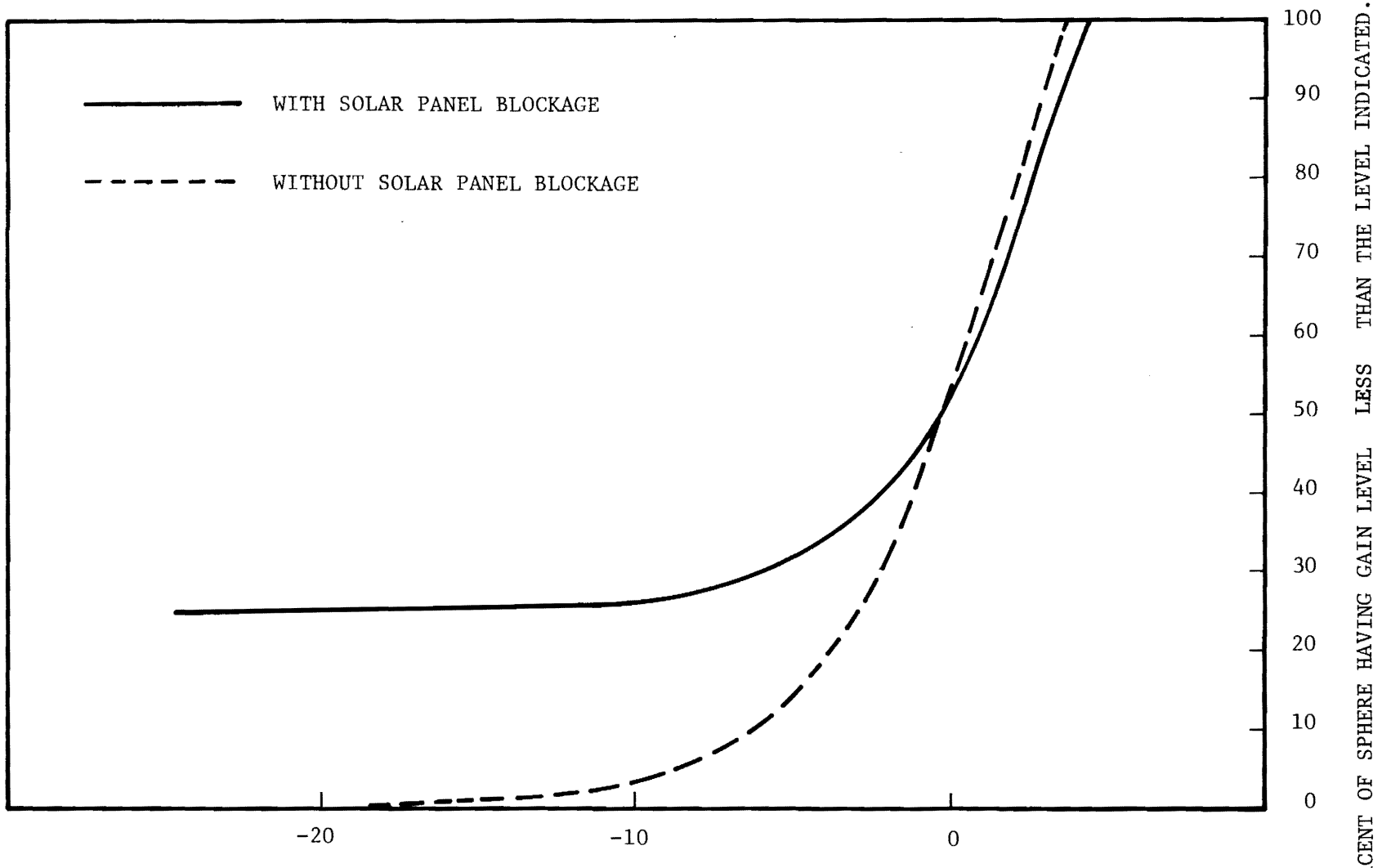

Figure 10. Power distribution function for two elements located on the SERT-C satellite and having 10-dB horizon tapers and $\theta - \phi$ pointing directions of (90,90) and (90,270).

$$P_t = \int_0^{\pi} \int_0^{2\pi} P(\theta,\phi)\ R^2 \sin\theta\ d\theta\ d\phi\ . \tag{6}$$

The directivity expression of Equation (4) then reduces to

$$D = \frac{4\ P_m(\theta,\phi)}{\int_0^{\pi} \int_0^{2\pi} P(\theta,\phi)\ \sin\theta\ d\theta\ d\phi}\ . \tag{7}$$

For the present situation where $P(\theta,\phi)$ is known as a discrete set of calculated points, and $d\theta$ and $d\phi$ are non-zero constants, Equation (7) becomes

$$D = \frac{4\pi\ P_m(\theta,\phi)}{\Delta\theta\ \Delta\phi \sum_i \sin\theta_i \left[\sum_j P(\theta_i,\phi_j)\right]}\ . \tag{8}$$

A summary of certain key coverage levels for several of the arrays investigated is given in Tables I (no blockage considered) and II (blockage). The three-dimensional power patterns and coverage functions corresponding to these cases are included in Appendix II.

It is apparent from these two tables that most of the candidates appear acceptable when looking strictly at the coverage numbers. Other factors warrant consideration however, when selecting the optimum antenna configuration. For example, four-element arrays have an inherent 6-dB power splitter loss while two-element arrays suffer only a 3-dB loss (neither loss is reflected in Tables I and II). Also, the four element arrays produced radiation patterns which fluctuated significantly (e.g., see Figure 7) throughout the entire range of θ and Φ. Additionally, it is known from the antenna element survey that the candidates which are commensurate with 5-10 dB horizon tapers (e.g., quadrifilar helix) are too narrowband to cover both of the frequencies of interest, while the spiral with a 10-20 dB horizon taper can handle both frequencies efficiently. The conclusions thus drawn from this theoretical modeling section are that two elements are probably more desirable than four elements, and that the broadband spiral can provide coverage levels almost as high as the narrowband quadrifilar. Both

Table I

CALCULATED PERCENT COVERAGE LEVELS (USING SCALAR METHOD) FOR DIFFERENT NUMBERS OF ELEMENTS PLACED ON THE SERT-C SATELLITE. SOLAR PANEL BLOCKAGE WAS NOT INCLUDED.

Number of Elements	90° Edge Taper	θ (°)	φ (°)	Peak Directivity	50% Level	35% Level	20% Level	10% Level	5% Level
1	10 dB	90	90	6.65	-5.3	-13.8	--	--	--
1	20 dB	90	90	8.99	-15.0	--	--	--	--
2	10 dB	90	90	3.64	-0.4	-1.9	-4.1	-6.3	-8.9
		90	270						
2	20 dB	90	90	5.98	-2.7	-6.0	-9.8	-14.2	-16.0
		90	270						
2	10 dB	45	90	4.81					
		45	270						
2	10 dB	0	90	8.59					
		0	270						
4	10 dB	90	45	4.85	-0.7	-2.8	-5.5	-8.7	-11.5
		90	135						
		90	225						
		90	315						
4	10 dB	45	45	6.02	-1.9	-4.2	-8.8	-13.2	-16.3
		45	135						
		45	225						
		45	315						
4	20 dB (Spirals)	45	45	5.92	-2.4	-6.7	-13.7	-21.6	-35.0
		45	135						
		45	225						
		45	315						
4	10 dB	90	45	4.89	-0.8	-2.8	-5.4	-8.4	-11.2
		45	135						
		90	225						
		45	315						
4	20 dB	90	45	4.58	-0.6	-3.2	-7.0	-11.3	-15.3
		45	135						
		90	225						
		45	315						
4	10 dB	90	45	4.89	-0.5	-1.9	-4.3	-7.2	-10.0
		45	135						
		120	225						
		45	315						
4	20 dB	120	45	4.33	-0.6	-2.7	-5.8	-9.5	-12.8
		45	135						
		120	225						
		45	315						
1	5 dB	90	90						
2	5 dB	90	90						
		90	270						
4	5 dB	90	45	5.32	-0.9	-3.0	-6.4	-10.4	-14.4
		90	135						
		90	225						
		90	315						
4	5 dB	45	45	6.20	-1.5	-3.8	-7.5	-11.6	-15.5
		45	135						
		45	225						
		45	315						
4	5 dB	90	45	5.47	-1.1	-3.2	-6.1	-9.6	-12.6
		45	135						
		90	225						
		45	315						
4	5 dB	120	45	5.18	-0.8	-2.7	-5.4	-8.5	-11.7
		45	135						
		120	225						
		45	315						

Table II

CALCULATED PERCENT COVERAGE LEVELS (USING SCALAR METHOD) FOR DIFFERENT NUMBERS OF ELEMENTS PLACED ON THE SERT-C SATELLITE. SOLAR PANEL BLOCKAGE WAS INCLUDED.

Number of Elements	90° Edge Taper	θ (°)	ϕ (°)	Peak Directivity	50% Level	35% Level	20% Level	10% Level	5% Level
1	5 dB	90	90						
1	10 dB	90	90						
1	20 dB	90	90						
2	5 dB	90	90						
		90	270						
2	10 dB	90	90	4.25	-0.4	-3.7	--	--	--
		90	270						
2	20 dB	90	90	6.29	-3.8	-9.8	--	--	--
		90	270						
2	5 dB	45	90						
		45	270						
2	10 dB	45	90						
		45	270						
2	20 dB	45	90						
		45	270						
4	5 dB	90	45	6.37	-1.9	-7.4	--	--	--
		90	135						
		90	225						
		90	315						
4	10 dB	90	45	5.76	-1.6	-5.7	--	--	--
		90	135						
		90	225						
		90	315						
4	20 dB	90	45	5.18	-1.1	-5.7	--	--	--
		90	135						
		90	225						
		90	315						
4	5 dB	45	45	6.70	-2.2	-7.5	--	--	--
		45	135						
		45	225						
		45	315						
4	10 dB	45	45	6.25	-2.0	-6.0	--	--	--
		45	135						
		45	225						
		45	315						
4	20 dB	45	45	5.97	-2.3	-7.5	--	--	--
		45	135						
		45	225						
		45	315						
4	5 dB	90	45	6.26	-1.9	-6.7	--	--	--
		45	135						
		90	225						
		45	315						
4	10 dB	90	45	5.49	-1.0	-5.0	--	--	--
		45	135						
		90	225						
		45	315						
4	20 dB	90	45	4.98	-0.9	-5.0	--	--	--
		45	135						
		90	225						
		45	315						
4	5 dB	120	45	6.21	-1.8	-6.2	--	--	--
		45	135						
		120	225						
		45	315						
4	10 dB	120	45	5.22	-0.6	-4.6	--	--	--
		45	135						
		120	225						
		45	315						
4	20 dB	120	45	5.33	-1.2	-5.7	--	--	--
		45	135						
		120	225						
		45	315						

of these two candidates were investigated on the antenna range by recording radiation distribution plots and making a decision based on those results.

D. Scale Model Measurements

Two sets of scale model measurements were made. The first set consisted of measurements of the principal plane patterns only of the three recommended antenna types: crossed-dipole, quadrifilar helix, and spiral. The second set of scale model measurements included the quadrifilar helix and the cavity-backed spiral as antenna elements and consisted of complete conical pattern measurements.

1. Preliminary Scale Model Measurements

Dimensions of the scale model of the SERT-C spacecraft utilized in the antenna radiation pattern measurements are presented in Figure 11. The model was scaled by a factor of 4.1:1 in frequency or 1:4.1 in size. The appropriate drawings received from NASA LeRC were used in determining the dimensions of the scale model.

The preliminary scale model pattern measurements were performed for two reasons: (1) to determine if, in fact, these three antenna elements had principal plane radiation patterns similar to the radiation patterns used in the theoretical model, and (2) to determine which of the three element types should be further evaluated. As a result of these tests it was confirmed that these antenna elements did possess similar radiation pattern characteristics as we had anticipated, and only one of the three element types was eliminated as a further candidate, this being the crossed-dipole element. The circular polarization property of the crossed-dipole element deteriorates to linear polarization on the horizon, whereas the quadrifilar helix and the spiral elements maintain good circularity.

As previously stated, the three antenna types for the preliminary scale model measurement program were the crossed-dipoles, quadrifilar helix, and the cavity-backed spiral. The principal plane radiation patterns of five configurations of each antenna type were measured:

(1) one element mounted on one side of the spacecraft and perpendicular to the skin,

(2) two elements mounted on opposite sides and perpendicular to the spacecraft skin,

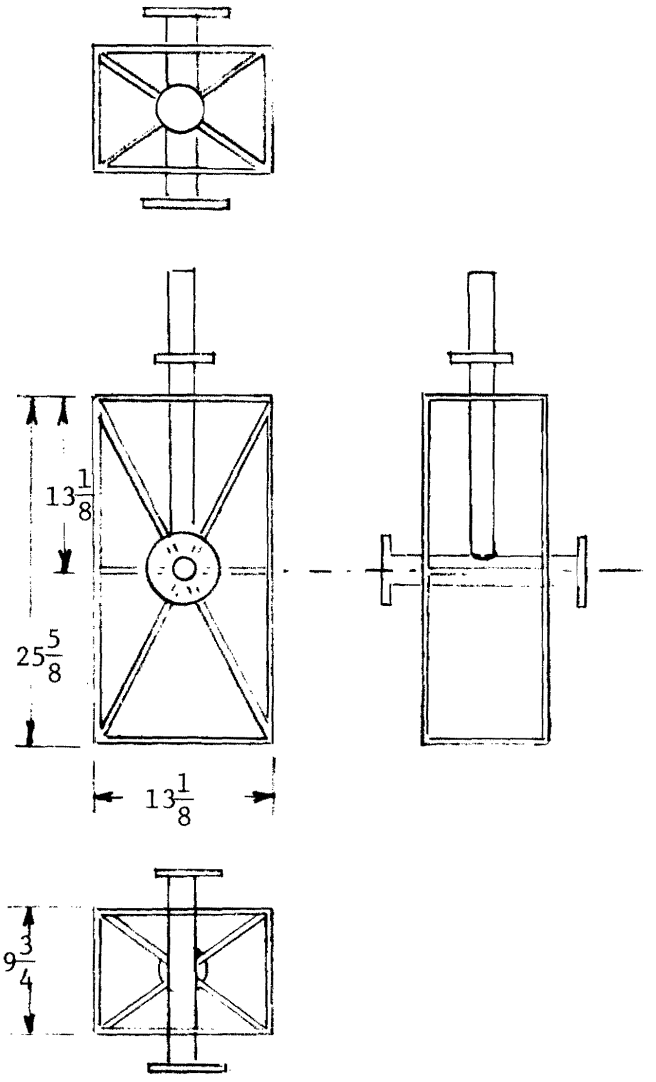

Figure 11. Scale Model Frame Dimensions in Inches.

(3) four elements mounted perpendicular to the spacecraft skin and positioned at approximately the azimuth angles of 45°, 135°, 225° and 315°,

(4) four elements mounted at 45° with respect to the spacecraft skin, positioned as in (3), and facing toward the solar arrays (the solar arrays were not mounted during this preliminary test phase), and

(5) four antenna elements mounted in pairs on opposite sides of the spacecraft near the center and positioned at 45° with respect to the skin.

Principal plane radiation patterns at four different polarizations (vertical, horizontal, LHC and RHC) were measured. These patterns indicated that the four quadrifilar elements mounted at 45° with respect to the spacecraft skin as in (4) above and the two quadrifilars mounted as in (2) above give the best principal plane coverage. In addition, the two cavity-backed spirals mounted as in (2) above gave adequate coverage. The quadrifilar element and the cavity-backed spiral gave consistently better pattern coverage than did the crossed-dipoles. Based on these data, it was decided to continue measurements on the scale model using the quadrifilar element and the cavity-backed spiral. It was noted during these measurements that nulls for RHCP tended to be filled in when the polarization was changed to LHCP. Also, the nulls in LHCP patterns are located in different spatial positions than those of RHCP. Photographs of the elements are shown in Figure 12.

2. Radiation Distribution Pattern Measurements on 1:4.1 Scale Model SERT-C Spacecraft

The antenna range at Lockheed-Georgia was utilized for further pattern measurements. This range was equipped with the necessary equipment for obtaining radiation pattern contour plots as the polar radiation patterns were being plotted. The scale frequency was 9.2 GHz. The patterns were measured utilizing first RHC polarization and then LHC polarization. The circularity of the illuminating horn is presented in Figures 13 and 14. Pattern measurements were performed on the scale model both with and without the solar panels attached. Tabulated in Table III are the different configurations of antennas and the patterns that were measured.

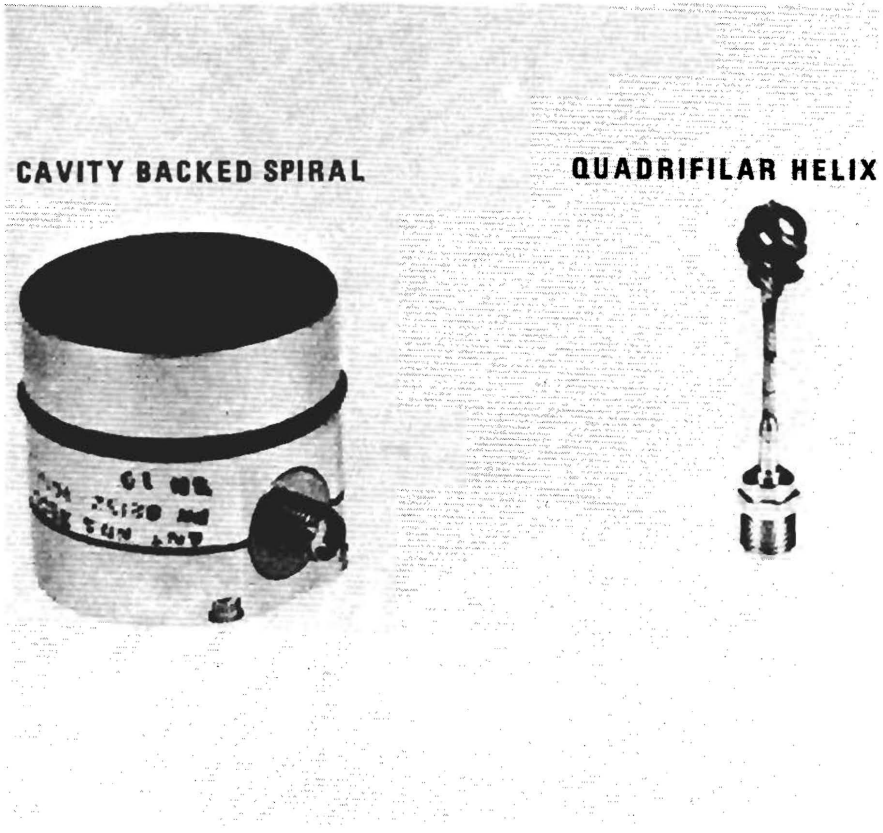

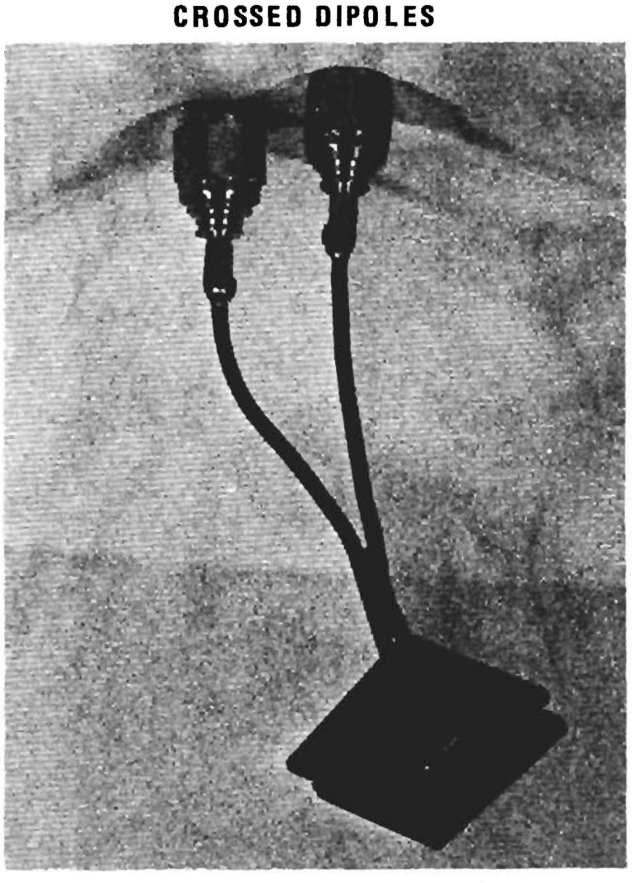

Figure 12. Photographs of the Three Antenna Elements (Scaled).

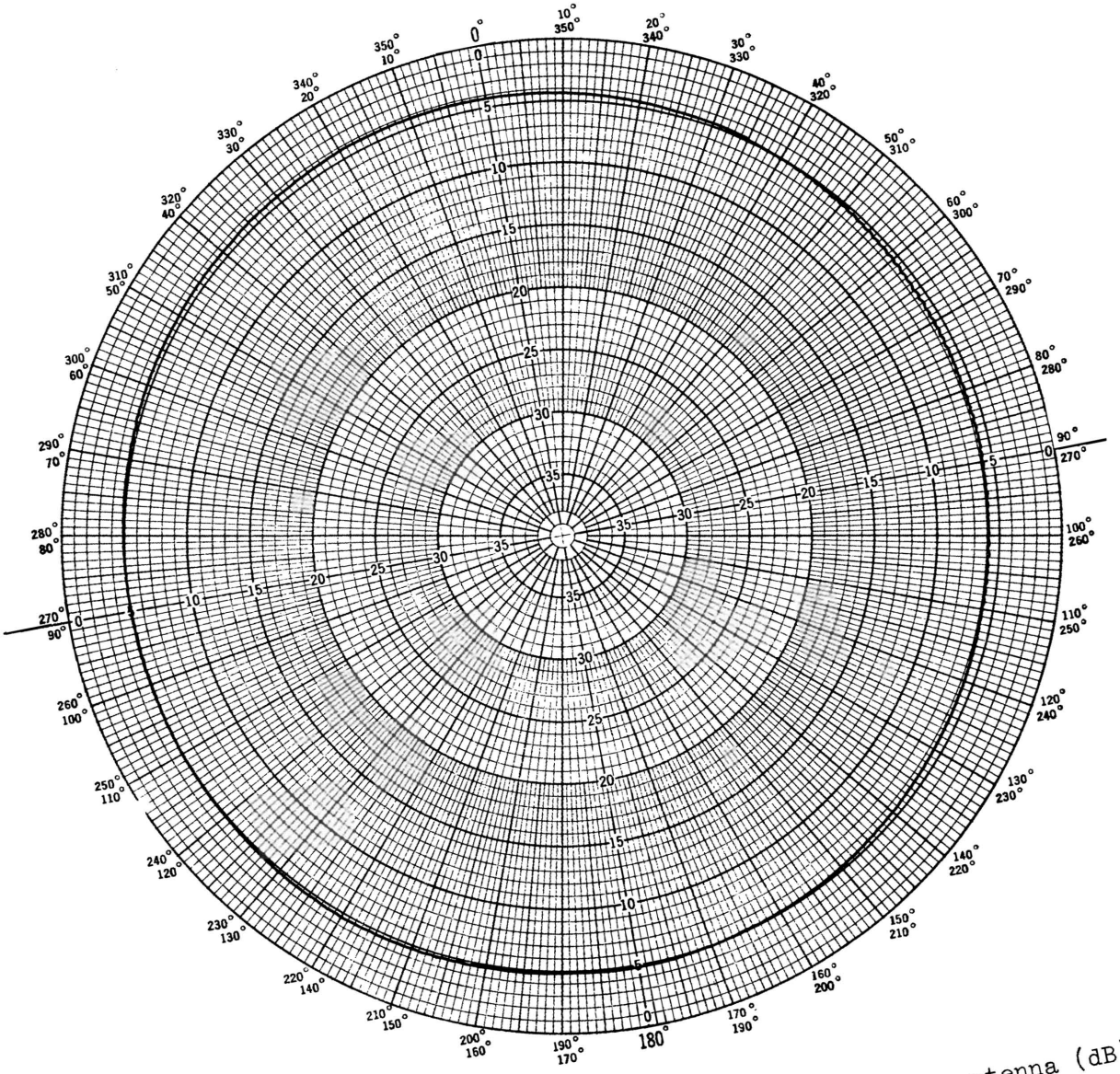

Figure 13. Circularity plot of RHCP illuminating antenna (dB).

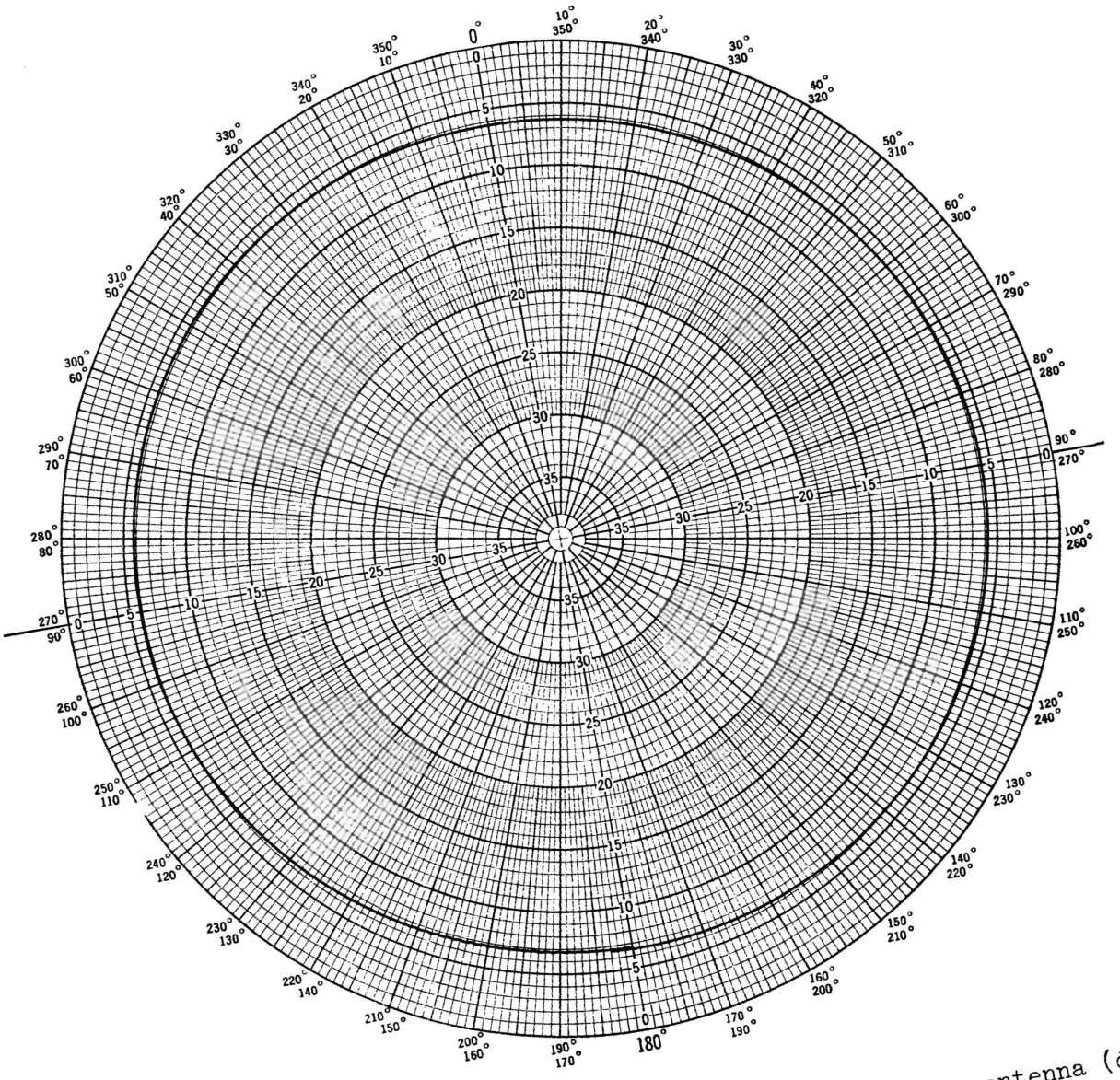

Figure 14. Circularity plot of LHCP illuminating antenna (dB).

Table III

SCALE MODEL ANTENNA PATTERN MEASUREMENTS

Element Type and Number	Location	Type Patterns and Polarization	Solar Panels
2 Spirals	Opposite Sides of Spacecraft	Polar Plots, RHC, LHC Contour Plots, RHC	None
Same	Same	Same	0°
Same	Same	Same	45°
Same	Same	Principal Plane RHC	90°
2 Quadrifilars	Opposite Sides of Spacecraft	Polar Plots, RHC, LHC Contour Plots, RHC	None 0° and 45°
Same	Same	Same	
Same	Same	Principal Plane RHC	90°
4 Spirals	45° with respect to spacecraft; approx. 90° separation in azimuth between antenna elements	Polar Plots, RHC	None
4 Quadrifilars	Same	Contour Plots, RHC	None
4 Quadrifilars	45° with respect to spacecraft; closely spaced pairs placed on opposite sides of spacecraft	Polar Plots Contour Plots, RHC	None

After analyzing all the contour plots of data without solar panels it was decided that the two-element arrays, either cavity-backed spirals or quadrifilars, gave sufficient radiation pattern coverage. The four-element arrays produced scalloped radiation patterns due to the interference between antenna elements. The final choice of antenna type was the cavity-backed spiral based on bandwidth and pattern coverage requirements.

The radiation contour plots that were made at the Lockheed-Georgia outdoor test range are shown in Figure 15 through Figure 22. The results of the two-spiral array are plotted in Figure 23 for the case of no panels. Compare this with Figures 24 and 25 for the two-spiral array with solar panels at 0^{o} and 45^{o}, respectively. The contours of the "no solar panel" case are much smoother than the contour plots with solar panels. This is also observed in the polar plots found in Appendix III. The solar panels cause a scalloping effect of the radiation pattern, but the overall coverage level is not decreased much by the solar panels.

The data from Figures 23, 24, and 25 were fed into a computer program to determine actual percentage coverage for the three cases of the two-spiral arrays with no solar panels, with solar panels at 0^{o}, and with solar panels at 45^{o}. The calculated probability based on measured data that the gain level is above -10 dBi for the worst case with solar panels was about 50 percent. This compares with 68 percent with no solar panels. Thus, the solar panels cause diffraction effects but do not necessarily block out large sectors of the antenna radiation pattern. This 50 percent actual coverage agrees well with the predicted coverage level. It should be pointed out that this actual coverage increases substantially if the ground station antenna polarization can be changed.

The four-element array radiation contour plots of Figures 15 through 17 are included to show that the deep nulls are more numerous than for the two-element array. The computer percentage coverage levels for the four-element arrays based only on the theoretical analysis indicated better coverage than was actually obtained by the model measurements. From Table I it is indicated that a four-element array of spirals would provide a 65 percent probability of coverage above -10 dBi. As indicated in Figures 15, 16 and 17 the area of -10 dBi coverage is small.

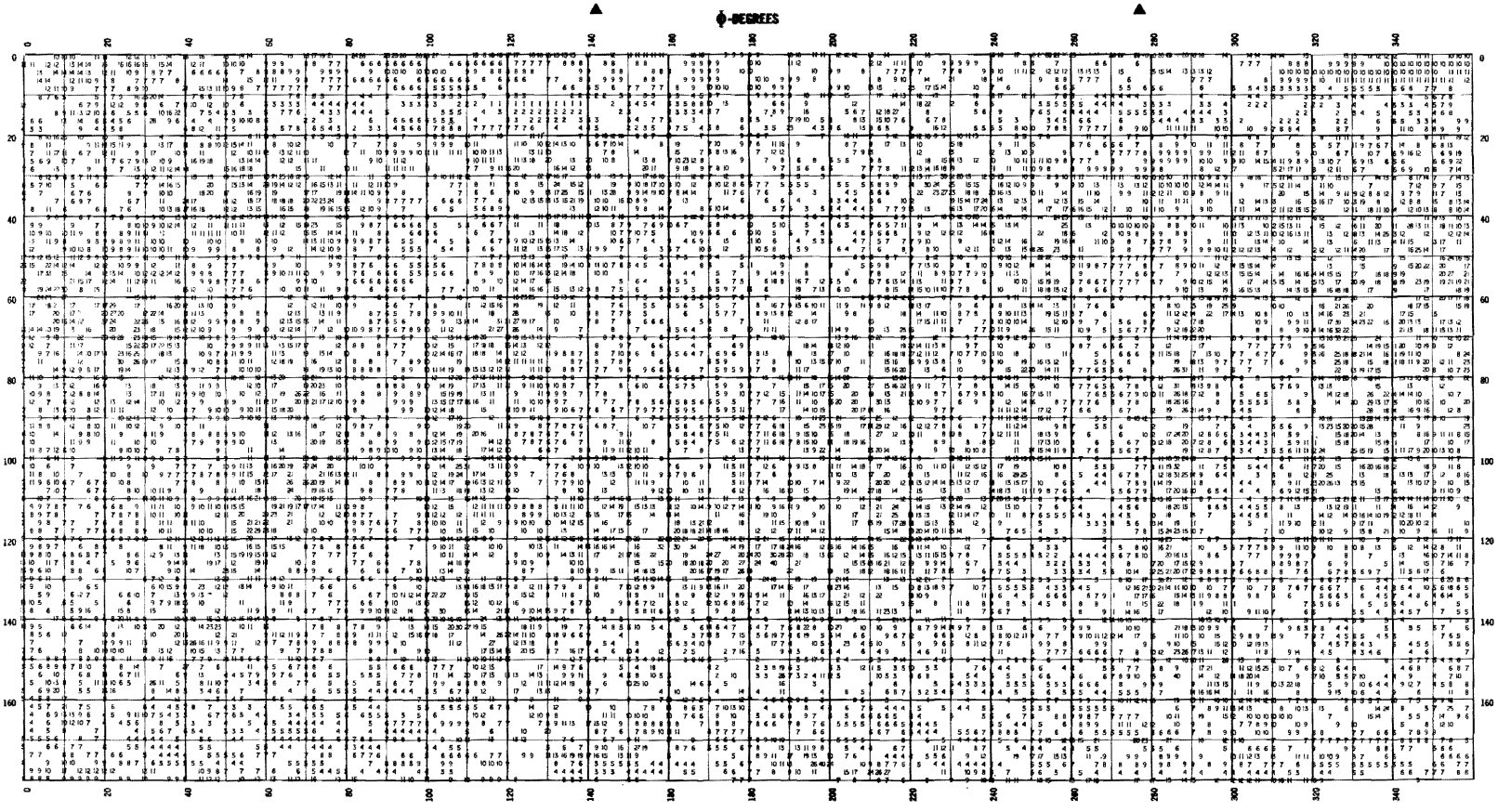

Figure 15. RDP plot - 4 quads - inboard ports - bent 45°. (Level marked 2 is -3 dBi gain).

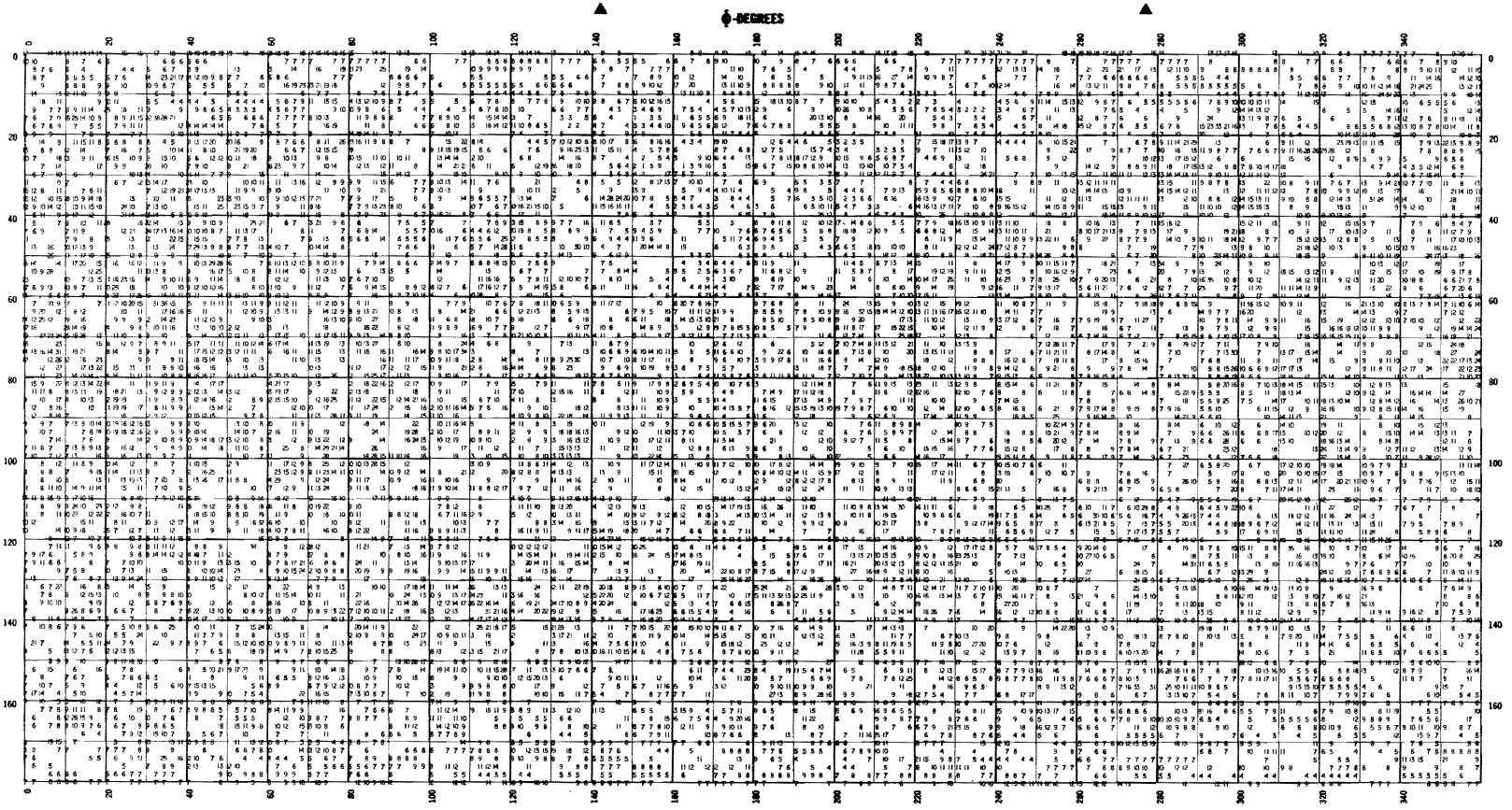

Figure 16. RDP plot - 4 quads - outboard ports - bent 45°. (Level marked 2 is -3 dBi gain).

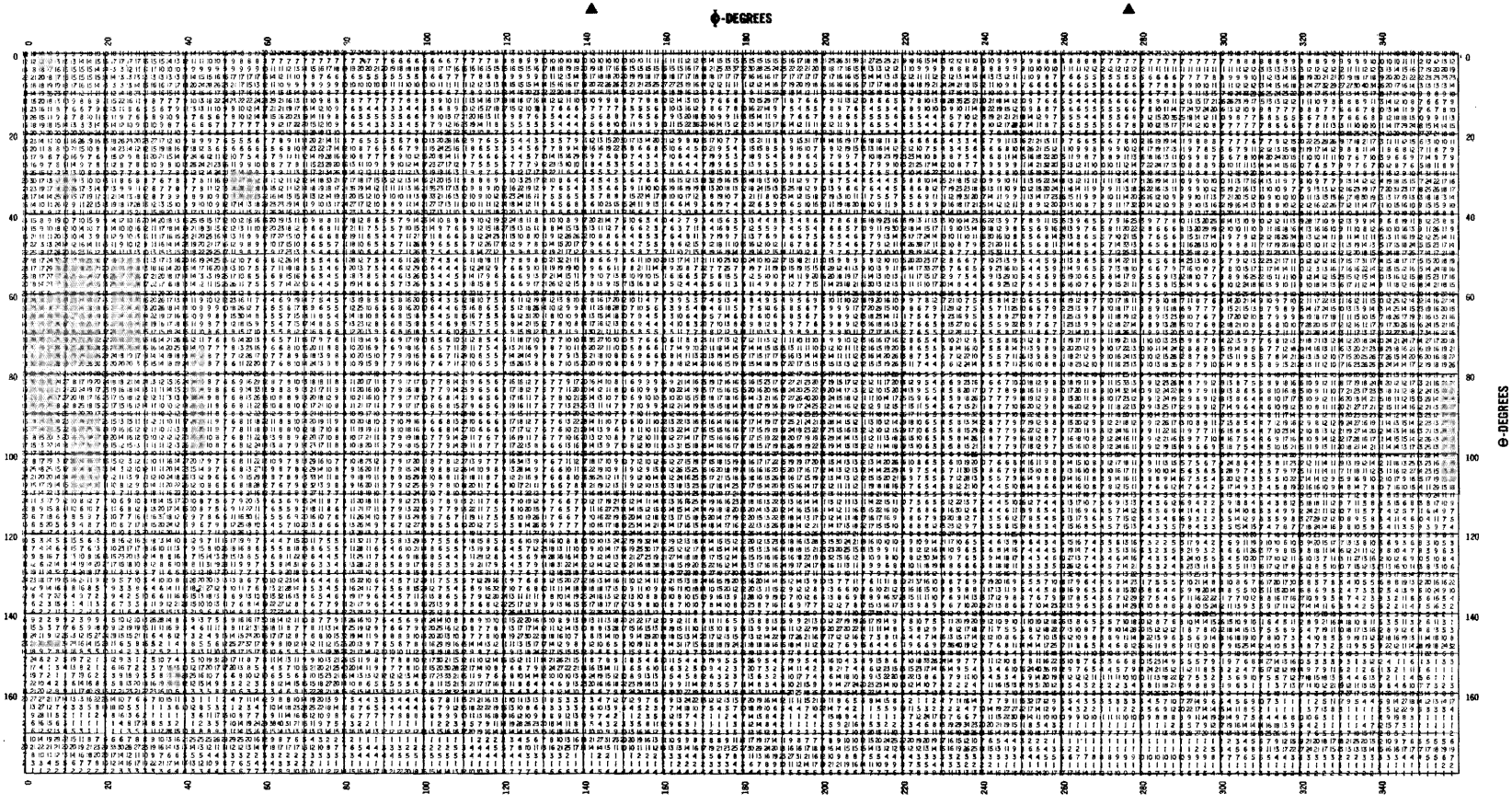

Figure 17. RDP plot - 4 quads - outboard port - normal to skin.
(Level marked 1 is -3 dBi gain).

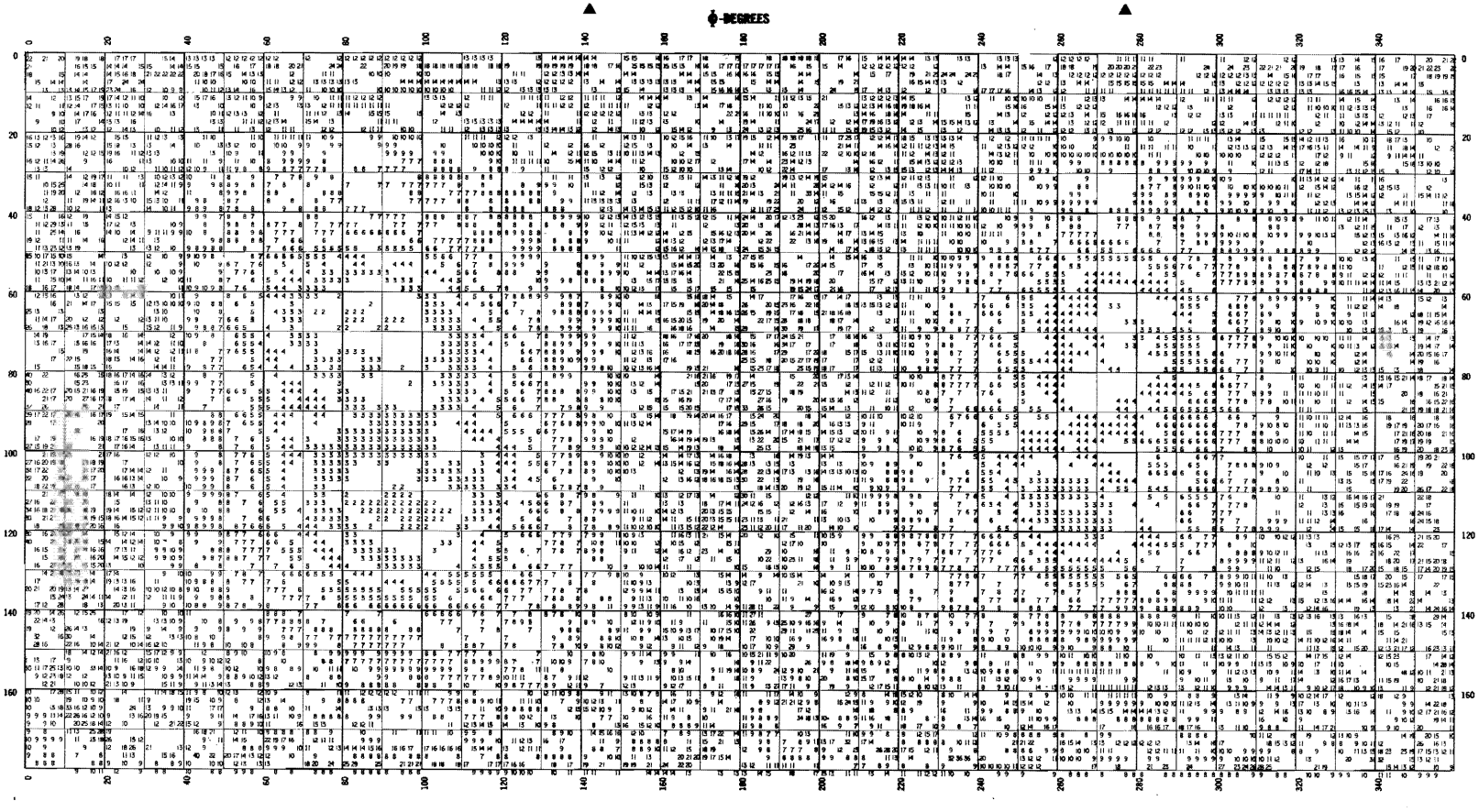

Figure 18. RDP plot - 2 spirals - center ports - normal to skin - no solar panels. (Level marked 2 is 0 dBi gain)

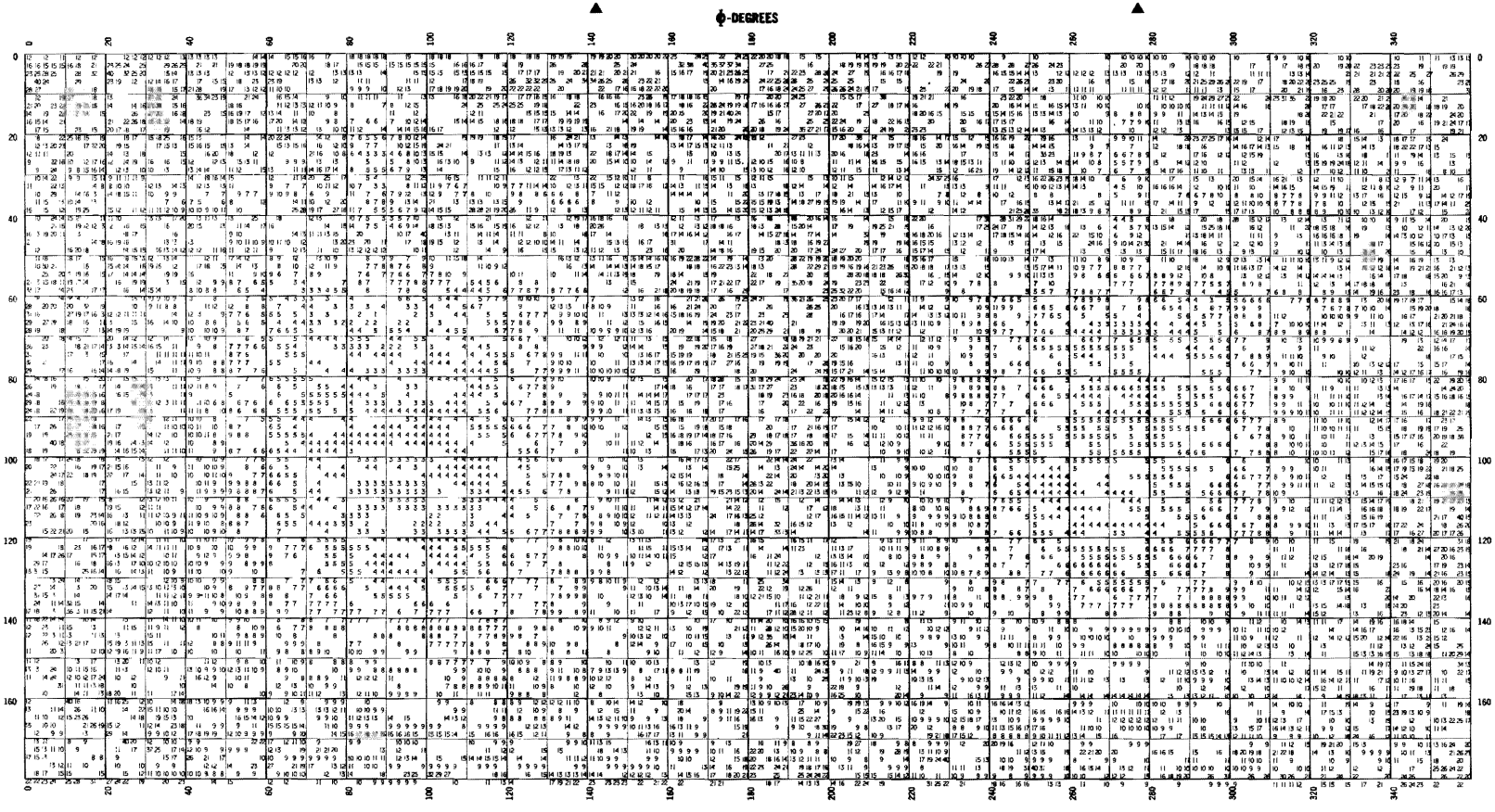

Figure 19. RDP plot - 2 spirals - center ports, solar panels 0°.
(Level marked 1 is 0 dBi gain)

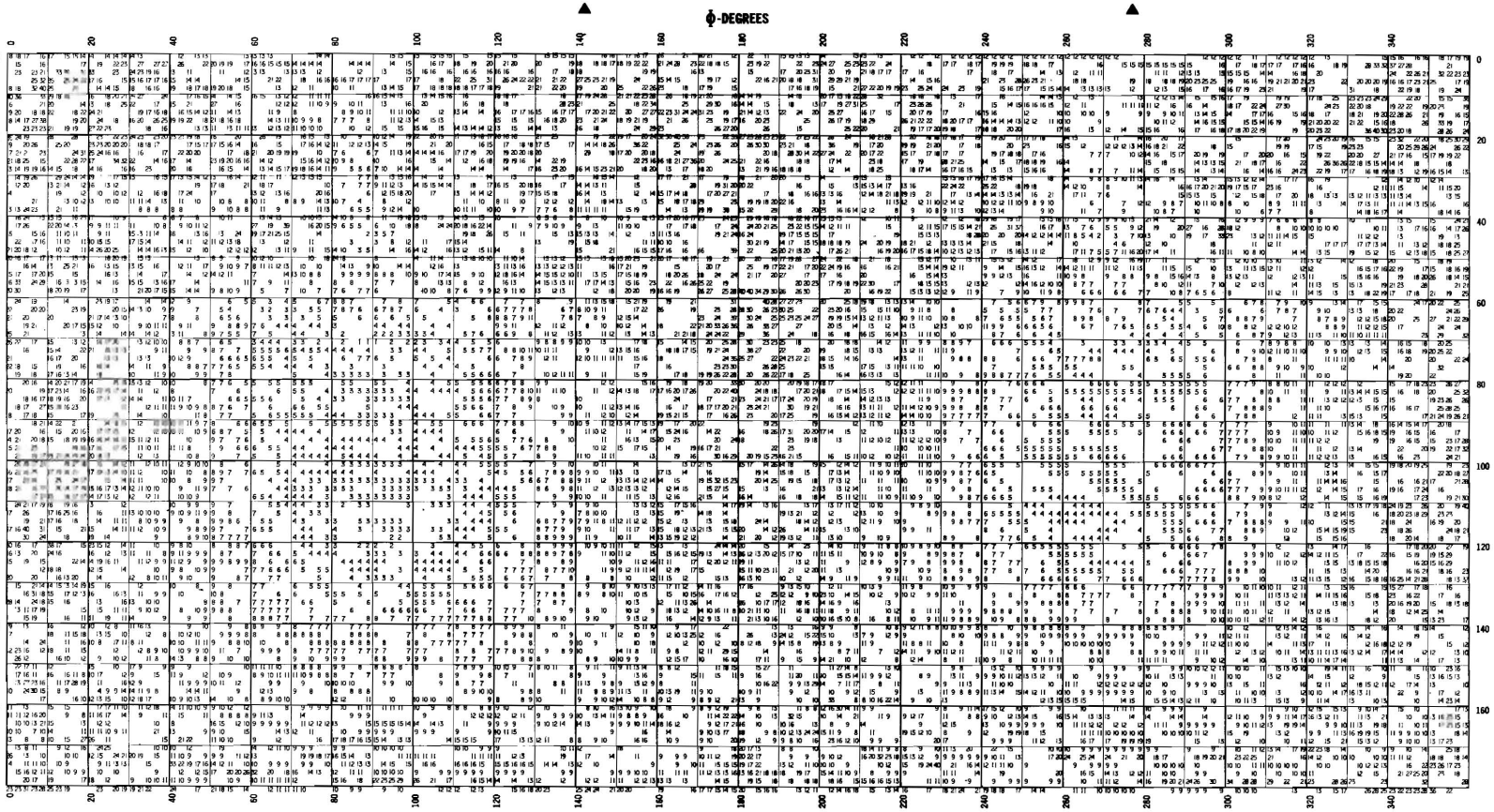

Figure 20. RDP plot - 2 spirals - center ports - solar panels 45°.
(Level marked 1 is 0 dBi gain)

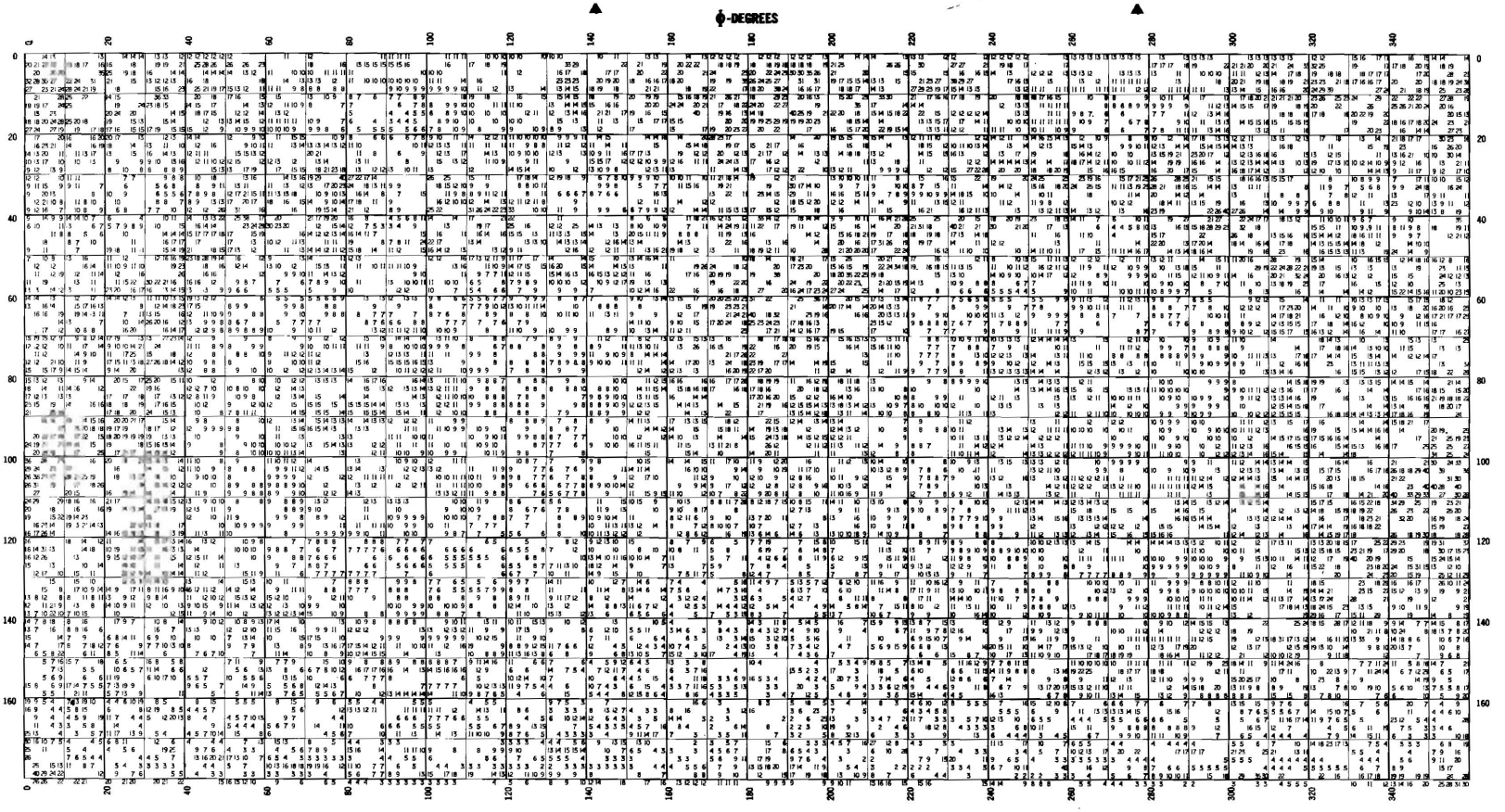

Figure 21. RDP plot - 2 quads - center ports - solar panels at 0°.
(Levels marked 2 are + 2 dBi gain)

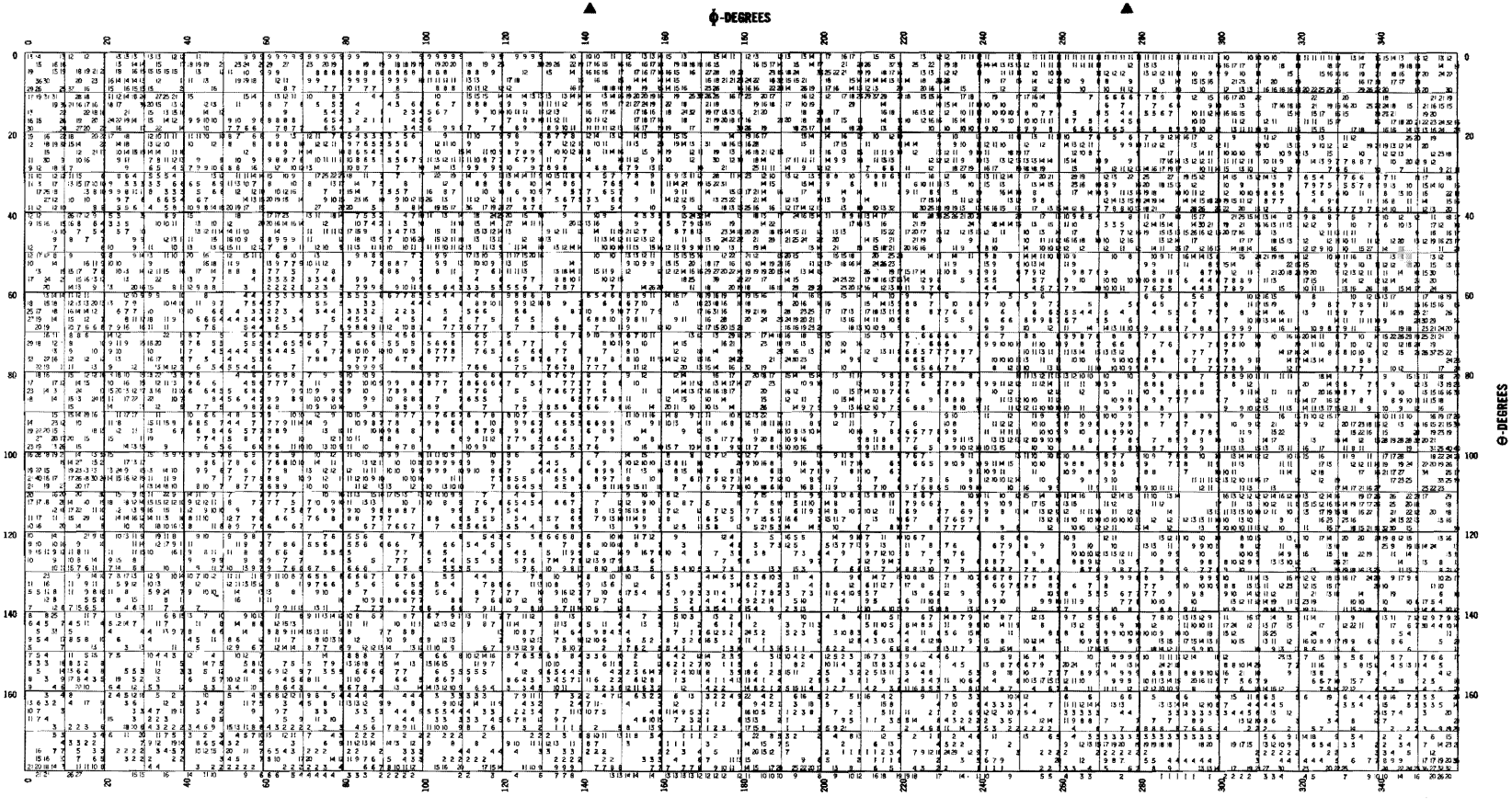

Figure 22. RDP plot - 2 quads - center ports - solar panels at 45°.
(Levels marked 1 are + 2 dBi gain)

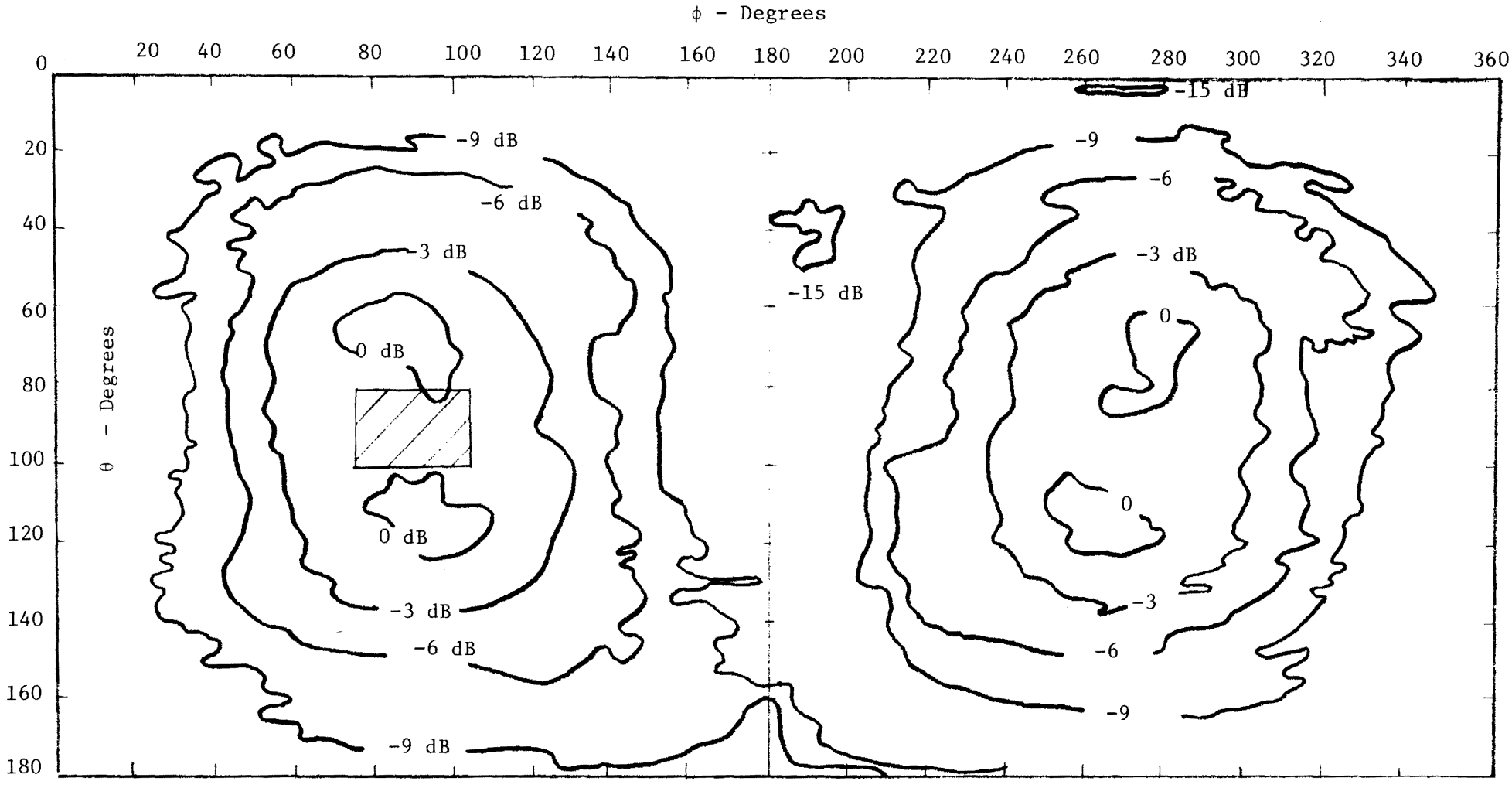

Figure 23. Partial RDP Contour Plot - 2 Spirals - No Solar Panels. (Crosshatched area is beamed toward earth in orbit raising phase.)

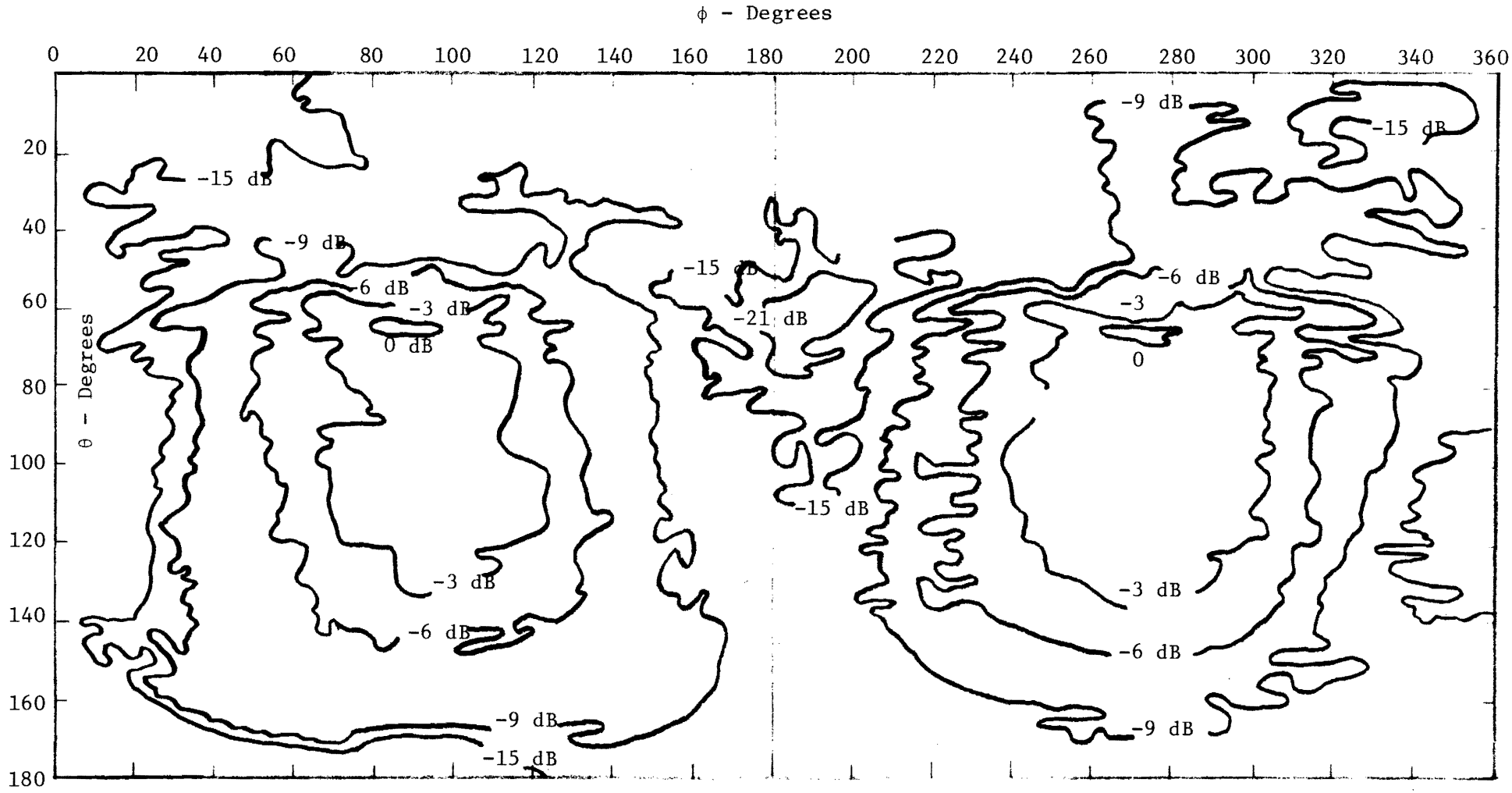

Figure 24. Partial RDP Contour Plot - 2 Spirals - Solar Panels at 0°.

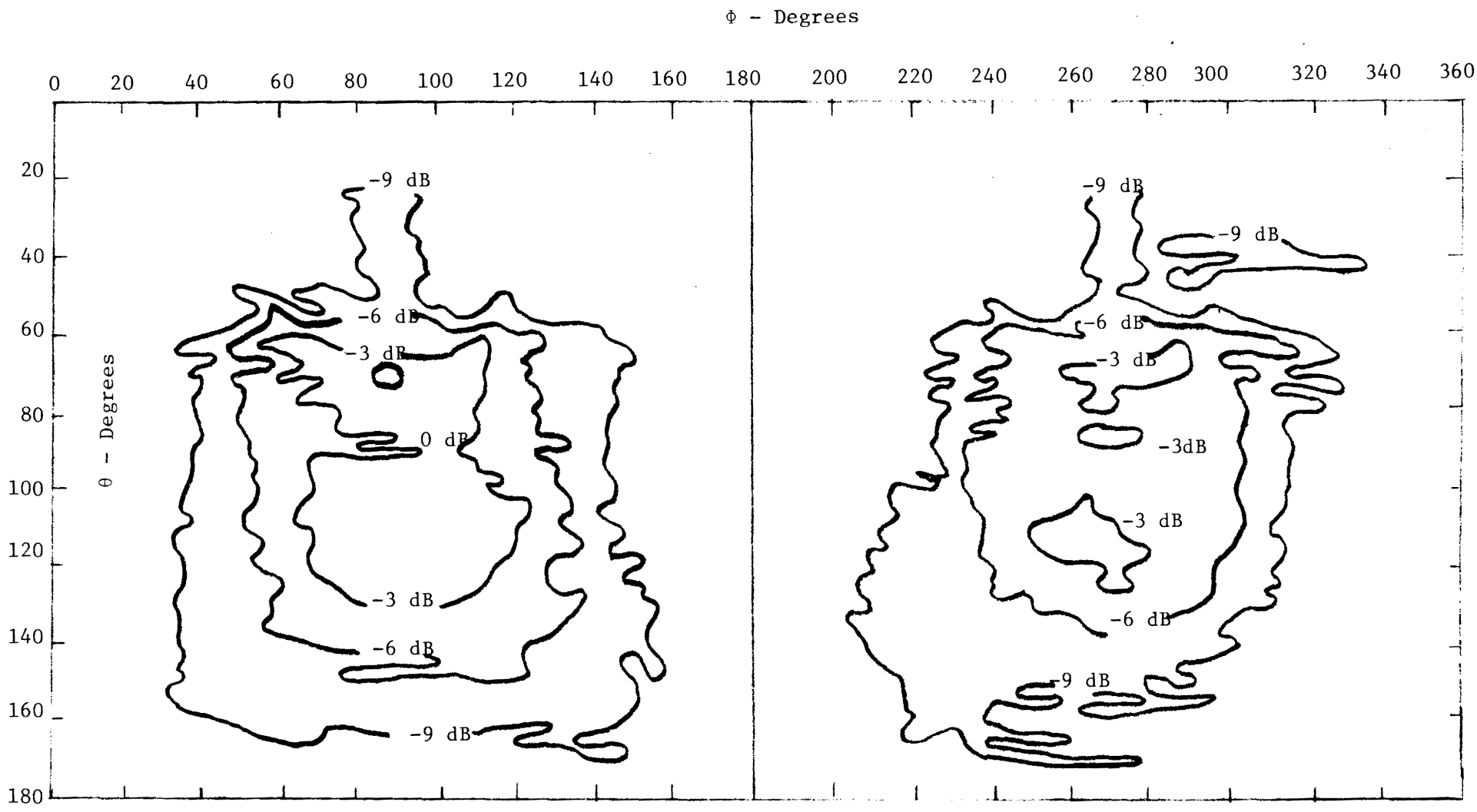

Figure 25. Partial RDP Contour Plot - 2 Spirals - Solar Panels at 45°.

At this point it should be noted that the approach taken by Georgia Tech on this program was to meet the antenna radiation pattern coverage levels with the simplest spacecraft antenna system possible. Since the computer analysis early in the program showed that either a two-element or four-element array would meet the design goals, we felt that the scale model measurements would corroborate this. There are orientations of the spacecraft where deep nulls occur and communication would probably be lost with a single ground station. But is is unlikely that communications would be totally lost if more than one ground station is involved. Also the coverage level increases significantly if the ground station antenna polarization can be changed from RHCP to LHCP or to elliptical polarization.

The remaining contour plots are included for completeness, i.e., all the conditions that were run on the pattern range have been included. The maximum gain levels that are shown on the four-element spiral array patterns correspond to an antenna system gain of -3 dBi, whereas the maximum level on the two-element spiral array contours refer to a gain of 0 dBi.

The two plots of Figures 26 and 27 were computed from the scale model measurement data. As indicated in Figure 26 the solar panels block a significant amount of the coverage of two quadrifilar helices. The two-element array of spirals was not affected as much by the solar panels as shown in Figure 27.

3. Coordinate System

In the orbit raising phase the three 30-cm ion thrusters are directed west with the high gain antenna and TV camera directed east. The face of the spacecraft directed toward the earth has the single 8-cm ion thruster. The face directed away from the earth is the side of the spacecraft where the 8-cm thruster and the radar antenna are mounted. With respect to the coordinate system (Figure 28) used in the scale model radiation pattern measurements, the spacecraft look angle toward the earth at an elevation angle of $\theta = 90^{\circ}$ and an azimuth angle of Φ near 90° (see Figure 23). The S-band antennas are mounted on the spacecraft in locations where one of the antennas has a low gain beam pointed toward the earth in the orbit raising phase. The other antenna is pointed in the direction θ,Φ of 90°, 270°.

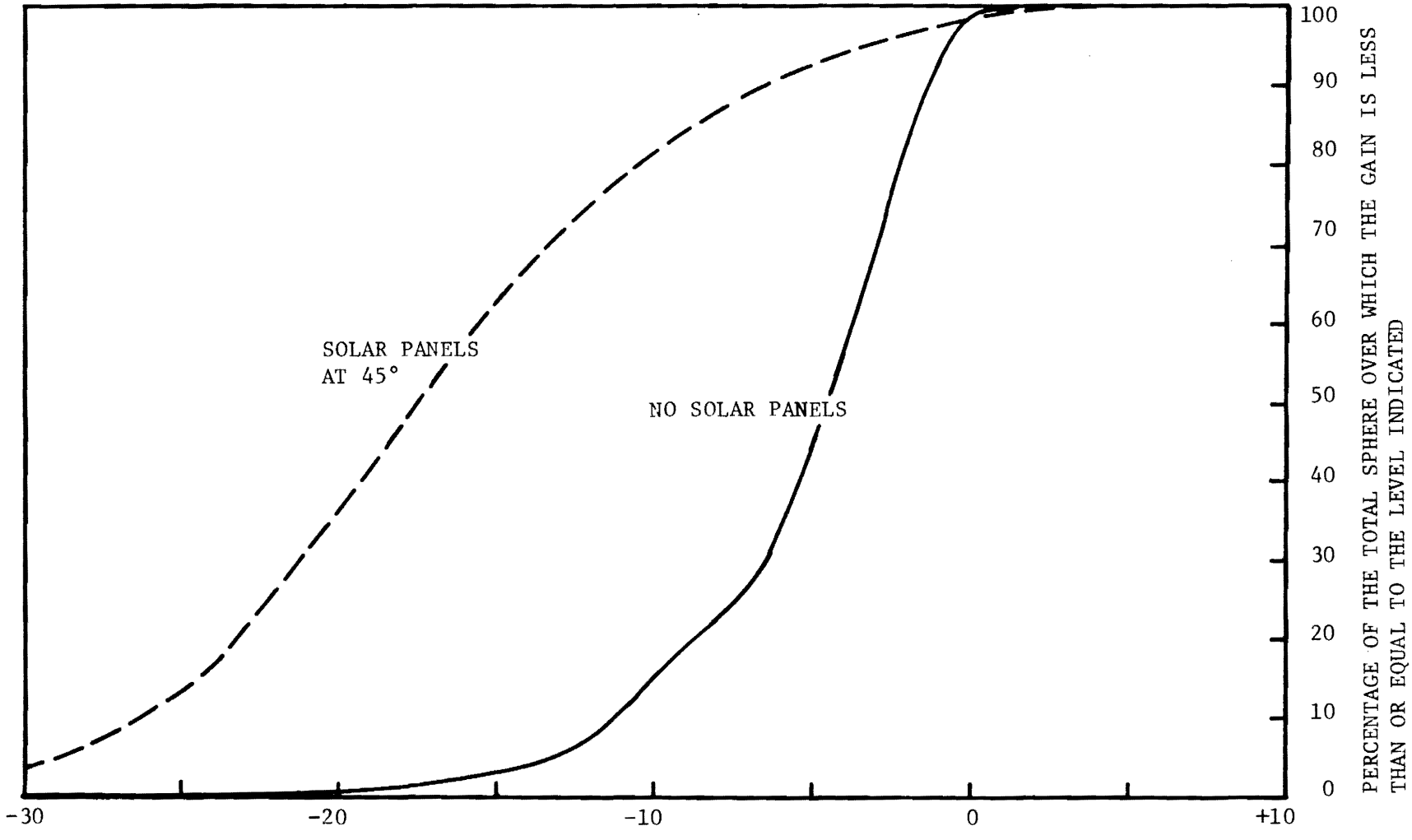

Figure 26. Actual Percent Coverage for Two-Element Array of Quadrifilar Antennas.

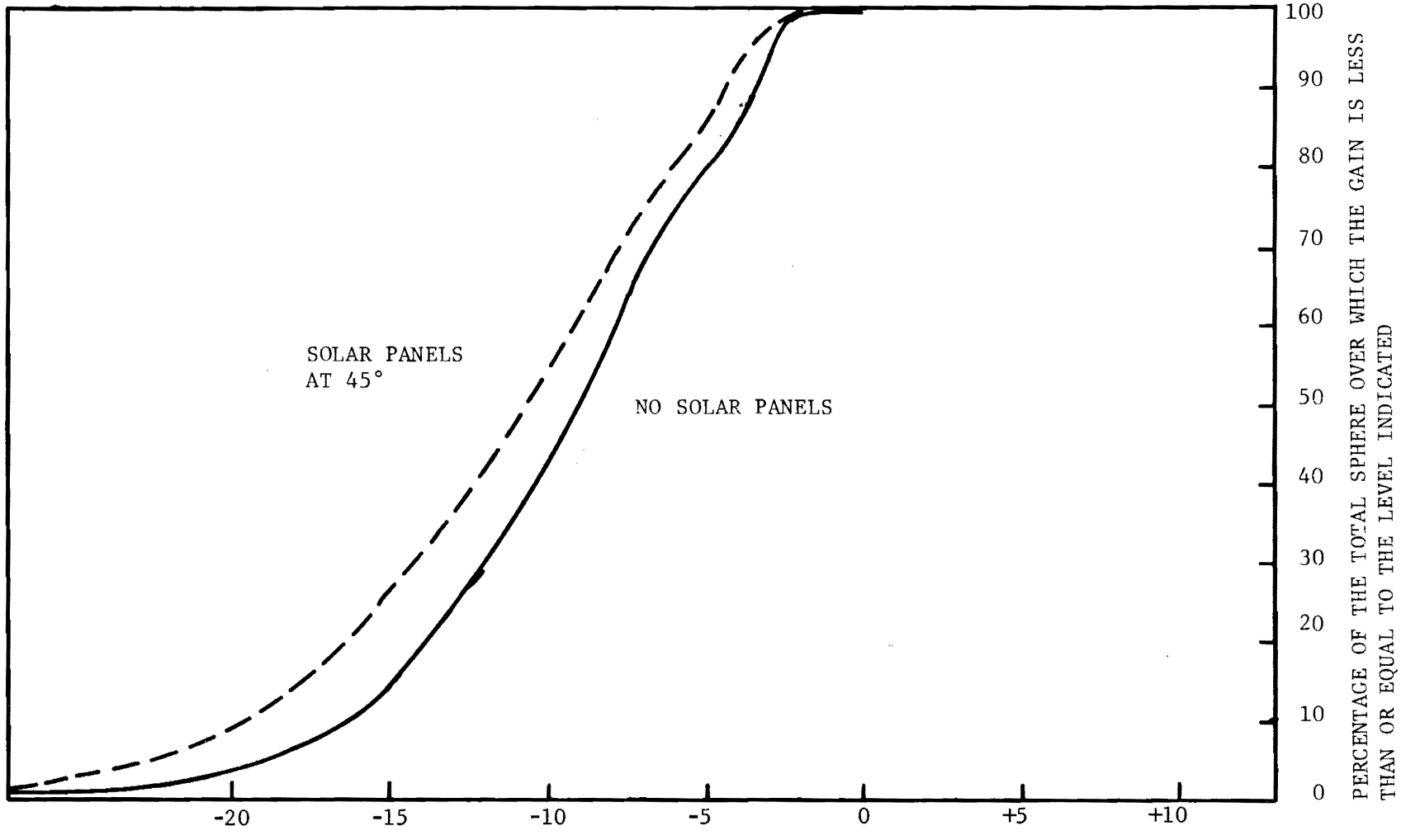

Figure 27. Actual Percent Coverage for Two-Element Array of Cavity-Backed Spiral Antennas.

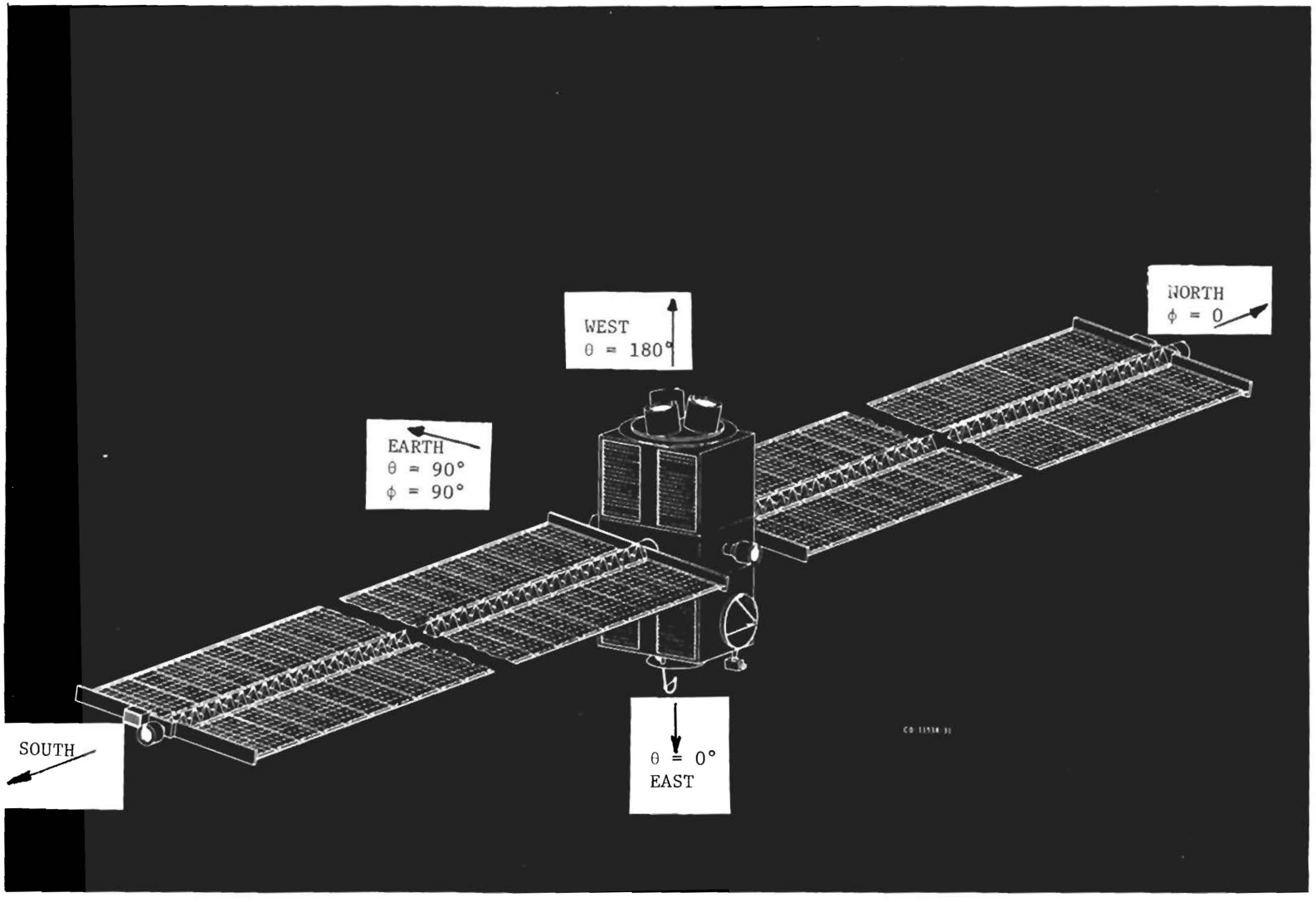

Figure 28. Coordinate system for scale model radiation pattern measurements.

The three 30-cm ion thrusters of our scale model were directed along the $\theta = 180^{o}$ coordinate in the scale model measurements. The solar panels were located at θ, Φ of 90^{o}, (0^{o}, 180^{o}). Scale model patterns were run with the solar panels oriented at 0^{o}, 45^{o} and 90^{o}. The 0^{o} solar panel orientation had the panels in parallel with the long dimension of the spacecraft body. See Figure 28 for an explanation of coordinate system.

4. Scale Model and Antenna Elements

The scale model was a replica of the SERT-C to the following degree:

(a) The rectangular portion of the satellite was duplicated utilizing drawings CR635333 and CR635334 provided by NASA LeRC.

(b) The 30-cm ion engines located on bottom of craft were simulated by cylindrical sections of the metal (Figures 30 and 39).

(c) A conical metal section attachment plate was included on the scale model as indicated in Figures 31 and 33.

(d) The solar panels were made of screen wire and aluminum tubing (Figure 37).

Shop drawings of the scale model are presented in Figures 29 through 41. The dimensions noted on the drawings are in inches. Photographs of the scale model are shown in Figures 42 and 43. The conical attachment plate and 30-cm ion engine replication are shown in Figure 42.

The model is shown as it was mounted on the outdoor range tower in Figure 43. Due to the wind velocity additional wooden supports were used, mainly to protect the gears in the tower drive system. A number of antenna radiation patterns were run with and without wooden supports to determine adverse effects of supports. Fortunately the interference was so small that it could be neglected.

The scaled antenna elements are shown in Figures 12 and 44. The quadrifilar helix was wound at Georgia Tech. Element patterns indicated that the quadrifilar did possess a broad radiation pattern and was circularly polarized. The circular polarization characteristic was obtained by the length and diameter of the individual elements [3]. The crossed-dipole element is shown in Figure 12 and was constructed from a copper-clad fiber

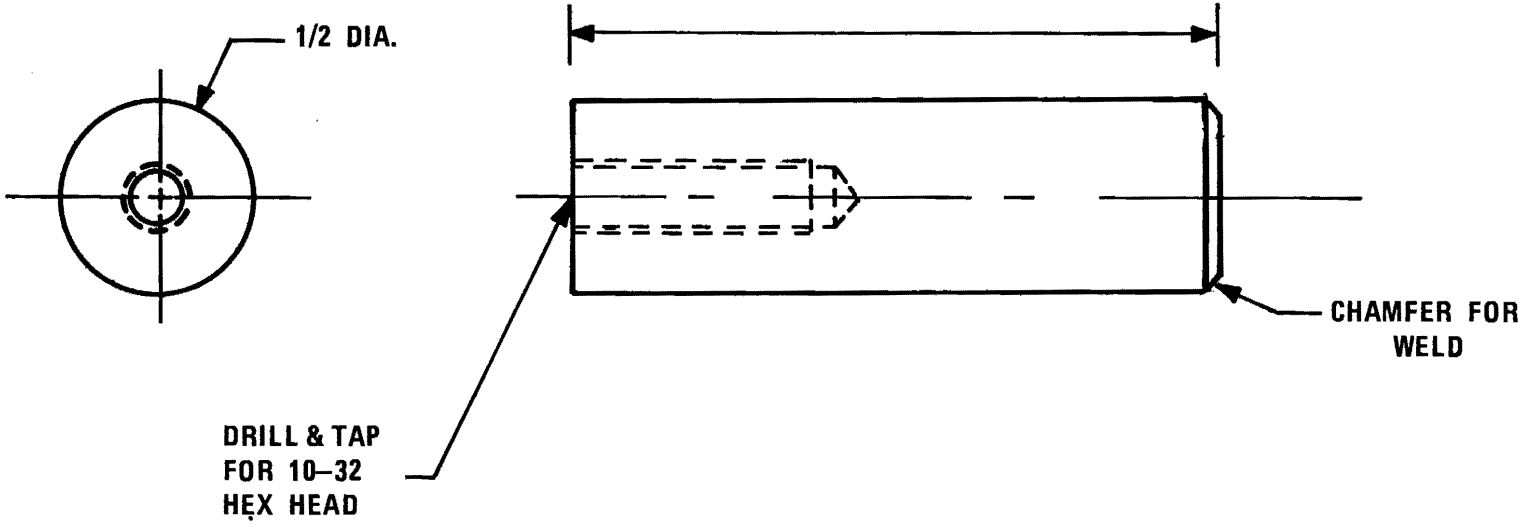

MAT'L: 1/2 ALUMINUM ROD
REQ'D: 4

SCALE: 2:1

A1651–001
DWG D100
RRS 9–30–74

Figure 29. Scale Model Part.

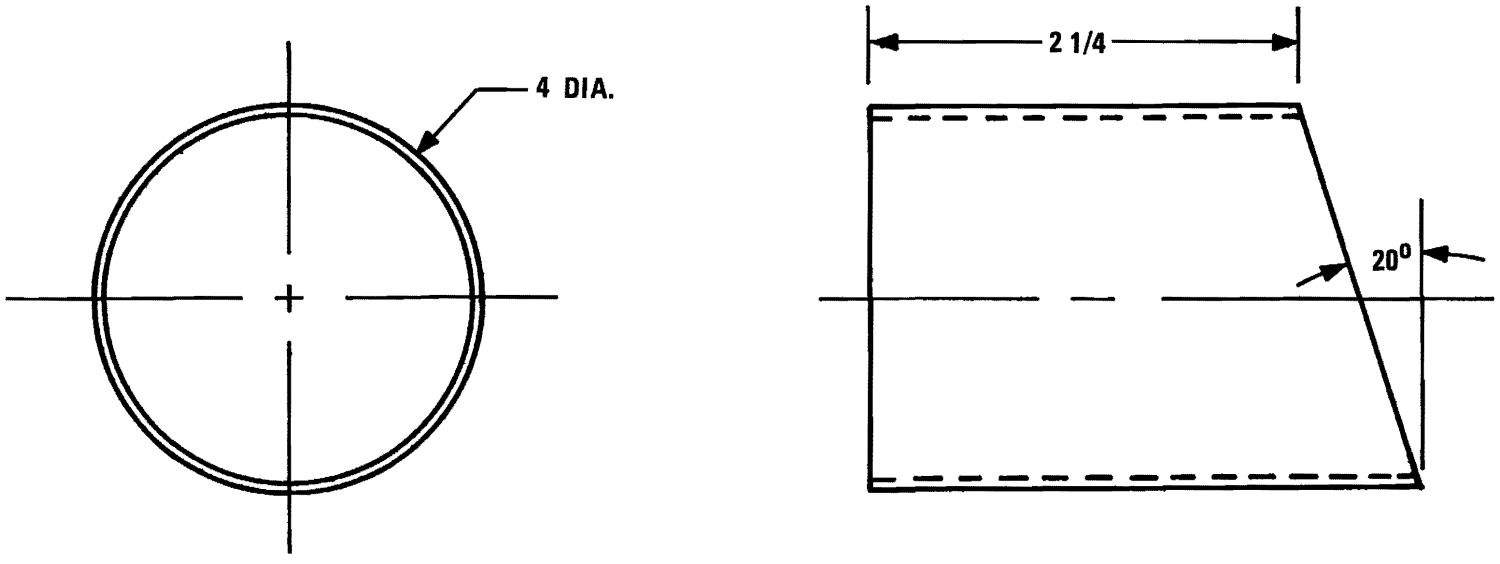

MAT'L: 4 O. D. 0.072 WALL
ALUMINUM TUBING
REQ'D: 3

NOT TO SCALE

A1651–001
DWG D101
RRS 9–30–74

Figure 30. Ion Engines-Scale Model.

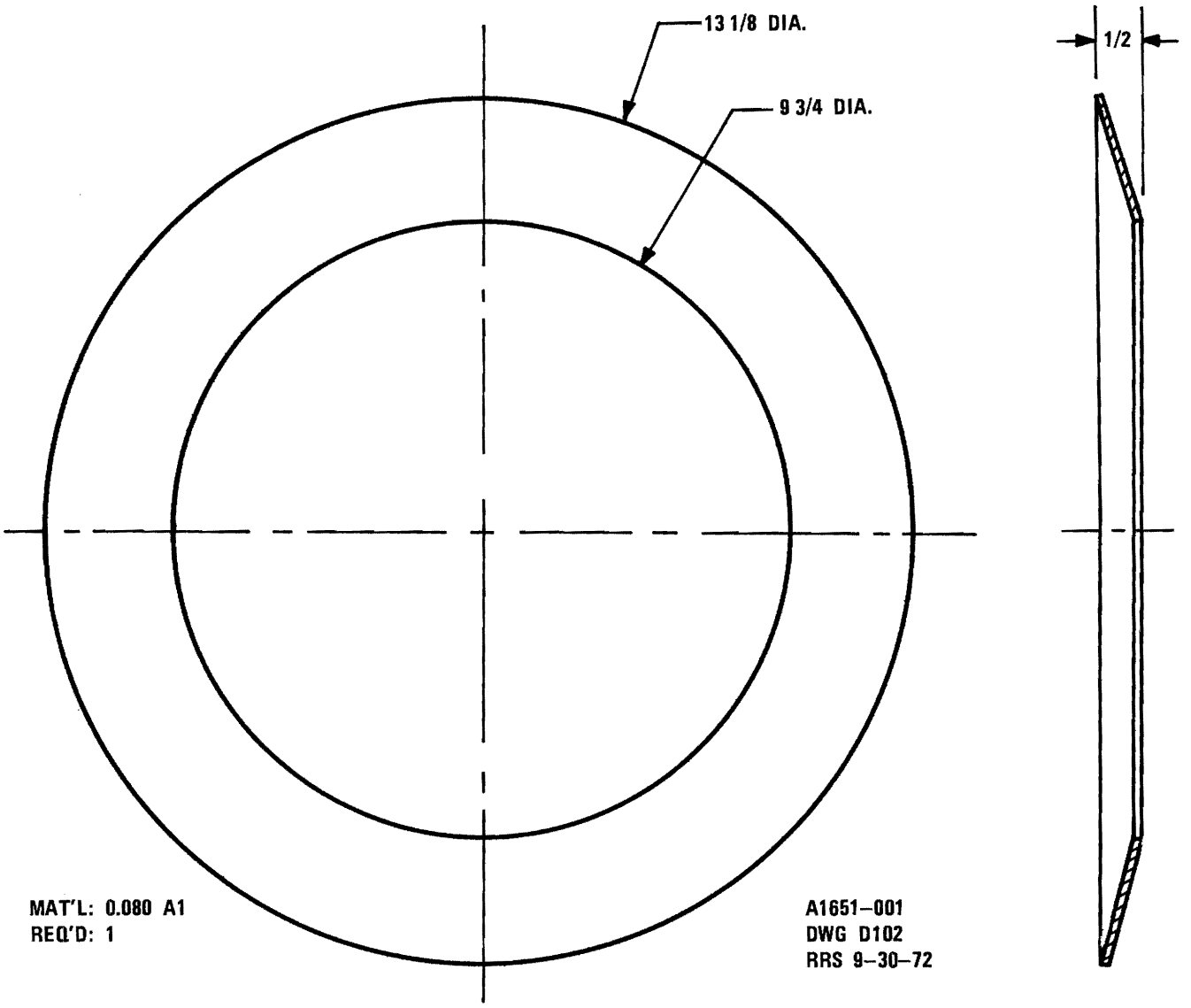

Figure 31. Conical Mounting Bracket-Scale Model.

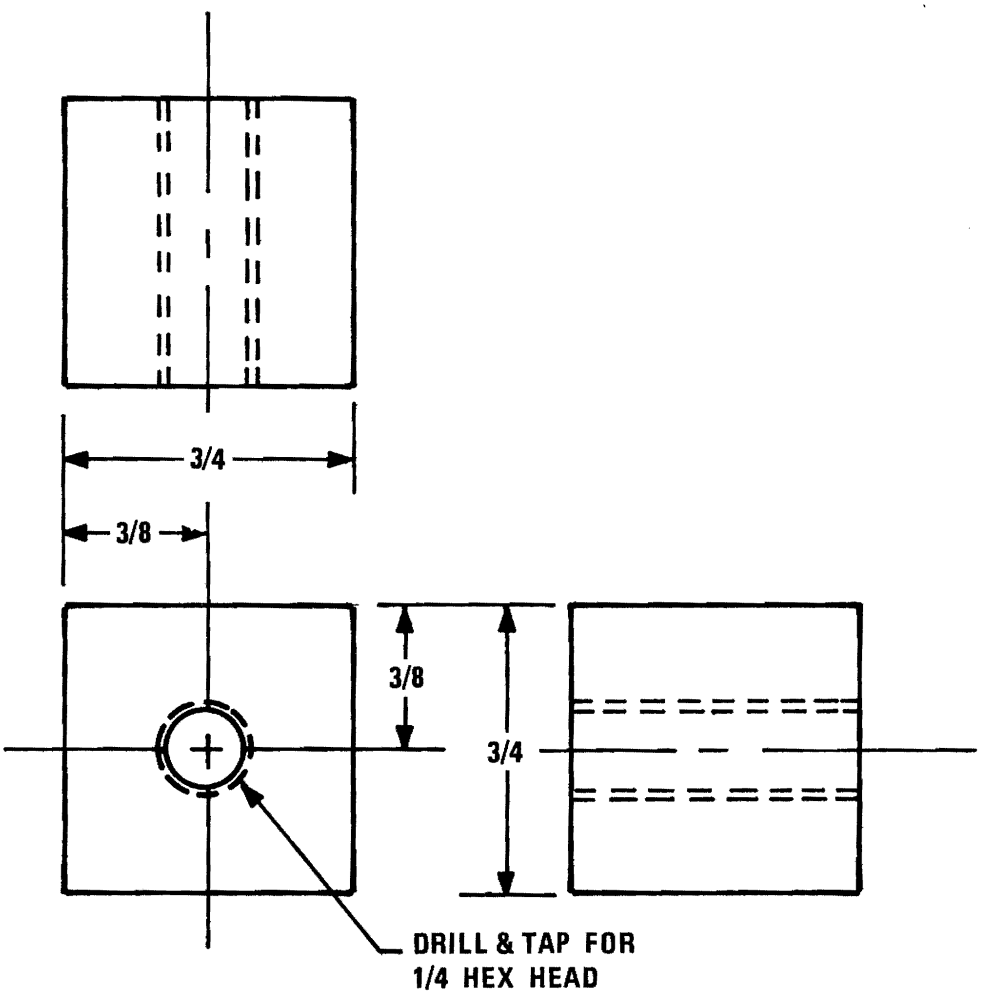

MAT'L: ALUMINUM
REQ'D: 4

A1651–001
DWG D103
RRS 9–30–74

Figure 32. Scale Model Part.

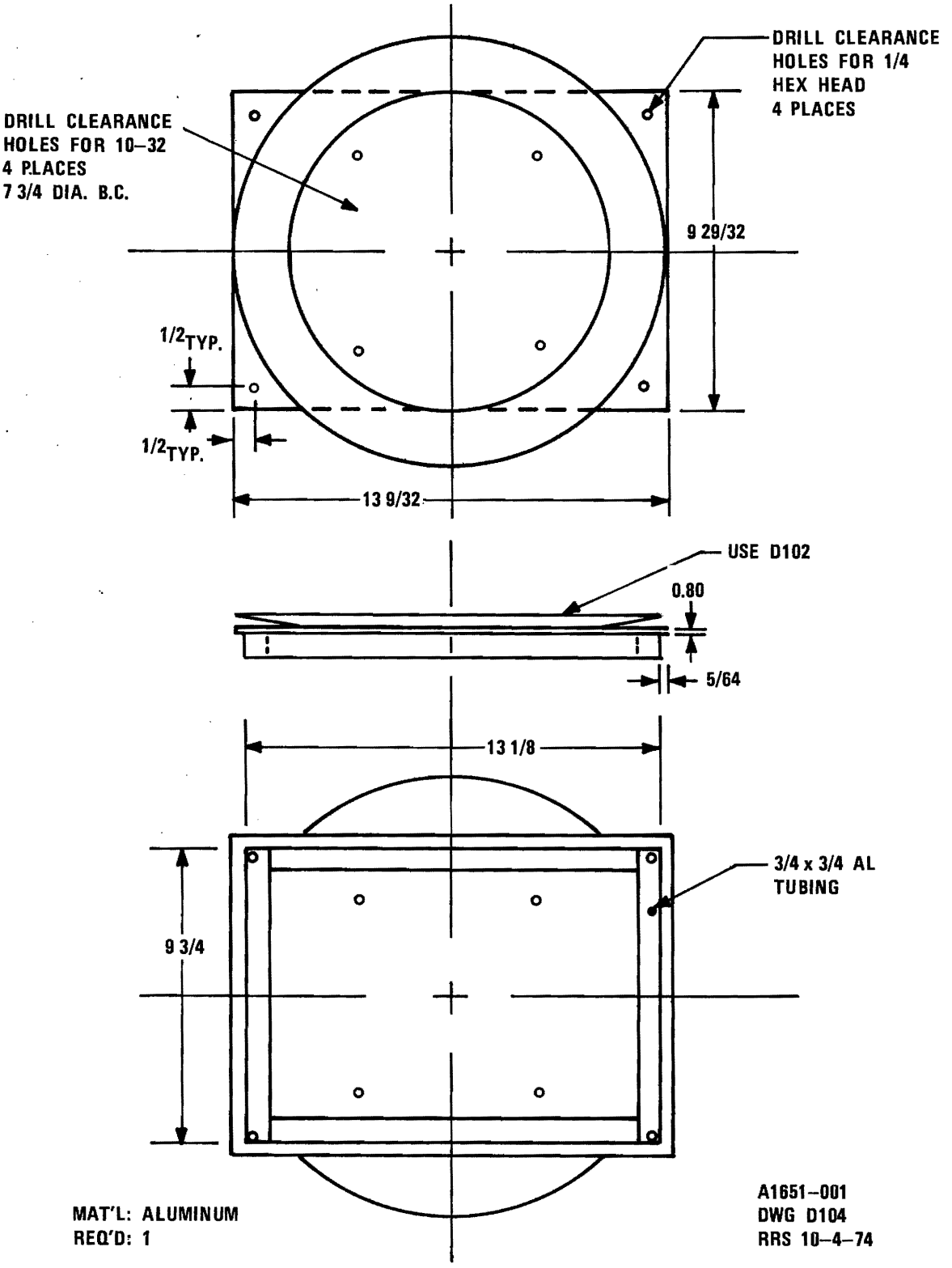

Figure 33. Scale Model Assembly Drawing.

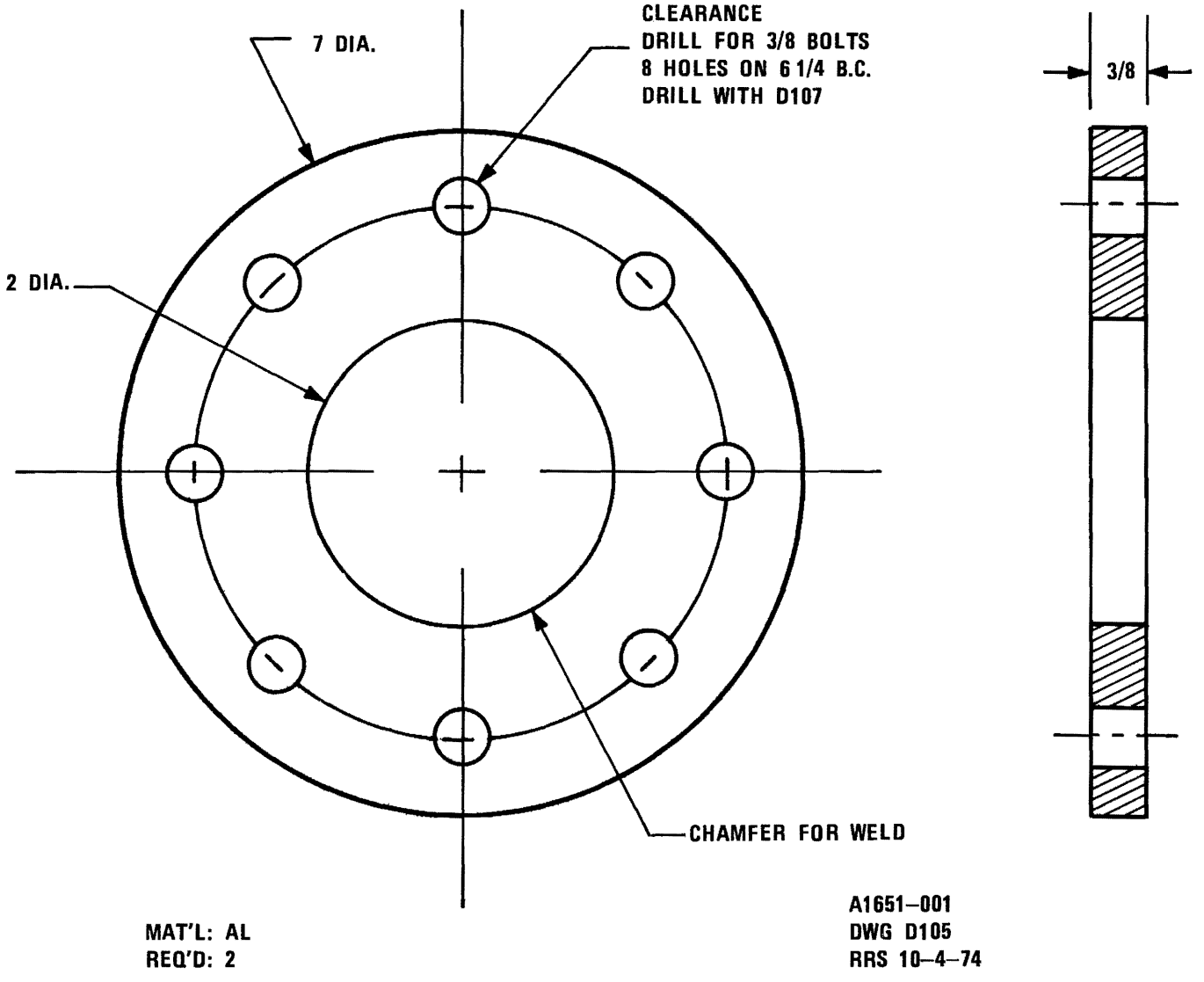

Figure 34. Solar Panel Attachment Ring - Scale Model.

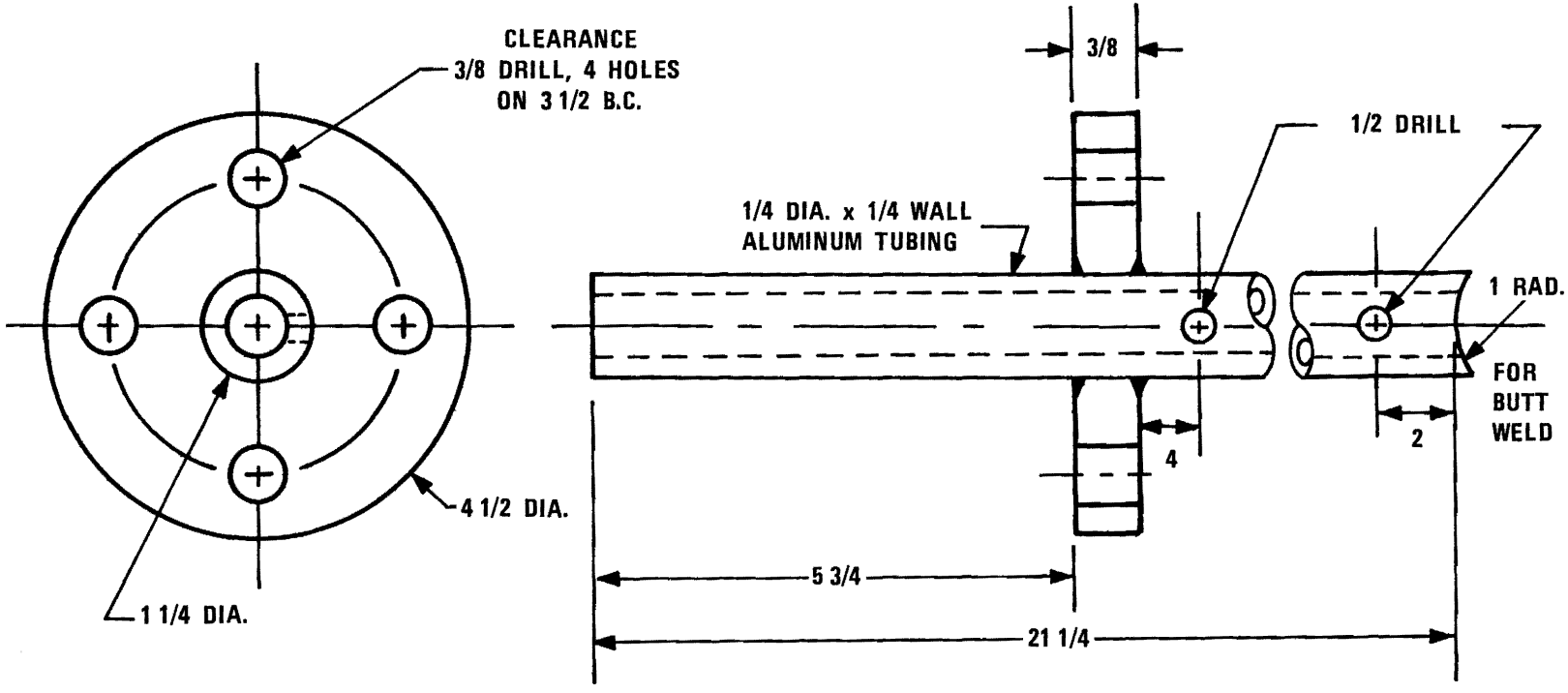

MAT'L: AL
REQ'D: 1

A1651-001
DWG D106
RRS 10-7-74

Figure 35. Scale Model Mounting Bracket.

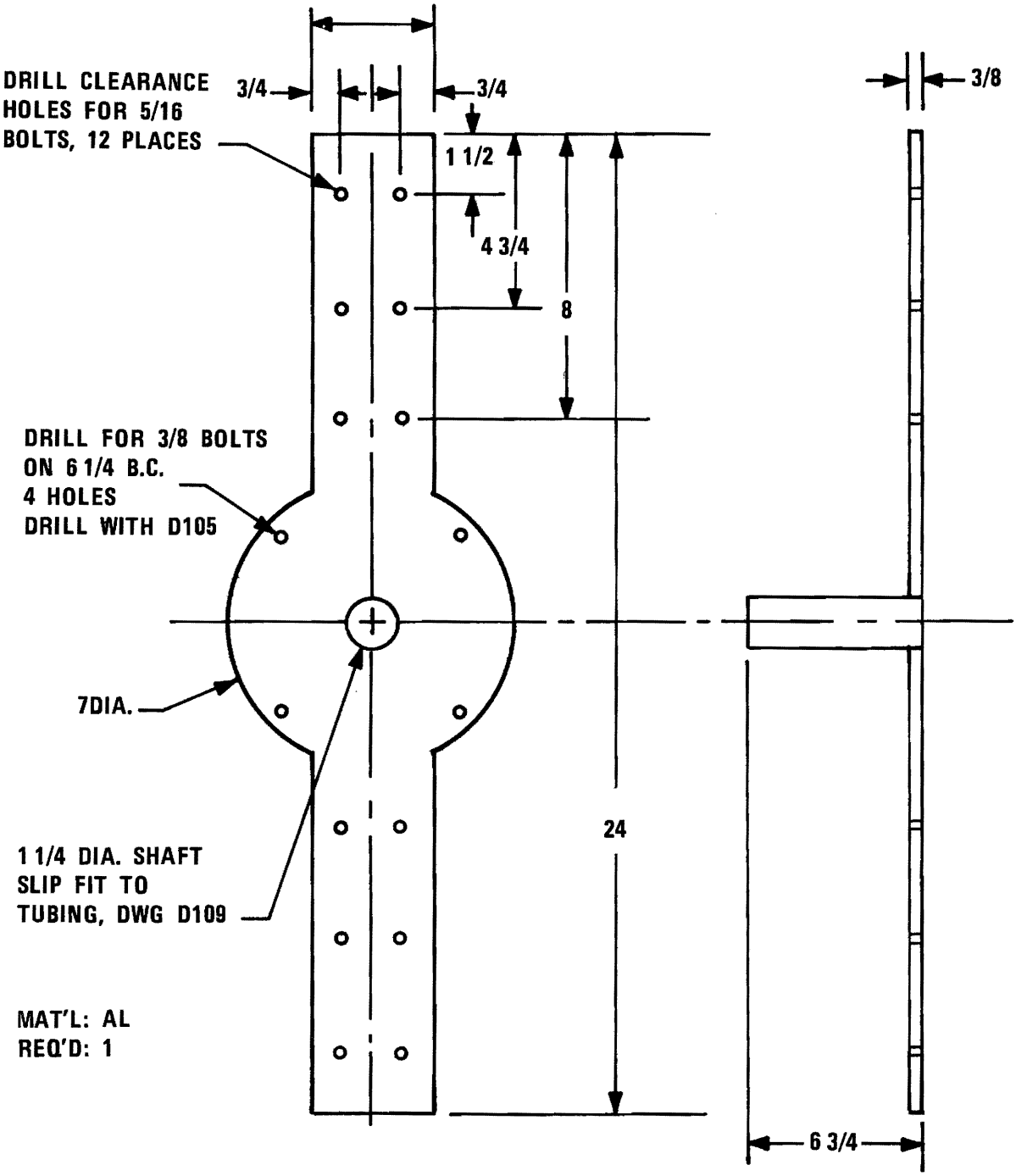

Figure 36. Solar Panel Mounting Bracket, Scale Model.

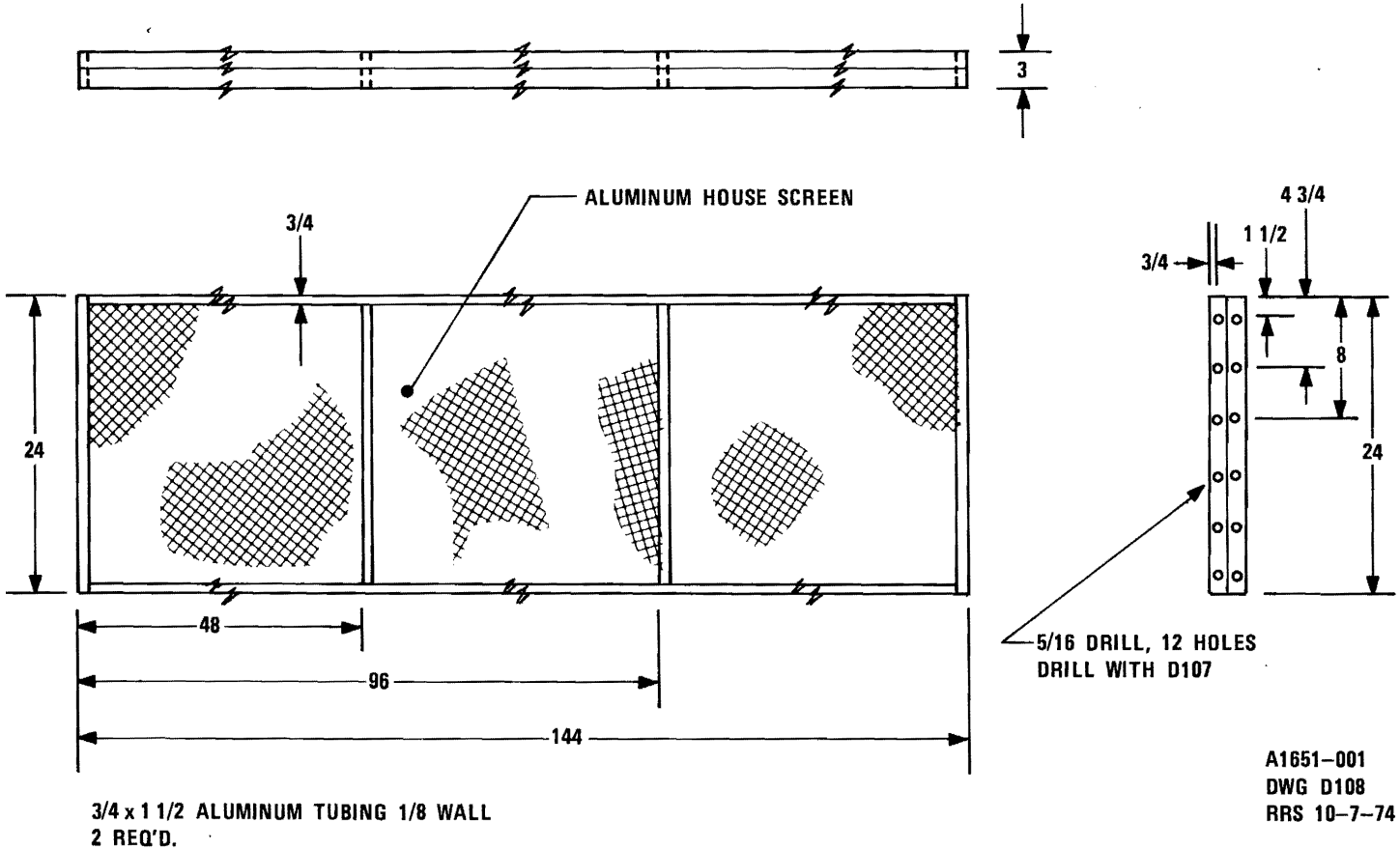

Figure 37. Solar Panels - Scale Model.

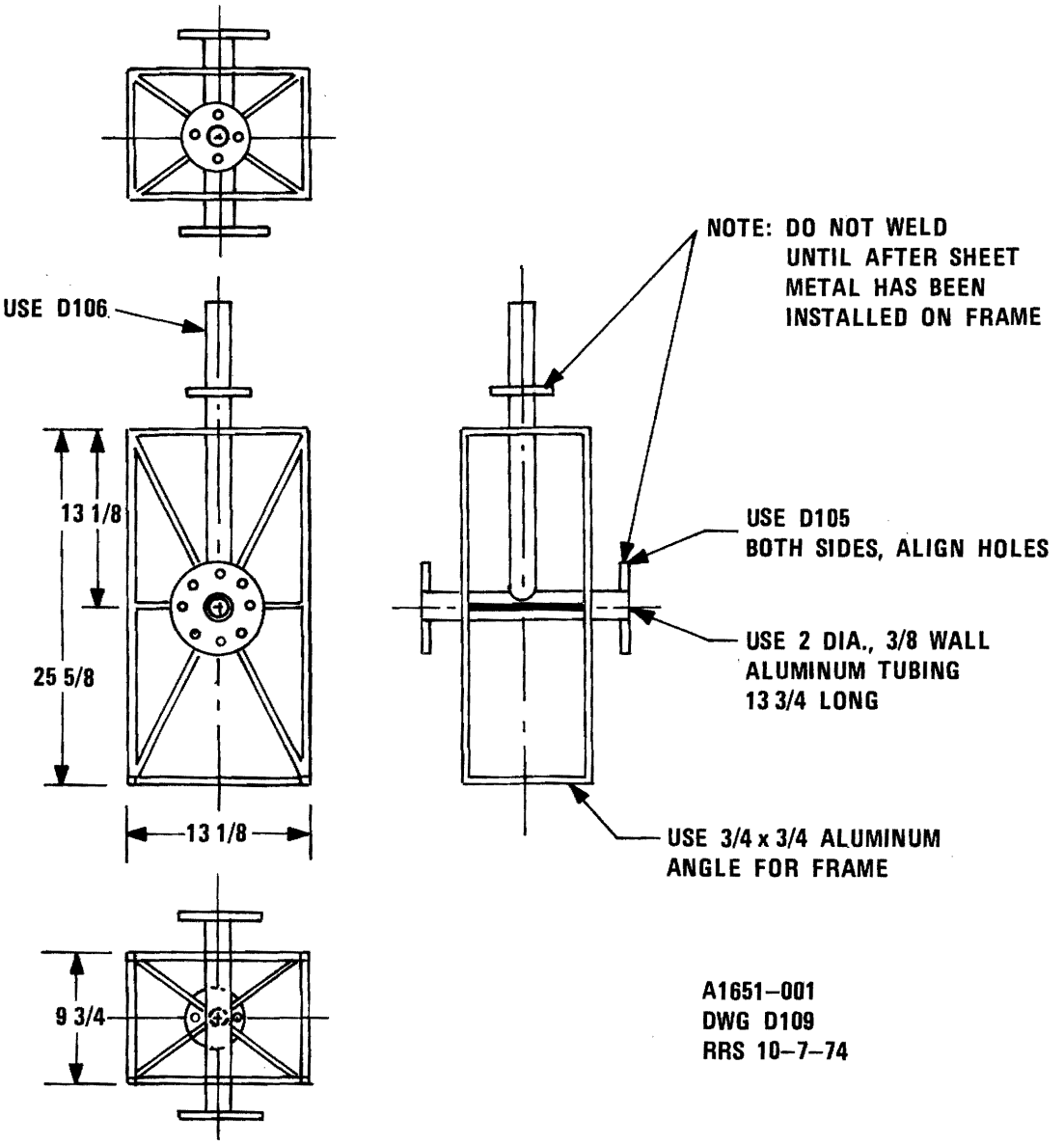

Figure 38. Scale Model Assembly Drawing w/o 30-cm Ion Engines.

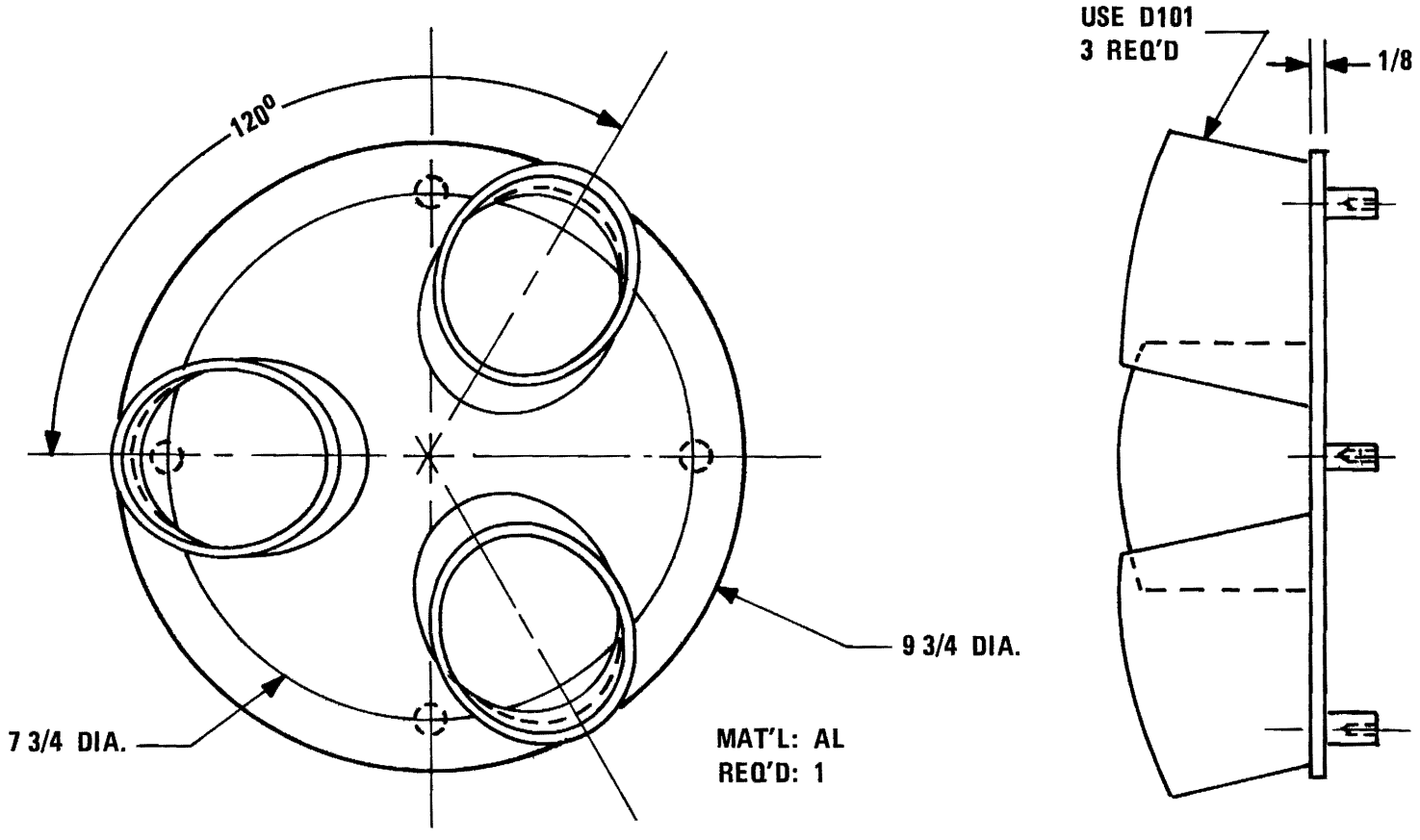

Figure 39. Ion Engine Simulation - Scale Model.

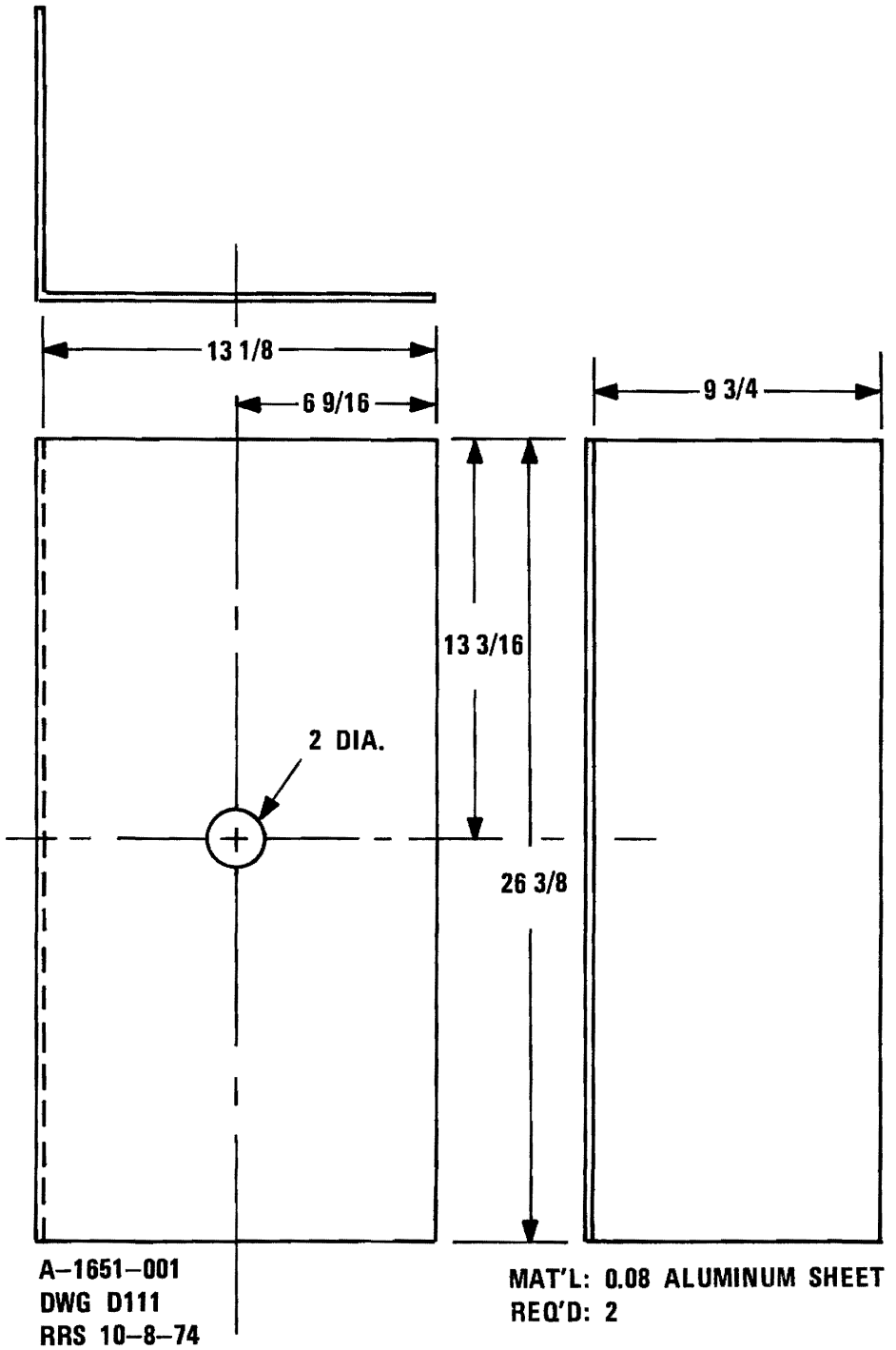

Figure 40. Scale Model Sidewalls.

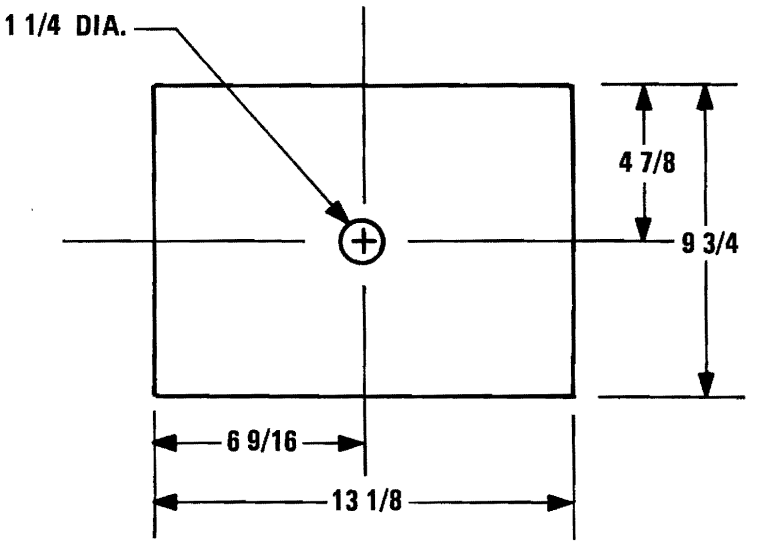

A1651–001
DWG D112
RRS 10–8–74

MAT'L: 0.08 AL
REQ'D: 1

Figure 41. Scale Model Top.

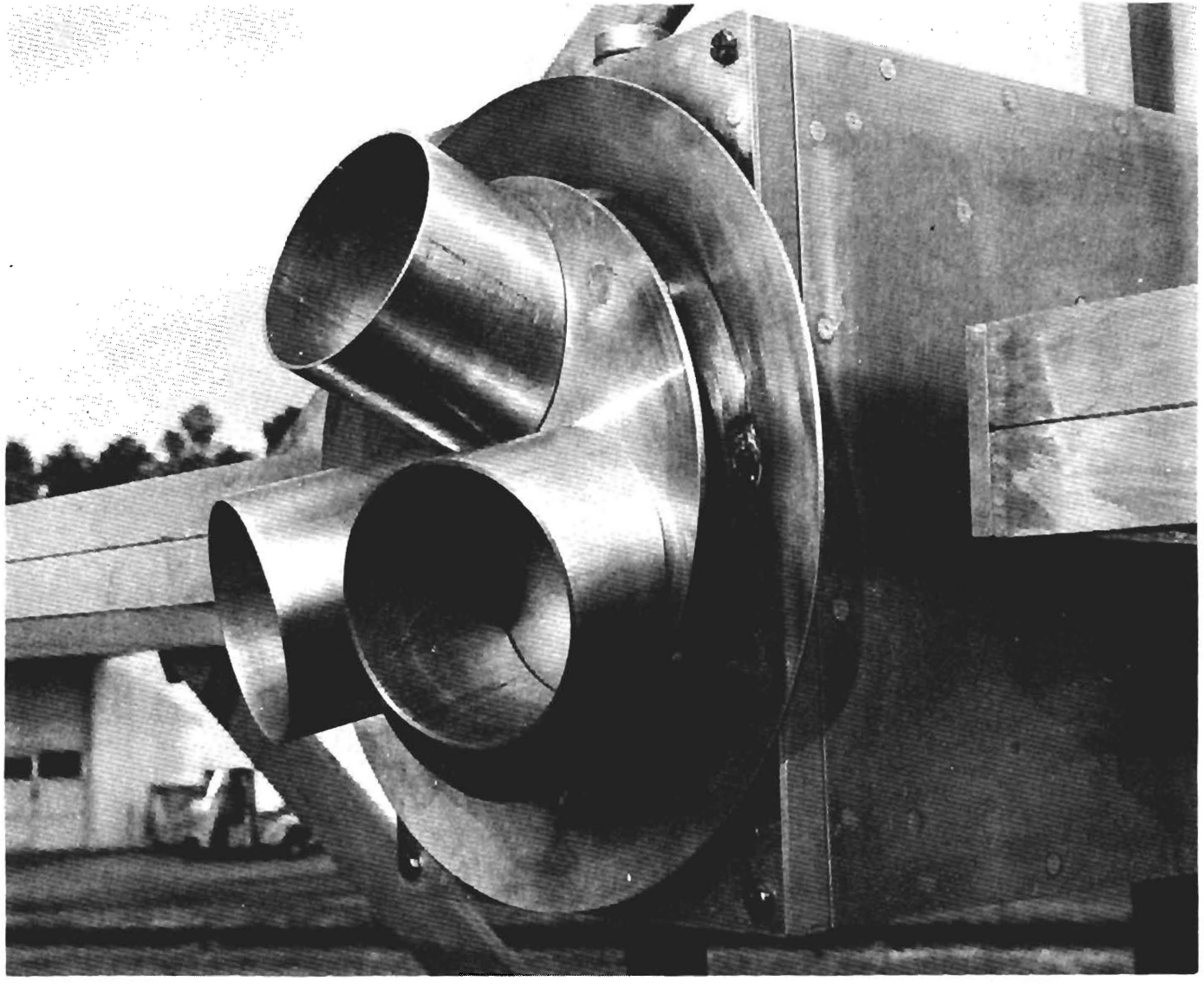

Figure 42. Scale model of SERT-C 30-cm ion engines mounted on antenna test model.

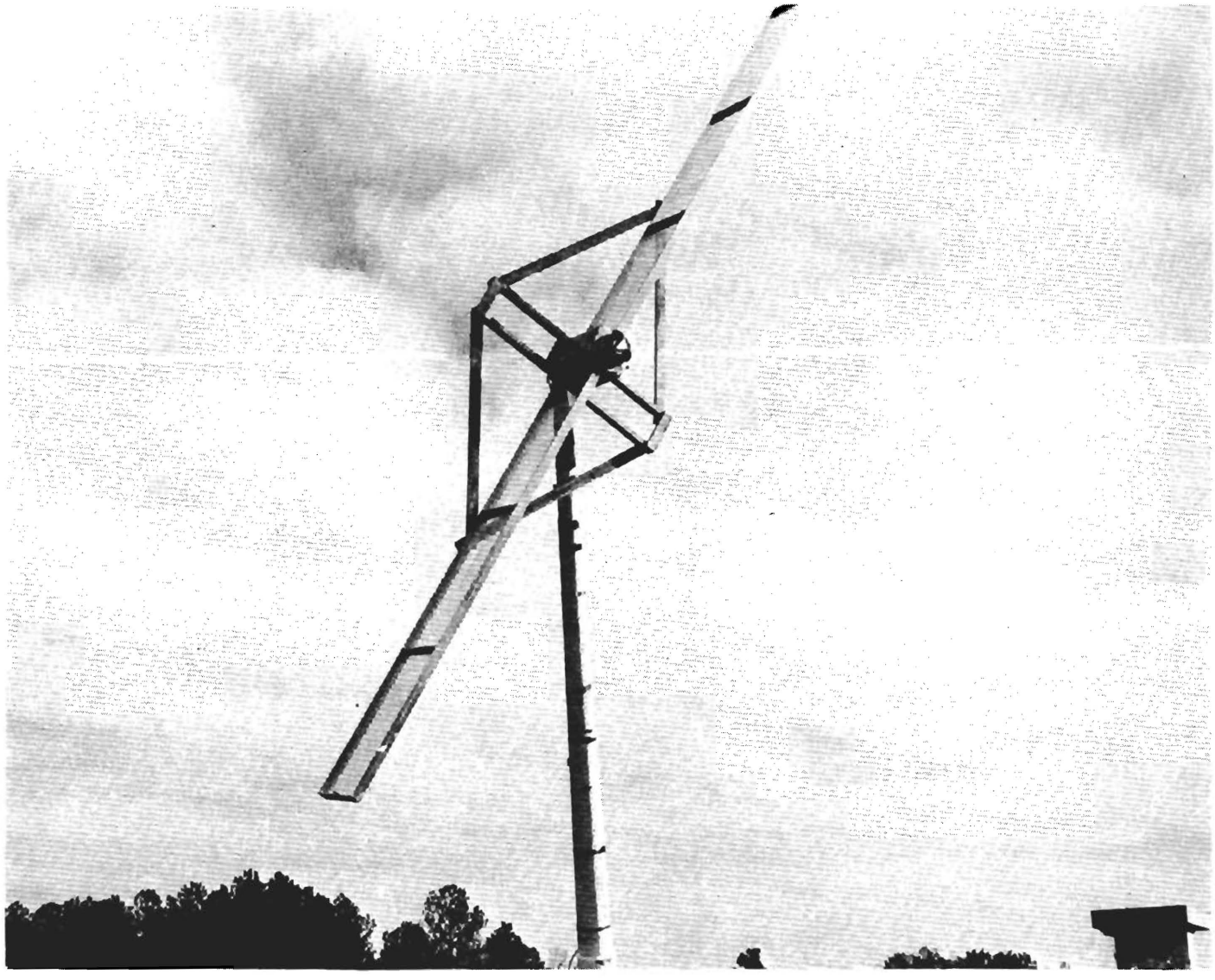

Figure 43. Scale model of SERT-C mounted on test range.

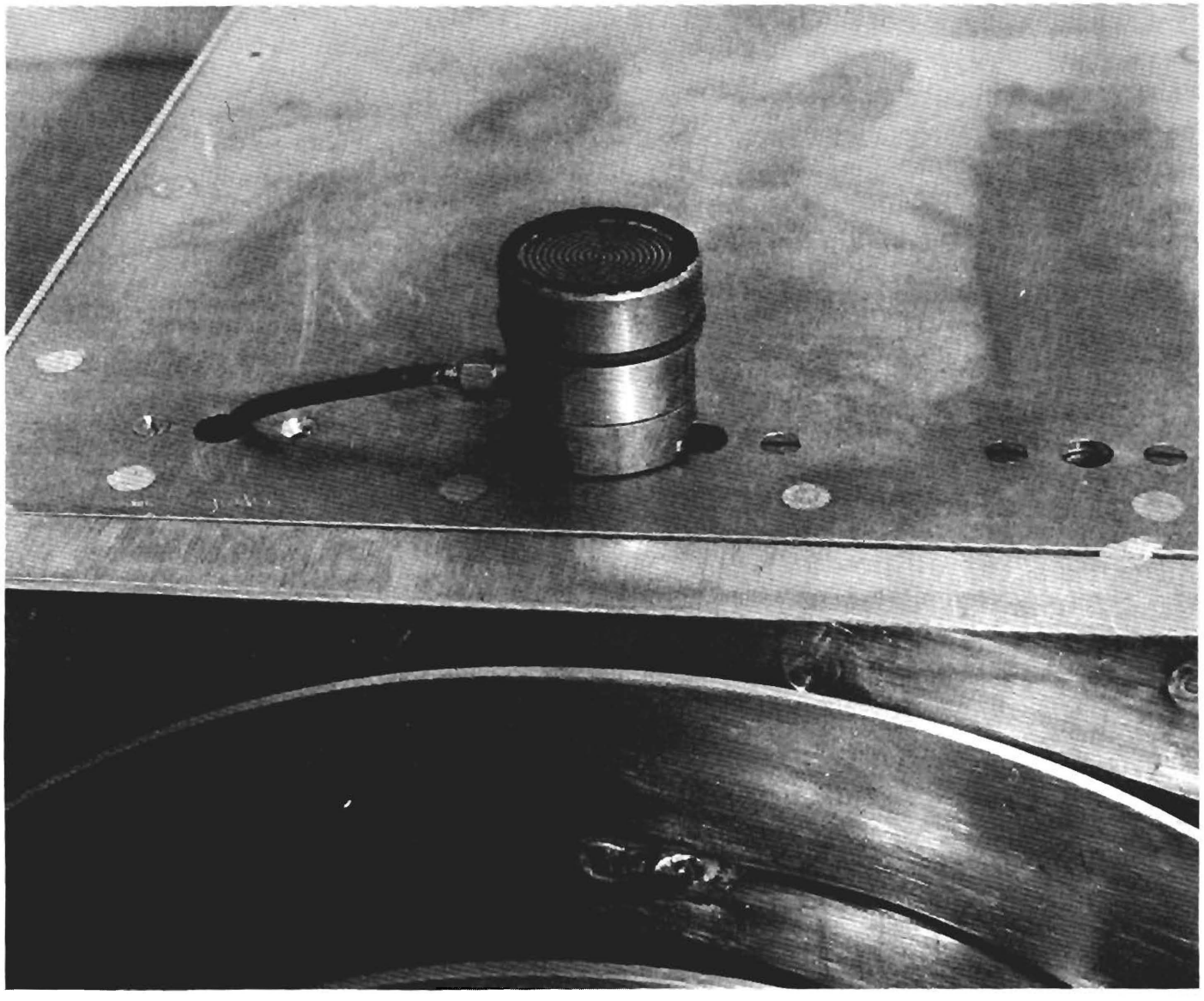

Figure 44. Photograph of cavity-backed spiral antenna mounted on scale model of SERT-C.

board and utilized a flat reflector of copper. Good crossed-dipole pattern, impedance, and polarization characteristics were obtained by empirical methods.

The scale model spiral antennas were items that were a part of our inventory. The spiral is shown mounted to the satellite model in Figure 44. This particular spiral has excellent RF characteristics from 8 GHz to 18 GHz. Our scaled operating frequency was 9.2 GHz.

After tests were completed on the scale model, two spirals were fabricated in our shop and mounted to the model. These antennas will remain attached to the scale model for demonstration activities.

5. Scale Model Electrical Considerations

To obtain contour and polar pattern plots of the omnidirectional array which include the effects of the solar array, it was necessary to model the system. The theoretical basis for the proposed modeling approach was based on the principle of electrodynamic similitude developed by Stratton [10]. In free-space, the principle states that if the linear dimensions of an antenna and the operating wavelength are reduced in a 1:1 ratio, the basic electrical characteristics of the antenna remain unchanged. In summary, an appropriate modeling approach is the following scaling:

$\ell_o' \rightarrow \ell_o/n$	ℓ_o = full scale dimension, n = scaling factor
$f_o' \rightarrow nf_o$	f_o = frequency
$\sigma_o' \rightarrow n\sigma_o$	σ_o = conductivity
$\mu_o' \rightarrow \mu_o$	μ_o = complex permeability
$\epsilon_o' \rightarrow \epsilon_o$	ϵ_o = complex permittivity

where the primed values are the scaled parameters. The physical dimensions of the full-scale antenna were scaled down by a factor n; frequency and σ were scaled up by the factor n; while ϵ_o and μ_o of the model remained unchanged.

The scaling factor n must be properly chosen in order to accommodate the following:

* reasonable model dimensions for duplicating antenna elements
* reasonable model dimensions for radiation pattern measurements
* practical instrumentation and measurement techniques

A major intent of modeling is to obtain a replica of the full-scale situation in a small, manageable form factor. The model must be amenable to relatively easy fabrication and handling. A scale frequency of 9.2 GHz was used, i.e., the scaling factor, n, equaled 4:1. A scale frequency of 9.2 GHz allows the use of coaxial components and permitted the scale model spacecraft with solar panels to be tested on the radiation pattern measurement ranges. The radiation patterns of each single scale model element were compared with those of a full scale antenna element prior to any array testing.

E. Full Scale Antenna Measurements

The S-band cavity-backed spiral antennas were mounted on a full-scale model of the SERT-C spacecraft for VSWR measurements, gain measurements, and power handling capability measurements. The full-scale spacecraft model consisted of the rectangular frame fabricated from aluminum sheets (Figure 45). The solar panels were not included in these measurements.

The two antennas were Transco Products, Inc. Model 9C1800 high power cavity-backed spirals mounted on opposite faces of the spacecraft ground plane. The location of the antennas is presented in Figure 46. One view of the antenna is shown in Figure 47. The antennas were connected through equal length coaxial cables to the sum port of a Technical Research and Manufacturing 4-port 0° and 180° hybrid junction, Model HS-506. The difference port of the hybrid junction was terminated with a 50-ohm load.

1. VSWR and Impedance Measurements

The impedance and VSWR of the antenna system were determined from discrete frequency measurements from 2.0 GHz to 2.35 GHz. The antenna system (two antennas plus 2 coaxial cables and hybrid junction) VSWR is tabulated in Table IV as a function of frequency. These data are plotted in Figure 48. The specification for maximum VSWR was 1.5:1. As noted in Table IV, the antenna system just does fall within specifications.

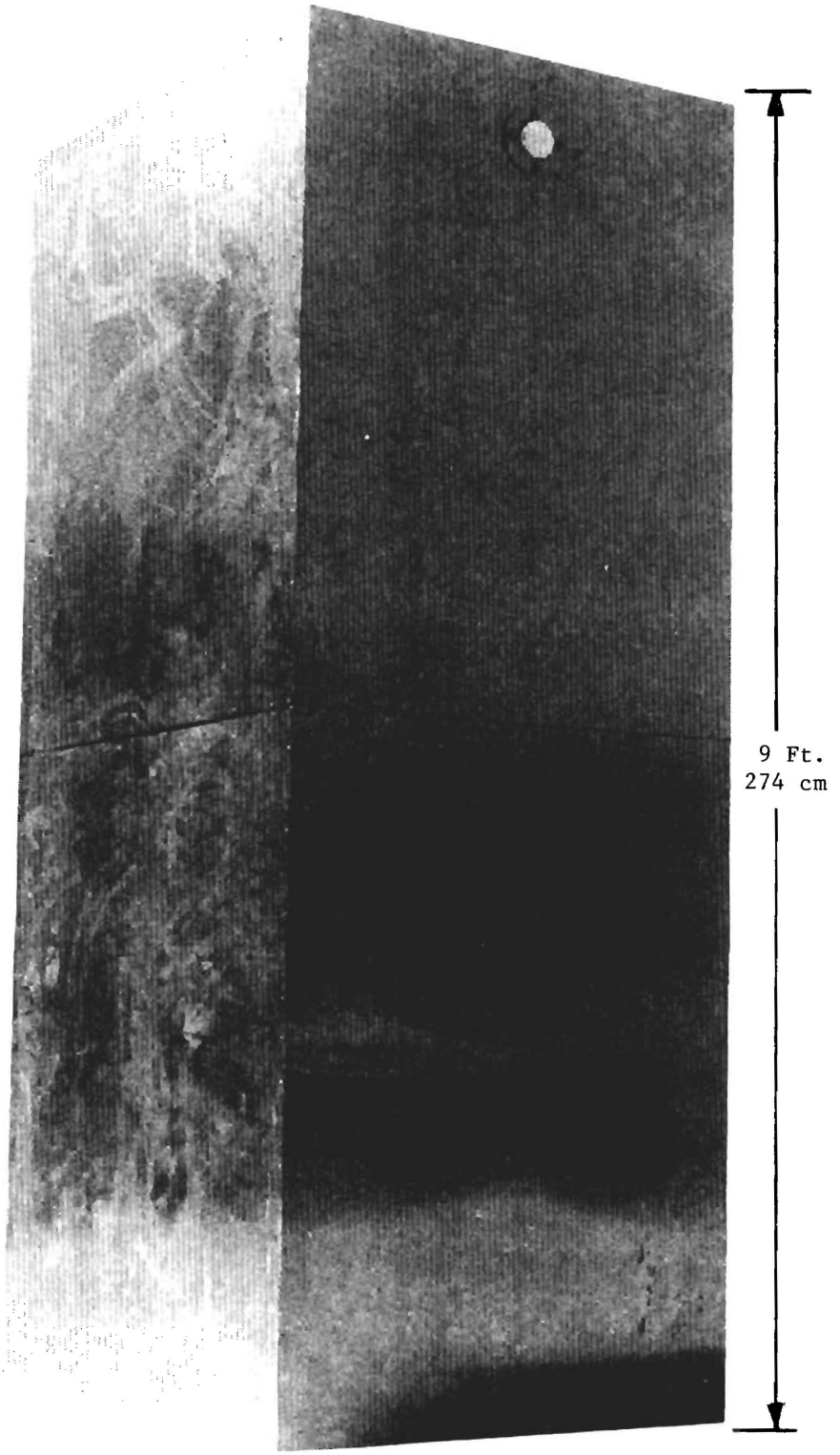

Figure 45. Full Scale S-Band Antenna Mounted on Aluminum Frame.

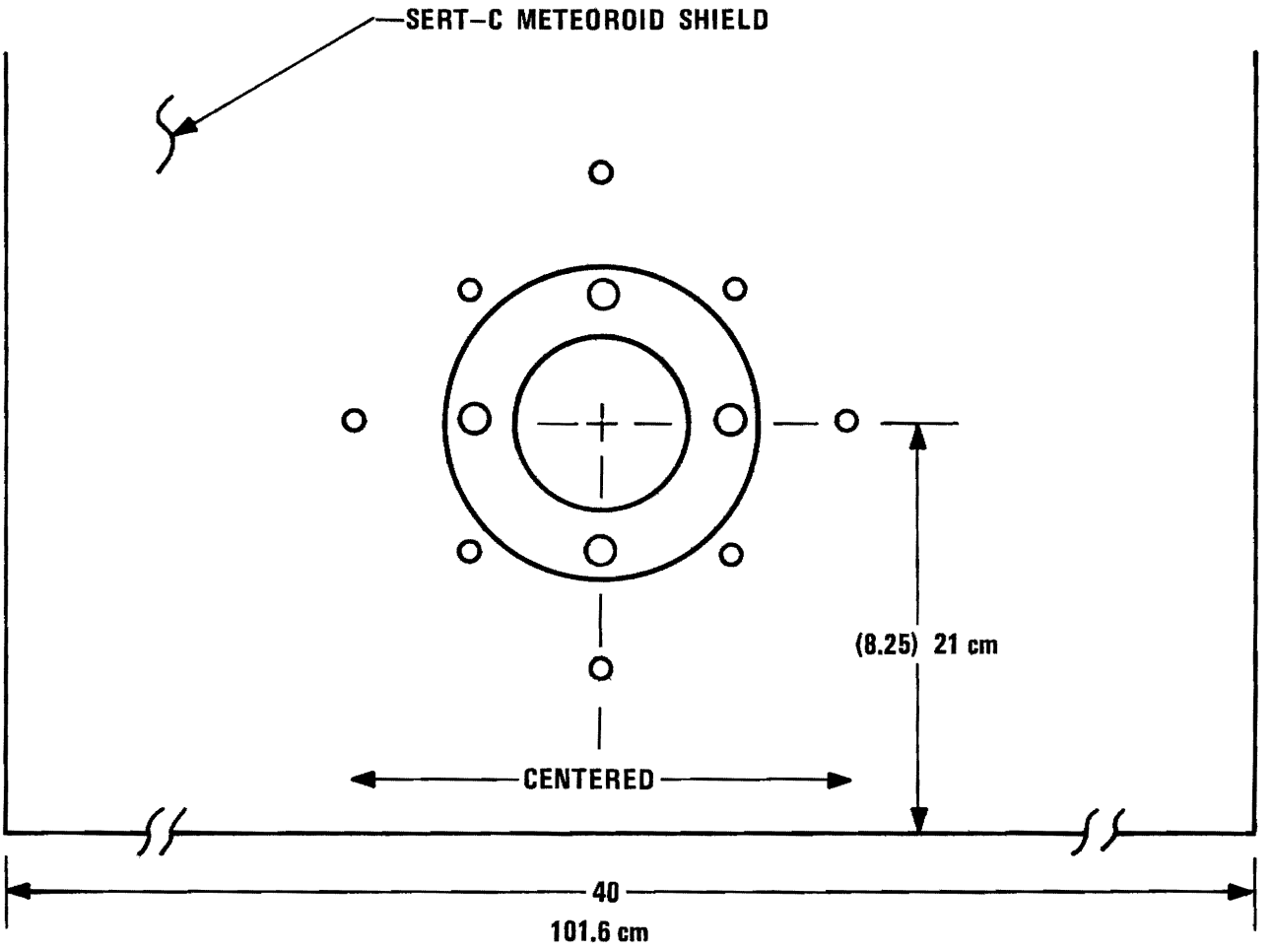

Figure 46. Location of Antenna on Face of Spacecraft-
21 cm from end of spacecraft mounting ring.

Figure 47. Side view of S-Band cavity-backed spiral antenna.

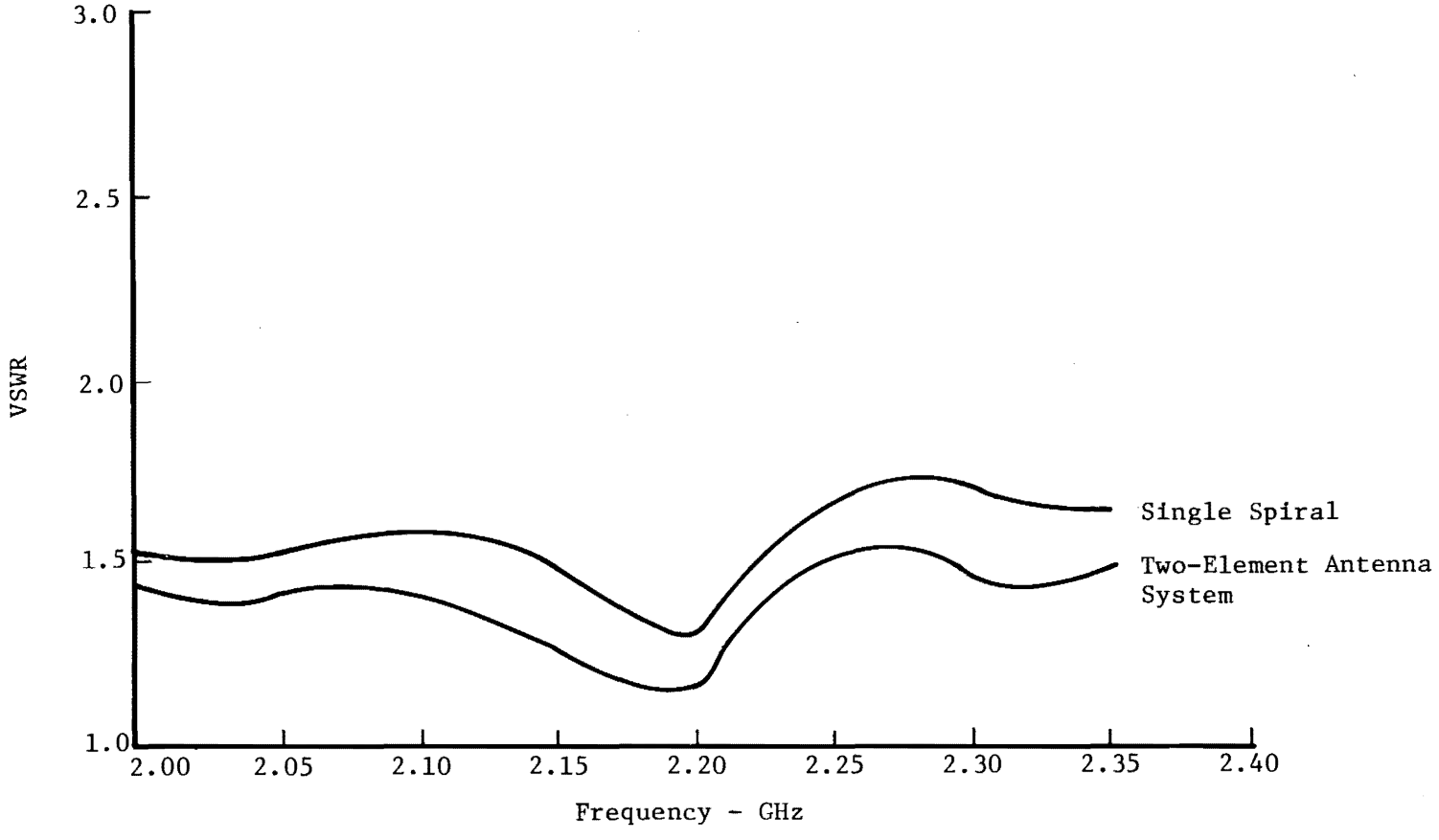

Figure 48. VSWR of Single Cavity-Backed Spiral Antenna and VSWR of Proposed SERT-C Antenna System.

TABLE IV

VSWR vs. FREQUENCY FOR S-BAND
CAVITY-BACKED SPIRALS

Frequency	Both Spirals Plus Hybrid Junction VSWR	Single Spiral VSWR
2.0	1.43	1.55
2.05	1.4	1.57
2.1	1.42	1.6
2.15	1.32	1.5
2.2	1.23	1.37
2.25	1.53	1.64
2.3	1.5	1.72
2.35	1.52	1.7

Individual antenna measurement data indicate a VSWR greater than 1.5:1 over most of the frequency range of concern (see Table IV). The reduction in VSWR of the two is due to the power divider which has some loss and to the interaction between elements.

The impedance of the antenna system is plotted on the Smith Chart of Figure 49. This is a typical impedance plot for two parallel-fed spiral antennas. It was noted during the scale model measurements that the solar panels had little, if any, effect on the VSWR or impedance of the antenna system.

A block diagram of the impedance and VSWR measurement equipment is shown in Figure 50. The data of Figure 49 and the data of Table IV are the impedance and VSWR data, respectively, of the input to the four-port hybrid junction.

2. Gain Measurements

The standard gain horn technique [11] of determining the maximum gain of the antenna system was used. The antenna system of the full-scale model of the SERT-C satellite was illuminated by a circularly polarized source antenna. The power level at the output of the four-port hybrid junction was measured. The full-scale model was replaced by a standard gain horn of known gain vs. frequency characteristics. The power level at the output of the standard gain horn was noted. The difference in measured power levels was an indication of the gain of the antenna system. The system gain including the losses in the coaxial cables and the four-port hybrid was measured to be -3.0 dB with respect to a linear isotropic radiator. Since the polar plots of Appendix III and the contour plots of Figures 23 and 24 are for circular polarization, the maximum gain level is 0 dB as indicated in the figures.

3. Power Handling Measurements

The antenna system was subjected to 20 watts of CW power at a frequency of 2.47 GHz to determine if any adverse effects occurred. The block diagram of this measurement set-up is shown in Figure 51. An AIL High Power Oscillator was used in generating the RF signal. The signal from the

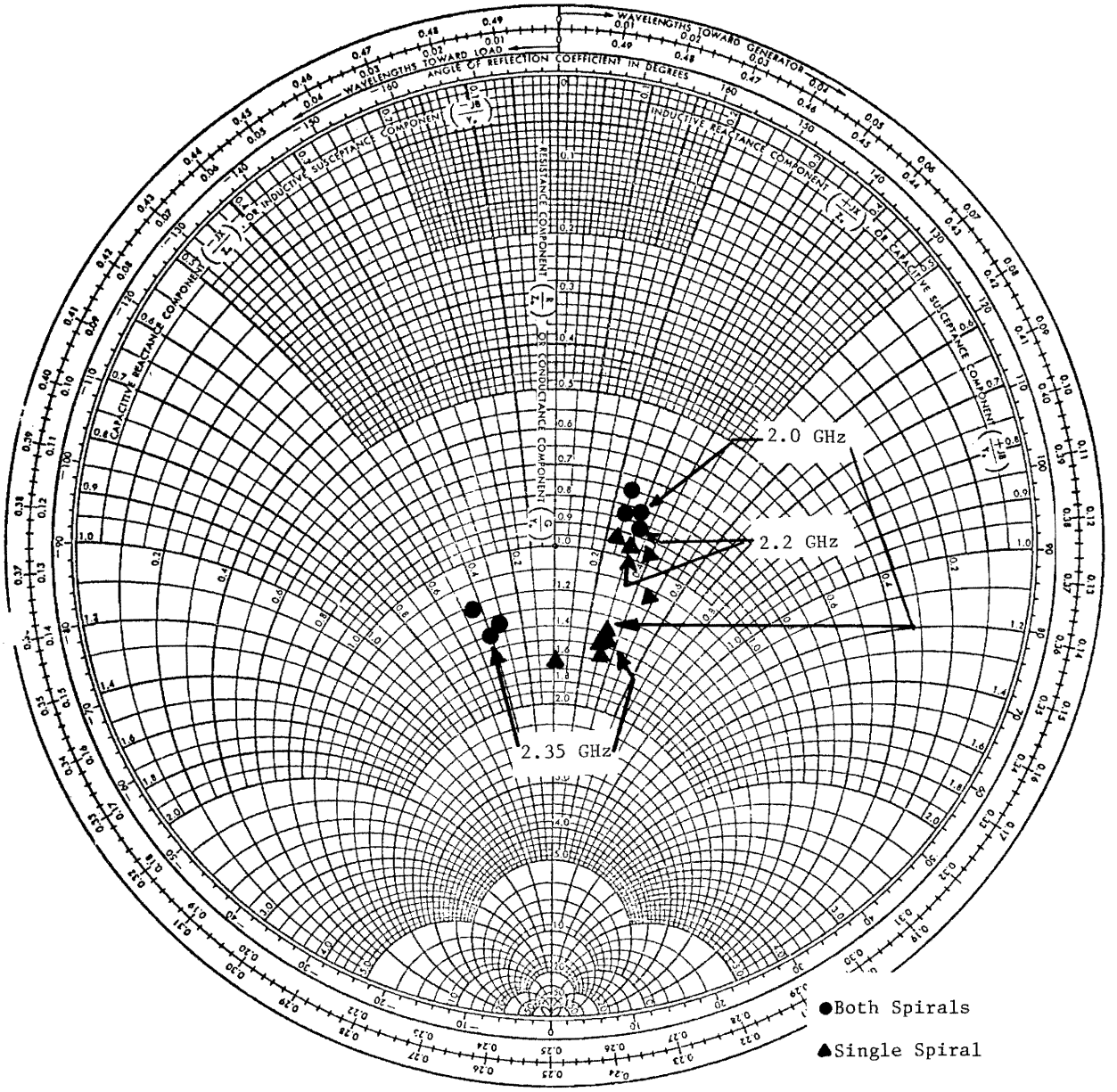

ANTENNA	LOCATION	EQUIPMENT
AIRCRAFT _____	ALTITUDE _____	ATTITUDE _____
REMARKS _____		FREQUENCY _____
ENGINEER	FILE NO.	DATE

Figure 49. Smith Chart Indicating Impedance of S-Band Antenna Array.

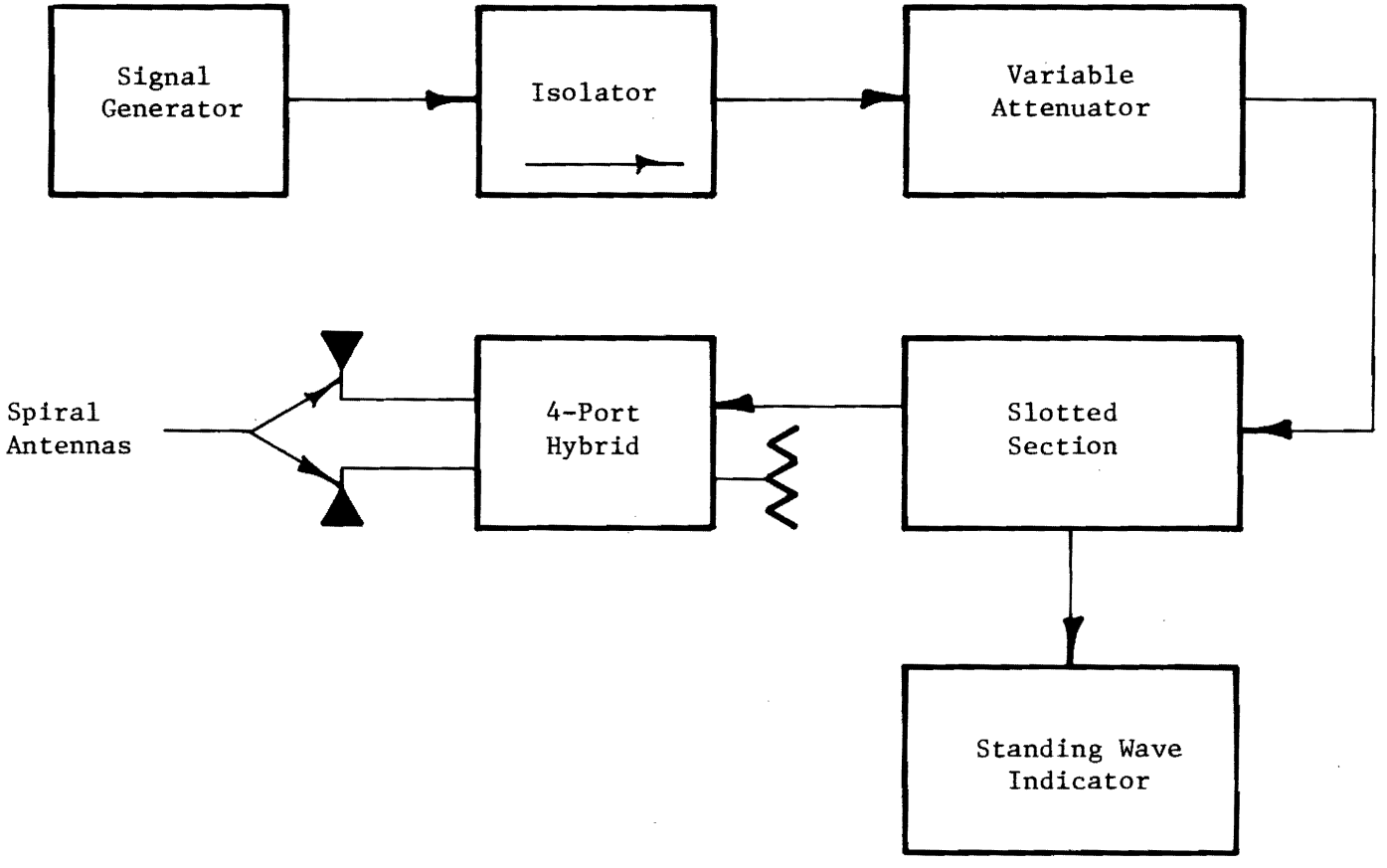

Figure 50. Block Diagram of Test Equipment for VSWR Measurements.

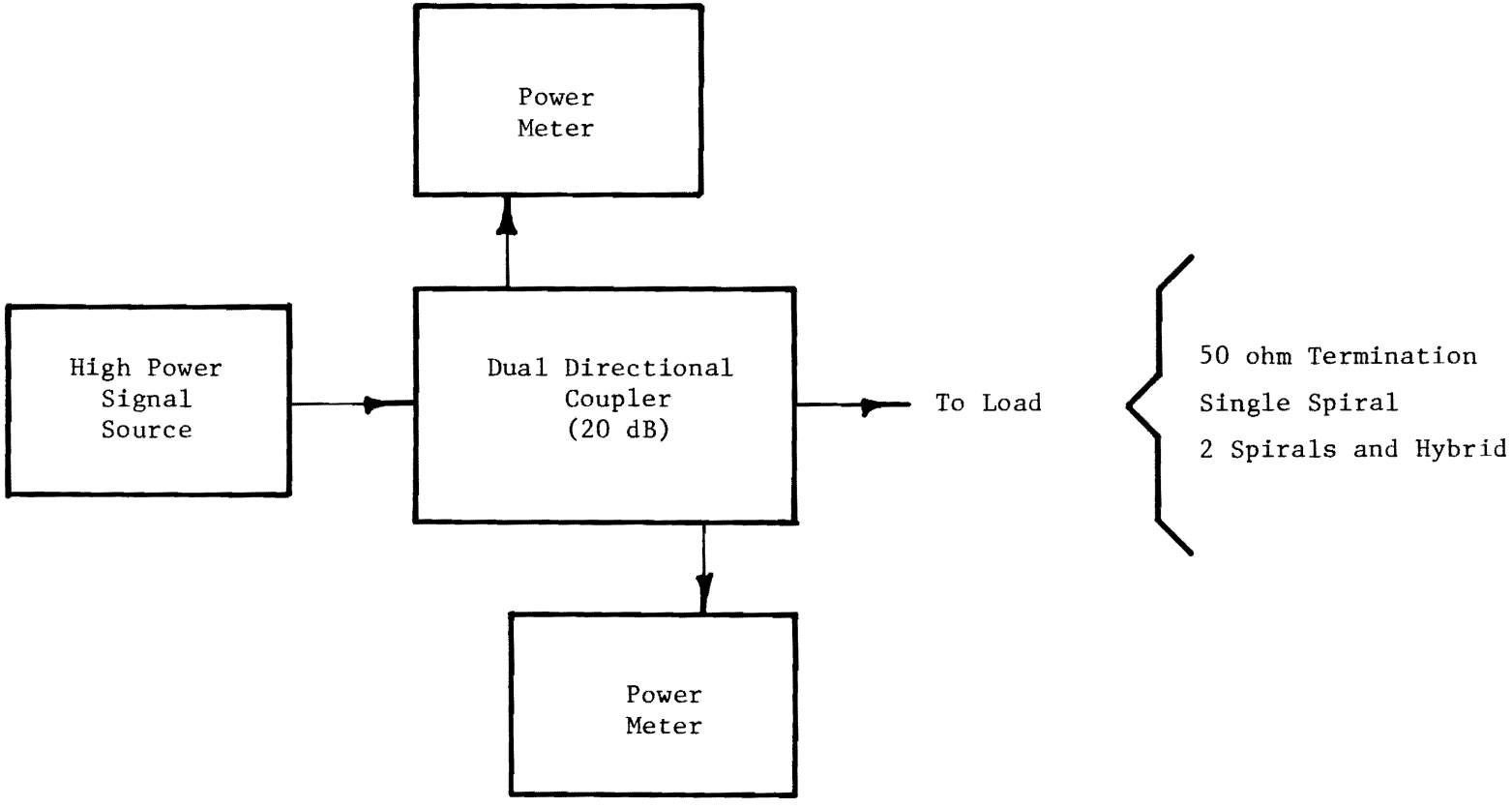

Figure 51. Block Diagram for High Power Antenna Tests.

high power source was connected to the input of the four-port hybrid and the incident and reflected powers to the hybrid-antenna system were recorded. The incident power was increased slowly from zero power to 20 watts.

The power handling measurements were performed with the antennas mounted on the full-scale model and the sequence was as follows:

a. Measured incident and reflected power of a high power 50 ohm termination - CW.
b. Measured incident and reflected power of a high power 50 ohm termination - 30 kHz FM.
c. Measured incident and reflected power of a single spiral - CW.
d. Measured incident and reflected power of a single spiral - 30 kHz FM.
e. Measured incident and reflected power of hybrid - 2 element spiral configuration - CW.
f. Measured incident and reflected power of hybrid - 2 element spiral configuration - 30 kHz FM.

These data were plotted and are presented in Figures 52 through 57. No adverse effects were noted as the power level was increased to at least 20 watts. This was expected since the hybrid junction and antennas were designed to handle much higher power levels.

F. Mechanical Considerations

The mechanical design effort was performed to insure that the transmitting spiral antennas chosen for use on the SERT-C satellite will perform properly in the space environment. The antennas procured for this purpose meet the microwave performance requirements and surpass the environment specifications of MIL-E-5400. The mounting arrangement for the antennas must have the inherent capability of meeting the physical constraints imposed by the satellite environment with adequate strength and without excessive weight or manufacturing cost. Of course, the antenna mount must not inhibit the transmitting capability of the antennas.

A cross-sectional drawing of the antenna mounting arrangement appears in Figure 58. This design provides access to the antennas from the exterior of the satellite. Effective electrical isolation is provided by use of a

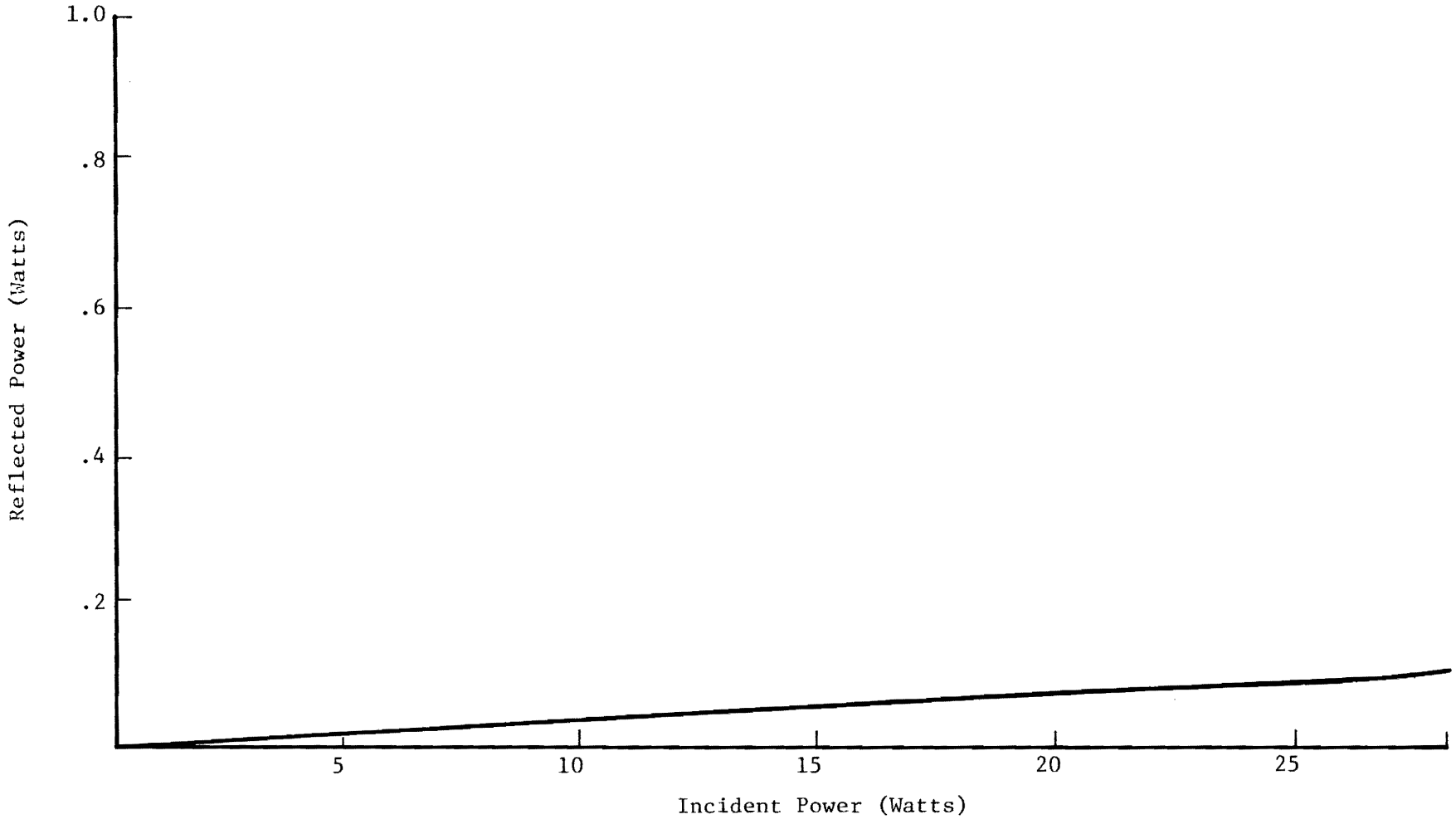

Figure 52. Incident vs. Reflected Power for 50 ohm Load Termination CW.

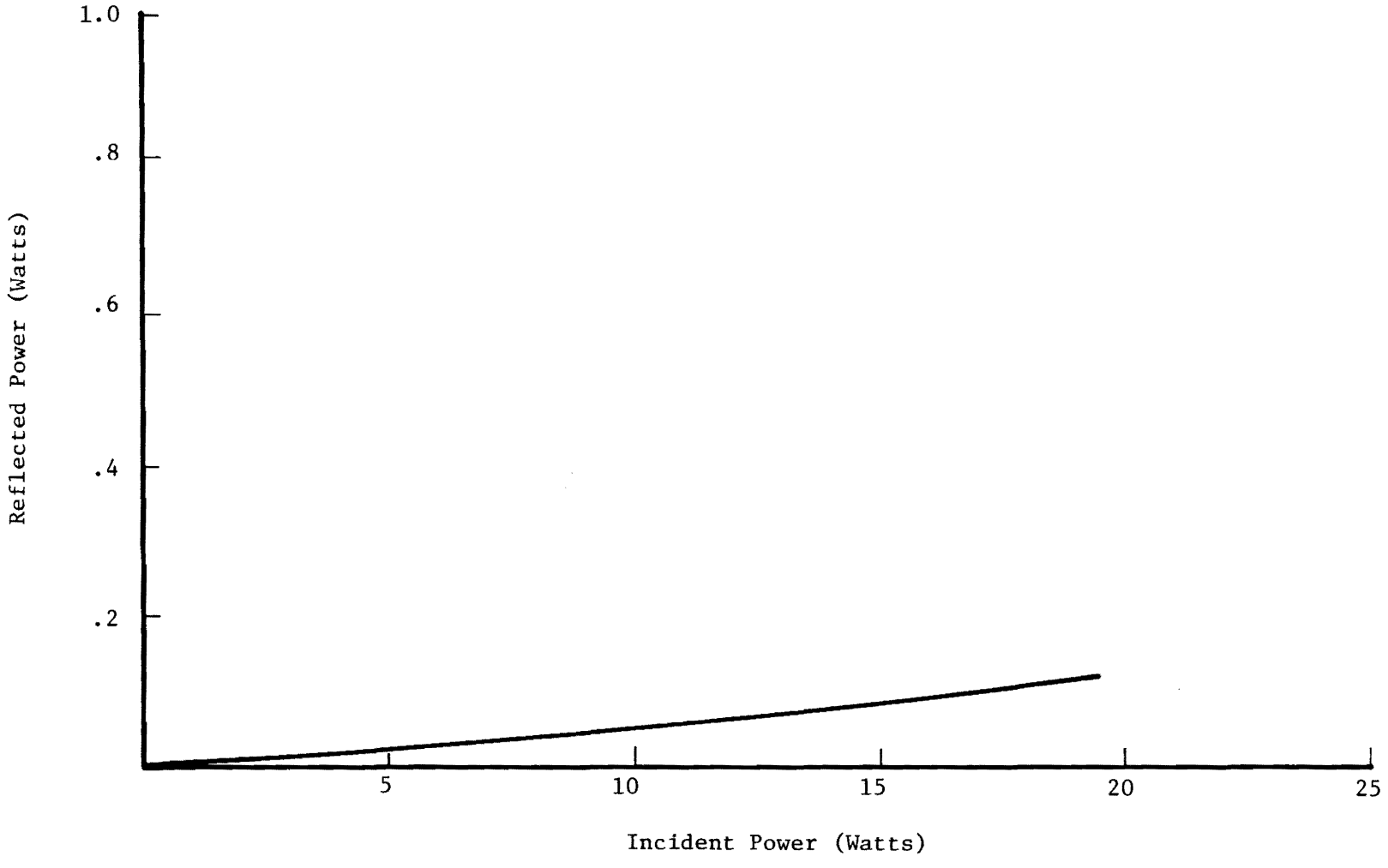

Figure 53. Incident vs. Reflected Power for 50 ohm Load
30 kHz FM.

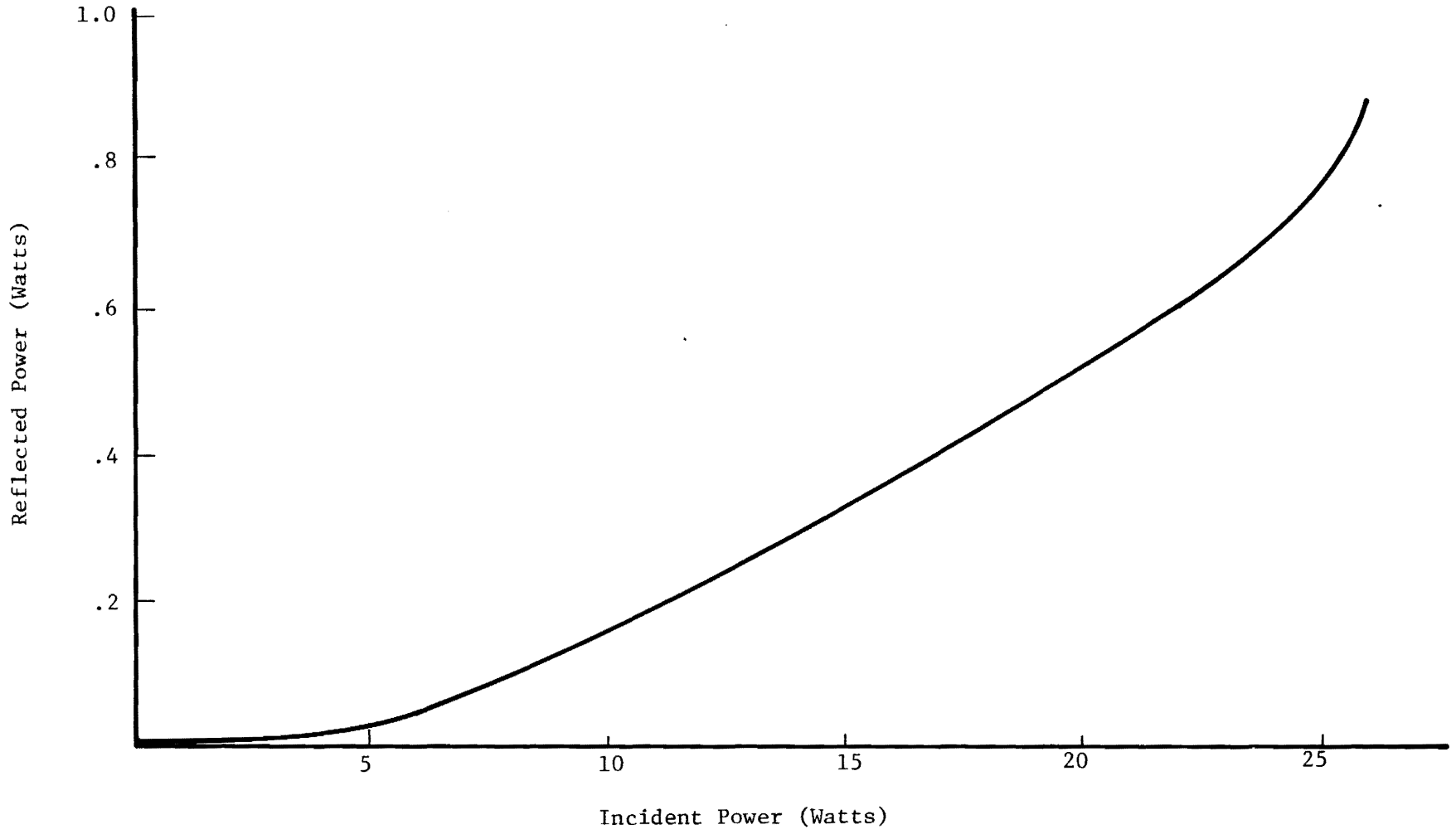

Figure 54. Incident vs. Reflected Power for Single Spiral CW.

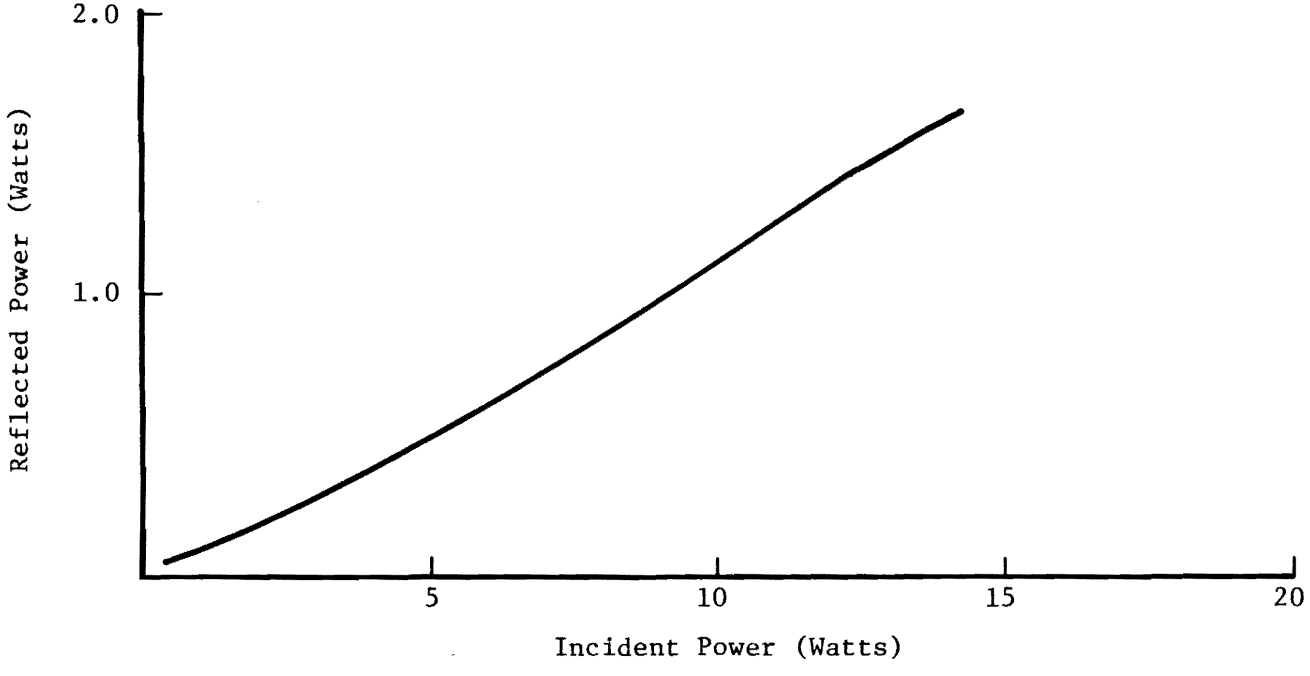

Figure 55. Incident vs. Reflected Power for Single Spiral 30 kHz FM.

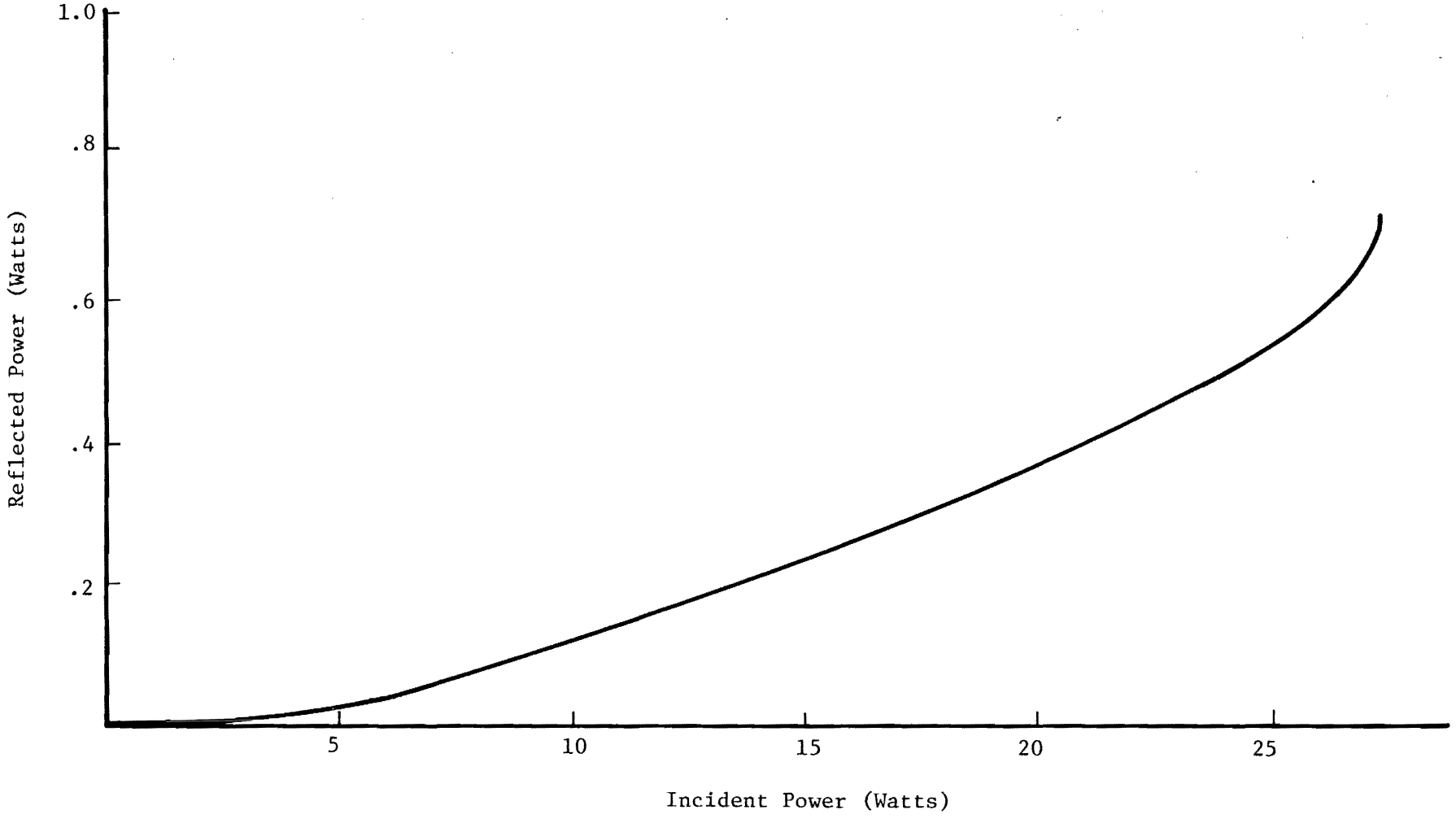

Figure 56. Incident vs. Reflected Power for Both Spirals CW.

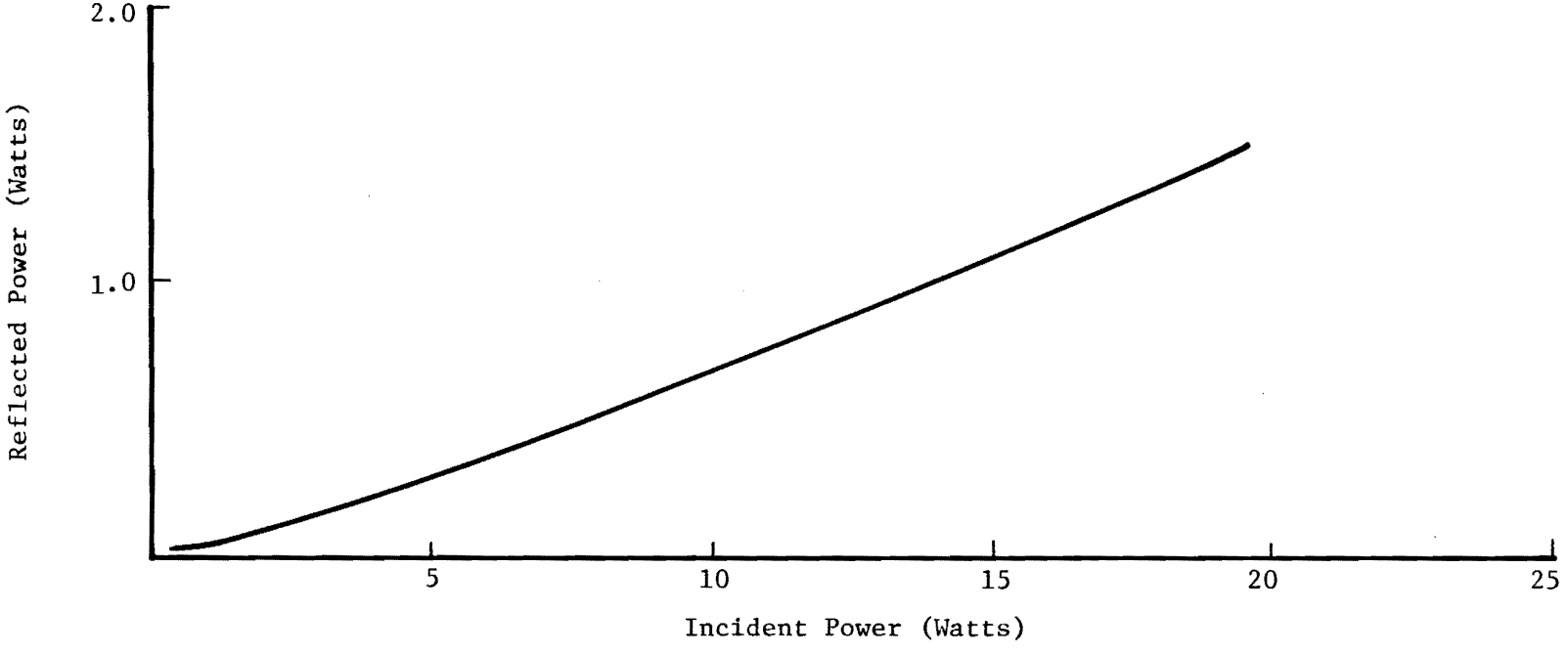

Figure 57. Incident vs. Reflected Power for Both Spirals 30 kHz FM.

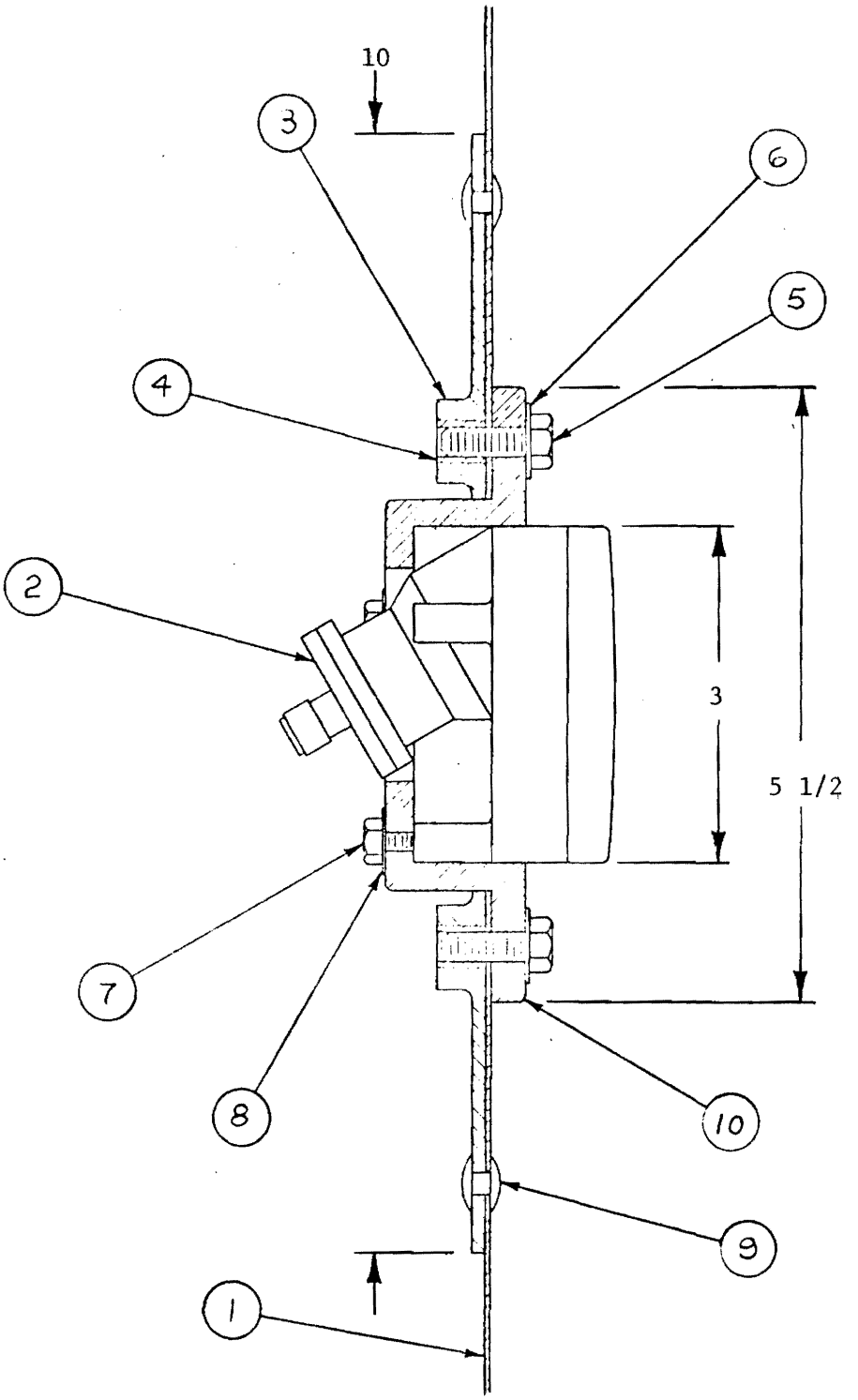

CIRCULAR CROSS SECTION

1. METEOROID SHIELD
2. SPIRAL ANTENNA
3. WALL DOUBLER
4. KEENSERT
5 & 7. WIRE-LOCK SCREWS
6 & 8. CONICAL LOCKWASHERS
9. RIUETS
10. ANTENNA MOUNT

FIGURE 58

SERT-C SPIRAL ANTENNA MOUNT

nylon mounting adapter. An aluminum wall doubler stiffens the meteoroid shield in the area of the antenna and provides the necessary attachment surfaces.

The estimated weight of the antenna and mount are as follows:

Spiral antenna	0.227 kg (0.50 lbs.)
Mount Adapter (nylon)	0.154 kg (0.34 lbs.)
Wall Doubler (aluminum)	0.409 kg (0.90 lbs.)
Screws (stainless steel)	0.018 kg (0.04 lbs.)
Rivets (aluminum)	0.005 kg (0.01 lbs.)
Total	0.813 kg (1.79 lbs.)

The two spiral antennas will add approximately 1.625 kg (3.6 lbs.) to the weight of the satellite. The hybrid junction and cabling will add 0.23 kg (0.5 lbs.) to the weight for a total system weight of 1.855 kg (4.1 lbs.).

The structural design of satellite hardware is governed by such factors as accelerations, thermal stability, vibrations, materials, compatibility, and shock. The primary loads experienced by the antenna are the vibratory and static accelerations from the launching engines. Secondary loadings arise from stage separating, engine acoustic pressures and maneuvers. The acceleration loading provided by the booster rarely exceeds 20g and lateral thrust rarely more than a one g peak. Design levels of 30g and 3g laterally are used. For shock, it is believed that the amplitude rarely exceeds 40g, or the duration more than 20 msec. This max-max combination almost never occurs [12].

Taking a maximum load of 40g the rivets must sustain a force of 1.79 lbs x 40g = 71.6 lbs. The 5/32 diameter rivets used can withstand a load of 750 pounds each. Eight rivets are used to insure that the assembly does not translate or vibrate independently of the SERT-C meteoroid shield.

The thermal environment seen by the antenna system orbiting about the earth is determined mainly by (1) the direct solar radiation (442 BTU/hr.ft^2); (2) the reflected solar radiation or albedo, of the earth (172 BTU/hr.ft^2); (3) the emitted radiation of the earth (65 BTU/hr.ft^2); (4) R.F. heat generation within the antennas and (5) conduction heat transfer paths to the satellite [13]. The relative magnitude of the various heat transfer

mechanisms determines the cyclic temperature variation of the antennas. For design purposes an extreme range of $-200^{o}F$ to $+200^{o}F$ is used.

The fact that different materials expand or contract at different rates with temperature change will create problems in the antennas and their mountings. The significant material property to be considered is the coefficient of thermal expansion, α. The coefficient related expansion to temperature change by the relation:

$$\delta = \alpha L \Delta T,$$

where

δ = thermal expansion (in.)

α = coefficient of thermal expansion ($in/in\text{-}^{o}F$)

L = original length (in.)

ΔT = temperature change (^{o}F).

For the materials being used

$\alpha = 4.5 \times 10^{-5}$ for type 6/6 nylon

$\alpha = 12.8 \times 10^{-6}$ for aluminum

Nylon expands 3-1/2 times as much as aluminum. The antenna is aluminum, the mounting adapter is nylon. If the temperature drops from $70^{o}F$ to $-200^{o}F$ the antenna diameter will decrease to

$$3 \text{ in} + \delta = 3 \text{ in} + 12.8 \times 10^{-6} \text{ (3 in.)}(-270^{o}F) = 2.99 \text{ in.}$$

For the same temperature change the diameter of the nylon mount will decrease to

$$3 \text{ in} + \delta = 3 \text{ in.} + 4.5 \times 10^{-5} \text{ (3 in)}(-270^{o}) = 2.96 \text{ in.}$$

There is an interference of 2.99 in. - 2.96 in. = 0.03 in. The hole in the nylon mount adapter is therefore machined to a diameter of 3.030 to avoid compressive stresses in the antenna. For the nylon adapter mounted in the aluminum wall doubler, the 3.5 in. diameter requires a hole of 3.014 in. for a temperature rise of $130^{o}F$. Likewise the three antenna mounting

holes are machined 0.004 in. oversize to avoid bending stresses in the antenna mounting legs.

The properties of type 6/6 nylon are:

Dielectric constant, 60 Hz	4.2
Tensile strength	11,800 psi
Specific gravity	1.14
Specific heat	.72 BTU/lb.
Linear coefficient of thermal expansion	4.5×10^{-5} in/in-^{o}F
Thermal conductivity	1.7 BTU in/hr.-ft^{2}-^{o}F
Melting point	490^{o}F
Water absorption, 24 hr.	1.5%

Prolonged exposure to solar ultraviolet and X-ray radiation can cause embrittlement, softening, and changes in electrical properties of plastics. Also to be considered are the effects of Van Allen and Solar Wind proton, electron, and alpha particle impingement and rocket exhaust plume contaminants. Nylon has been recommended for use as machined forms for spacecraft antennas. It has a radiation damage threshold of 5×10^{7} rads. Its ultraviolet and vacuum stability is fair.

III. RECOMMENDED CONFIGURATION

The antenna design has been previously described in Section II; thus this Section will serve as a summary of the design. Two high-power cavity-backed spiral antennas fed in-phase through a four-port hybrid device are proposed as the telemetry and command antenna system for the SERT-C spacecraft. This system meets all design specifications. The VSWR of the system is somewhat higher than desired but is typical of spiral antennas. The two-element antenna system provides fifty percent coverage of a 4π steradian angle with a gain level greater than -10 dBi. This can be enhanced by having the ground station change antenna polarization.

A photograph of the cavity-backed spiral antenna is presented in Figure 47. A drawing of the nylon mounting structure and antenna is shown in Figure 58. The antenna is 7.6 cm (3 inches) in diameter and weighs approximately 8 ounces. The weight of the antennas, mounting jackets, and hybrid junction is approximately 1.855 kg (4.1 lbs).

Each antenna is placed into the nylon jacket and the jacket is mounted to the spacecraft. A circular hole with sufficient clearance for the nylon mounting ring will need to be cut into the satellite skin (see Figure 58). The drawing of the nylon mounting jacket is shown in Figure 59.

The gain of the RHC polarization antenna system is -3 dB with respect to a linearly polarized radiator. Contour plots of the antenna system radiation patterns were presented in Figures 19 and 20. For comparison observe Figure 22 which is a contour plot for the two-element quadrifilar helix array. The coverages are very similar for the two antenna systems. The polar plots of the antenna system radiation patterns are presented in Appendix III. An analysis of the polar plots and/or the radiation pattern contour plots indicates deep nulls occurring at the angles shown in Table V.

At first glance it would seem that this is relatively poor coverage, but if you consider the case of opposite polarization, LHC, then these nulls are filled in and the percent coverage is increased significantly. Comparisons of the polar plots of Appendix III lead to this conclusion.

The scale model measured results compared favorably with the predicted pattern data, although the solar panels did shadow the signal more than

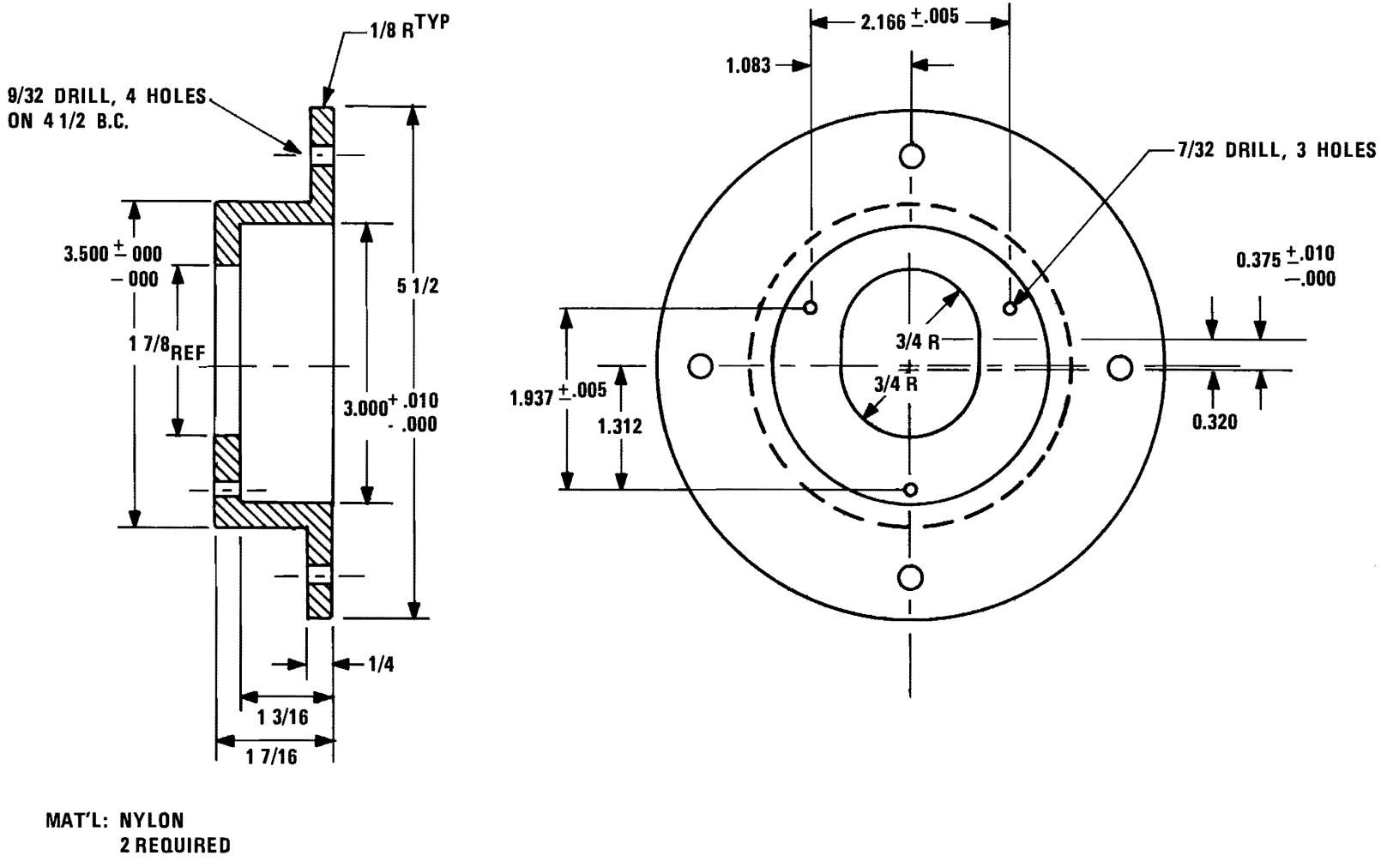

MAT'L: NYLON
2 REQUIRED

Figure 59. Antenna Mounting Bracket - Nylon.

TABLE V

LOCATION OF NULLS IN RADIATION PATTERNS OF TWO-ELEMENT SPIRAL ARRAY (RHC)

θ (deg)	ϕ (deg)
10	25
25	10, 22
30	185
50	180
75	194, 352
80	195, 352
105	188, 346
120	192, 342
145	348
160	172, 185
170	165, 355
178	52, 206

anticipated for the two-element quadrifilar array. The panels caused a scalloping effect on the radiation patterns. Based on measured data there is a 50 percent probability that the gain is greater than -10 dBi over a 4π steradian angle for the two-element array of cavity-backed spirals.

The antenna element can be painted with a non-metallic paint that will reflect a major portion of the incident rays of the sun and, thus, the temperature cycling effects are minimized. Also, the antenna element will withstand 100 watts of CW power, which is a good indication that it will withstand fairly high temperatures. The antenna mounting bracket is fabricated from nylon, which is an excellent material for use on exterior surfaces of spacecraft (see Section II.F.)

IV. CONCLUSIONS

A number of general conclusions can be drawn from the results of this program:

(1) The scalar technique of computing radiation patterns proved a useful method for large beamwidth antennas mounted on large structures. (The scalar technique is a low cost computation method as compared to the moment method and the geometrical theory of diffraction (GTD) technique).

(2) Two-element arrays of cavity-backed spirals meet the radiation pattern coverage considerations, whereas, the solar panels reduced the coverage of the two-element quadrifilar helix to an unacceptable level. The quadrifilar helix has a 5-10 dB pattern taper whereas the spiral has a 10-20 dB taper. The spiral array provides a gain greater than -10 dBi over 50 percent of a 4π steradian angle.

(3) The coverage is increased significantly if the ground station has the capability to change polarization from RHC to LHC or to elliptical polarization (polarization diversity).

(4) The quadrifilar helix element had a bandwidth (VSWR $\leq$ 1.5:1), less than 10 percent. The cavity-backed spiral bandwidth is much greater although the VSWR is near 1.5:1. The two-element array of cavity-backed spirals was chosen because of its bandwidth and its radiation pattern characteristics.

(5) The solar panels produce more diffraction effects than shadowing effects. The overall radiation pattern coverage of the two-element spiral array was not decreased significantly by the solar panels. The solar panels do not affect system VSWR.

(6) Scale model techniques have proved to be an effective method of obtaining radiation pattern data from antennas mounted on large bodies.

(7) It is recommended that at least two ground stations maintain communications with the satellite during its orbit raising

period. It is strongly recommended that the ground stations possess the capability to change polarizations.

(8) The antennas are essentially flush-mounted and thus the 30-cm ion engine exhausts should not affect antenna operation.

(9) The antennas are mounted so that the connecting cables are accessible external to the spacecraft.

APPENDIX I

Athena H and Apollo S-Band Omnidirectional Antenna Systems

S-BAND ANTENNA SYSTEMS

A number of pertinent published articles are listed in the Bibliography, Section VI. As a sampling of these, consider the following past efforts to provide omnidirectional coverage at S-Band frequencies [ref. 5].

> "The following paragraphs, narrating the history of the antenna system for the Athena H are presented to illustrate the moral that when numbers of antennas are discussed, 'more is not necessarily better.'
>
> In March 1969, Granger Associates, then Dorne and Margolin, Inc., submitted a proposal to Atlantic Research Corporation outlining a design for the S-band antenna system for the Athena H Missile.
>
> A set of six slanted monopole elements arrayed circumferentially around the missile was proposed. The diameter of the missile in the area available for antenna mounting was 40", or 7.6λ. The elements would be fed to produce a phase rotation which would result in right hand circular polarization in the direction of vehicle travel, and left hand circular in the opposite direction. It was thought, at the time, that three of the six elements would be fed at a reduced power level in an attempt to lessen the effect of complete cancellation in certain directions. It was predicted, however, that sectors would remain, both fore and aft, in which the amplitude and phase summation would result in circular polarization of the sense opposite to that desired, and so a polarization diversity system at the ground receiving station was suggested.
>
> The six-element S-band system produced a multilobed pattern, as expected. The attempt to reduce null depth by feeding alternate elements with reduced power produced inconclusive results, however, mainly because the changes in the patterns were slight and difficult to analyze as relative power levels were changed. It was then decided to try a three-element array, with the surprising result that the null structure with only three antennas was better than with six. Coverage from the statistical or percentage-area point of view, was also improved.
>
> The coverage of the three-element system was very good. The patterns showed somewhat the same gain in the forward direction as in the aft direction with the major nulls located in the roll plane between Θ = 80° to θ = 100°. The critical area where more coverage is preferred is in the forward cone, θ = 0° to θ = 60° where the vehicle is acquired by the down range receiving station as the vehicle comes over the horizon.

The possibility of obtaining adequate pattern coverage with half the originally contemplated number of antenna elements was very attractive, for this approach permitted two three-element antenna systems to be installed allowing 100 percent redundancy of S-band telemetry with the use of two transmitters and without the need for a diplexer. (It is of interest to note that three antennas and associated cables and power divider weigh less, and cost less, than a diplexer.) Additional patterns were run for the R and D telemetry antenna system, which is located forward where the diameter of the vehicle is 24". The investigation here started with a three-element array and ended with a two-element array. The two-element array provided sufficient coverage and was thus chosen. Thus, 'more is not necessarily better'."

Also, consider the Apollo S-band omnidirectional antenna system as taken from Reference 6:

"Patterns of the Apollo S-band omnidirectional antenna system were taken at the NASA Manned Spacecraft Center to help establish the signal strength margins between the Apollo spacecraft and the Manned Space Flight Network ground stations. The function of the antenna is to provide two-way Doppler tracking, and pseudorandom-noise ranging; up-link voice and up-data on the spacecraft receive frequency of 2106.4 MHz; and down-link voice, telemetry, and data information on the spacecraft transmit frequency of 2287.5 MHz.

Patterns of a full-scale model were taken to achieve greater accuracy and higher reliability. The four omnidirectional antennas are flush mounted on the side of the command module, which is covered with ablation material to keep the interior of the vehicle cool enough so that the three astronauts will survive the heat of reentry. When patterns were first taken using a 1/3-scale model, the ablation material that consisted of plastics and resins could not be reliably scaled with respect to the loss tangent and dielectric constant. In addition, the difficulty in obtaining mechanical tolerances resulted in significant pattern errors. Full-scale data were measured with ablation material in the uncharred and charred conditions, since communication is required both before and after reentry.

The following spacecraft configurations were tested:

(1) Command module (CM)
(2) Command and service module (CSM)
(3) CSM/lunar module (LM) ascent stage only (docked)
(4) CMS and LM (docked)

The four antennas which were tested are quartz-embedded, cavity-backed helices manufactured by Amecom, Inc., Division of Litton Industries.

The antenna is covered with ablative material 0.7 inches thick. The four antennas are located at the maximum radius point of the CM at station X = 20.766 inches for roll position of ϕ = 45°, ϕ = 135°, ϕ = 225° and ϕ= 315°. The recessed or hot-side antennas are located at ϕ = 135° and ϕ = 225°, near the positive Z-axis of the spacecraft. The cold-side antennas are flush mounted with the surface of the ablator and are located at ϕ = 45° and ϕ= 315°. To simulate the dielectric effects of the ablator, a special cork material was used. The dielectric properties of the heat shield at S-band are δ = 1.85 and tan δ = 0.022. The entire CM, except for a 7.5-inch radius circle around each of the two hot-side antennas, is covered with a conductive coating. Aluminum foil was used to simulate the conductive coating on the CM.

In measuring the radiation patterns for various spacecraft orientations, conical patterns were obtained by rolling the spacecraft about the X-axis (ϕ-variation) for fixed aximuth values of θ. The results of the measurements for the CSM configuration are shown in the partial contour pattern of Figure 60. The contour levels on the pattern enclose an area which has an absolute gain equal to or greater than the contour level specified referenced to a right-circularly polarized isotropic source. From the pattern, it is noted that the main beam occurs near the axis of the antenna around the θ= 90° and ϕ = 135° area and where the gain is 3.6 to 6.6 decibels. The approximate coverage from this antenna is in the second quadrant and ranges from ϕ= 90° to ϕ = 180°. In this region, the worst-case level in the nose region is near the positive X-axis and is seen to be -6.4 decibels. In the tail region near the negative X-axis, the worst case gain is -16.4 decibels. The patterns for the other configurations tested are similar to the one in Figure 60, except that the gains in the nose and tail regions are affected by the changes in module shadowing. For example, with the complete LM attached to the nose of the CM, the lowest level near the positive X-axis is reduced to -21 decibels.

The attachment of the SM to the CM causes a reduction of 12.4 decibels in the level near the negative X-axis (tail) from -4 decibels without the SM to -16.4 decibels with the SM."(The effects of vehicle shadowing to the gains are given in Table VI.)

After a review of other reports similar to the Athena H antenna and the Apollo antenna, it was decided that it would be appropriate to investigate a number of two-element and four-element arrays for the SERT-C satellite.

Table VI

SUMMARY OF MEASURED GAINS
FOR ANTENNA LOCATED AT $\Phi = 135°$

[Spacecraft Transmit Frequency = 2287.5 MHz]

Gain[a]	CM ONLY	SCM	CSM/LM ascent stage only	CSM/LM
Maximum-main beam	6.0	6.6	6.4	6.0
Worst case - nose (positive X-axis)	-5.0	-6.4	-9.6	-21
Worst case - tail (negative X-axis)	-4.0	-16.4	-16.6	-16

[a]The gains are in decibels and are referenced to a perfect right-circularly polarized isotropic level.

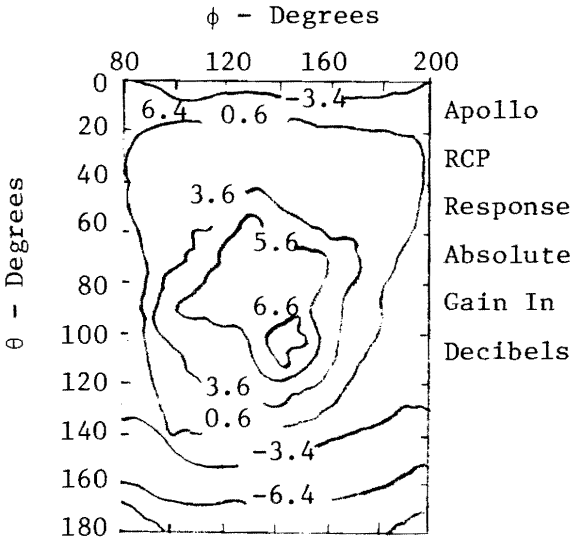

Figure 60. Representative CSM Pattern.

APPENDIX II

Calculated Radiation Pattern Coverage for 2-and 4-Element Arrays With/Without Solar Panels

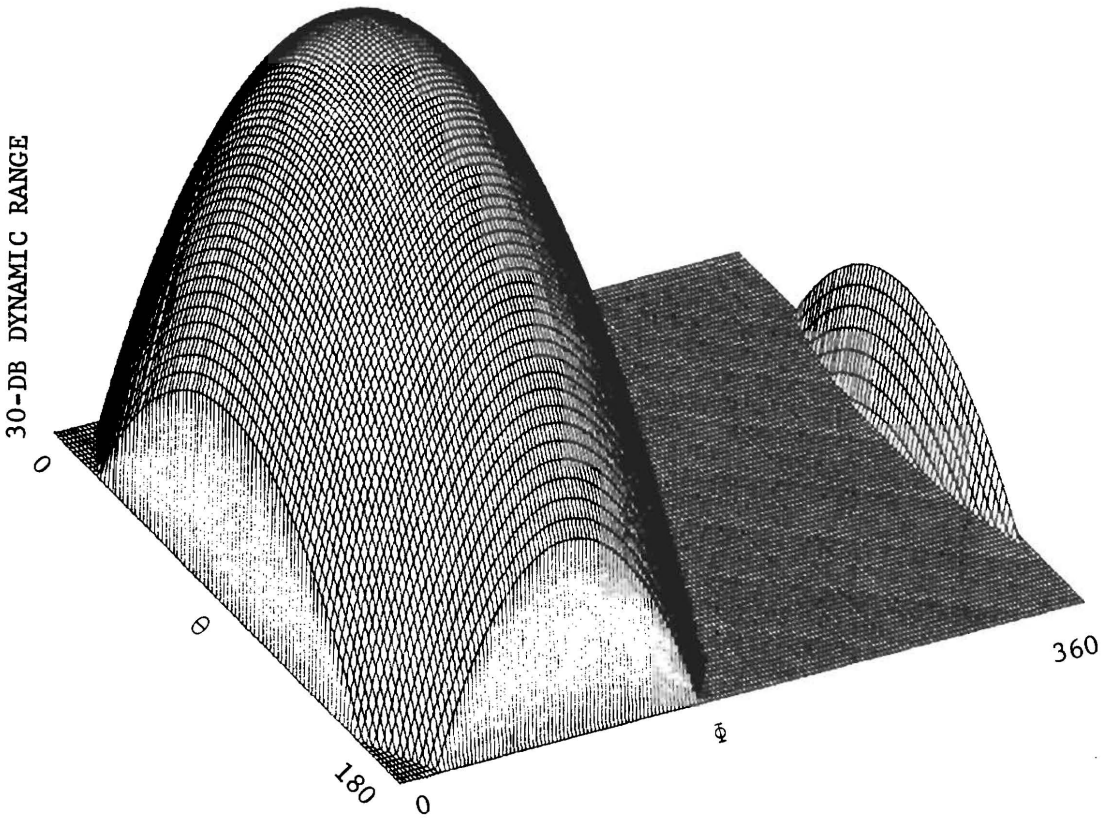

Figure 61. Calculated radiation pattern from a 1 element array located on the SERT-C satellite. The elements have a 20 dB taper 90^{o} away from boresight. The elements have θ - Φ pointing directions of (90, 90). Solar panel blockage was not included.

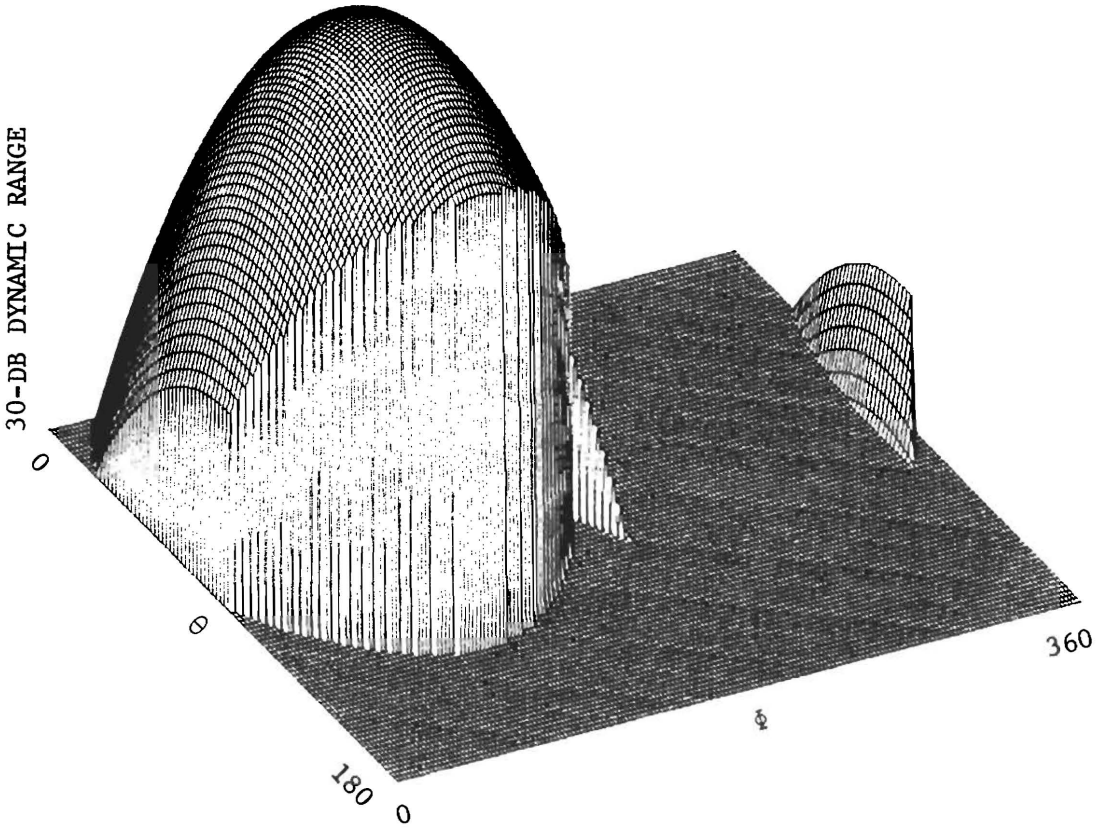

Figure 62. Calculated radiation pattern from a 1 element array located on the SERT-C satellite. The elements have a 20 dB taper 90^{o} away from boresight. The elements have θ - Φ pointing directions of (90,90). Solar panel blockage was included.

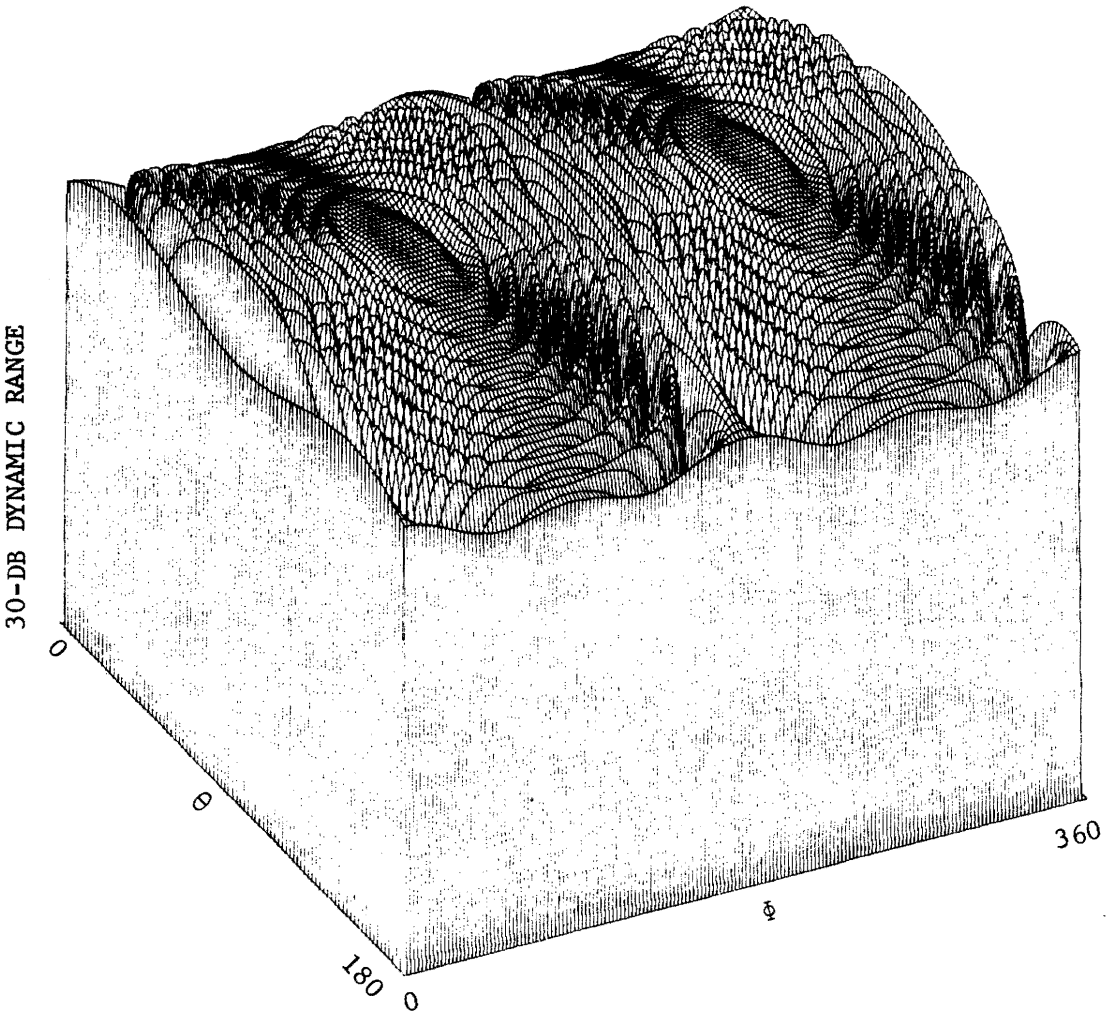

Figure 63. Calculated radiation pattern from a 2 element array located on the SERT-C satellite. The elements have a 5 dB taper 90° away from boresight. The elements have θ - Φ pointing directions of (90, 90) and (90, 270). Solar panel blockage was not included.

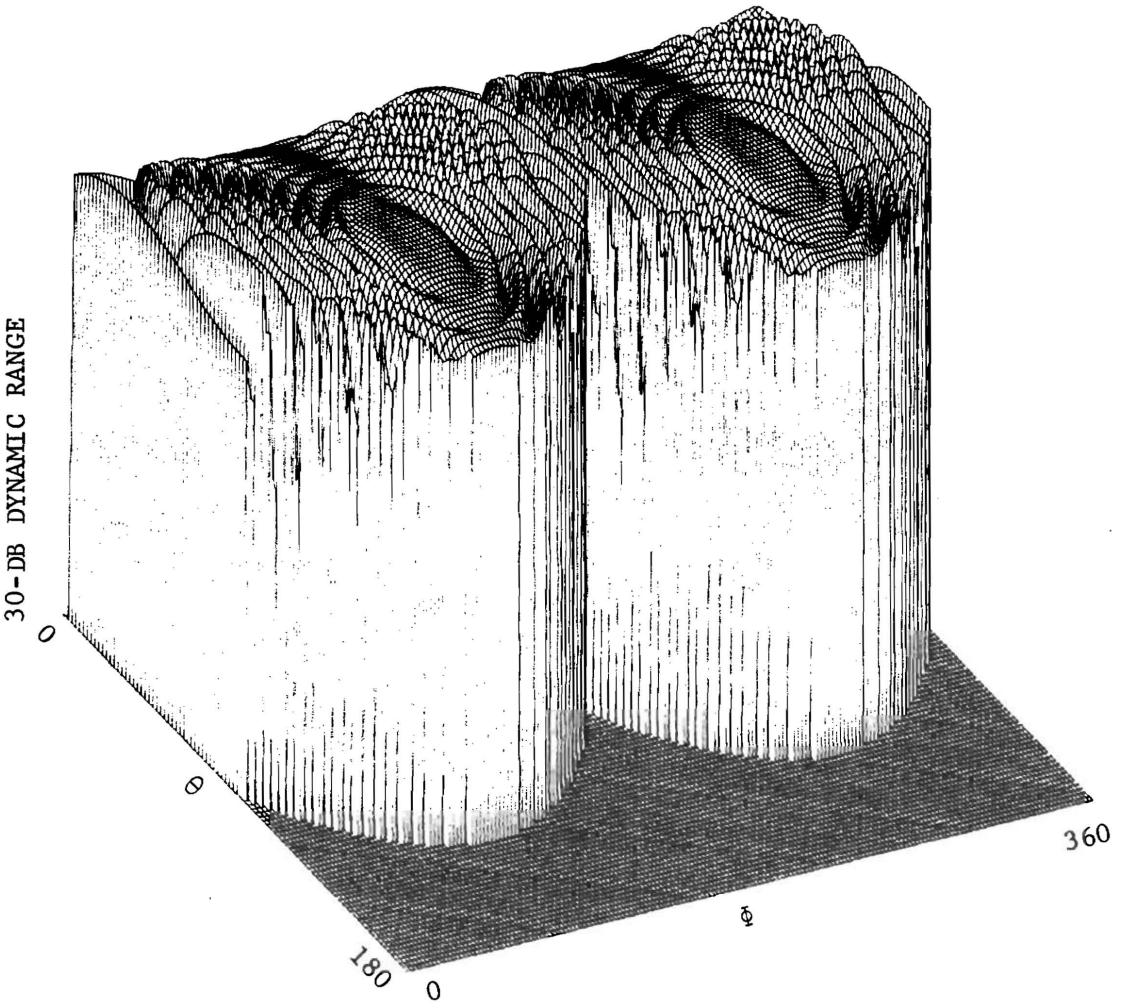

Figure 64. Calculated radiation pattern from a 2 element array located on the SERT-C satellite. The elements have a 5 dB taper 90° away from boresight. The elements have θ - Φ pointing directions of (90, 90) and (90, 270). Solar panel blockage was included.

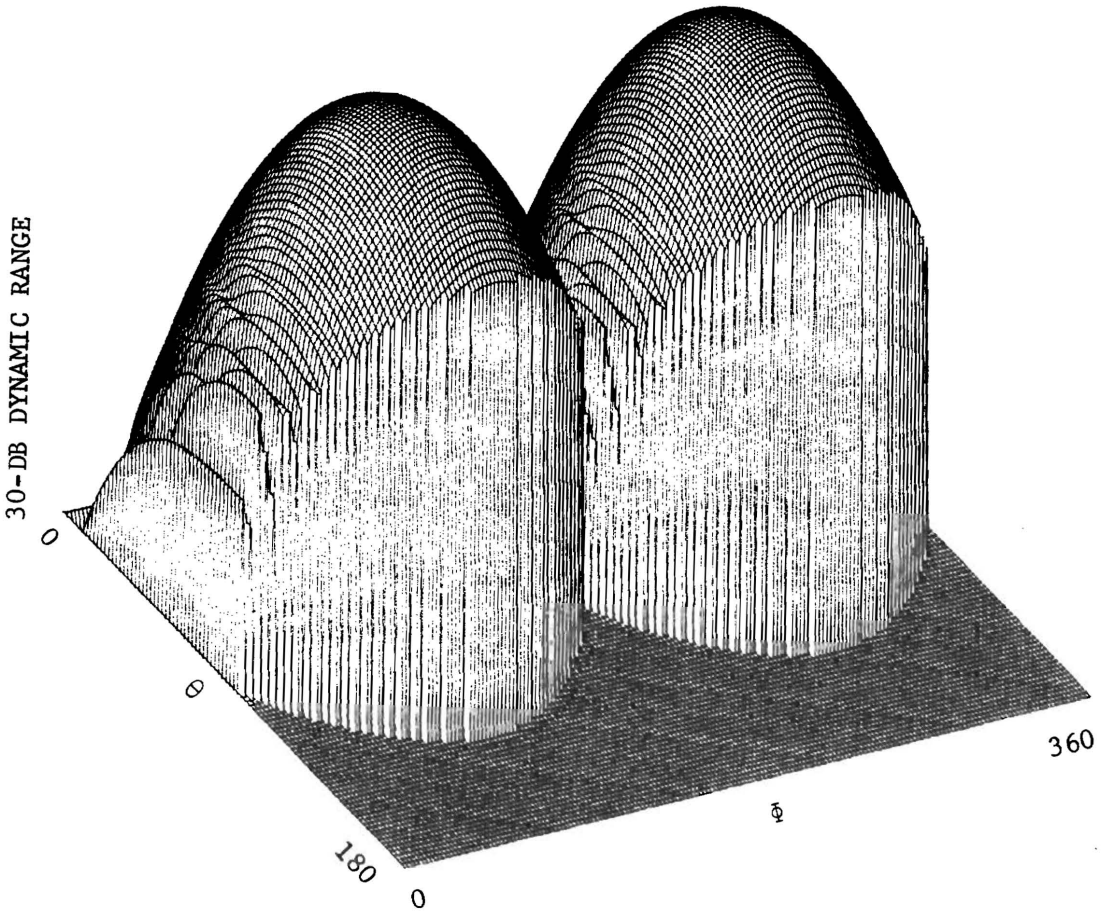

Figure 65. Calculated radiation pattern from a 2 element array located on the SERT-C satellite. The elements have a 20 dB taper 90° away from boresight. The elements have θ - Φ pointing directions of (90, 90) and (90, 270). Solar panel blockage was included.

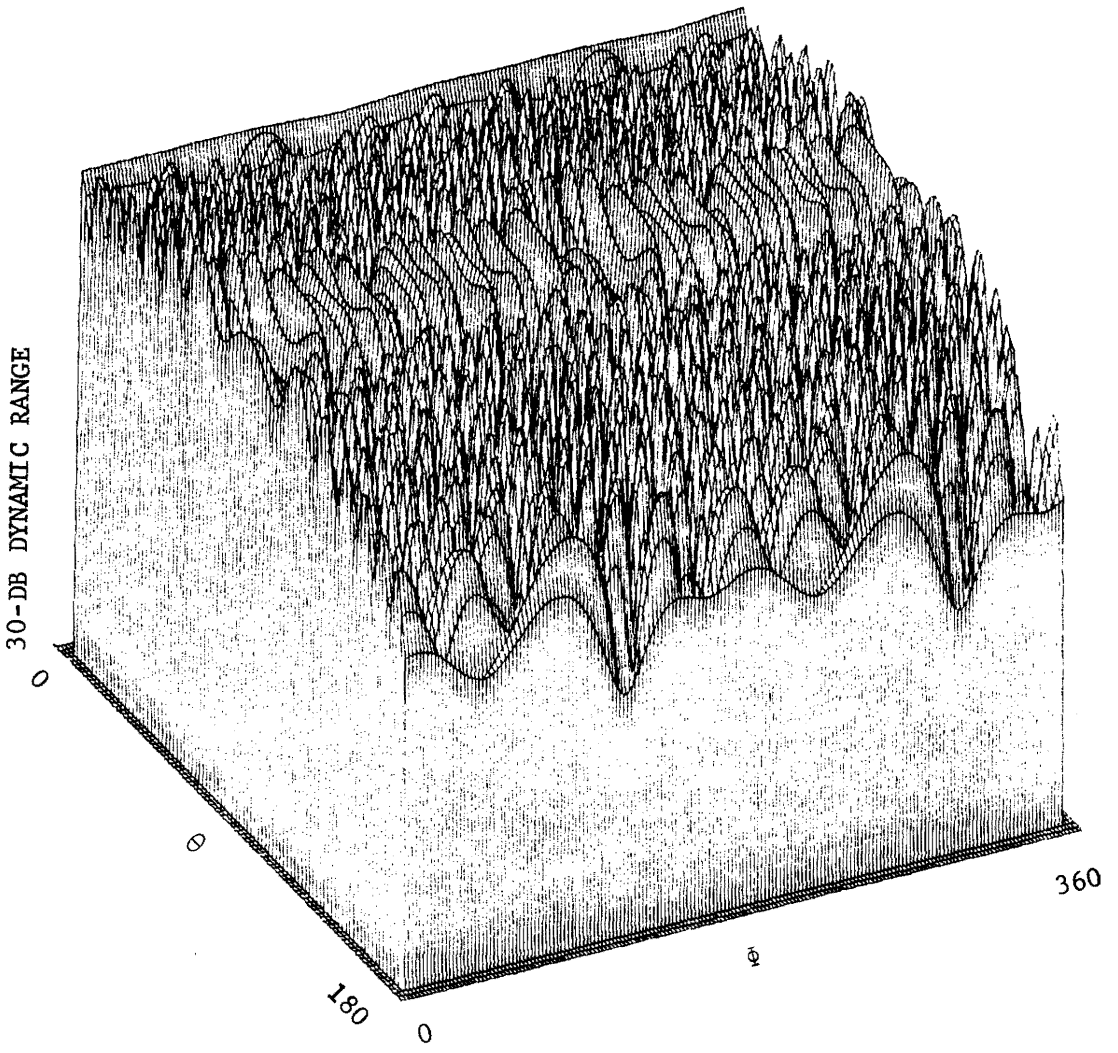

Figure 66. Calculated radiation pattern from a 4 element array located on the SERT-C satellite. The elements have a 5 dB taper 90° away from boresight. The elements have θ - Φ pointing directions of (90, 45), (45, 135), (90, 225), and (45, 315). Solar panel blockage was not included.

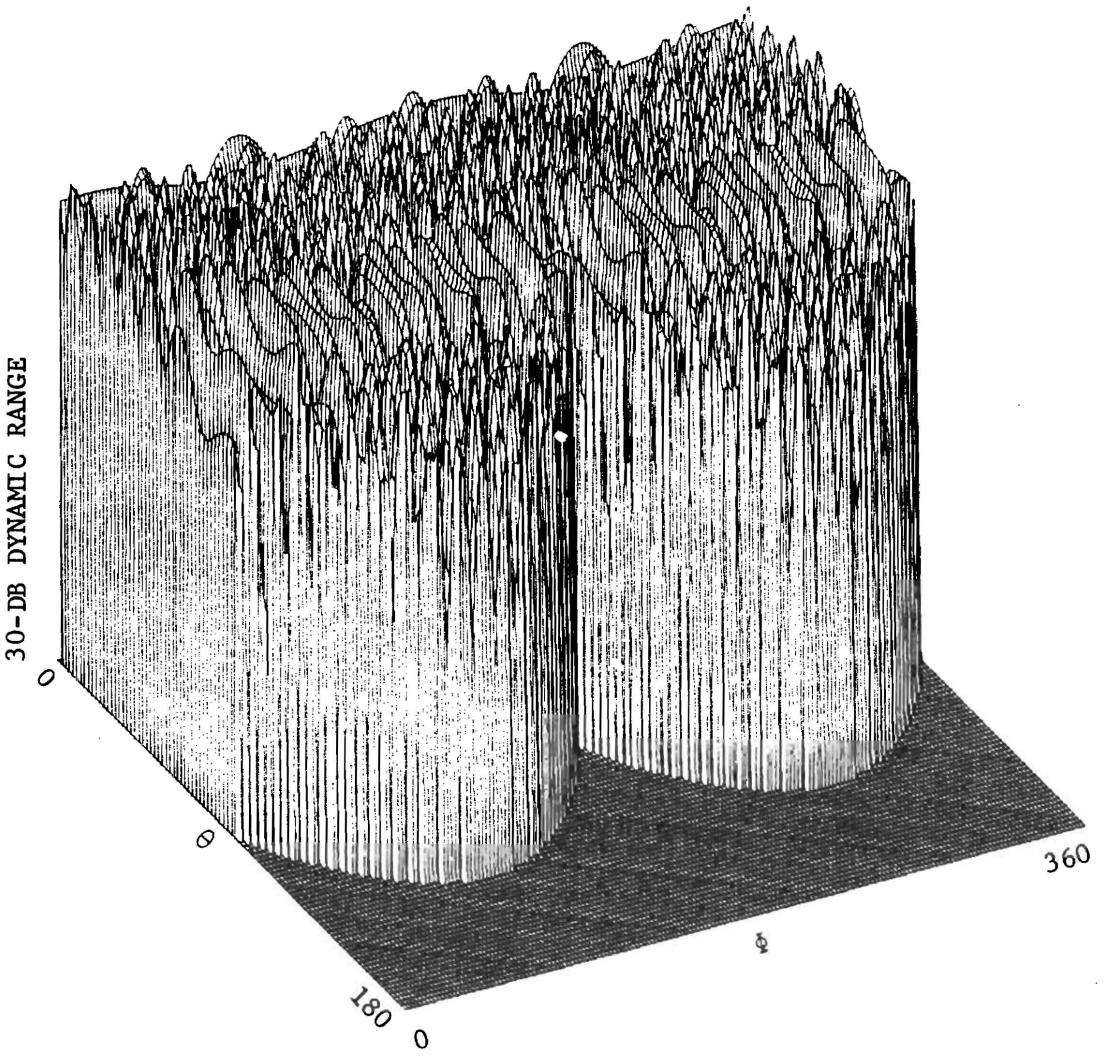

Figure 67. Calculated radiation pattern from a 4 element array located on the SERT-C satellite. The elements have a 5 dB taper 90° away from boresight. The elements have θ - Φ pointing directions of (90, 45), (45, 135), (90, 225), and (45, 315). Solar panel blockage was included.

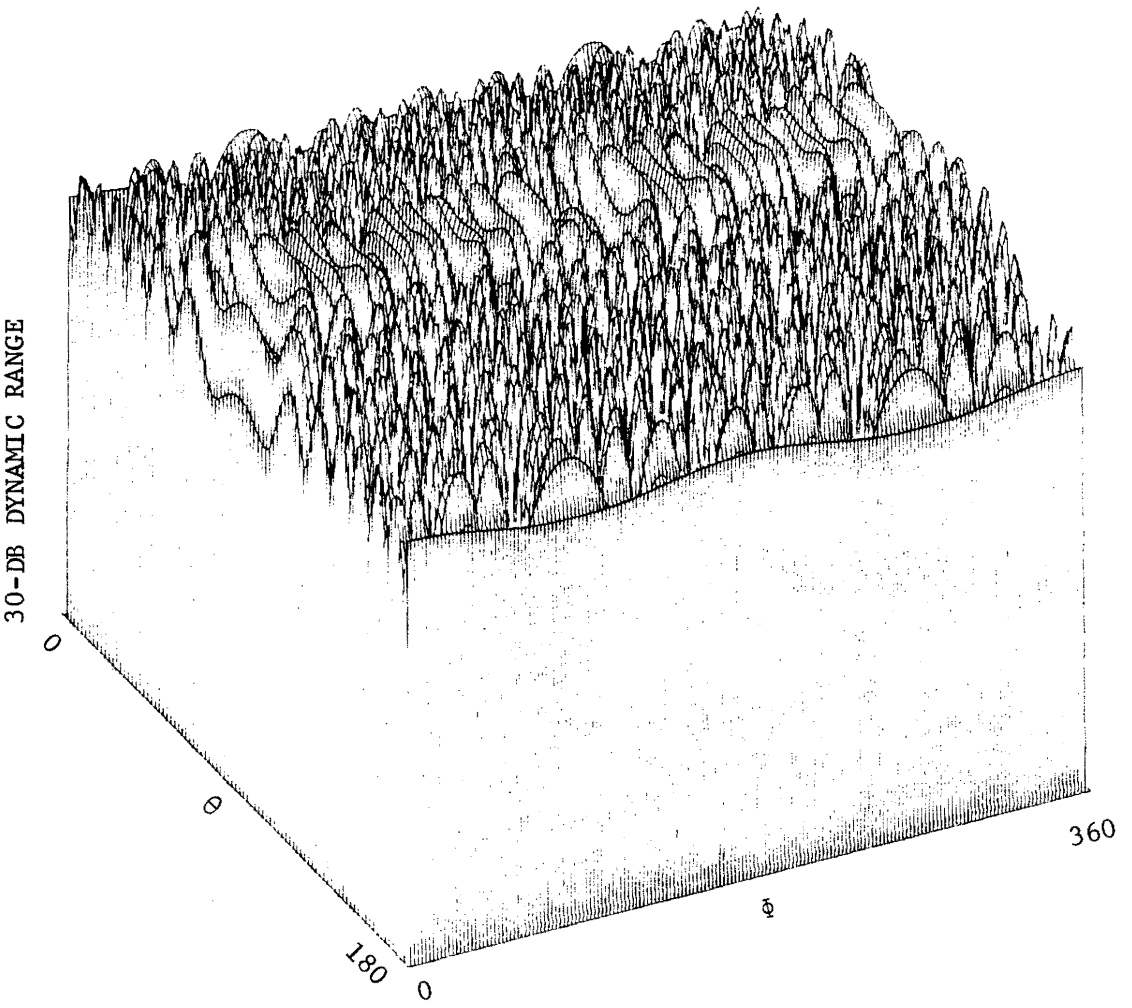

Figure 68. Calculated radiation pattern from a 4 element array located on the SERT-C satellite. The elements have a 5 dB taper 90° away from boresight. The elements have θ - Φ pointing directions of (90, 45), (90, 135), (90, 225) and (90, 315). Solar panel blockage was not included.

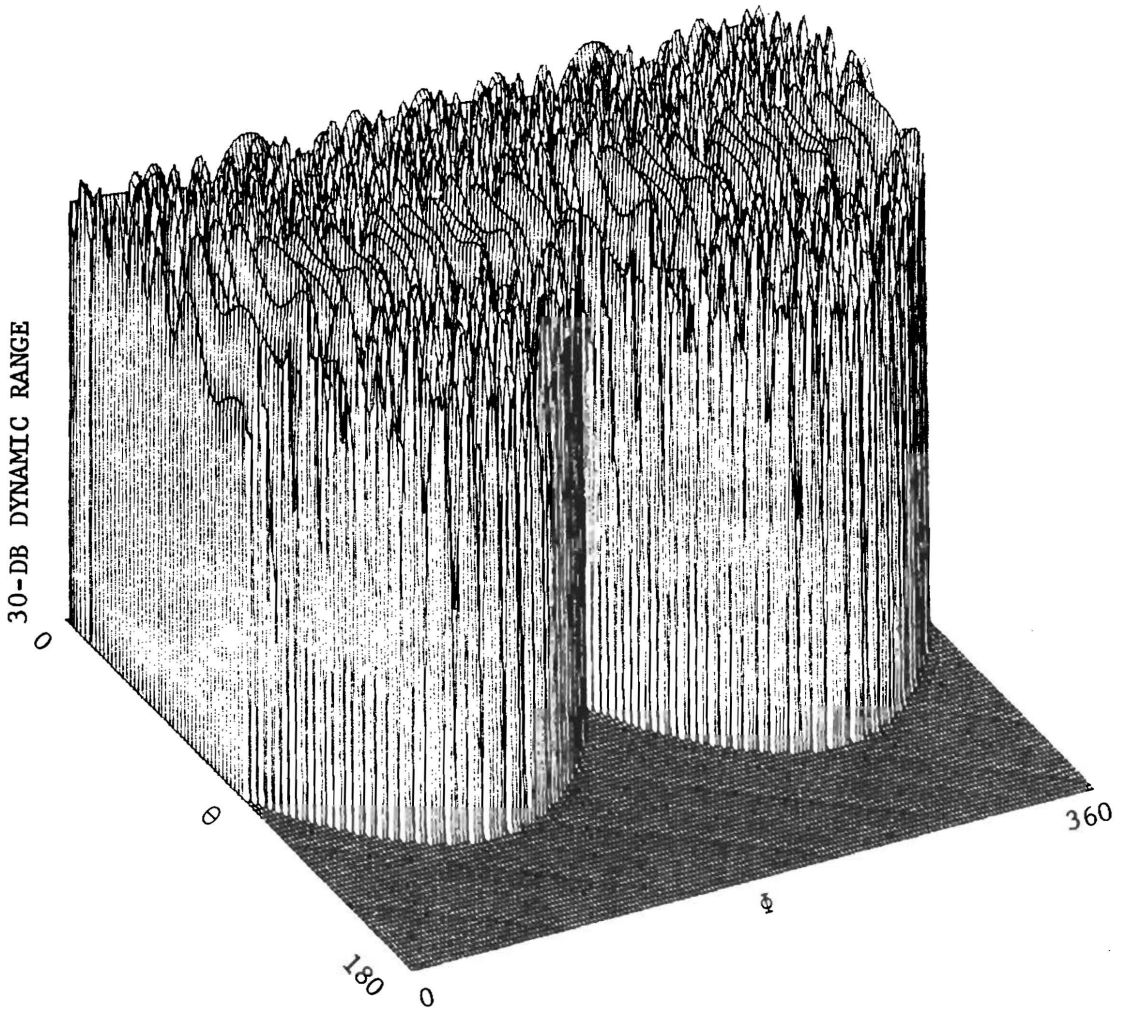

Figure 69. Calculated radiation pattern from a 4 element array located on the SERT-C satellite. The elements have a 5 dB taper 90^{o} away from boresight. The elements have θ - Φ pointing directions of (90, 45), (90, 135), (90, 225), and (90, 315). Solar panel blockage was included.

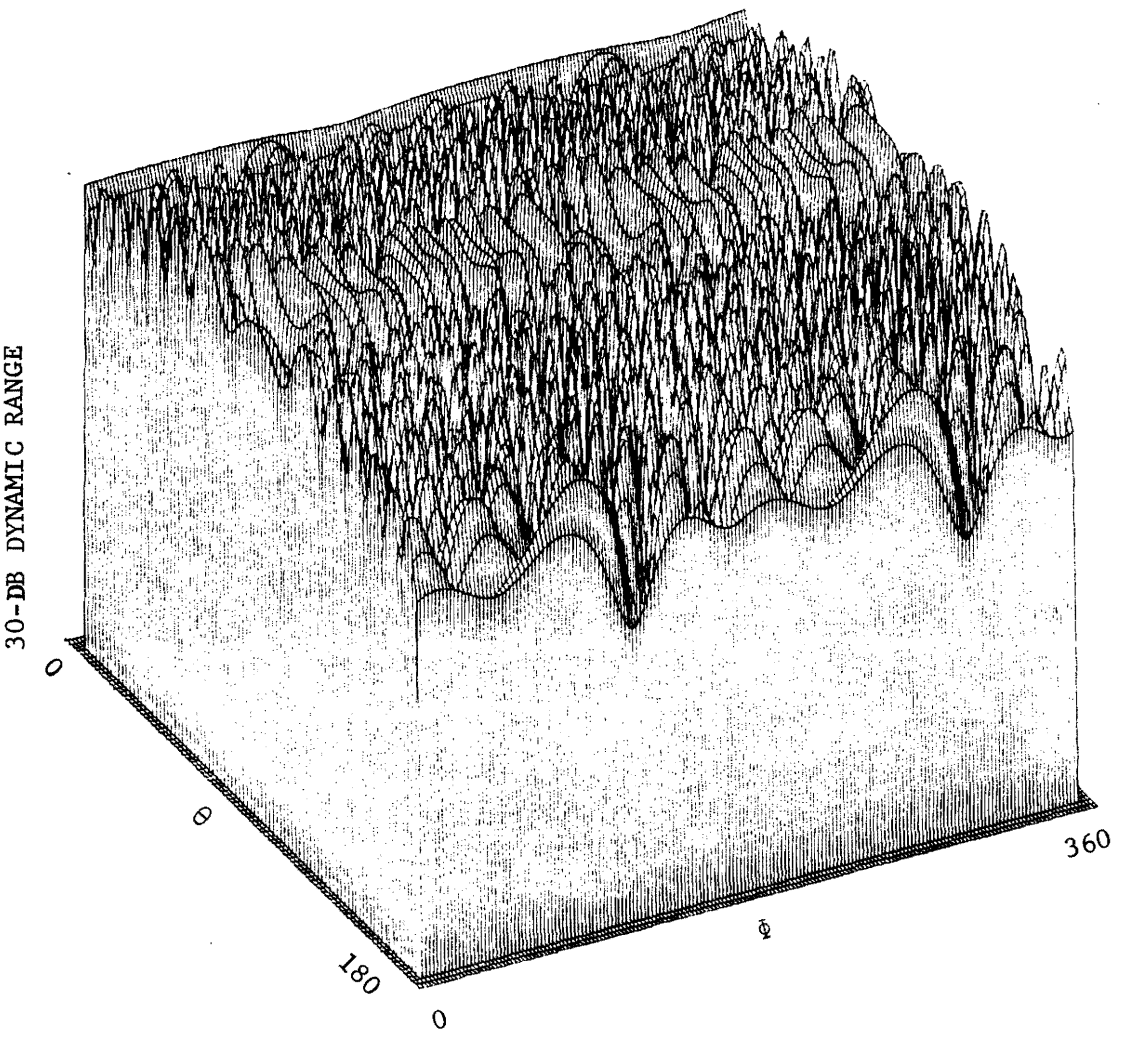

Figure 70. Calculated radiation pattern from a 4 element array located on the SERT-C satellite. The elements have a 5 dB taper 90^{o} away from boresight. The elements have θ - Φ pointing directions of (120,45), (45, 135), (120, 225), and (45, 315). Solar panel blockage was not included.

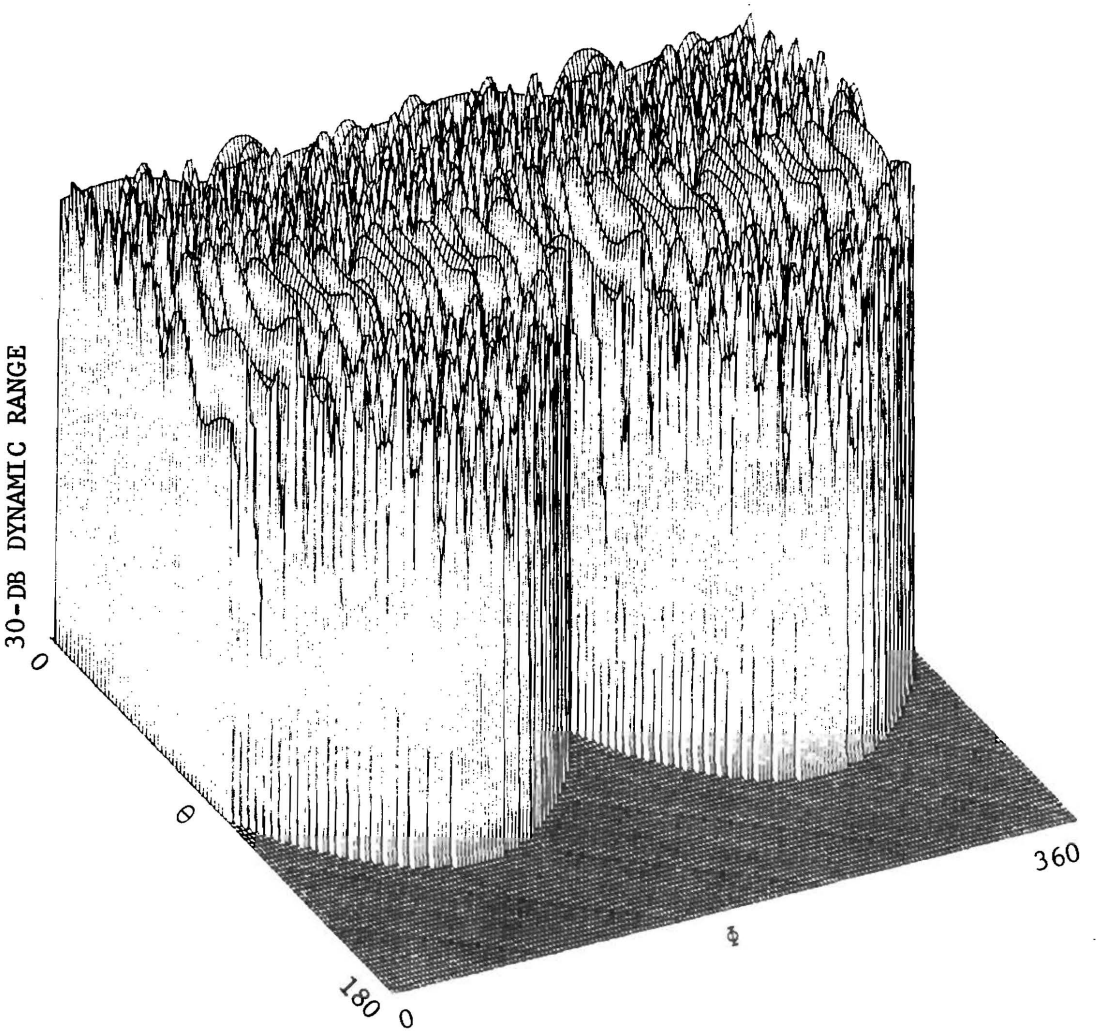

Figure 71. Calculated radiation pattern from a 4 element array located on the SERT-C satellite. The elements have a 5 dB taper 90^{o} away from boresight. The elements have θ - Φ pointing directions of (120, 45), (45, 135), (120, 225), and (45, 315). Solar panel blockage was included.

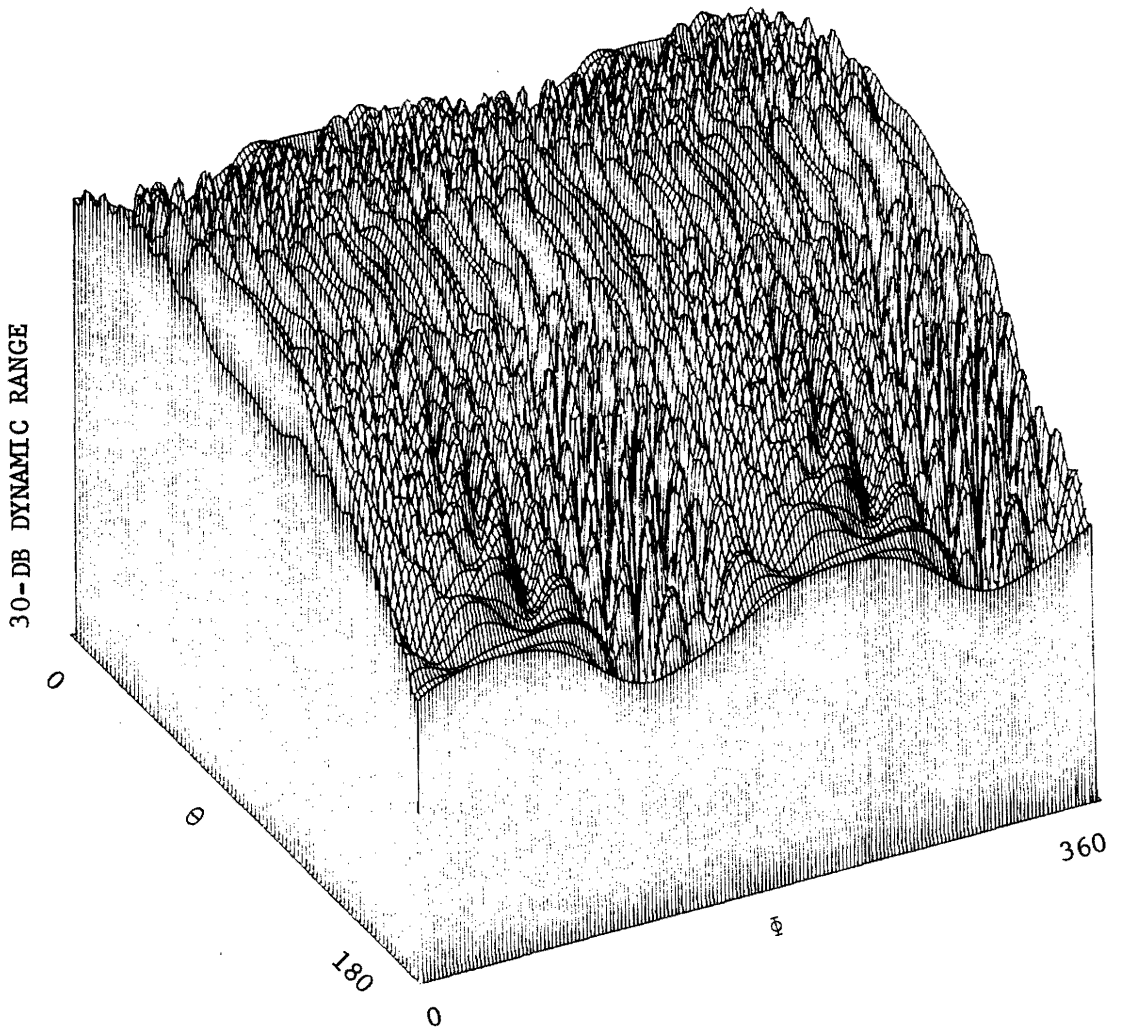

Figure 72. Calculated radiation pattern from a 4 element array located on the SERT-C satellite. The elements have a 10 dB taper 90^{o} away from boresight. The elements have θ - Φ pointing directions of (90, 45), (45, 135), (90, 225), and (45, 315). Solar panel blockage was not included.

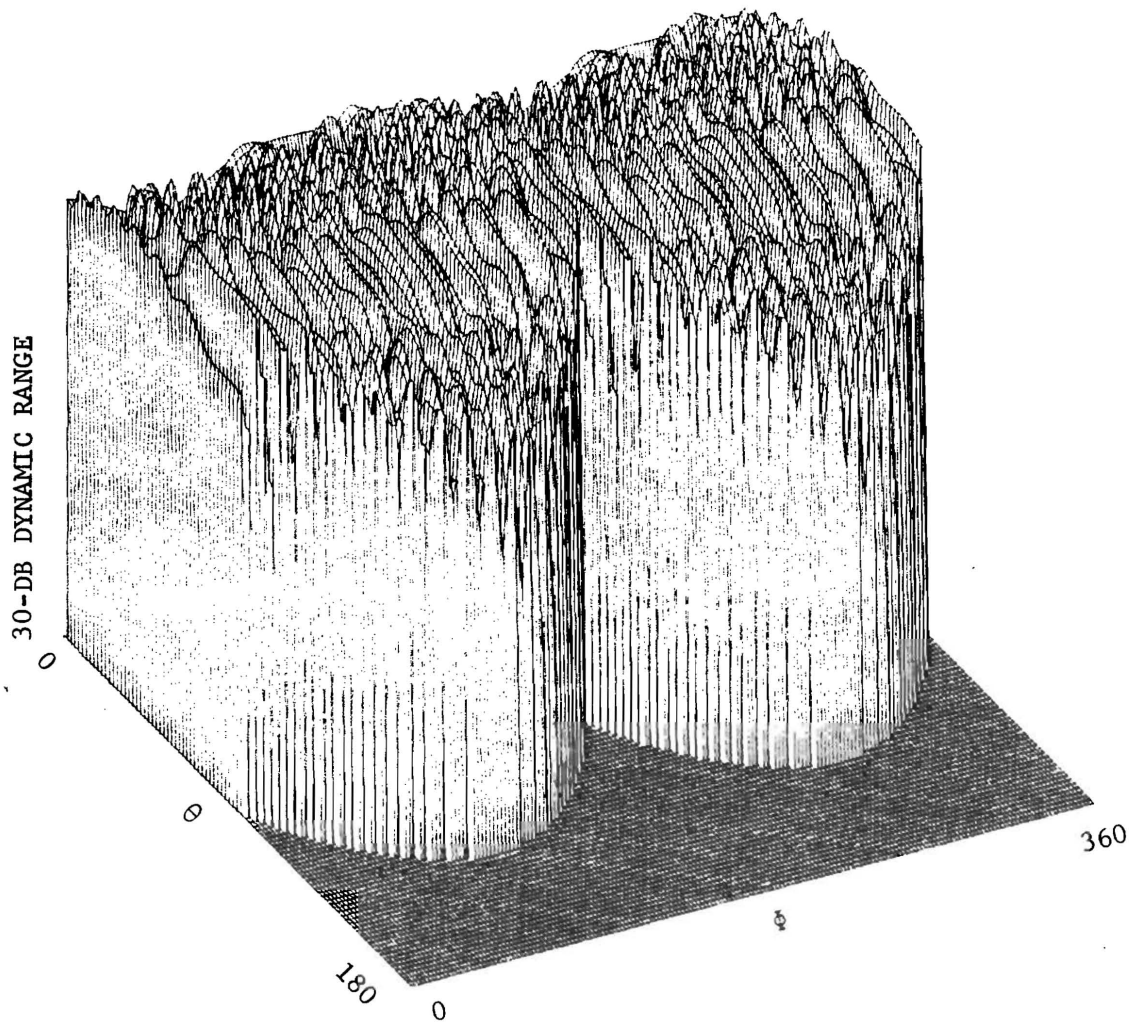

Figure 73. Calculated radiation pattern from a 4 element array located on the SERT-C satellite. The elements have a 10 dB taper 90^{o} away from boresight. The elements have θ - Φ pointing directions of (90, 45), (45, 135), (90, 225), and (45, 315). Solar panel blockage was included.

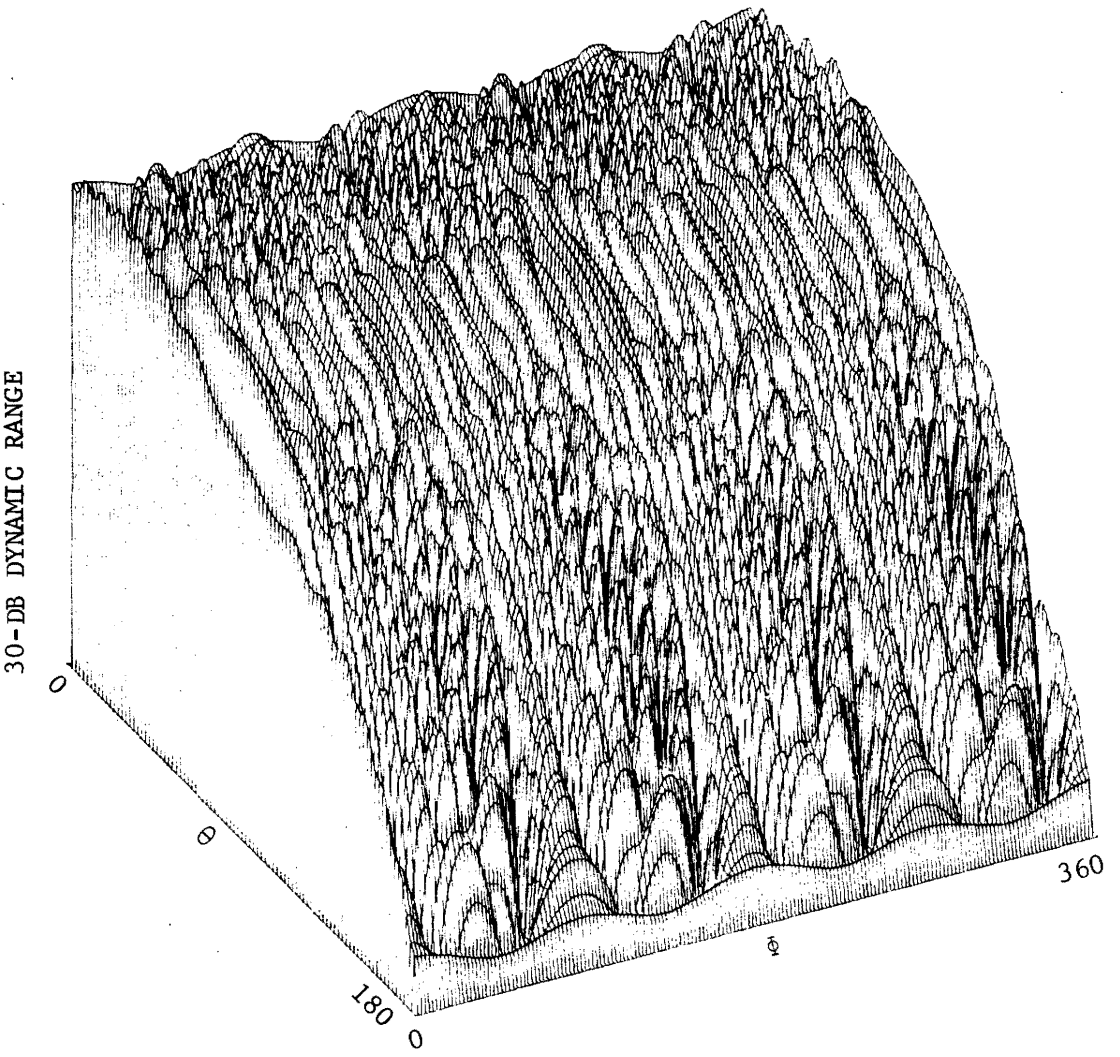

Figure 74. Calculated radiation pattern from a 4 element array located on the SERT-C satellite. The elements have a 10 dB taper 90° away from boresight. The elements have θ - Φ pointing directions of (45, 45), (45, 135), (45, 225), and (45, 375). Solar panel blockage was not included.

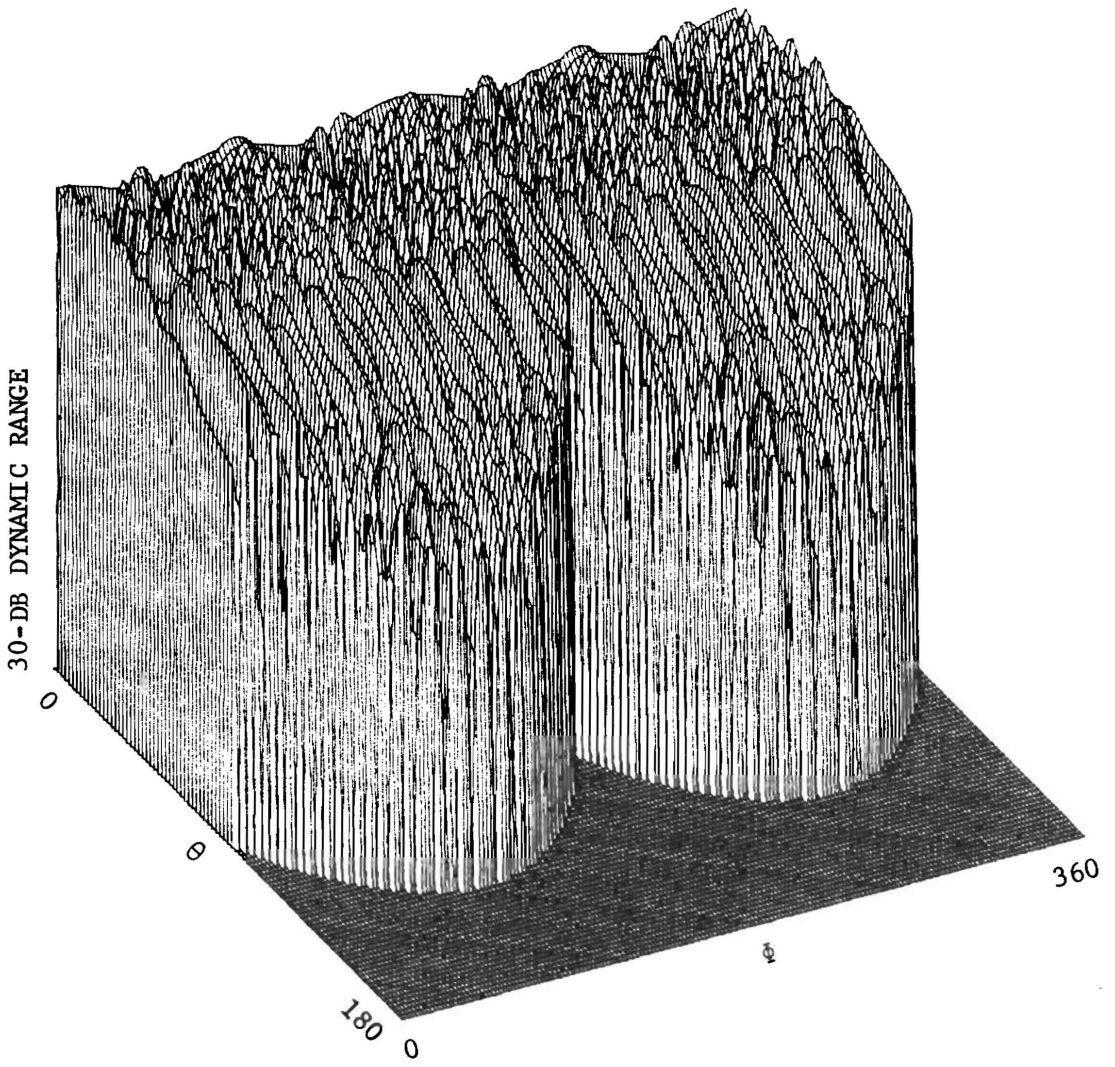

Figure 75. Calculated radiation pattern from a 4 element array located on the SERT-C satellite. The elements have a 10 dB taper 90° away from boresight. The elements have θ - Φ pointing directions of (45, 45), (45, 135), (45, 225), and (45, 315). Solar panel blockage was included.

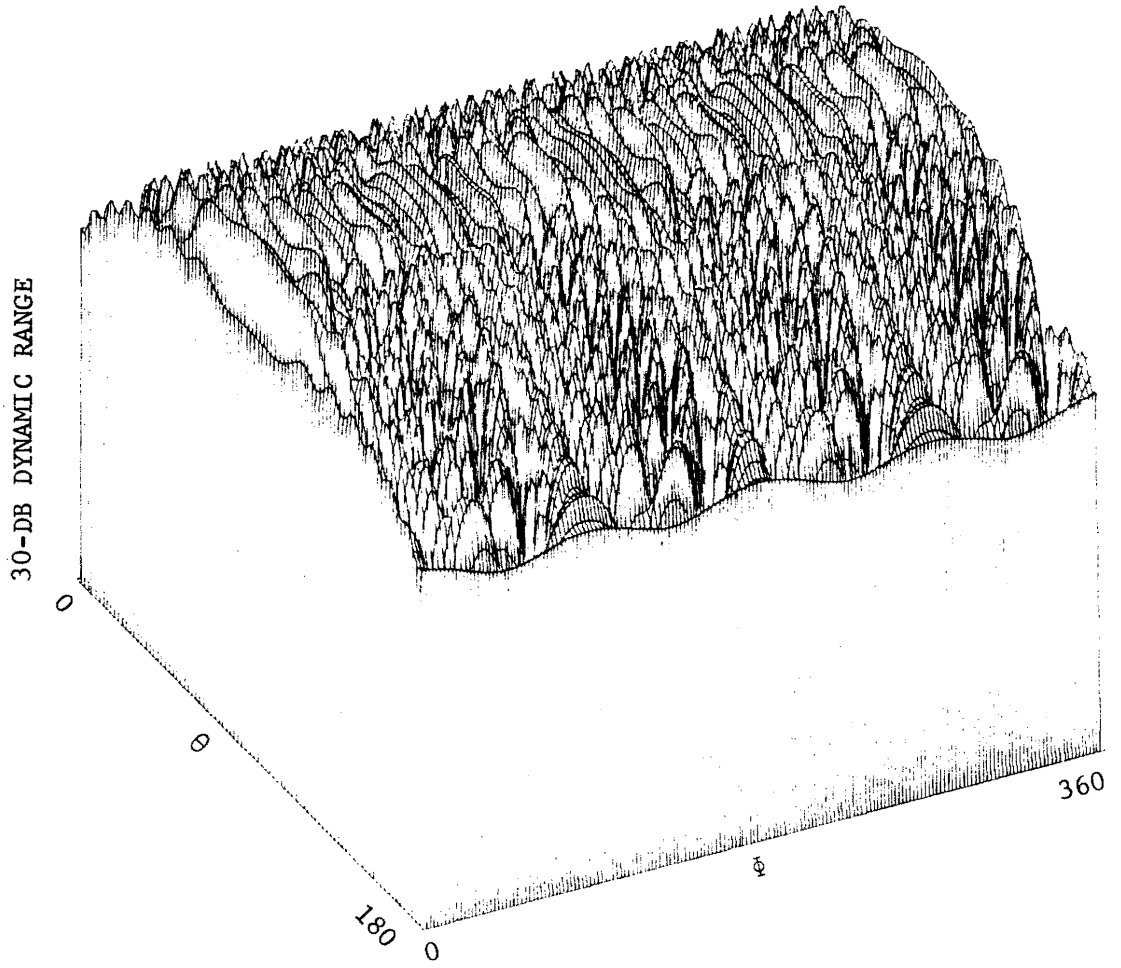

Figure 76. Calculated radiation pattern from a 4 element array located on the SERT-C satellite. The elements have a 10 dB taper 90^{o} away from boresight. The elements have θ - Φ pointing directions of (90, 45), (90, 135), (90, 225), and (90, 315). Solar panel blockage was not included.

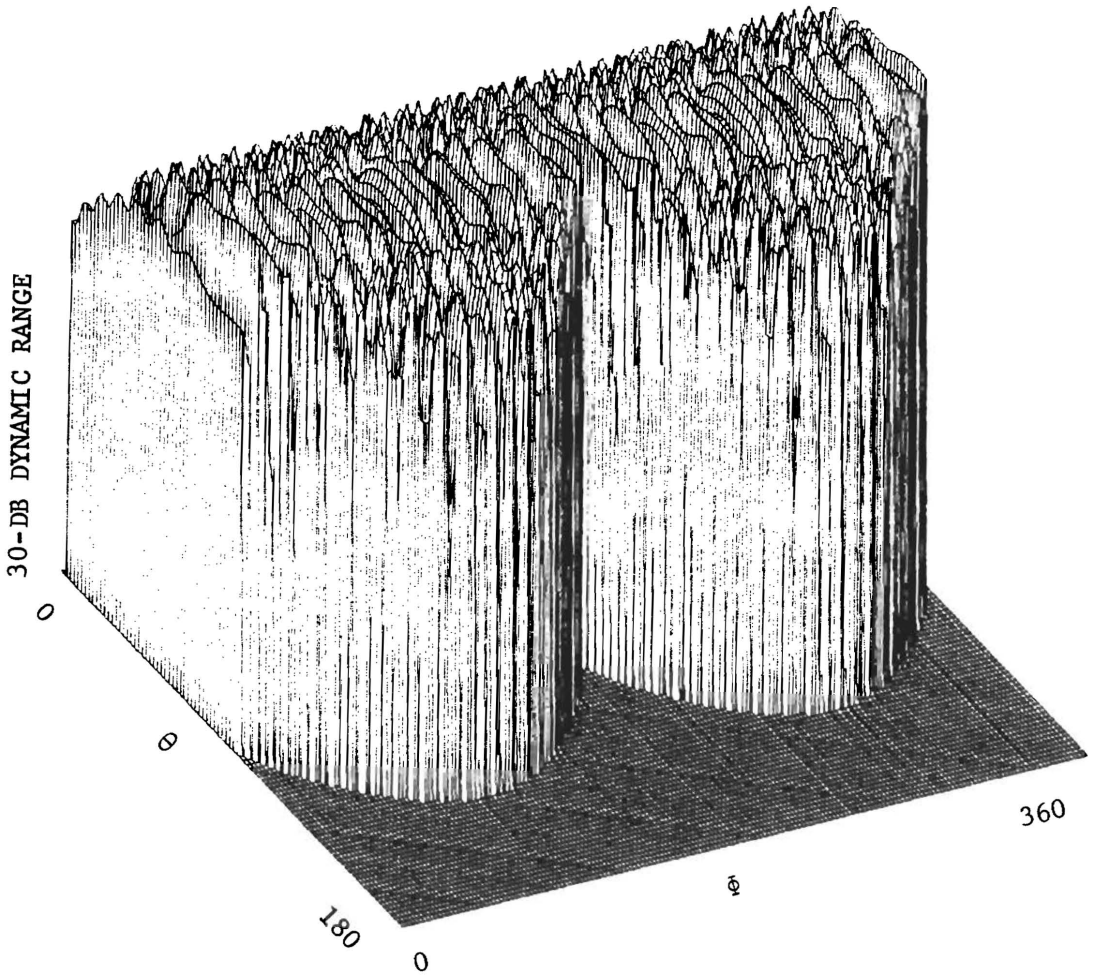

Figure 77. Calculated radiation pattern from a 4 element array located on the SERT-C satellite. The elements have a 10 dB taper 90° away from boresight. The elements have θ - Φ pointing directions of (90, 45), (90, 135), (90, 225), and (90, 315). Solar panel blockage was included.

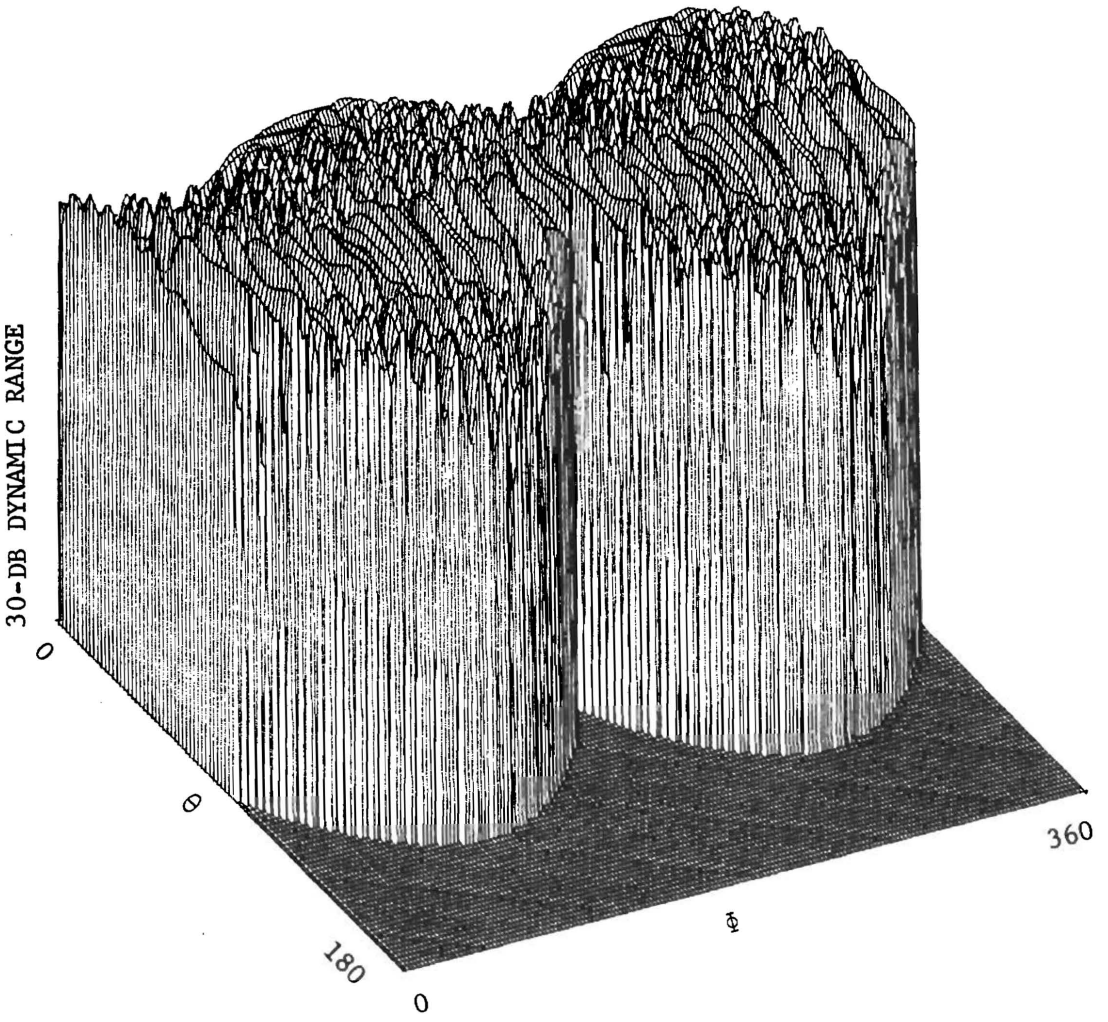

Figure 78. Calculated radiation pattern from a 4 element array located on the SERT-C satellite. The elements have a 10 dB taper 90° away from boresight. The elements have θ - Φ pointing directions of (120, 45), (45, 135) (120, 225), and (45, 315). Solar panel blockage was included.

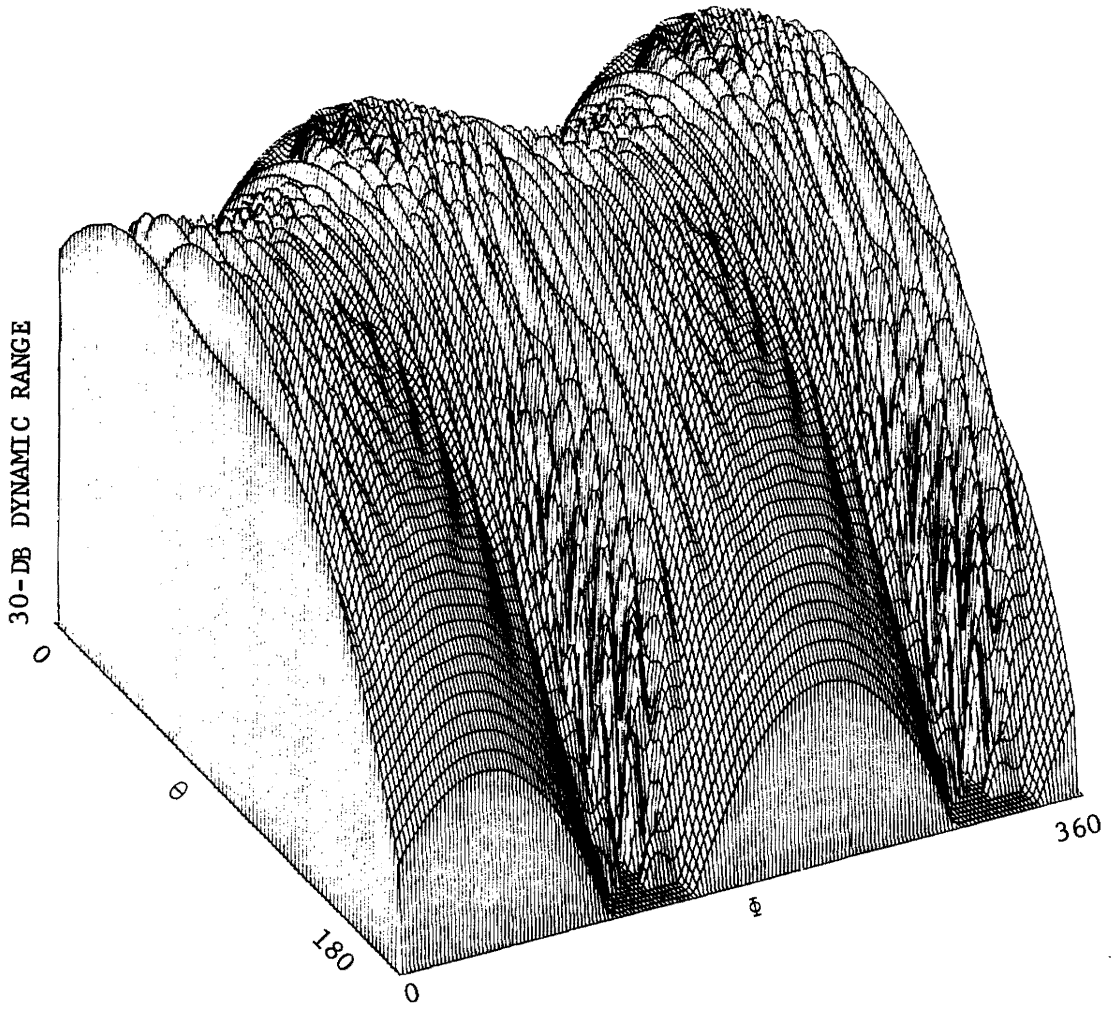

Figure 79. Calculated radiation pattern from a 4 element array located on the SERT-C satellite. The elements have a 20 dB taper 90^{o} away from boresight. The elements have θ - Φ pointing directions of (90, 45), (45, 135), (90, 225), and (45, 315). Solar panel blockage was not included.

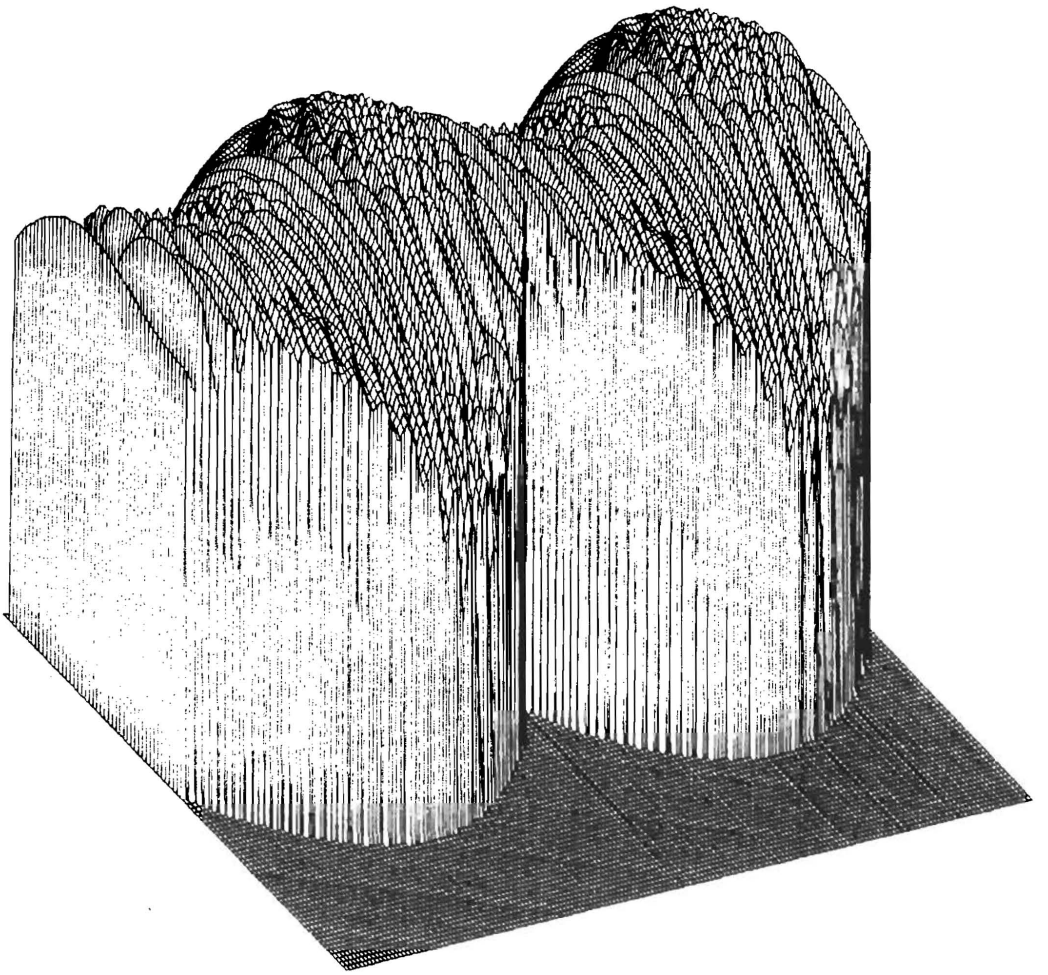

Figure 80. Calculated radiation pattern from a 4 element array located on the SERT-C satellite. The elements have a 20 dB taper 90^{o} away from boresight. The elements have θ - Φ pointing directions of (90, 45), (45, 135), (90, 225), and (45, 315). Solar panel blockage was included.

APPENDIX III

Polar Plots of 2 Spiral Array Radiation Patterns
With/Without Solar Panels, RHCP and LHCP.
Patterns Made with SERT-C Scale Model
(Full-Scale Dimensions Reduced by Factor of 4.1:1;
Test Frequency = 9.2 GHz).

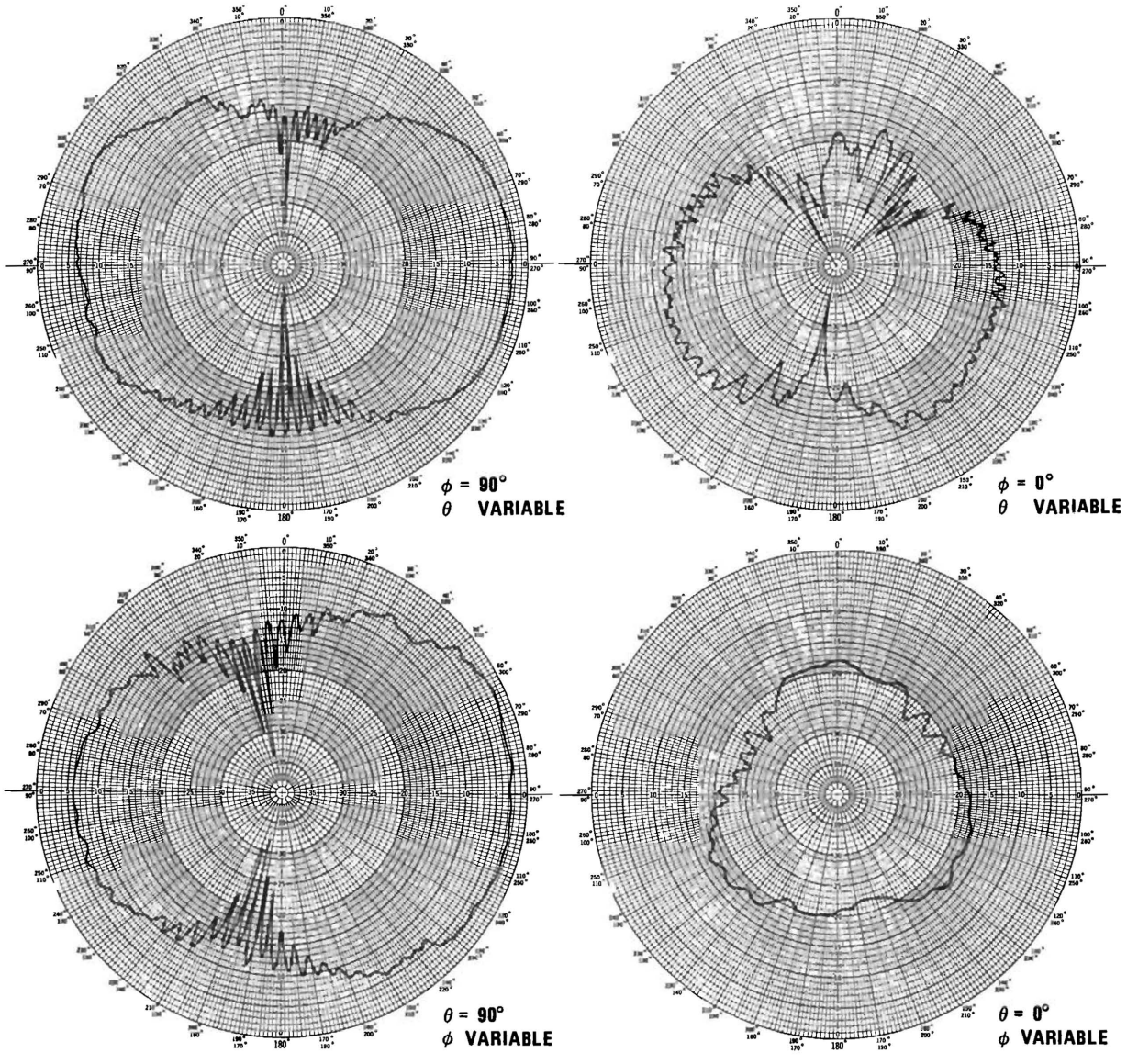

Principal Plane Patterns (dB), 2 Spirals, RHCP, No Solar Panels

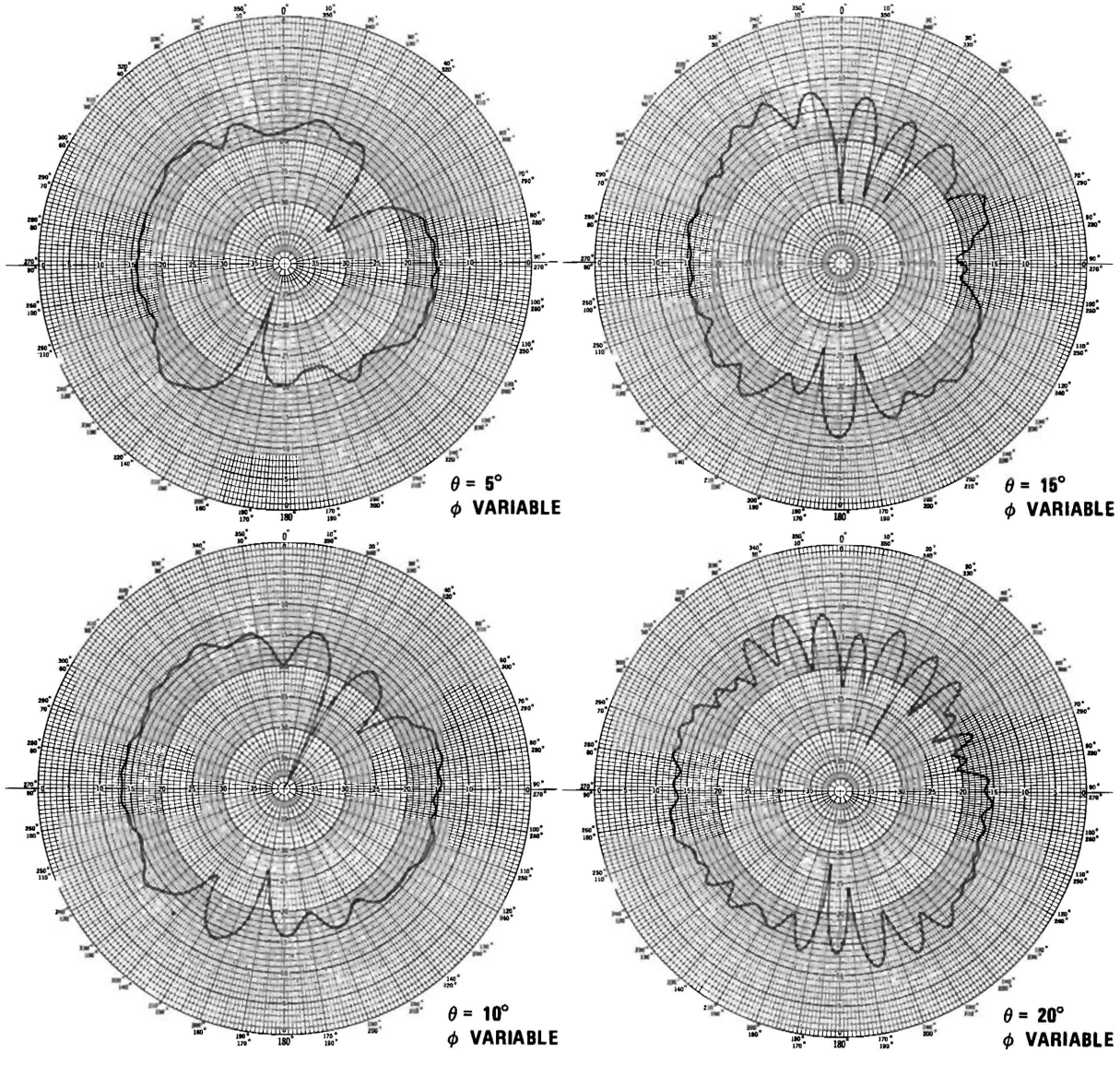

Conical Plots (dB), 2 Spirals, RHCP, No Solar Panels

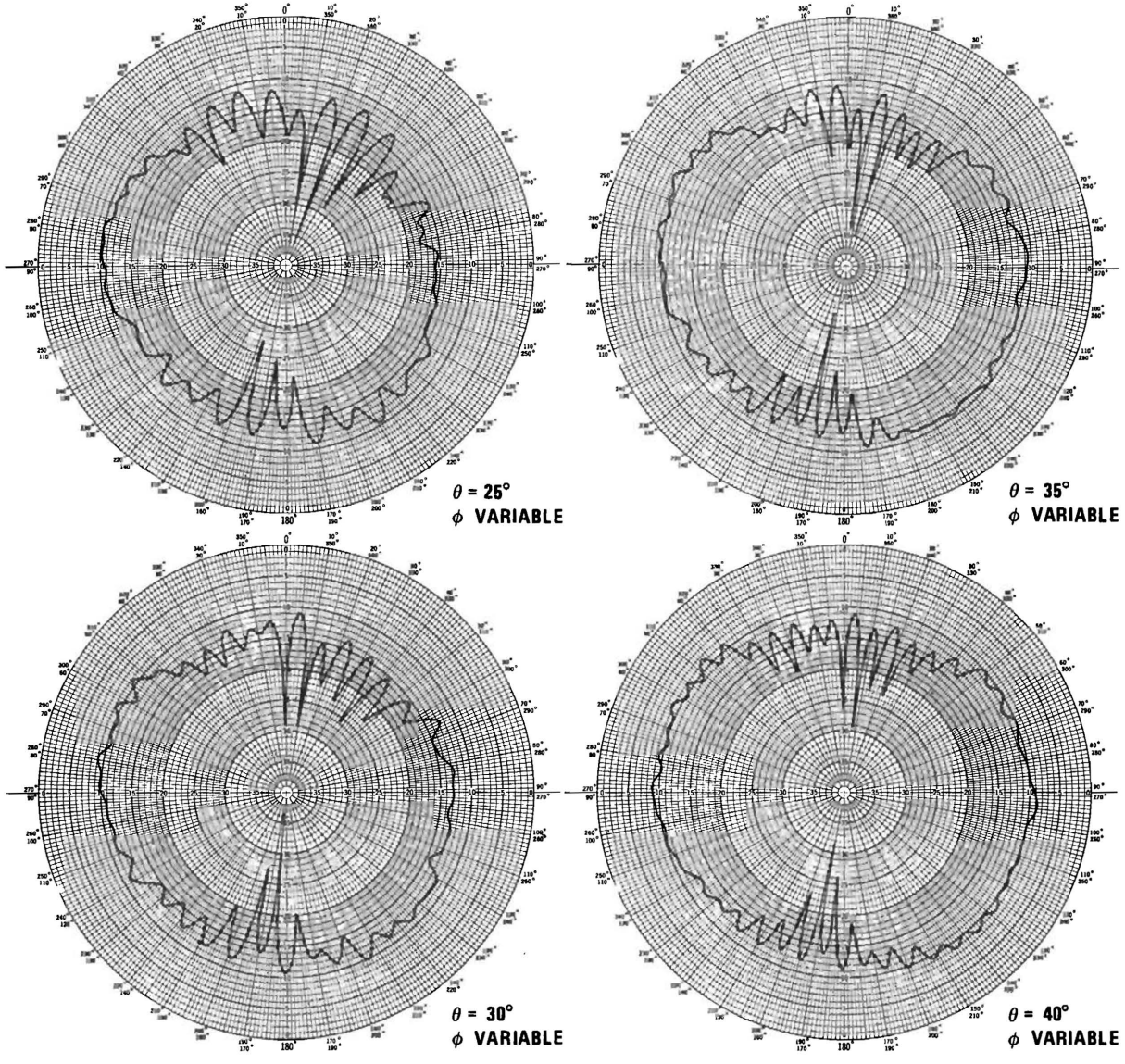

Conical Plots (dB), 2 Spirals, RHCP, No Solar Panels

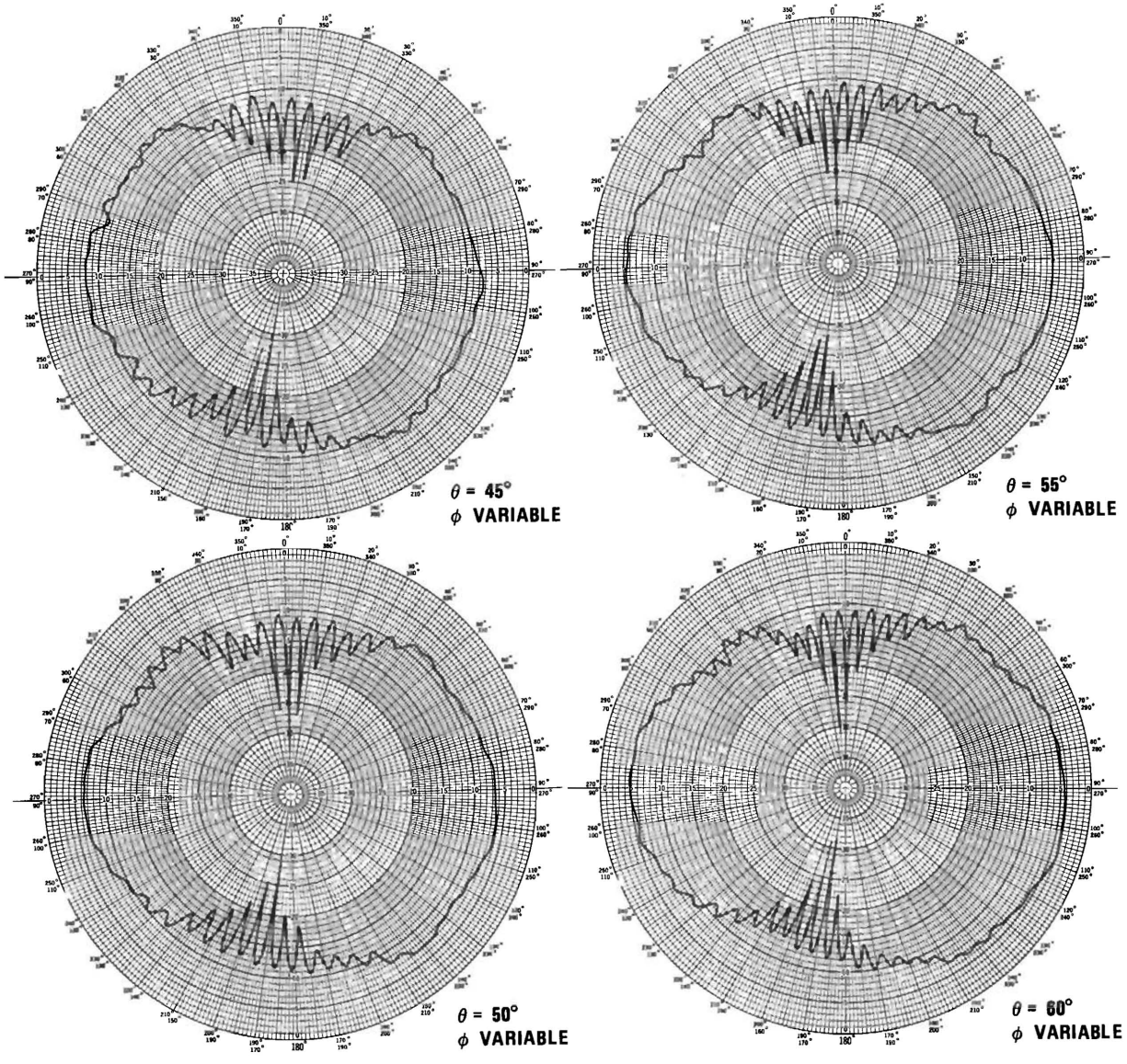

Conical Plots (dB), 2 Spirals, RHCP, No Solar Panels

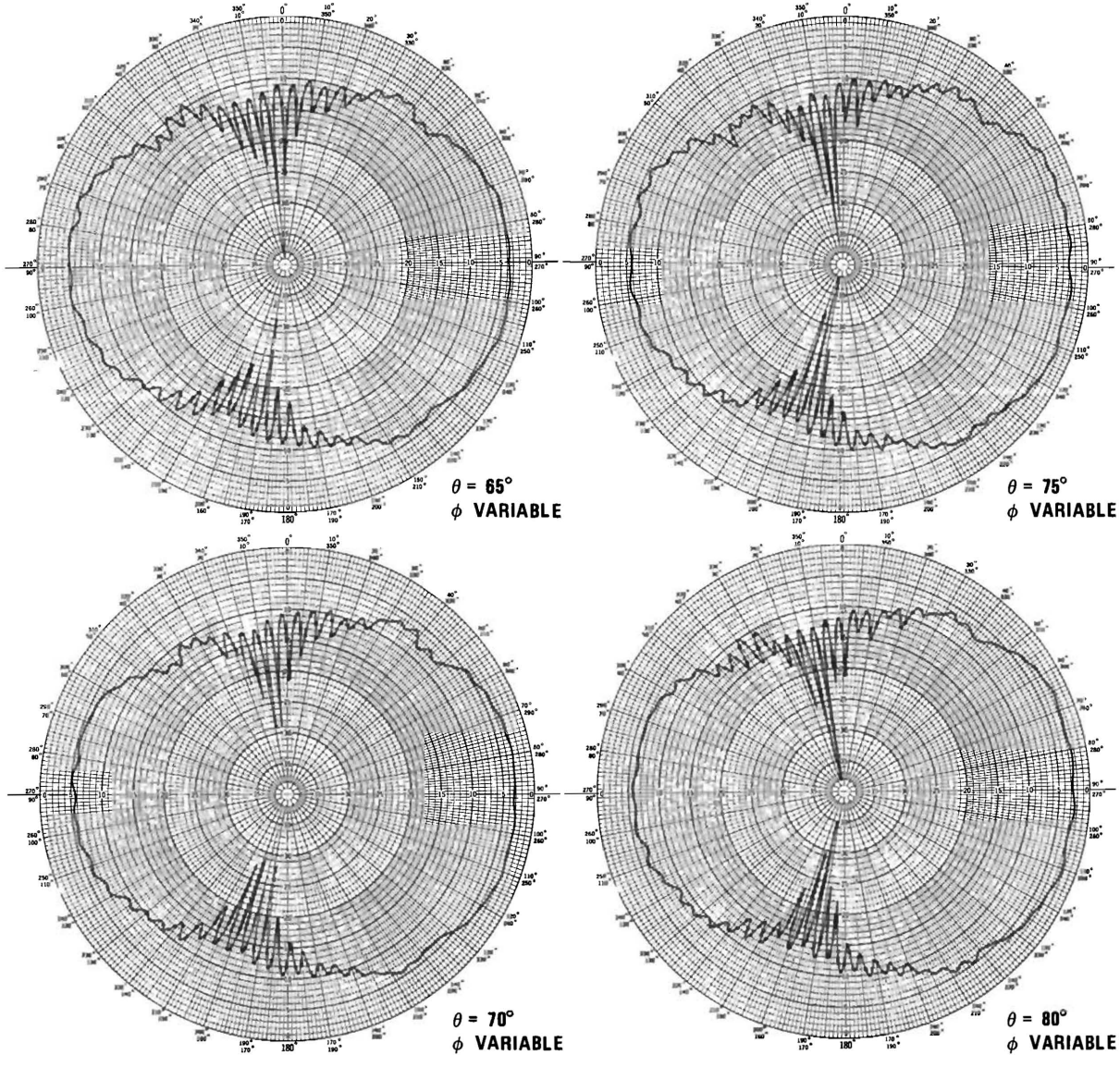

Conical Plots (dB), 2 Spirals, RHCP, No Solar Panels

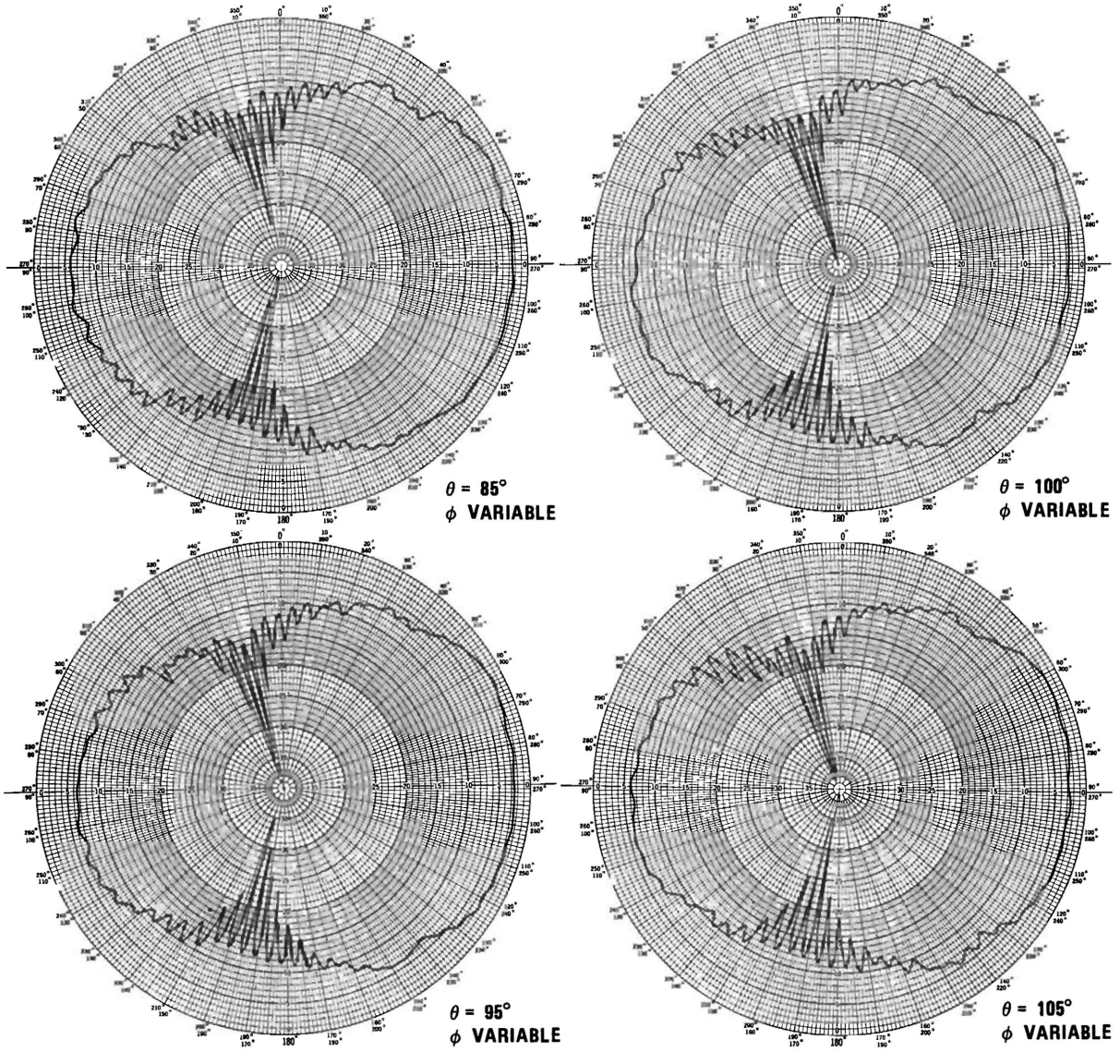

Conical Plots (dB), 2 Spirals, RHCP, No Solar Panels

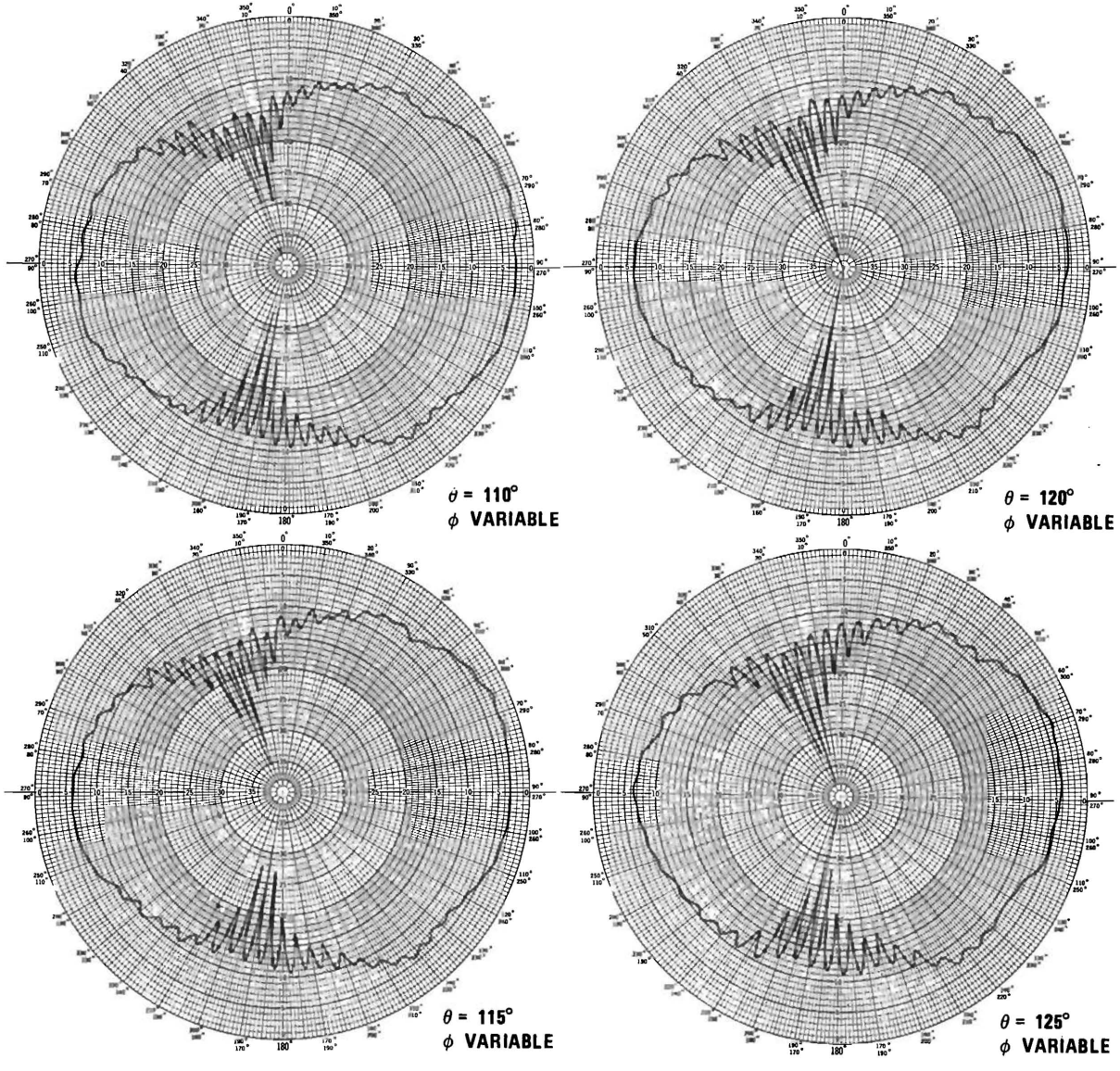

Conical Plots (dB), 2 Spirals, RHCP, No Solar Panels

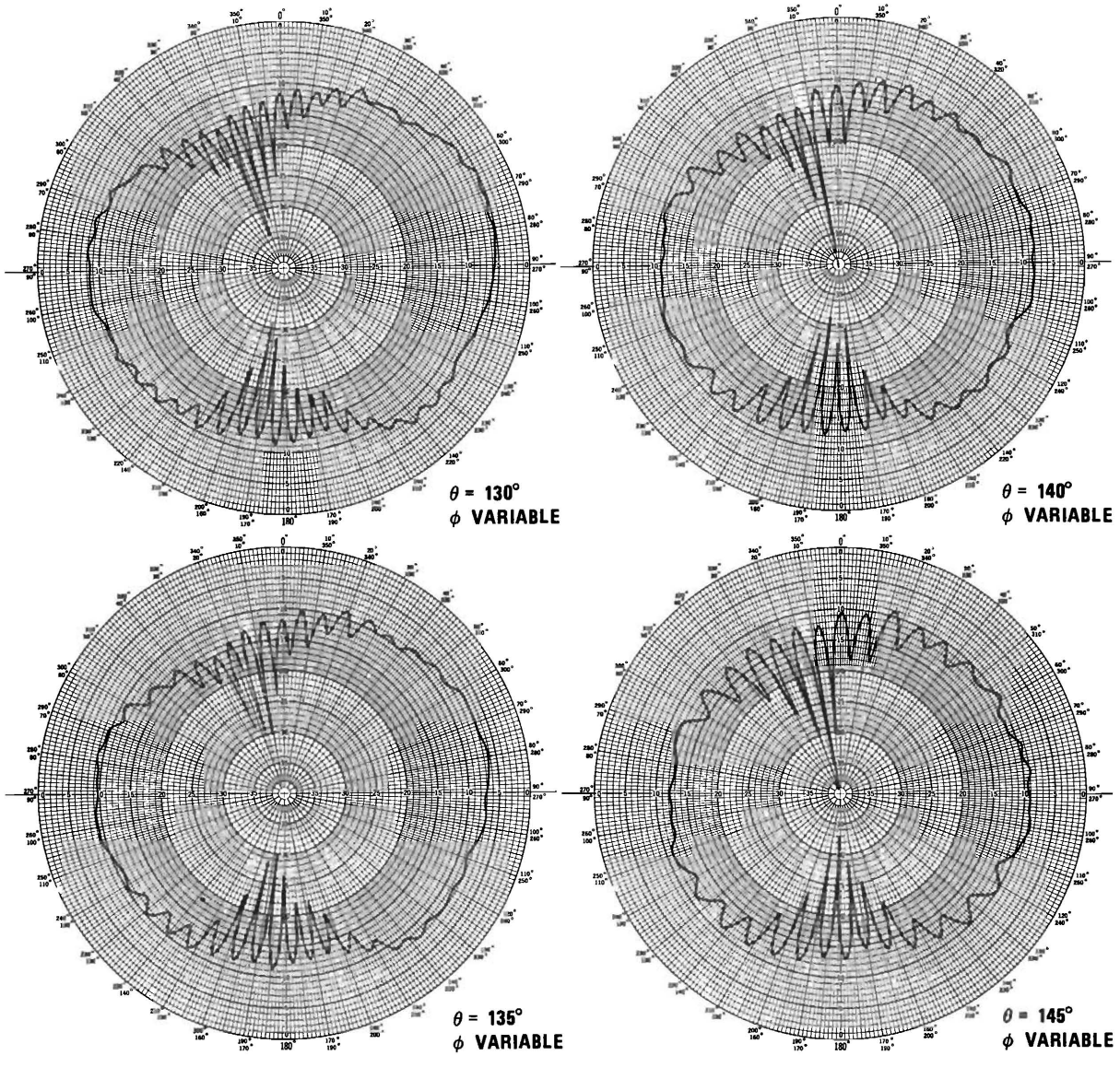

Conical Plots (dB), 2 Spirals, RHCP, No Solar Panels

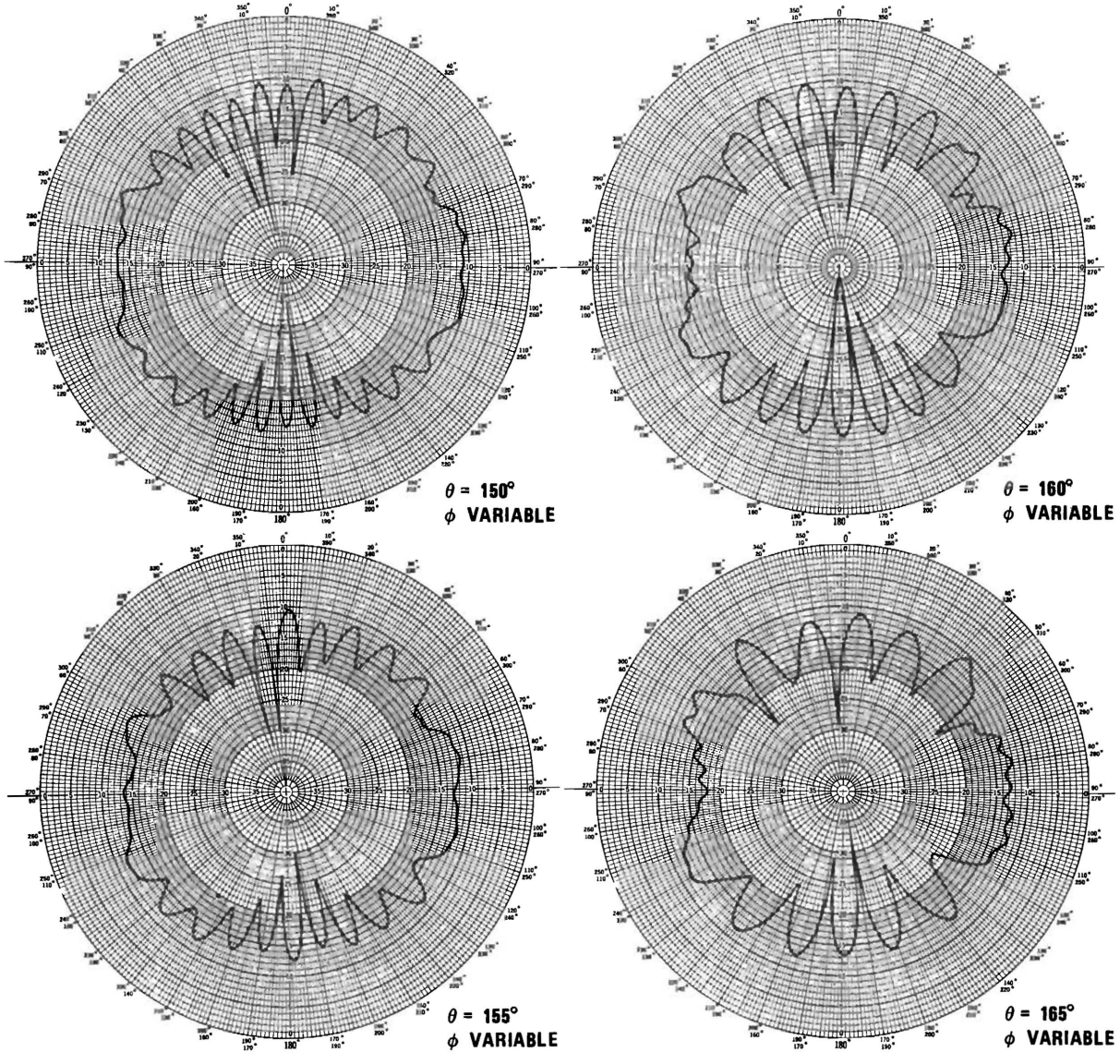

Conical Plots (dB), 2 Spirals, RHCP, No Solar Panels

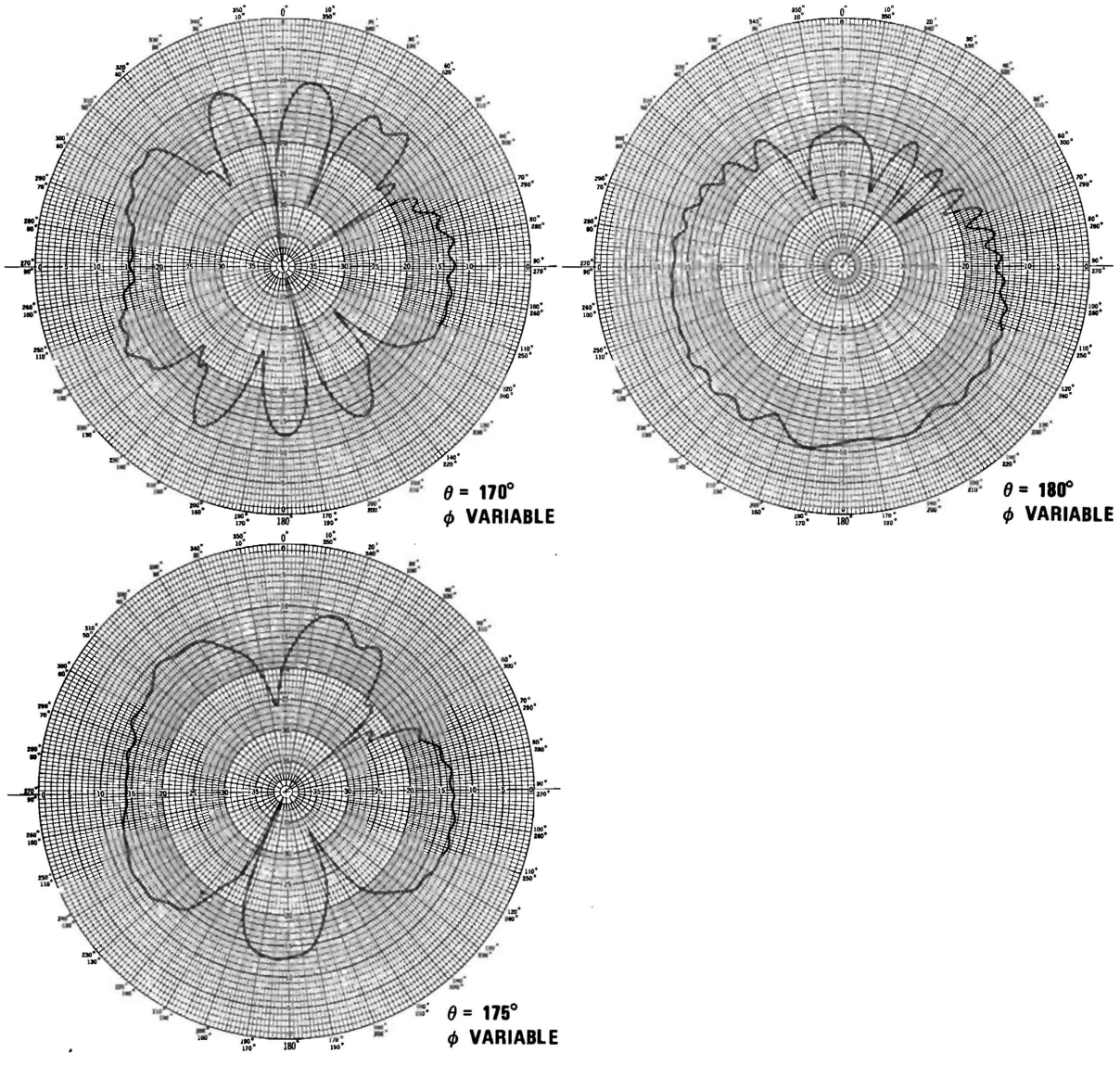

Conical Plots (dB), 2 Spirals, RHCP, No Solar Panels

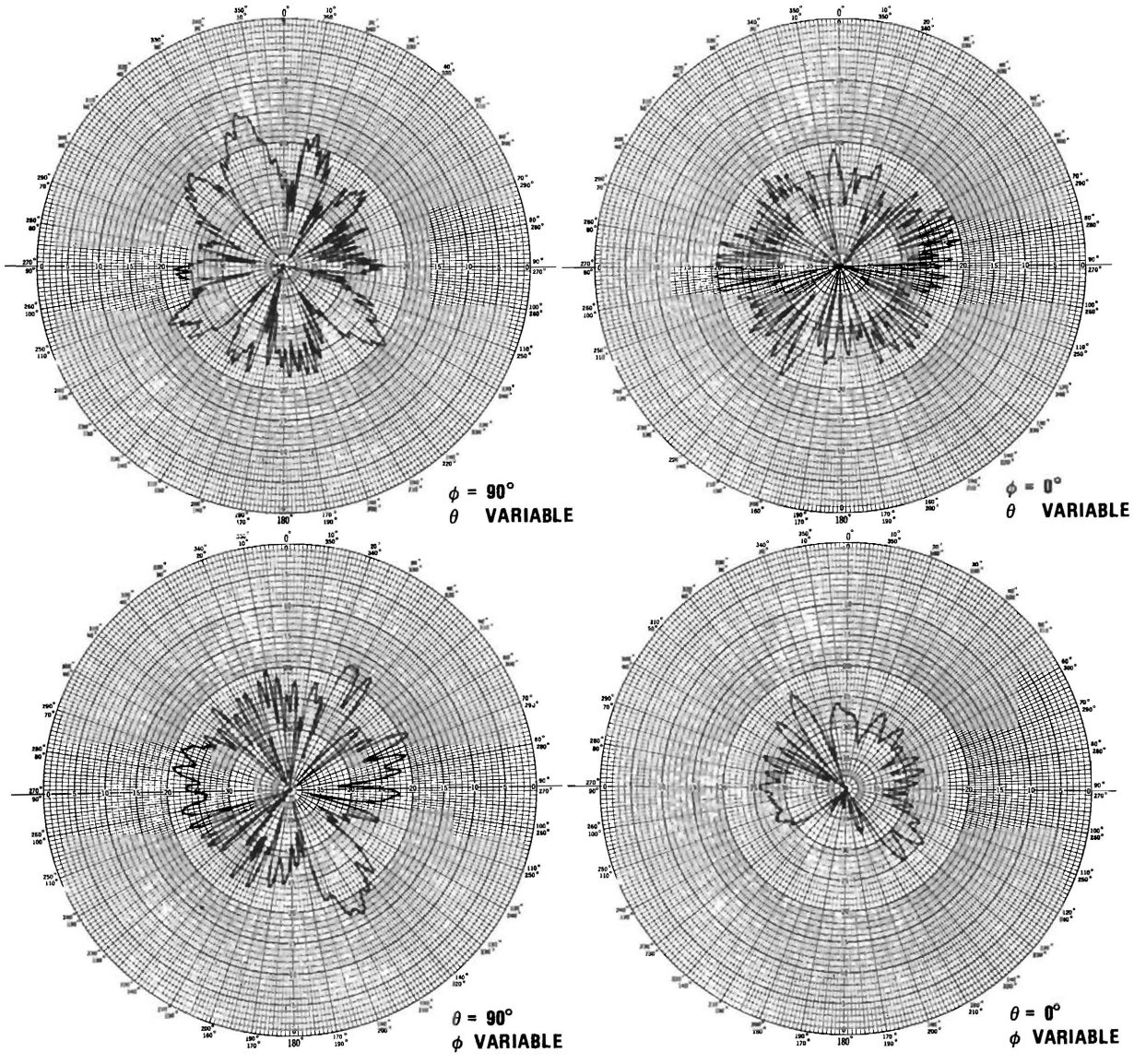

Principal Plane Patterns (dB), 2 Spirals, LHCP, No Solar Panels.

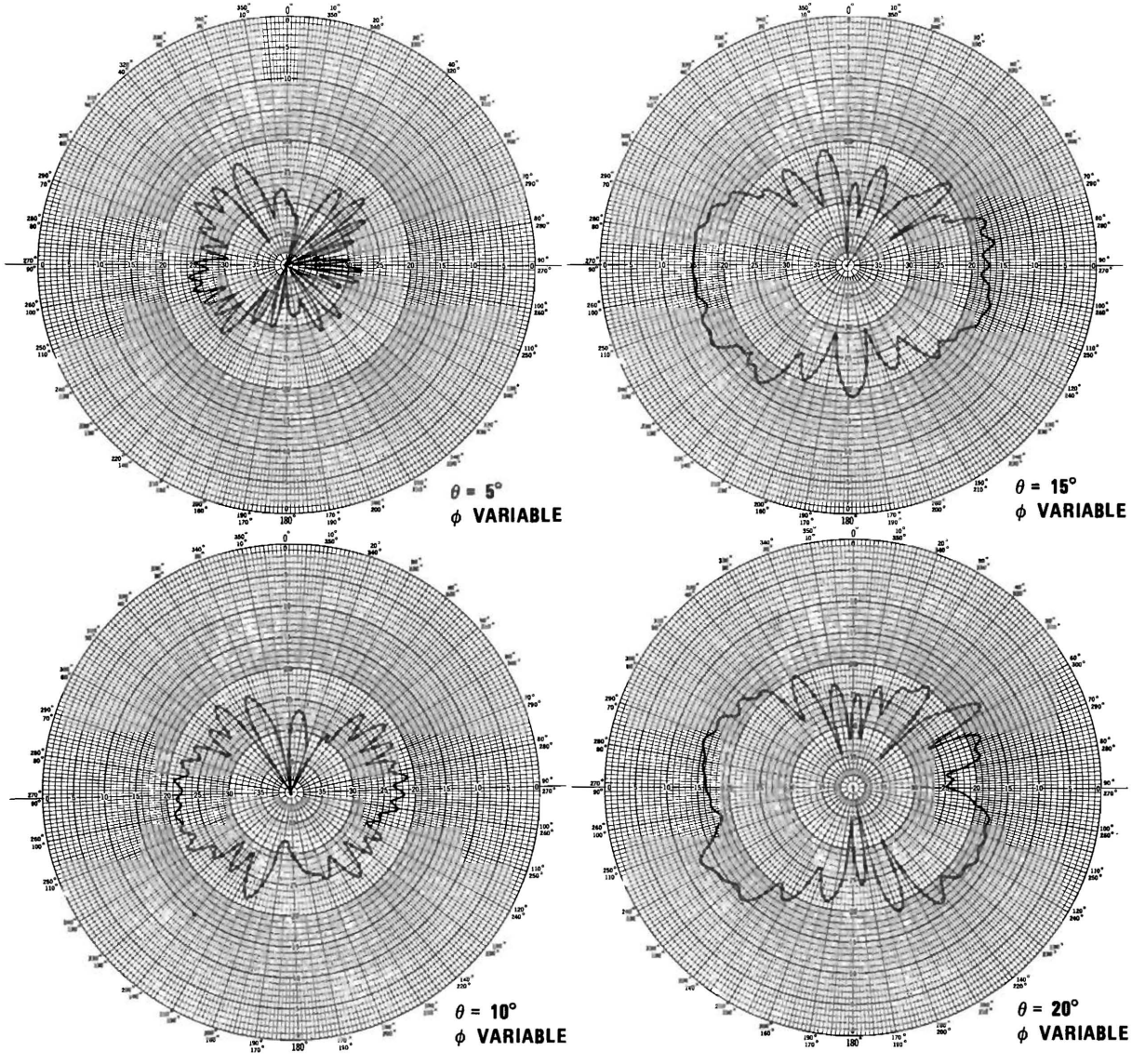

Conical Plots (dB), 2 Spirals, LHCP, No Solar Panels

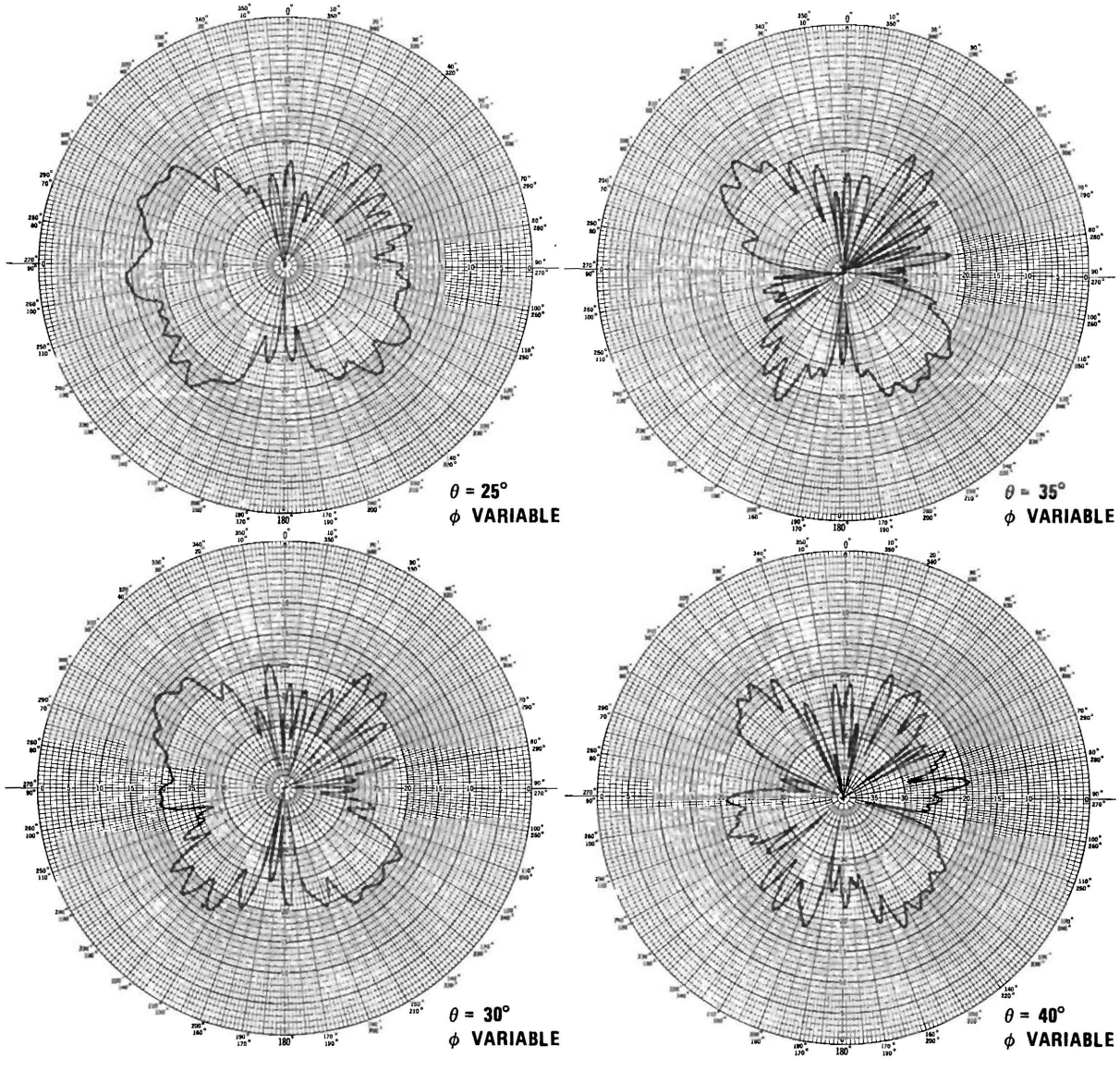

Conical Plots (dB), 2 Spirals, LHCP, No Solar Panels

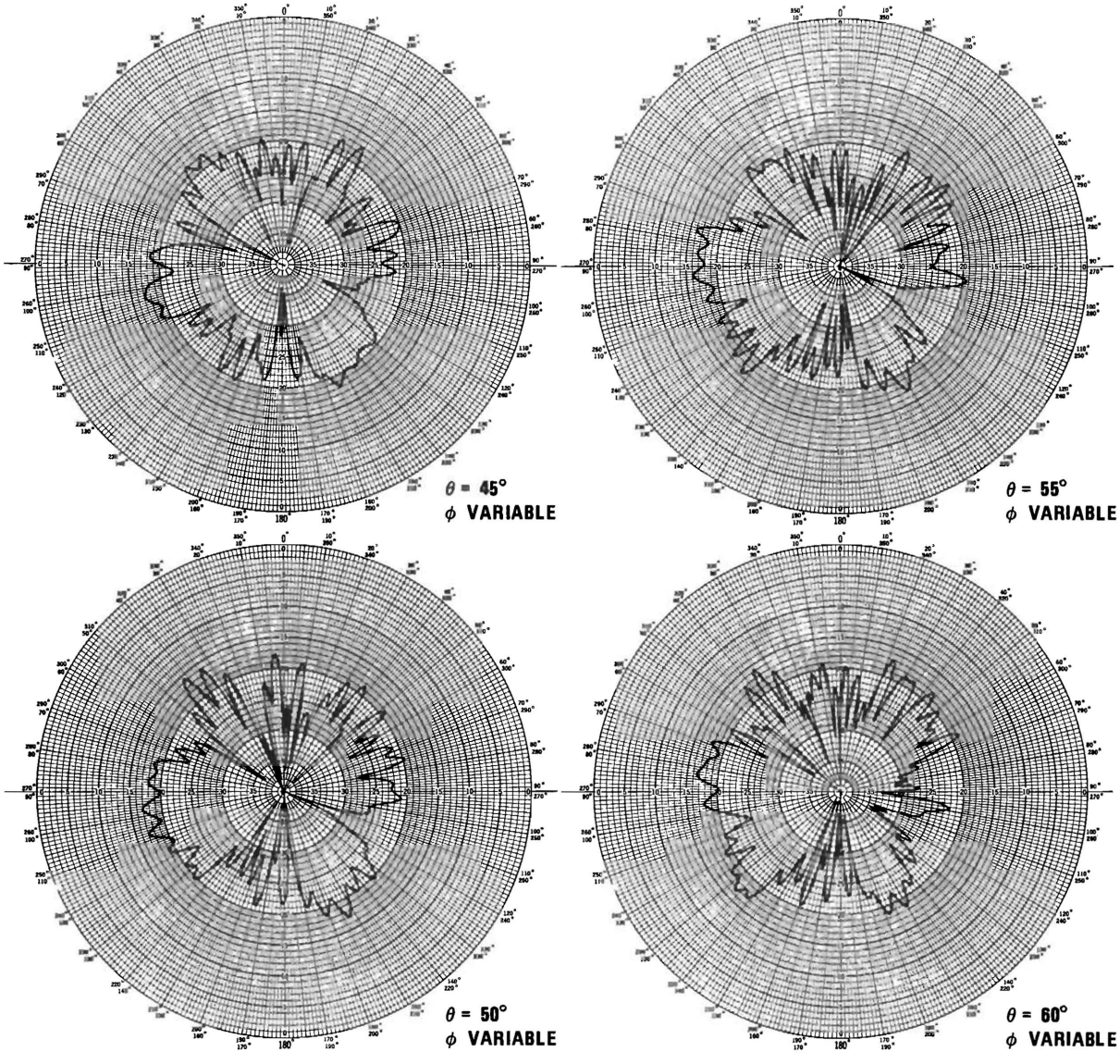

Conical Plots (dB), 2 Spirals, LHCP, No Solar Panels

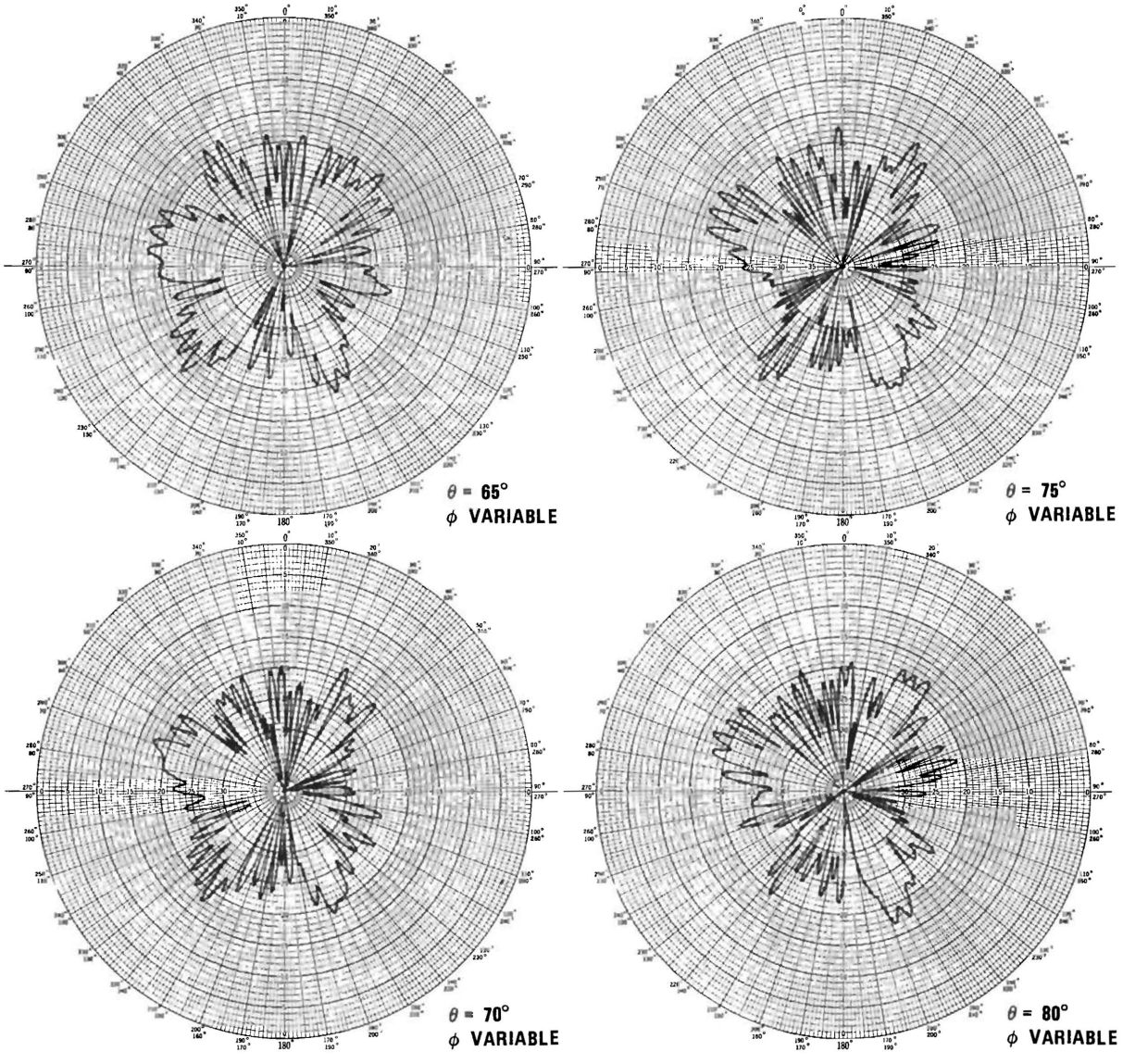

Conical Plots (dB), 2 Spirals, LHCP, No Solar Panels

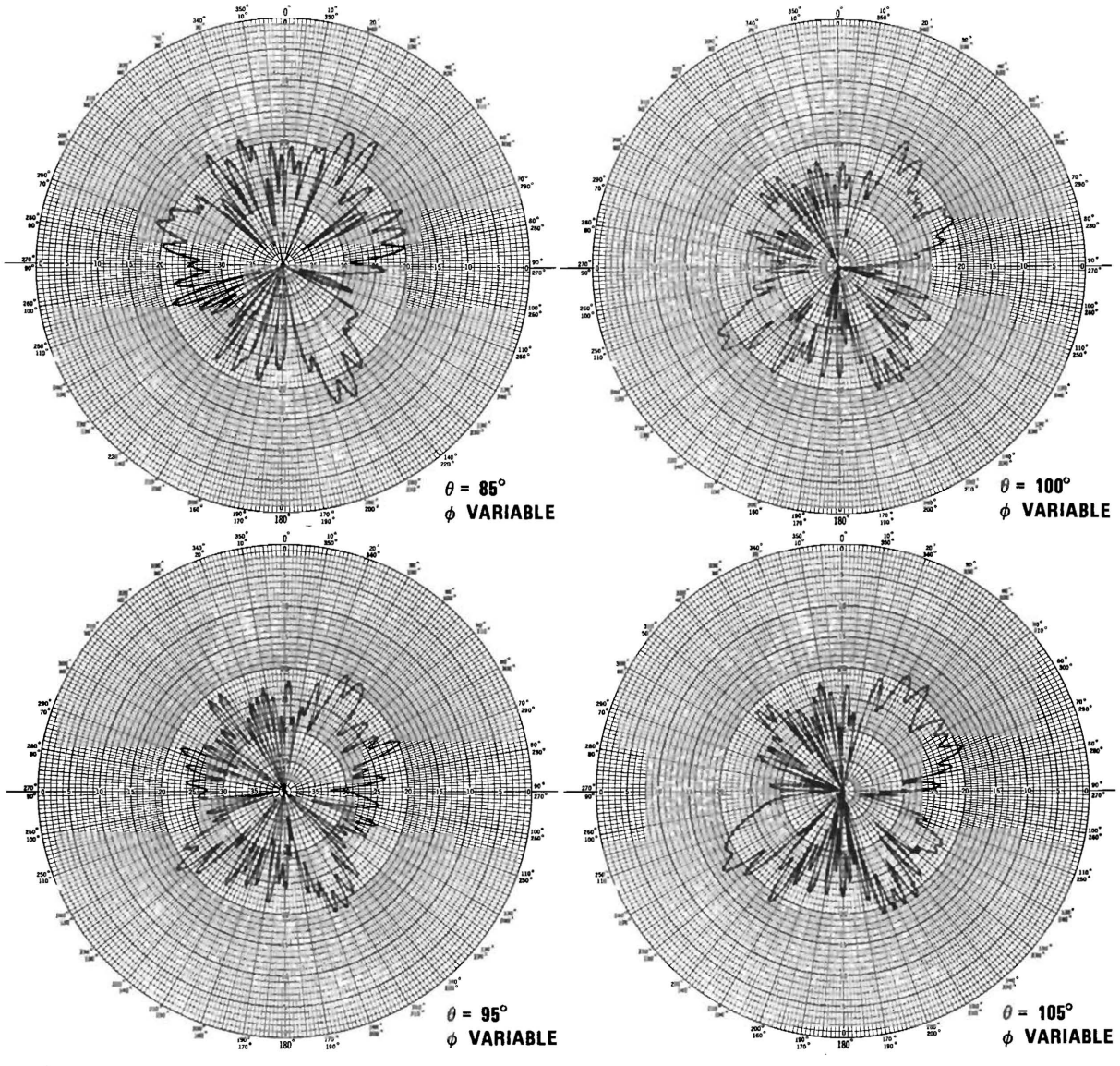

Conical Plots (dB), 2 Spirals, LHCP, No Solar Panels.

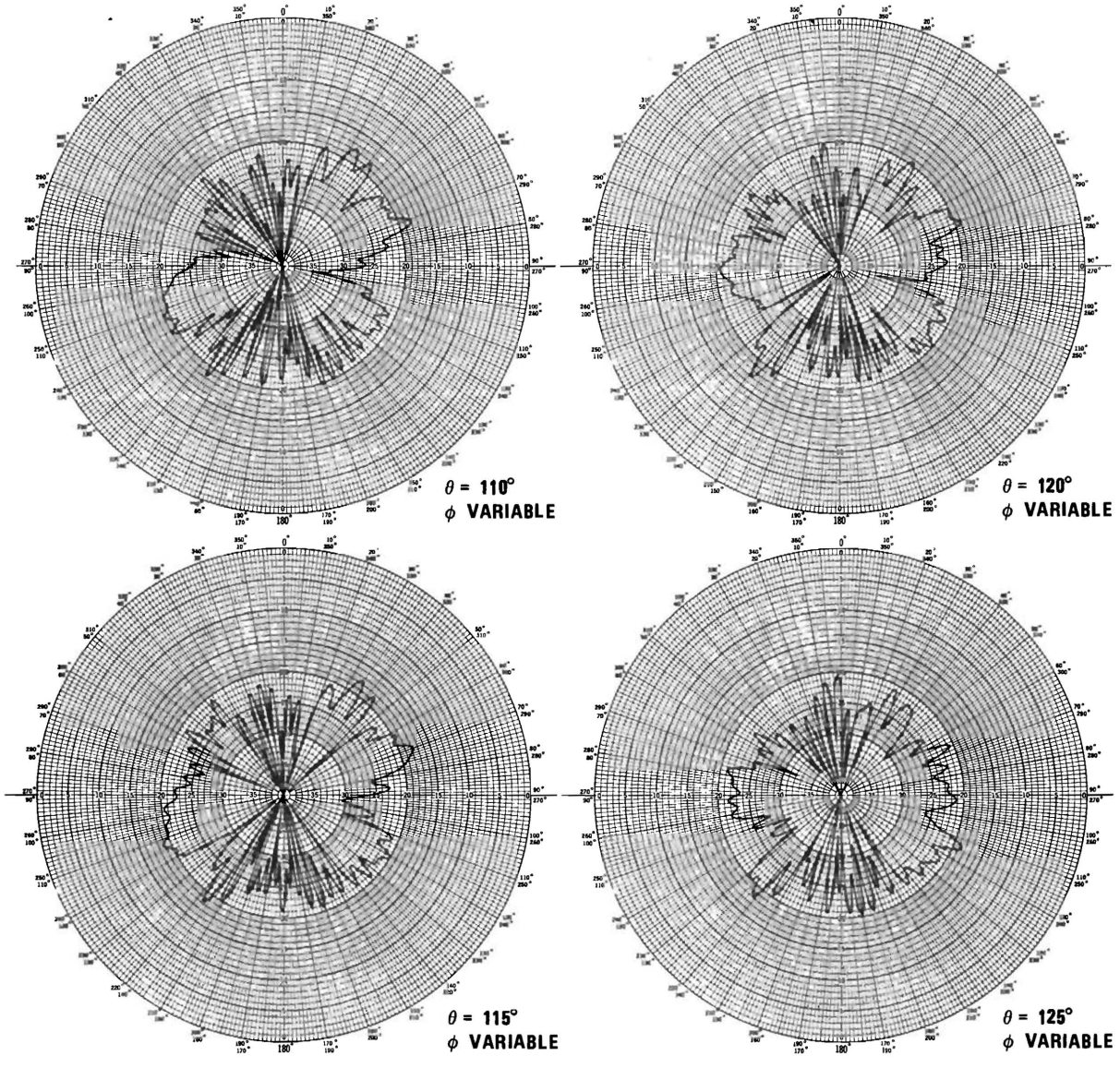

Conical Plots (dB), 2 Spirals, LHCP, No Solar Panels

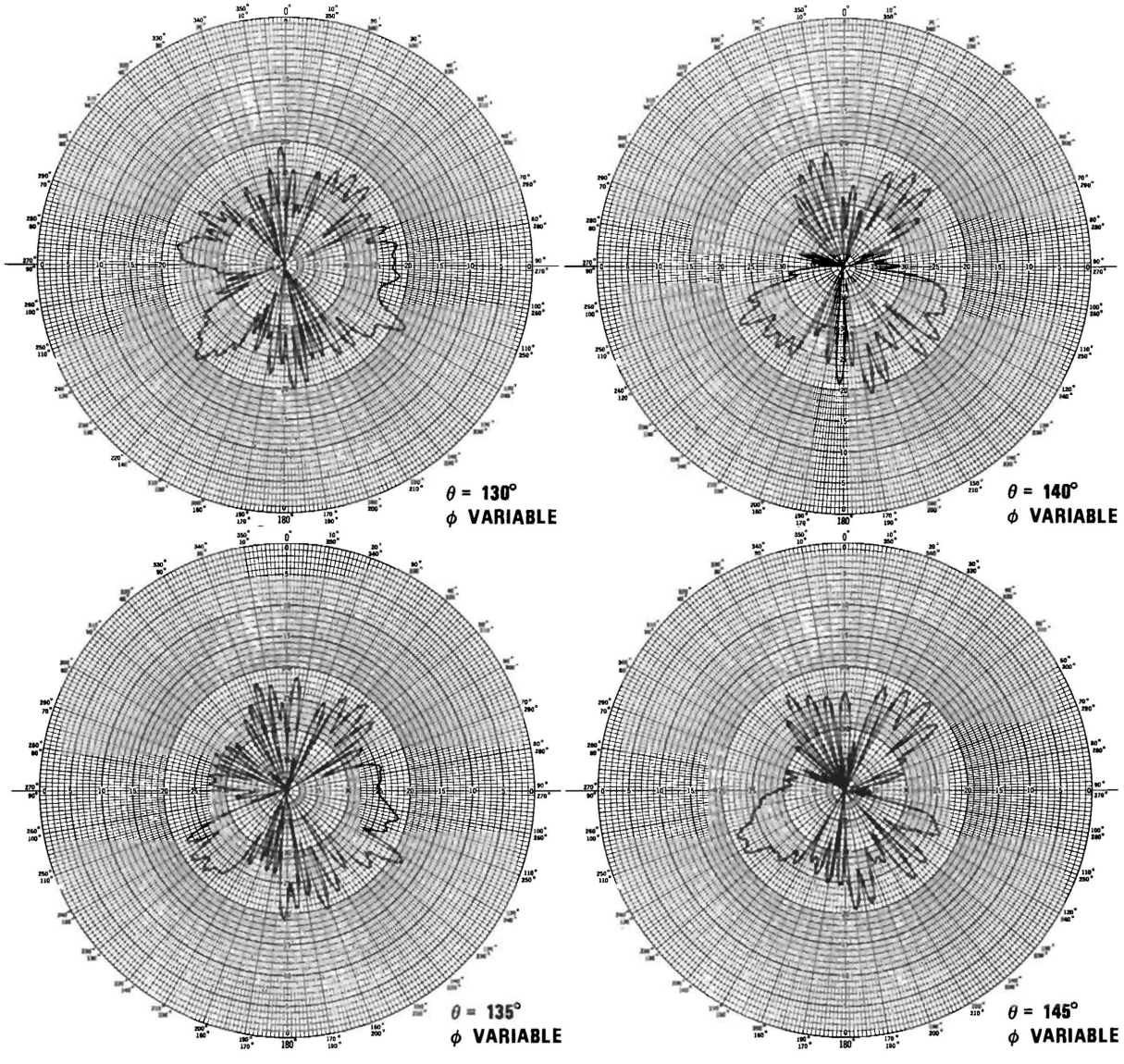

Conical Plots (dB), 2 Spirals, LHCP, No Solar Panels

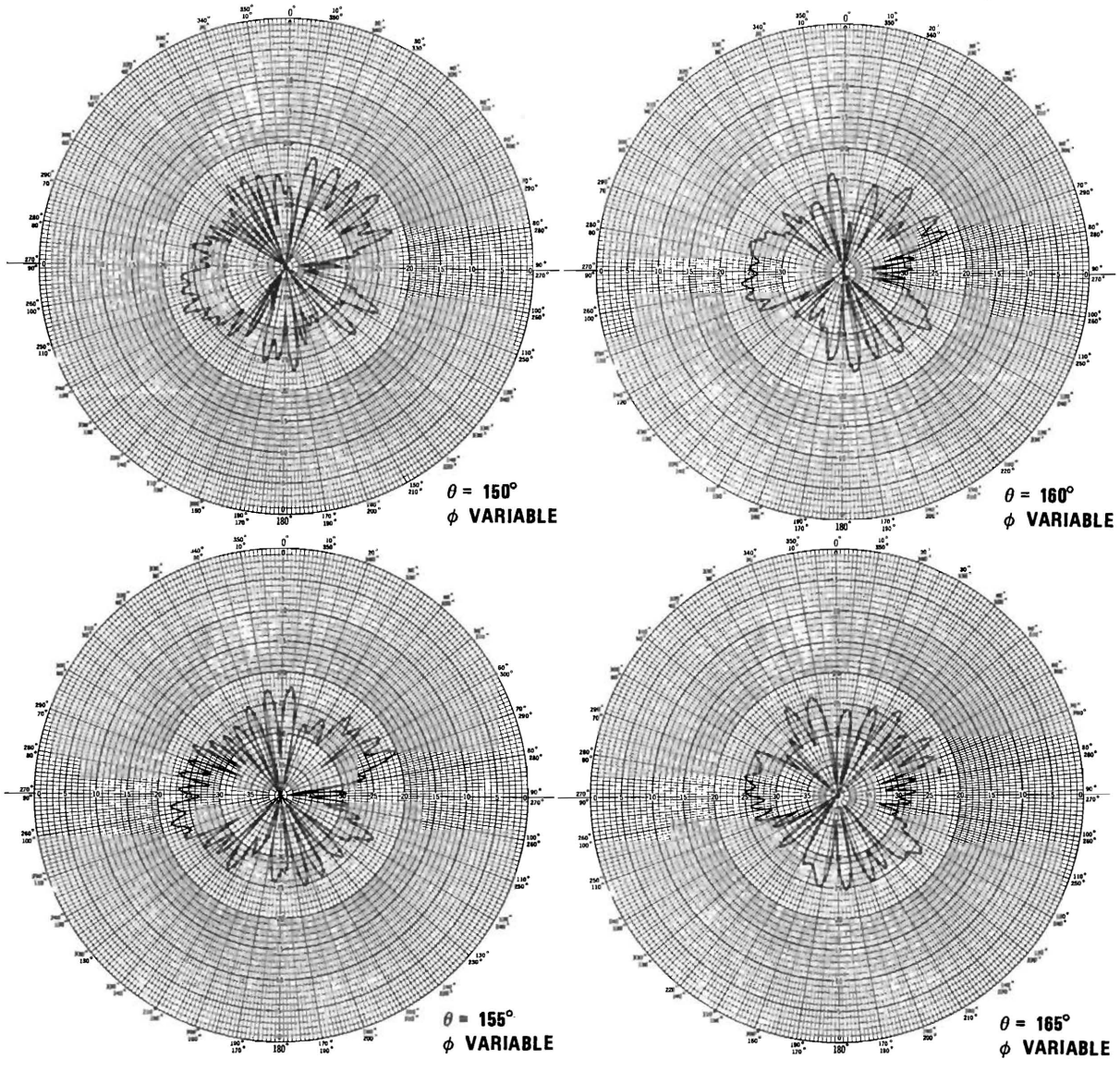

Conical Plots (dB), 2 Spirals, LHCP, No Solar Panels

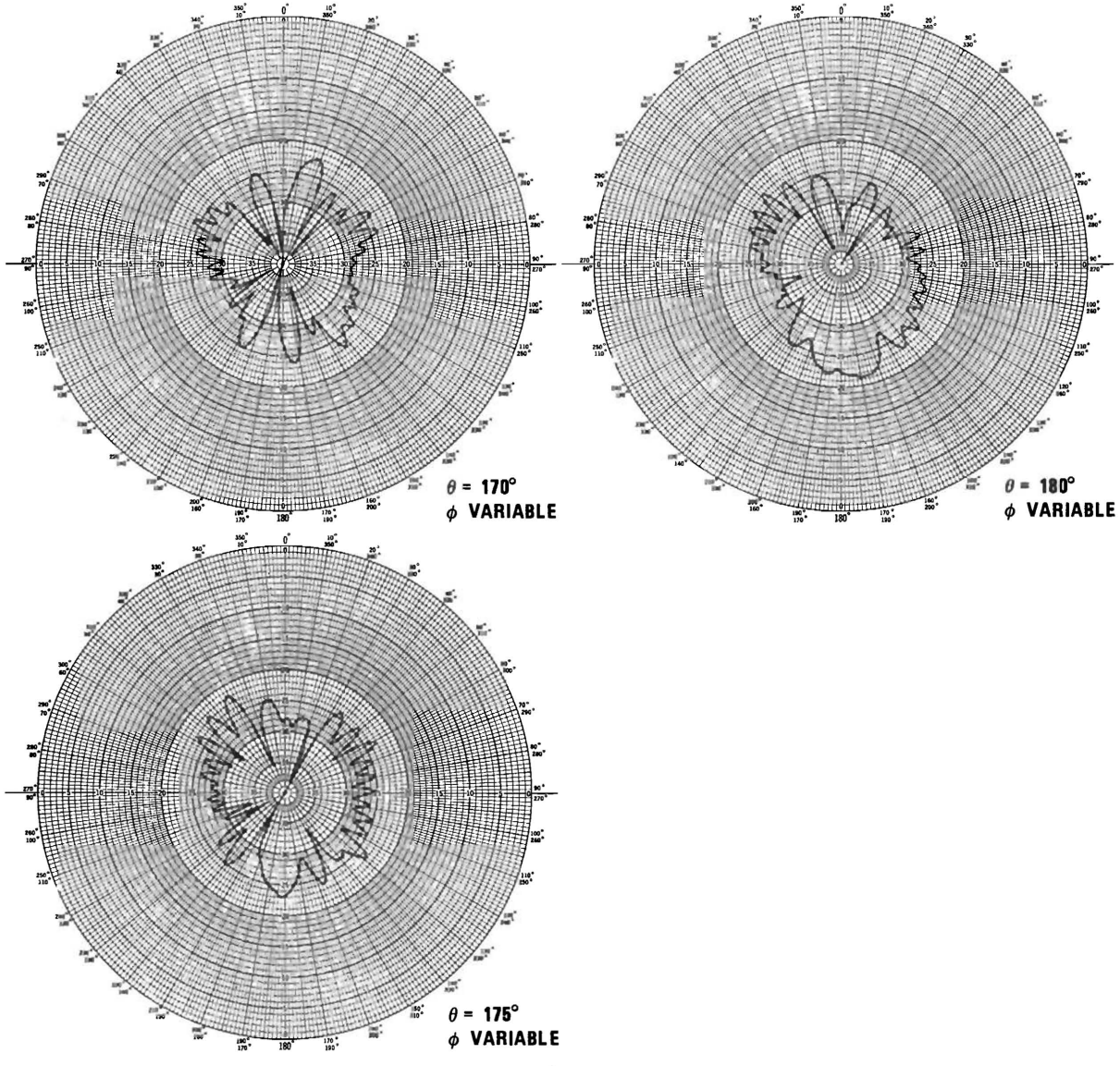

Conical Plots (dB), 2 Spirals, LHCP, No Solar Panels

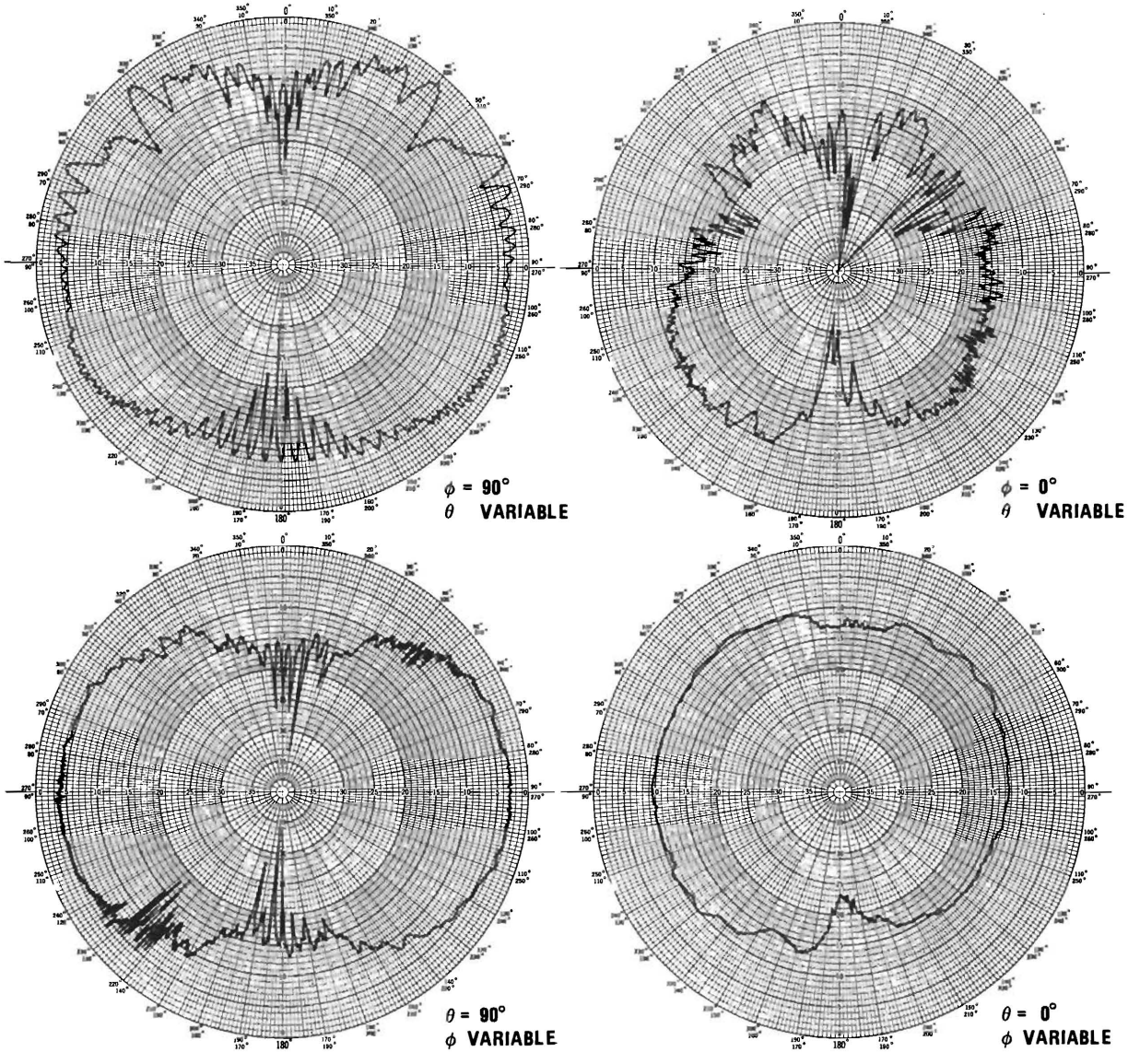

Principal Plane Patterns (dB), 2 Spirals, RHCP, Solar Panels at 0°.

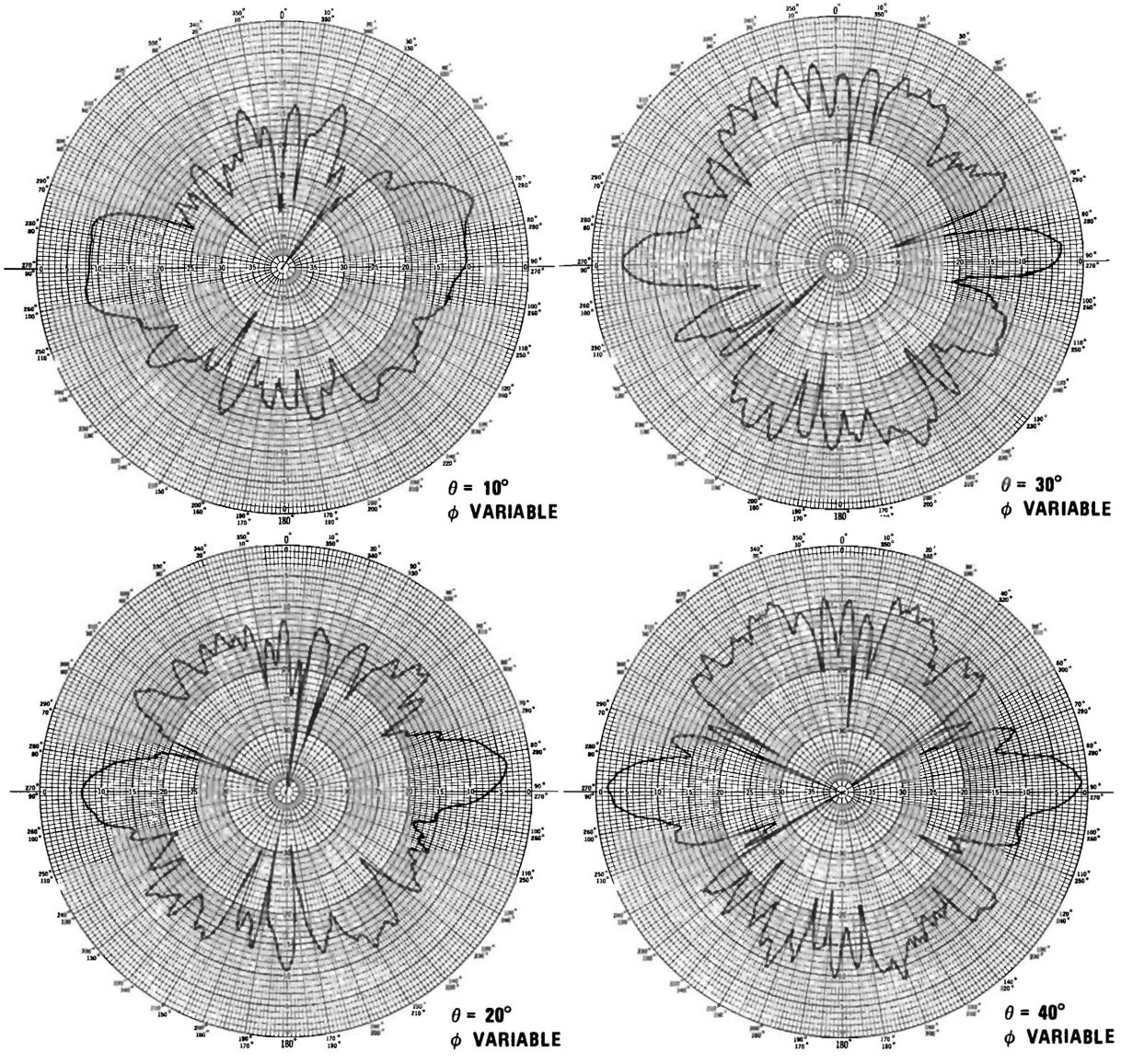

Conical Plots (dB), 2 Spirals, RHCP, Solar Panels at 0°

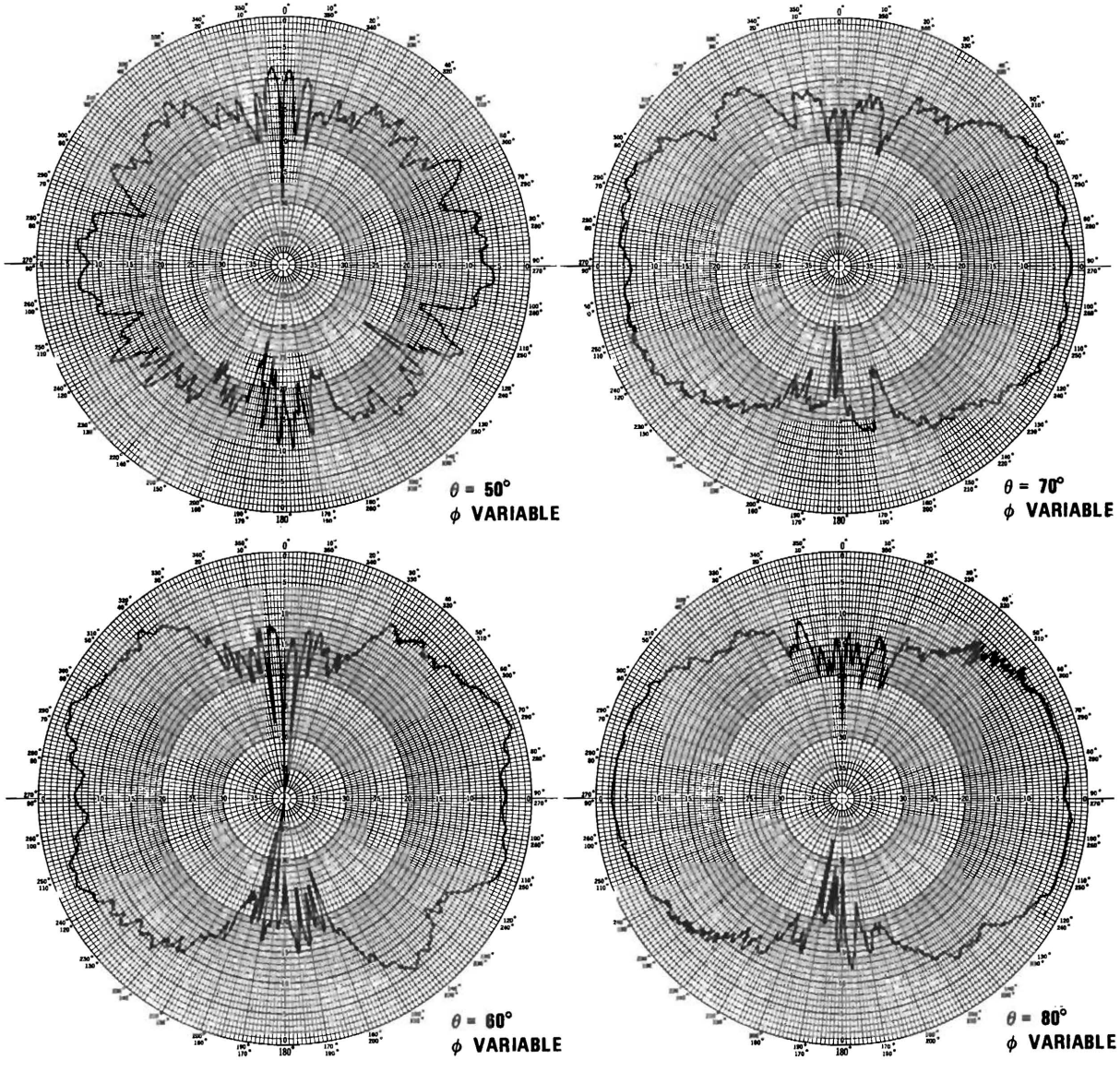

Conical Plots (dB), 2 Spirals, RHCP, Solar Panels at 0°

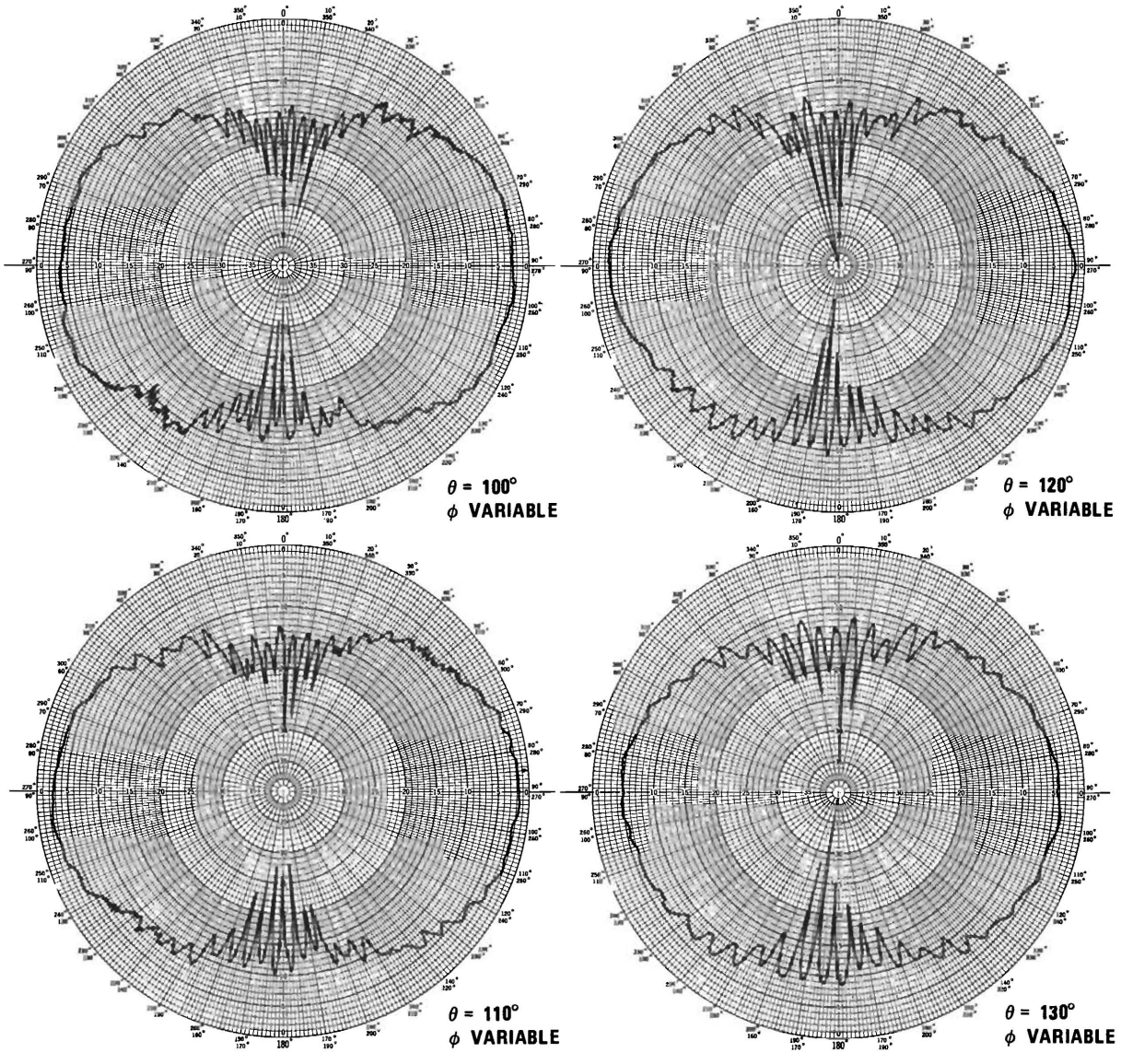

Conical Plots (dB), 2 Spirals, RHCP, Solar Panels at 0°

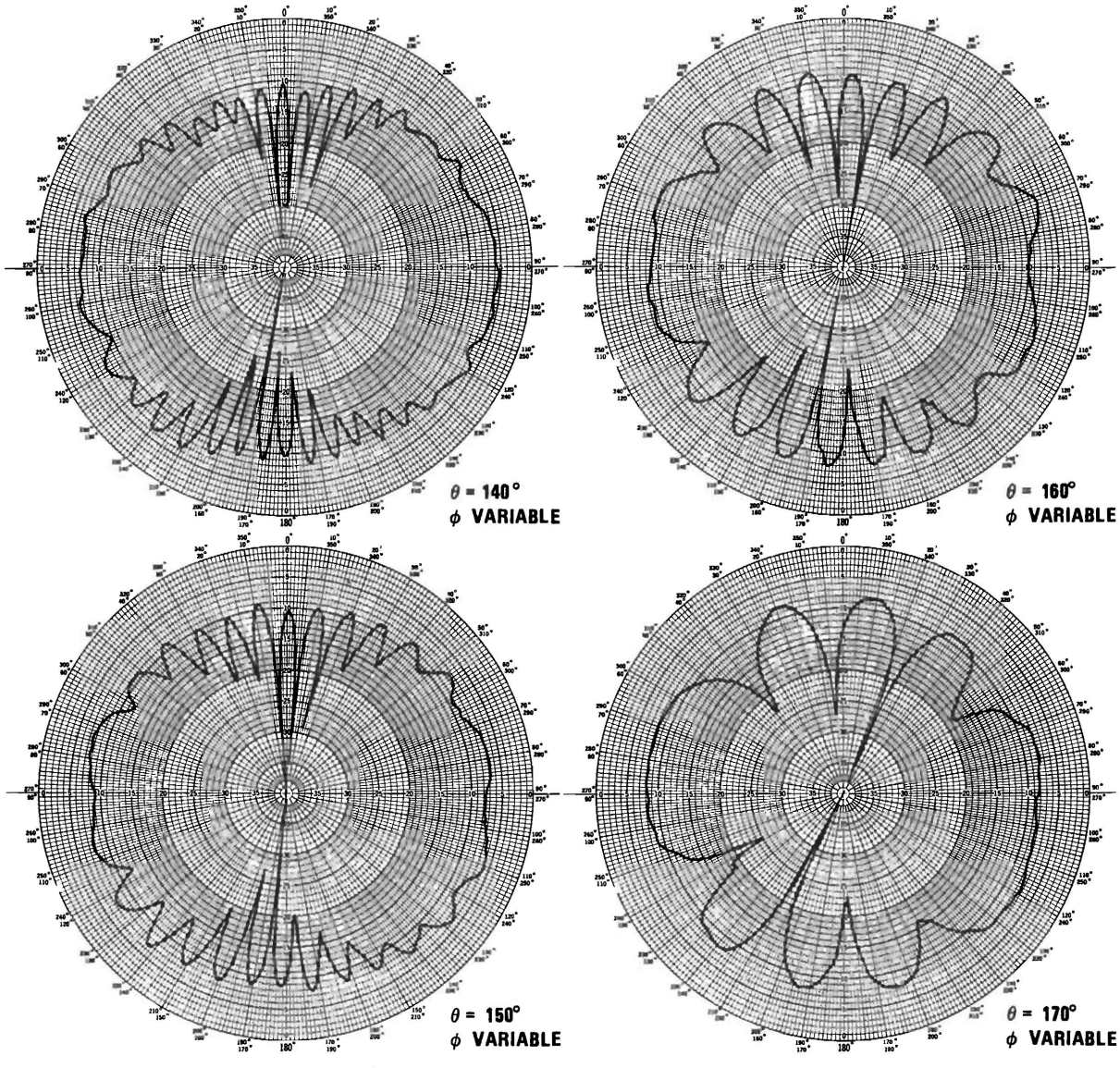

Conical Plots (dB), 2 Spirals, RHCP, Solar Panels at 0°

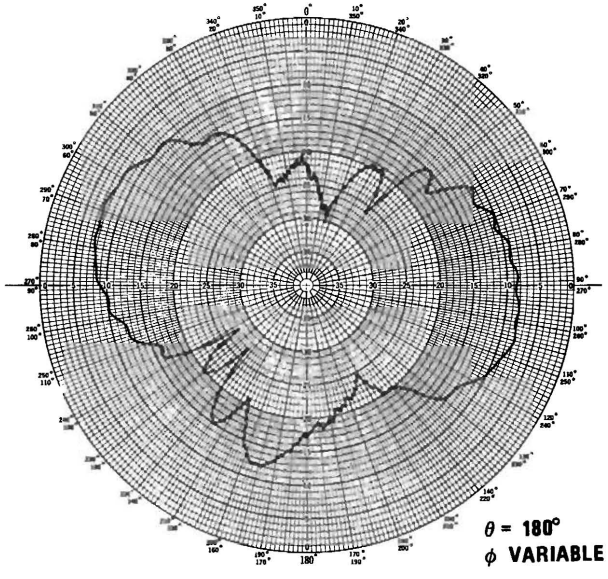

Conical Plots (dB), 2 Spirals, RHCP, Solar Panels at 0°

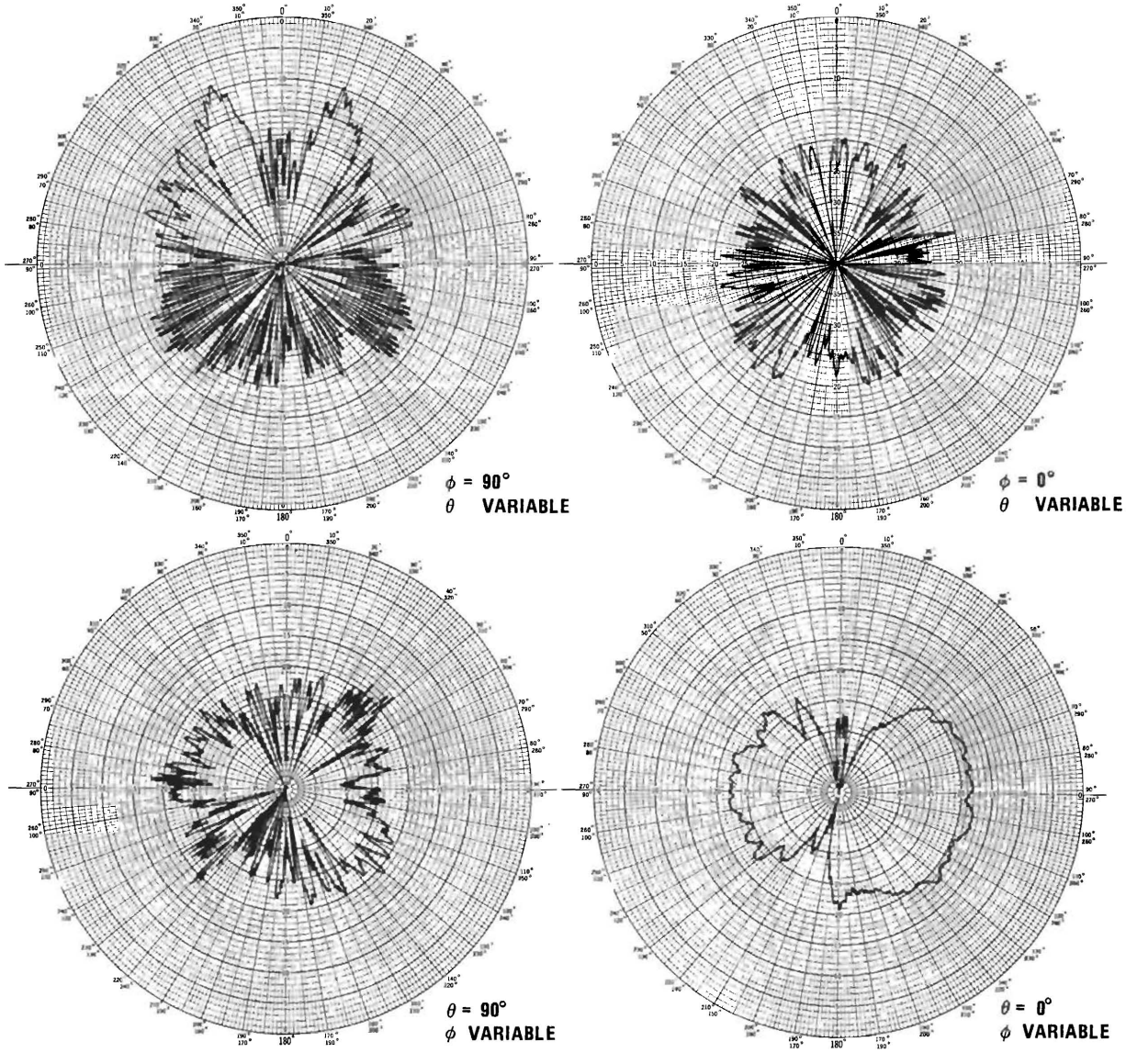

Principal Plane Patterns (dB), 2 Spirals, LHCP, Solar Panels at 0°.

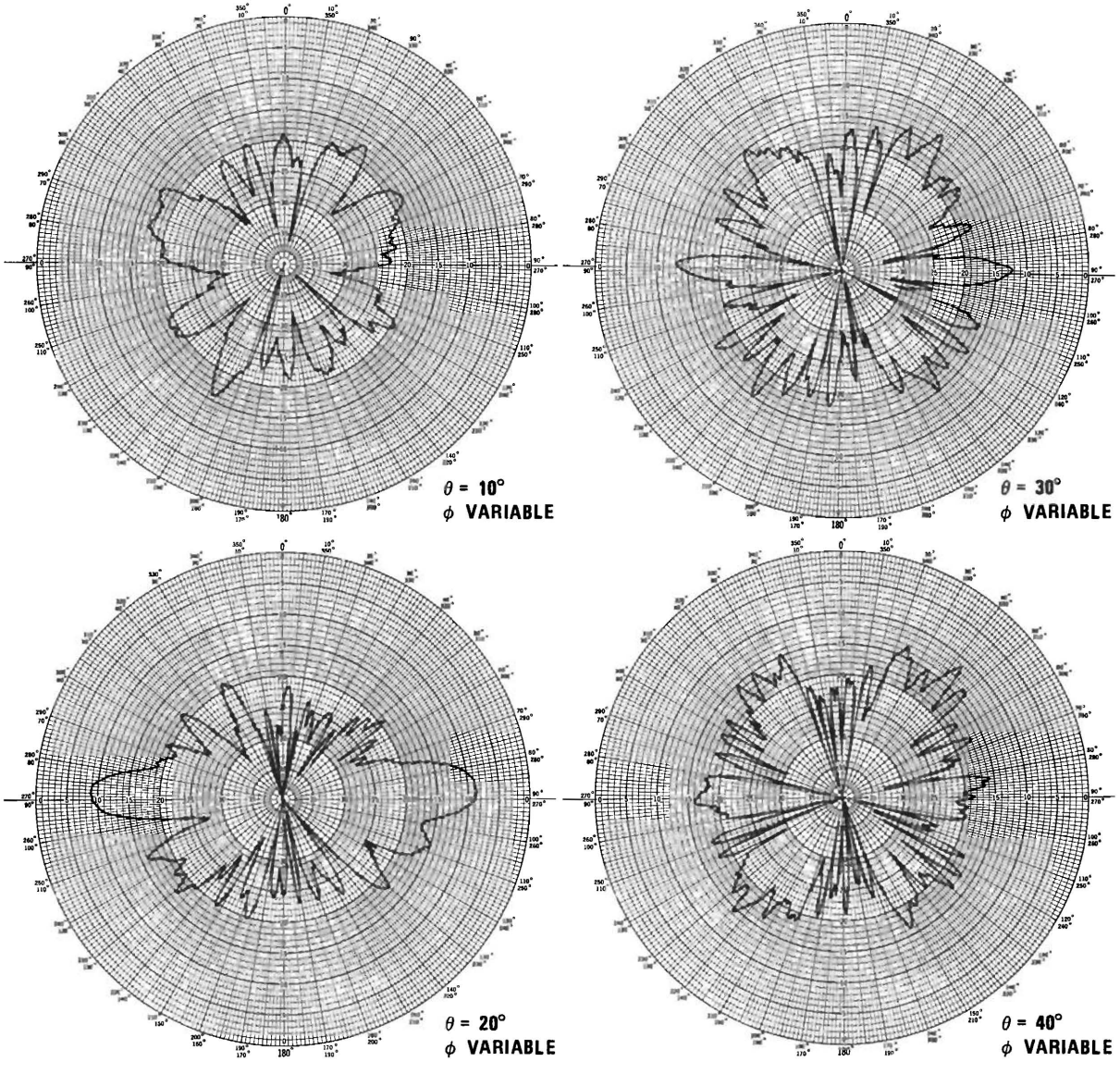

Conical Plots (dB), 2 Spirals, LHCP, Solar Panels at 0°

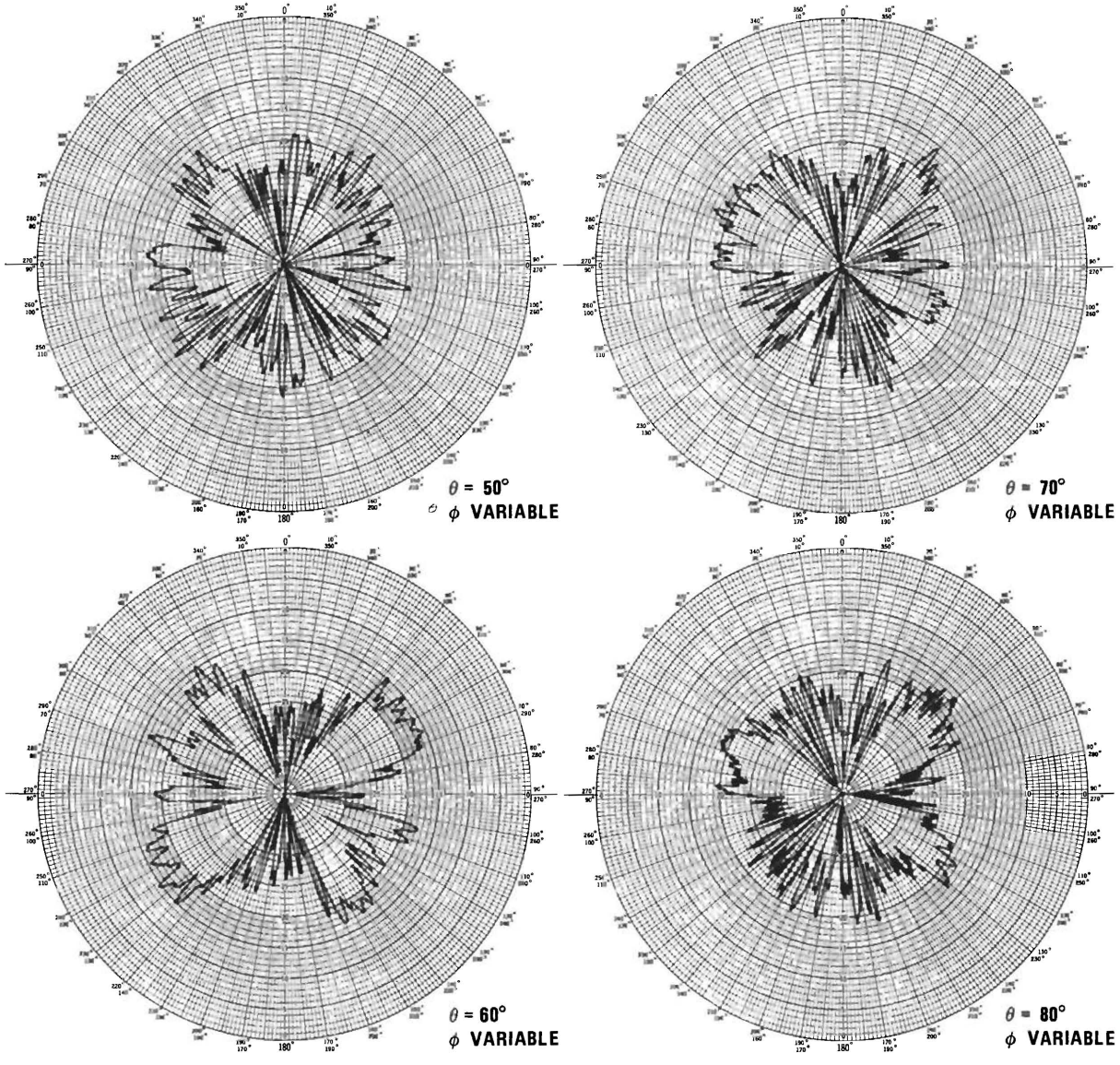

Conical Plots (dB), 2 Spirals, LHCP, Solar Panels at 0°

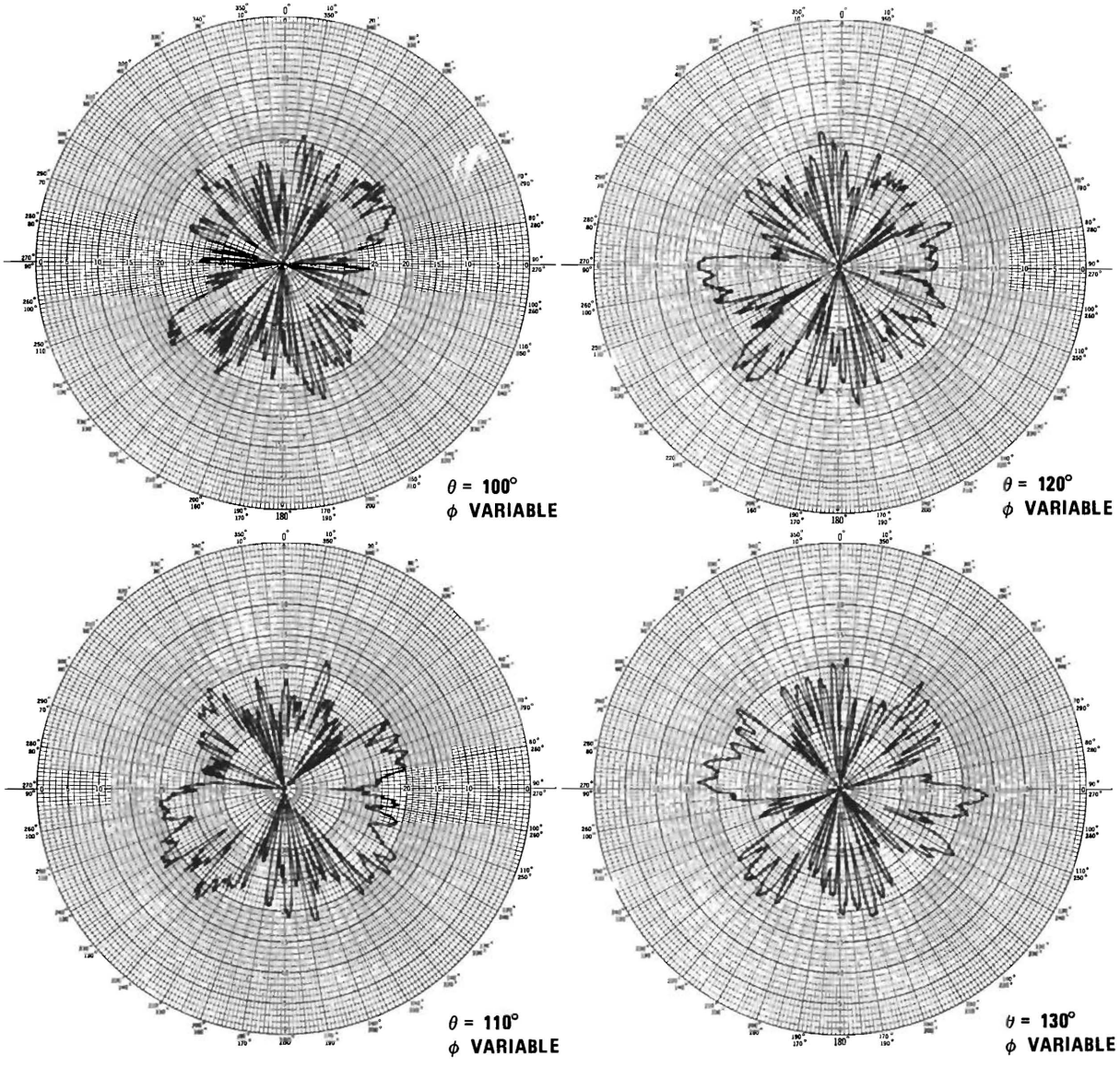

Conical Plots (dB), 2 Spirals, LHCP, Solar Panels at 0°

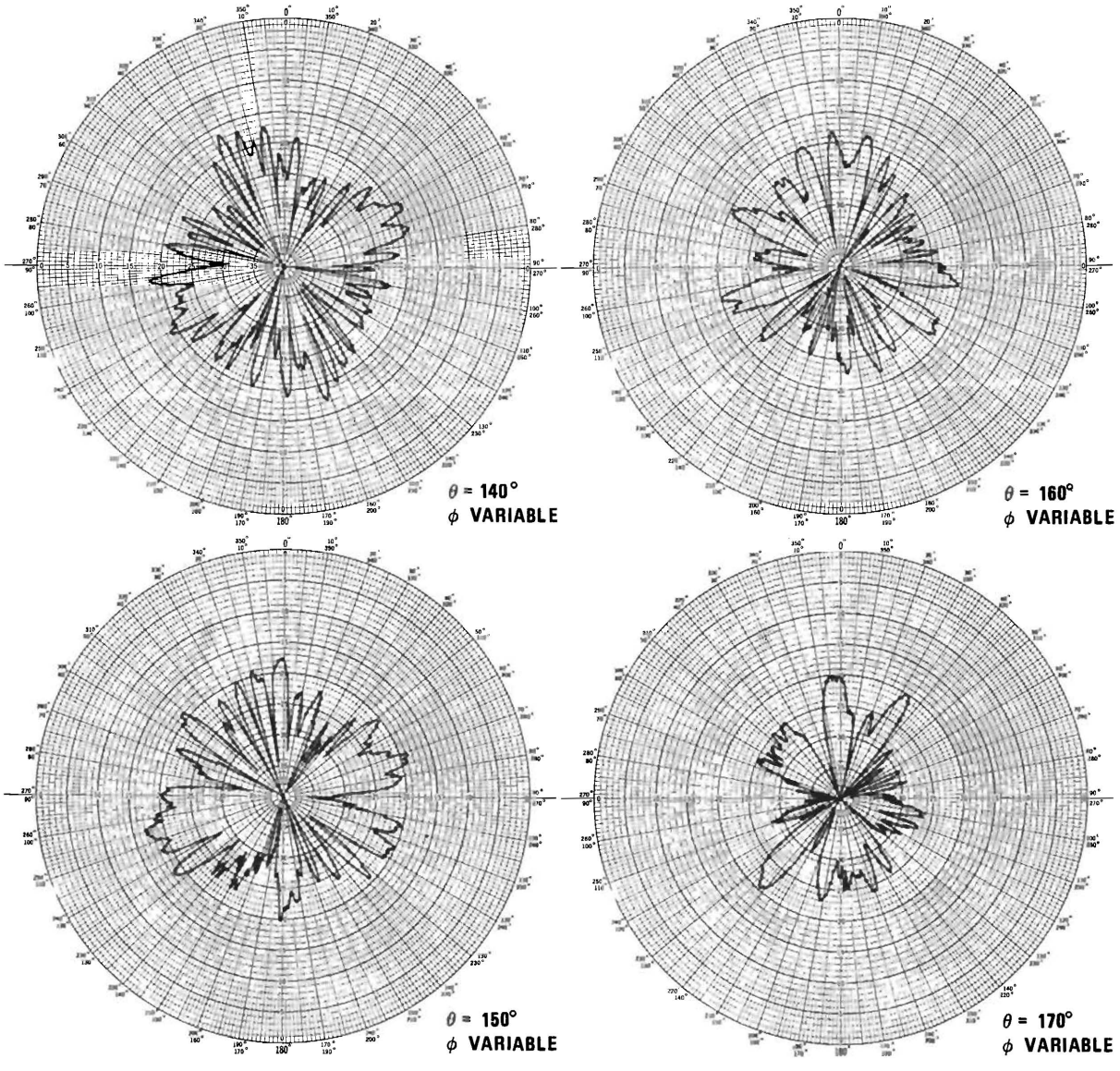

Conical Plots (dB), 2 Spirals, LHCP, Solar Panels at 0°

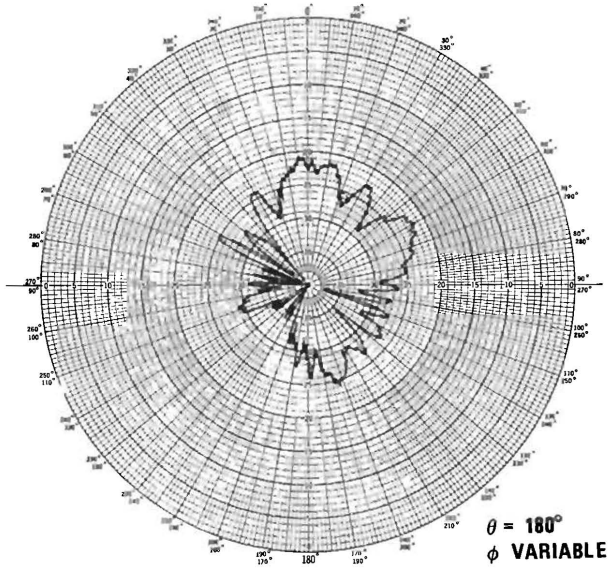

Conical Plots (dB), 2 Spirals, LHCP, Solar Panels at 0°

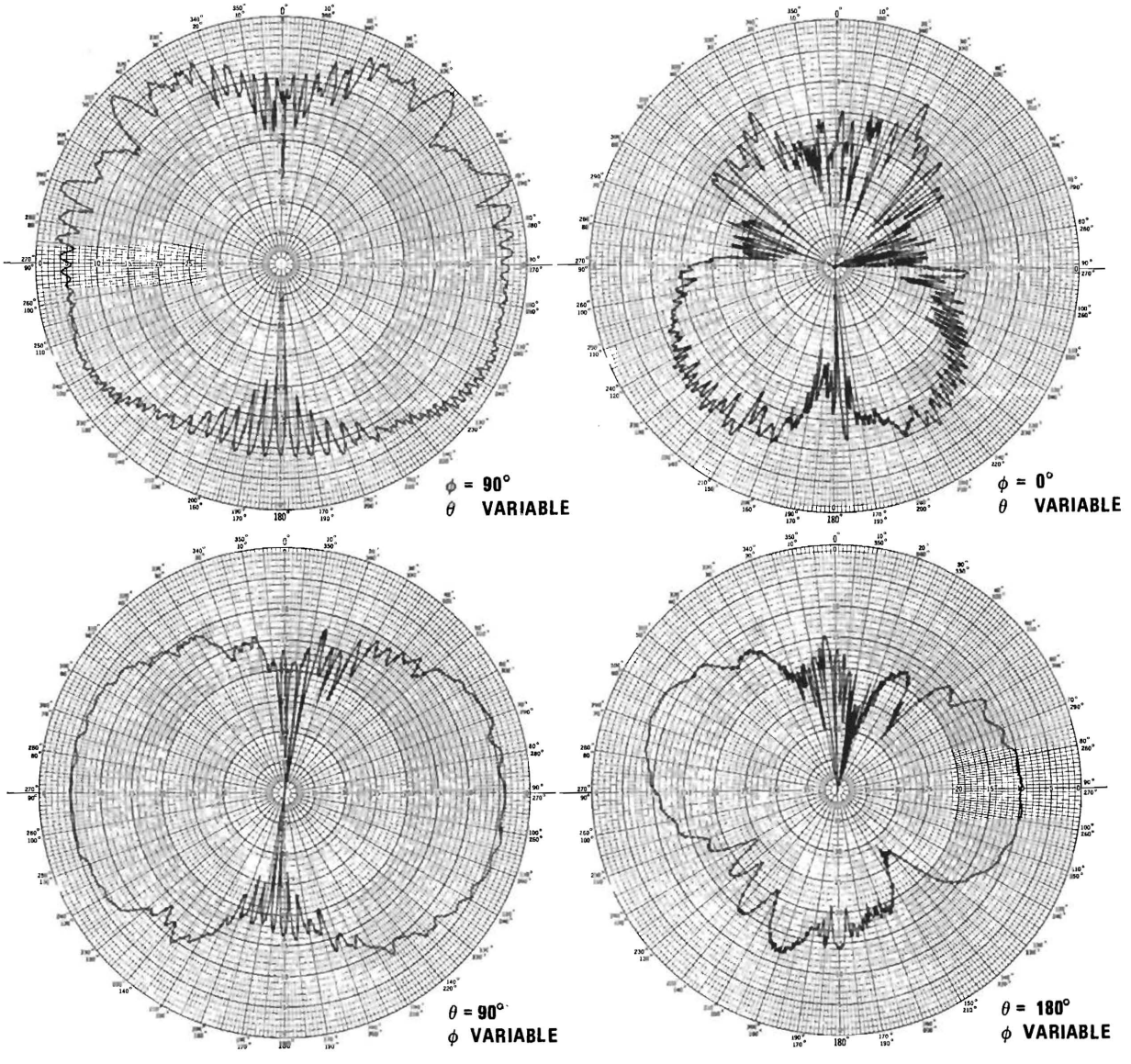

Principal Plane Patterns (dB), 2 Spirals, RHCP, Solar Panels at 45°

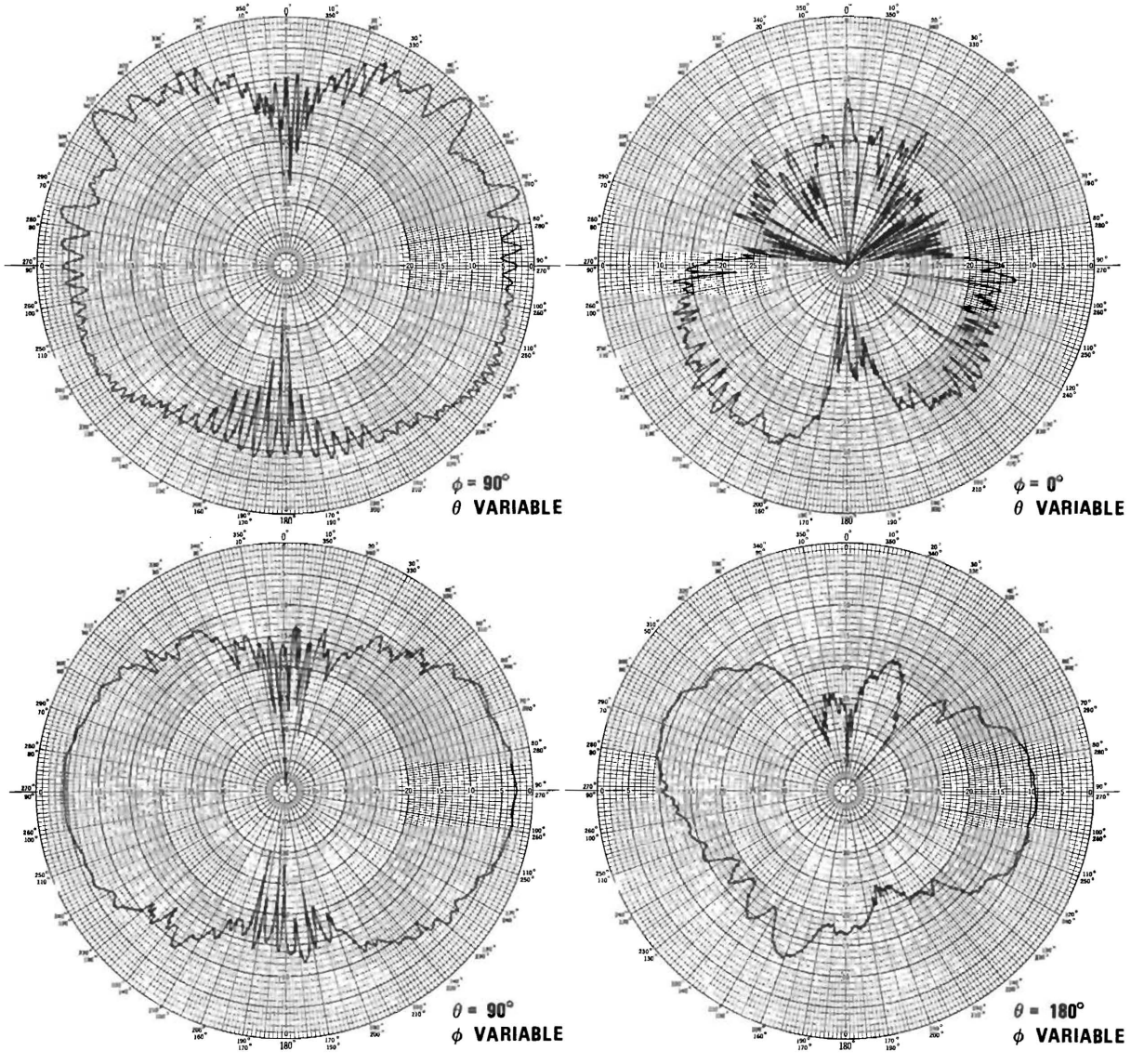

Principal Plane Patterns (dB), 2 Spirals, RHCP, Solar Panels at 90°

V. REFERENCES

1. Kilgus, C. C., "Resonant Quadrifilar Helix Design," Microwave Journal, December 1970, pp. 49-54.

2. Kilgus, C. C., "Multi-Element, Fractional Turn Helices," IEEE Trans. Vol. AP-16, July 1978, pp. 499-500.

3. Bricker, R. W., Jr. and H. H. Rickert, "An S-Band Resonant Quadrifilar Antenna for Satellite Communications," Symposium Digest of 1974 International IEEE/AP-S Meeting, June 10-12, 1974, pp. 78-82.

4. Munson, R. E., "Conformal Microstrip Antennas and Microstrip Phased Arrays," IEEE Trans. Vol. AP-22, January 1974, pp. 74-78.

5. Hill, J. E., "S-Band Antenna Systems for Missiles," NTC Proceedings, 1969, pp. 218-231.

6. Lindsey, J. F., III and L. Leopold, "S-Band Antenna Measurements for Manned Flight on the Apollo Program," Microwave Journal, December, 1969, pp. 71-74.

7. Croswell, W. F. and C. M. Knop, "On the Use of an Array of Circumferential Slots on a Large Cylinder as an Omnidirectional Antenna," IEEE Trans. AP-14, May 1966, pp. 394-396.

8. Feldman, N. E., "Antennas for Isotropic Coverage on Large D/Satellites," Proc.of the 14th International Astronautical Congress, Paris 1963 (Memorandum RM-3770, NASA July 1963).

9. Kuo, D. C., and B. J. Strait, "Improved Programs for Analysis of Radiation and Scattering by Configurations of Arbitrarily Bent Thin Wires," Prepared for AFCRL, Contract No. F19628-68-C-0180, AD-739 203, January 1972.

10. Stratton, J. A., Electromagnetic Theory, McGraw-Hill Book Co., 1941.

11. IEEE Transactions AP-13, "IEEE Test Procedure for Antennas," May, 1965.

12. Carl C. Osgood, Spacecraft Structures, Prentice-Hall, Inc., Englewood Cliffs, New Jersey, 1966.

13. Frank Kreith, "Radiation Heat Transfer and Thermal Control of Spacecraft," Publication No. 112, Oklahoma Engineering Experiment Station, Oklahoma State University, April, 1960.

14. John B. Rittenhouse and John B. Singletary, Space Materials Handbook, Third Edition, NASA SP-3051, 1969.

VI. BIBLIOGRAPHY

Anderson, R. E. and N. D. Hart, "A Look at UHF Telemetry Antennas for Aerospace Vehicles," The Microwave Journal, 9(1966) No. 4, p. 90-98.

Bangert, J. T. et al., "The Spacecraft Antennas," Bell System Technical Journal, 42 (1963) No. 7, pp. 869-897.

Bassett, H. L., "Antenna Systems for Group III Pershing Missile," Martin-Marietta Report OR-1416, January 1961.

Bassett, H. L., "Design of SPRINT S-Band Telemetry Antenna System," Martin-Marietta Report, January 1967.

Bugnolo, D. S., "A Quasi-Isotropic Antenna in the Microwave Spectrum," IRE Transactions AP-10, July 1962, pp. 377-383.

Cairns, F. V., "Measurement of Transmitter Gain as a Factor in Rocket Telemetry Link Performance," Canadian Aeronautics and Space Journal, February 1967, pp. 45-49.

Campbell, T. G., "An Extremely Thin, Omnidirectional Microwave Antenna Array for Spacecraft Applications," NASA TN D-5539, November 1969.

Charlton, T. E., et al., "A Waveguide Resonant Ring Antenna Yielding an Omnidirectional Pattern," Symposium on USAF Antenna Research and Development Programs, 1963.

Chen, C. C., "Turnstile Antenna for Space Communications," IEEE International Convention Record, 1966, Part 4, pp. 120-130.

Chu, T. S., "On the Use of Uniform Circular Arrays to Obtain Omnidirectional Patterns," IRE Transactions AP-7, October 1959, pp. 436-438.

Cockrell, C. R. and W. F. Croswell, "The Application of Circular Arrays to Spacecraft Antenna Problems," IEEE Transaction Aerospace, Vol.2, No. 2, April 1964, pp. 272-277.

Croswell,W. F. et al., "A Quasi-Omnidirectional Slot Array for Spacecraft Use at Microwave Frequencies," NASA TN D-4362, March 1968.

Croswell, W. F. and C. R. Cockrell,"An Omnidirectional Microwave Antenna for Use on Spacecraft, IEEE Transactions AP-17, July 1969, pp. 459-466.

Croswell, W. F. and C. M. Knop," On the Use of an Array of Circumferential Slots on a Large Cylinder as an Omnidirectional Antenna," IEEE Transactions AP-14, May 1966, pp. 394-396.

Croswell, W. F., et al., "A Dielectric Coated Circumferential Slot Array for Omnidirectional Coverage at Microwave Frequencies," IEEE Transactions AP-15,November 1967, pp. 722-727.

Dyson, J. D., "The Characteristics and Design of the Conical Log-Spiral Antenna," IEEE Transactions AP-13, July 1965, pp. 488-499.

Fradin, A. Z., "Synthesis of Radiators Approximating an Isotropic System," Radio Engineering and Electrophysics, 8(1963) pp. 779-783.

Fulton, F. F., "The Combined Radiation Pattern of Three Orthogonal Dipoles," IEEE Transactions AP-13, March 1965, pp. 323-324.

Galindo, V. and K.Green, "A Near-Isotropic Circularly Polarized Antenna for Space Vehicles," IEEE Transactions AP-13, November 1965, pp. 872-877.

Gregorwich, W. S., "An Electronically Despun Array Flush-Mounted on a Cylindrical Spacecraft," IEEE Transactions AP-22, January 1975, pp. 71-74.

Gregorwich, W. S., "An Omnidirectional Telemetry Antenna for Spacecraft," NTC Record, 1971, pp. 94-99.

IEEE Transactions AP-21, Special Issue on Antenna Measurements, edited by J. Searcy Hollis, July 1973.

Jones, J. E. and J. H. Richmond," Application of an Integral Equation Formulation to the Prediction of Space Shuttle Annular Slot Radiation Patterns," IEEE Transactions AP-22, January 1974, pp. 109-111.

Knudsen, H. L., "Radiation from Ring Quasi Arrays," IRE Transactions AP-4, July 1954, pp. 452-472.

Koob, K., "An Isotropic Antenna System with Six Orthogonally Polarized Radiators for Spacecraft Which are Large Compared to Wavelength," Bericht EP-109 der Messerschmitt - Bölkow-Blohm GmBh, July 1970.

Korvin, W. and R. B. Jackson," Antennas for Space Vehicles," Space and Aeronautics, November 1964, pp. 60-66.

Korvin, W. and G. G. Chadwick," Latest Word in Space Talk: It Can Come from Anywhere," Electronics, 30 May 1966, pp. 117-126.

Kraus, J. D., Antennas, McGraw-Hill Book Co., 1950.

Lindbergh, C. A., "A Shallow-Cavity UHF Crossed-Slot Antenna," IEEE Transactions AP-17, September 1969, pp. 558-563.

McQuaid, B. L., "Description of Computer Program to Analyze Gain Distribution of an Antenna System," NTC Proceedings, 1969, pp. 264-270.

Mathis, H. F., "A Short Proof that an Isotropic Antenna is Impossible," Proc. IRE 39, 1951, p. 970.

Mathis, H. F., "On Isotropic Antennas," Proc. IRE, 1954, p. 1810.

Mayer, R., "The Monopole and Dipole Omnidirectional Antenna," NTZ No. 9, 1968, pp. 549-552.

Neff, H. P. et al., "Circular Arrays Around Cylinders," Scientific Report No. 7, AFCRL-64-537, Univ. of Tennessee, Knoxville, June 1964.

Paul, B., "Shadows Produced by Spin-Stabilized Communication Satellite," AIAA Journal 2, No. 5, 1964, pp. 924-931.

Ricardi, J., "Directivity of an Array of Slots on the Surface of a Cylinder," Electronic Engineering, September 1967, pp. 578-581.

Riblet, H. B., "A Broadband Spherical Satellite Antenna," Proc. IRE, Vol. 48, April 1960, pp. 631-635.

Saunders, W. K., "On the Unity Gain Antenna," Electromagnetic Theory and Antennas, Edited by E. C. Jordan, Pergamon Press, New York, 1963, pp. 1125-1130.

Scott, W. G. and K. M. Soo Hoo," A Theorem on the Polarization of Null-Free Antennas," IEEE Transactions AP-14, No. 5, September 1966, pp. 587-590.

Shu, C. J., "Physical Limitations of Omnidirectional Antennas," Journal of Applied Physics 19, No. 12, 1948, pp. 1163-1175.

Wait, T. R., Electromagnetic Radiation from Cylindrical Structures, Pergamon Press, London, New York, 1959.

Waterman, A., and O. Henry, "Stripline Strap-On Antenna Array," Contract AF19628-69-C-0177, September 1971.

Weinschel, H. D., "Design of S-Band Telemetry Antennas," NTC Proceedings, 1969, pp. 317-329.

Wheeler, H. A., "Fundamental Limitations of Omnidirectional Antennas," Proc. IRE, December, 1947, pp. 1479-1484.

Wolff, F. M., "Antenna Pattern Analysis - A Computer Method," NTC Proceedings, 1969, pp. 232-247.

Woodward, O. M., "A Mode Analysis of Quasi-Isotropic Antennas," RCA Review 16, March 1965, pp. 42-74.